

1N-37-CR
20-1874

NA68-212

ENHANCED SIMULATION SOFTWARE FOR
ROCKET TURBOPUMP, TURBULENT, ANNULAR LIQUID SEALS

P. 291

FINAL REPORT

by

Drs. Satya Padavala and Alan Palazzolo (P.I.)
Texas A&M University
College Station, TX 77843-3123
(409)845-1251

To:

University of Alabama
at Huntsville, AL

and

NASA Marshall Space
Flight Center

TAMU Project 41670 ME
1/26/94

(NASA-CR-195239) ENHANCED
SIMULATION SOFTWARE FOR ROCKET
TURBOPUMP, TURBULENT, ANNULAR
LIQUID SEALS Final Report (Alabama
Univ.) 291 p

N94-27383

Unclass

G3/37 0209834

ABSTRACT

Dynamic Analysis of Arbitrary Profile Liquid Annular Seals and Transient Analysis with Large Eccentric Motion.

One of the main objectives of this work is to develop a new dynamic analysis for liquid annular seals with arbitrary profile and analyze a general distorted interstage seal of the Space Shuttle Main Engine High Pressure Oxygen Turbopump (SSME-ATD-HPOTP). The dynamic analysis developed is based on a method originally proposed by Nelson and Nguyen (1988a, 1988b). The original method used an approximation scheme based on *Fast Fourier Transforms* (FFT) to compute the circumferential gradients of the zeroth order variables of the eccentric solution. This method, in some cases, has problems with convergence at higher eccentricities. A simpler scheme based on cubic splines is found to be computationally more efficient and has better convergence properties at higher eccentricities than the original method. The first order solution of the original analysis is modified by including a more exact solution that takes into account the variation of perturbed variables along the circumference. A new set of equations for dynamic analysis are derived based on this more general model. The original method was developed for Moody's friction model. In the current work, a unified solution procedure that is valid for both Moody's and Hirs' models is presented.

Dynamic analysis based on the above improved method is developed for three

different models; a) constant properties, b) variable properties, c) thermal effects (energy equation) with variable properties.

Arbitrarily varying seal profiles in both axial and circumferential directions are considered. An example case of an elliptical seal with varying degrees of axial curvature is analyzed in detail. A case study based on predicted clearances (6 axial planes with 68 clearances/plane) of an interstage seal of the SSME-ATD-HPOTP is presented. Dynamic coefficients based on external specified load are introduced for seals, for the first time, to analyze seals that support a pre-load.

The other objective of this work is to study the effect of large rotor displacements of SSME-ATD-HPOTP on the dynamics of the annular seal and the resulting transient motion. Currently, the *linear model* of the annular seal employed at NASA Marshall Space Flight Center (MSFC) to estimate the seal forces during a transient motion of the turbopump uses a set of 6 dynamic coefficients computed at zero ($\epsilon = 0$) eccentricity. This model, while valid for a *small* motion of the rotor about the centered position, may not be accurate for large off-center operation of the seal. One of the objectives of this study is to identify the magnitude of these deviations and establish limits of effectiveness of using such a model. This task is accomplished by solving the *bulk flow model* seal governing equations directly for transient seal forces for any given type of motion, including motion with large eccentricities.

Based on the above study, an equivalence is established between linearized coefficients based transient motion and the same motion as predicted by the original governing equations. An innovative method is developed to model non-linearities in an annular seal based on dynamic coefficients computed at various static eccentricities. This method is thoroughly tested for various types of transient motion using bulk flow model results as a benchmark.

TABLE OF CONTENTS

CHAPTER		Page
I	INTRODUCTION	1
	1.1 Literature Survey	1
	1.2 Dynamic Analysis of an Annular Seal	5
	1.3 Current Work	8
	1.4 Original Contributions	13
II	CONSTANT PROPERTIES MODEL	15
	2.1 Bulk Flow Governing Equations	15
	2.2 Friction Factors	18
	2.3 Film Thickness	20
	2.4 Solution Procedure	23
	2.5 Perturbation Analysis	25
	2.5.1 Zeroth Order Equations	26
	2.5.2 First Order Equations	26
	2.5.3 Linearization of Friction Factors	27
	2.6 Zeroth Order Boundary Conditions	28
	2.7 Solution Procedure for Zeroth Order Equations	32
	2.7.1 Comparison with Nelson and Nguyen Approach	33
	2.7.2 Iterative Solution for Zeroth Order Equations	34
	2.7.3 Cubic Spline Interpolation	40
	2.7.4 Leakage	44
	2.7.5 Steady State Seal Forces	45
	2.7.6 Friction Loss	47
	2.8 First Order Boundary Conditions	48
	2.9 Solution Procedure for First Order Equations	48
	2.9.1 Comparison with Nelson and Nguyen's Approach	53
	2.9.2 Boundary Conditions of Assumed Variables	53
	2.9.3 Solution of First Order Equations	54
	2.10 Determination of Dynamic Coefficients	54
	2.11 Dynamic Coefficients based on External Load Specification	57
	2.11.1 Steady State Force Equilibrium Position	59
III	VARIABLE PROPERTIES MODEL	61

CHAPTER

Page

3.1	Thermophysical Properties Model	65
3.2	MBWR Equation of State	65
3.3	Bulk Flow Governing Equations	67
3.4	Comparison with San Andres (1991)	68
3.5	Perturbation Analysis	68
3.5.1	Zeroth Order Equations	69
3.5.2	First Order Equations	70
3.6	Zeroth Order Boundary Conditions	70
3.7	Reduction of Zeroth Order Equations	72
3.8	Solution Procedure for Zeroth Order Equations	74
3.9	Reduction of First Order Equations	75
3.10	First Order Boundary Conditions	77
3.11	Solution of First Order Equations	77
IV	THERMAL EFFECTS MODEL	80
4.1	Zeroth Order Equations	83
4.2	Zeroth Order Boundary Conditions	83
4.3	Solution Procedure for Zeroth Order Equations	85
4.4	Comparison of Current Analysis with San Andres <i>et al.</i>	86
4.5	First Order Solution	87
V	ARBITRARY PROFILE SEALS	88
5.1	Example of an Arbitrary Profile Seal: Elliptical Seal	89
5.2	Results	92
5.2.1	Straight Elliptical Seal vs. Straight Circular Seal	93
5.2.2	Linear Profile vs. Curved Profile	96
5.3	Case Study of a Distorted Seal of SSME-ATD-HPOTP	97
5.4	Directional Dependence of Dynamic Coefficients	100
VI	RESULTS	110
6.1	Childs and Lindsey (1993)	111
6.1.1	Work Summary	111
6.1.2	Comparative Study	113
6.1.3	Leakage, Concentric Tests	115
6.1.4	Dynamic Coefficients, Concentric Tests	117
6.1.5	Leakage, Straight Seal, Eccentric Tests	120
6.1.6	Dynamic Coefficients, Straight Seal, Eccentric Tests	120
6.1.7	Leakage, Slightly Convergent Seal, Eccentric	120

6.1.8	Dynamic Coefficients, Convergent Seal, Eccentric Tests	124
6.1.9	Conclusions	124
6.2	Childs and Kim (1985), Hirs Model	128
6.3	Scharrer and Nunez (1989)	129
6.4	Scharrer and Nelson (1990)	130
6.4.1	Smooth Seals	132
6.4.2	Rough Seals	132
6.5	Jenssen (1970)	134
6.6	Kanki and Kawakami (1984)	137
6.7	Falco <i>et al.</i> (1984)	142
6.8	Allaire <i>et al.</i> (1976)	145
6.9	Comparison of Variable Properties Model with Constant Properties Model	145
6.10	San Andres <i>et al.</i> (1992), Isothermal Case	147
6.11	San Andres <i>et al.</i> (1992), Adiabatic Case	151
6.12	Comparison of Current Analysis with Other Methods	151
VII	TRANSIENT ANALYSIS	159
7.1	Objectives	162
VIII	VARIOUS SEAL MODELS FOR TRANSIENT ANALYSIS	170
8.1	Transient Analysis with Bulk Flow Model	172
8.1.1	Transient Seal Forces with Bulk Flow Equations	173
8.2	Transient Analysis with Linear Model ($\epsilon = 0$)	174
8.3	New Method-I	174
8.3.1	Stiffness Force	175
8.3.2	Damping Force	176
8.3.3	Inertia Force	176
8.3.4	Theory	177
8.3.5	Evaluation of Integrals	181
8.3.6	Summation vs. Integration	184
8.3.7	Limitations of Method-I	184
8.4	New Method-II	185
8.4.1	Theory	186
IX	IMPLEMENTATION	190
9.1	Simulation Model	192

	9.2 Time Step for Transient Analysis	193
	9.3 Fluid Inertia Coefficients	193
	9.4 Computation of Fluid Forces	194
	9.5 Splines of Coefficients	196
	9.6 Transient Analysis Simulation Code: TRANSEAL	196
X	RESULTS	198
	10.1 Gradually Applied Loads (Ramp Function)	198
	10.1.1 Steady State Seal Forces vs. Spring Forces	204
	10.2 Harmonic Loads (Sinusoidal Function)	206
	10.3 High Frequency Loads (Sinusoidal Function)	212
	10.3.1 Fluid Inertia Forces at High Frequencies	213
	10.4 Suddenly Applied Loads (Step Function)	213
	10.5 Impulse Loads (Impulse Function)	222
	10.6 Combination Loads	223
	10.7 Comparison between Bulk Flow Model and Linear Model ($\epsilon = 0$)	229
	10.8 Comparison between Bulk Flow Model and New Method	229
	10.9 Conclusions	230
XI	SEAL CODES	234
	11.1 Tamuseal-I	234
	11.2 Tamuseal-II	234
	11.3 Tamuseal-III	235
	11.4 Tamuseal-IV	236
	11.5 Transeal	236
XII	CONCLUSIONS	238
	12.1 Future Work	240
	REFERENCES	242
	APPENDIX A	247
	APPENDIX B	250
	APPENDIX C	255
	APPENDIX D	256

CHAPTER	Page
APPENDIX E	257
APPENDIX F	258
APPENDIX G	261

LIST OF TABLES

TABLE	Page
6.1 Seal Geometry for Childs and Lindsey	112
6.2 Childs and Kim Check Case, Hirs' Model	129
6.3 Scharrer and Nunez, Rough Wavy Seal Case	130
6.4 Scharrer and Nelson, Partially Tapered Seals (Smooth), Taper=1.0 . .	132
6.5 Scharrer and Nelson, Partially Tapered Seals (Smooth), Taper=0.4 .	133
6.6 Scharrer and Nelson, Partially Tapered Seals (Smooth), Taper=0.0 .	133
6.7 Scharrer and Nelson, Partially Tapered Seals (Rough), Taper=1.0 . .	134
6.8 Scharrer and Nelson, Partially Tapered Seals (Rough), Taper=0.4 . .	135
6.9 Scharrer and Nelson, Partially Tapered Seals (Rough), Taper=0.0 . .	135
6.10 Scharrer and Nelson, Comparison with Childs and Kim, Taper=1.0, Rough	136
6.11 Scharrer and Nelson, Comparison with Childs and Kim, Taper=1.0, Rough	136
9.1 Table of Dynamic Coefficients for Seal Unit 3-02	197

LIST OF FIGURES

FIGURE	Page
1.1 A Pump Annular Seal (Vance, 1991)	2
1.2 Typical Seal Profiles	2
1.3 Predicted Clearance Profile for Seal, Unit 3-01	6
2.1 Differential Volume for Deriving the Continuity Equation	17
2.2 Differential Volume for Deriving the Momentum Equations	17
2.3 Diagram for Deriving General Seal Clearance Expression	21
2.4 Flow Chart of Solution Procedure, Nguyen (1988)	24
2.5 Boundary Conditions	29
2.6 Zeroth Order Boundary Conditions	29
2.7 Circumferential Grid	36
2.8 Grid for Numerical Integration	36
2.9 Leakage	45
2.10 Steady State Seal Forces	46
2.11 Force Geometry for Seal	46
2.12 Frictional Torque	47
2.13 Elliptical Whirl Orbit	49
2.14 Perturbation Orbit	51
2.15 Example of External Load acting on a Seal	58
2.16 External Load and External Load Angle	59

FIGURE		Page
3.1	Properties of Liquid Oxygen at 90°K	63
3.2	Properties of Liquid Hydrogen at 90°K	64
4.1	Zeroth Order Boundary Conditions	84
5.1	Examples of Seal Axial Profiles	88
5.2	Elliptical Seal	91
5.3	Elliptical Seal with Various Ellipticity Factors, δ	91
5.4	Normalized Direct Stiffness for Elliptical Seal (Straight), ($\delta=0$, $\delta=0.4$)	94
5.5	Normalized Cross Coupled Stiffness for Elliptical Seal (Straight), ($\delta=0$, $\delta=0.4$)	94
5.6	Normalized Direct Damping for Elliptical Seal (Straight), ($\delta=0$, $\delta=0.4$)	95
5.7	Normalized Leakage for Elliptical Seal (Straight), ($\delta=0$, $\delta=0.4$)	95
5.8	Normalized Direct Stiffness for Elliptical Seal (Curved)	98
5.9	Normalized Cross Coupled Stiffness for Elliptical Seal (Curved)	98
5.10	Normalized Direct Damping for Elliptical Seal (Curved)	99
5.11	Normalized Leakage for Elliptical Seal (Curved)	99
5.12	Load vs. Eccentricity for Distorted Seal, Unit 3-01	101
5.13	Leakage for Distorted Seal, Unit 3-01	101
5.14	Direct Stiffness for Distorted Seal, Unit 3-01	102
5.15	Cross Coupled Stiffness for Distorted Seal, Unit 3-01	102
5.16	Direct Damping for Distorted Seal, Unit 3-01	103
5.17	Definition of Angle of Line of Centers and Eccentricity Angle	104
5.18	Rotor and Minimum Film Thickness Coordinate Systems	104

FIGURE		Page
5.19	Variation of K_{xx} for Elliptical Seal	107
5.20	Variation of k_{xy} for Elliptical Seal	107
5.21	Variation of C_{xx} for Elliptical Seal	108
6.1	Leakage, Childs and Lindsey, Concentric Tests	116
6.2	Dynamic Coefficients, Childs and Lindsey, Concentric (10200 rpm) .	118
6.3	Dynamic Coefficients, Childs and Lindsey, Concentric (17400 rpm) .	119
6.4	Leakage, Childs and Lindsey, Straight Seal, Eccentric Tests	121
6.5	Dynamic Coefficients, Childs and Lindsey, Straight Seal, Eccentric (10200 rpm)	122
6.6	Dynamic Coefficients, Childs and Lindsey, Straight Seal, Eccentric (17400 rpm)	123
6.7	Leakage, Childs and Lindsey, Convergent Seal, Eccentric Tests	125
6.8	Dynamic Coefficients, Childs and Lindsey, Convergent Seal, Ec- centric (10200 rpm)	126
6.9	Dynamic Coefficients, Childs and Lindsey, Convergent Seal, Ec- centric (17400 rpm)	127
6.10	Scharrer and Nelson, A Partially Tapered Annular Seal	131
6.11	Seal Force at 3000 rpm, Jenssen	137
6.12	Seal Force at 5000 rpm, Jenssen	138
6.13	Seal Force at 7000 rpm, Jenssen	138
6.14	Seal Force, F, for Kanki and Kawakami	140
6.15	Direct Stiffness, K_{xx} , K_{yy} for Kanki and Kawakami	140
6.16	Cross Coupled Stiffness, k_{xy} , k_{yx} for Kanki and Kawakami	141
6.17	Direct Damping, C_{xx} , C_{yy} , for Kanki and Kawakami	141

FIGURE		Page
6.18	Cross Coupled Damping, c_{xy} , c_{yx} for Kanki and Kawakami	142
6.19	Direct Stiffness K_{xx} , K_{yy} , for Falco <i>et al.</i>	143
6.20	Cross Coupled Stiffness k_{xy} , k_{yx} for Falco <i>et al.</i>	143
6.21	Direct Damping, C_{xx} , C_{yy} , for Falco <i>et al.</i>	144
6.22	Direct Inertia, M_{xx} , M_{yy} for Falco <i>et al.</i>	144
6.23	Leakage, Q, for Falco <i>et al.</i>	145
6.24	Direct Stiffness, K_{xx} , K_{yy} , for Allaire <i>et al.</i>	146
6.25	Cross Coupled Stiffness, k_{xy} , k_{yx} , for Allaire <i>et al.</i>	146
6.26	Direct Damping, C_{xx} , C_{yy} for Allaire <i>et al.</i>	147
6.27	Direct Stiffness K_{xx} , K_{yy} , for Seal Unit 3-01	148
6.28	Cross Coupled Stiffness k_{xy} , k_{yx} , for Seal Unit 3-01	148
6.29	Direct Damping, C_{xx} , C_{yy} for Seal Unit 3-01	149
6.30	Direct Inertia, M_{xx} , M_{yy} for Seal Unit 3-01	149
6.31	Seal Force, F, for Seal Unit 3-01	150
6.32	Leakage, Q, for Seal Unit 3-01	150
6.33	Direct Stiffness K_{xx} , K_{yy} , for San Andres, Isothermal	152
6.34	Cross Coupled Stiffness k_{xy} , k_{yx} , for San Andres, Isothermal	152
6.35	Direct Damping, C_{xx} , C_{yy} for San Andres, Isothermal	153
6.36	Direct Inertia, M_{xx} , M_{yy} for San Andres, Isothermal	153
6.37	Seal Force, F, for San Andres, Isothermal	154
6.38	Leakage, Q, for San Andres, Isothermal	154
6.39	Temperature Rise, San Andres, Adiabatic	155

FIGURE	Page
6.40	Frictional Torque, San Andres, Adiabatic 155
6.41	Leakage, San Andres, Adiabatic 156
6.42	Stiffness, San Andres, Adiabatic 156
6.43	Damping, San Andres, Adiabatic 157
7.1	Circumferential Grid for Seal Coefficient Mapping 161
7.2	Variation of K_{xx} for unit 3-02 as a function of rotor position 163
7.3	Variation of C_{xx} for unit 3-02 as a function of rotor position 164
7.4	Variation of k_{xy} for unit 3-02 as a function of rotor position 165
7.5	Eccentric Motion: Type 1 167
7.6	Eccentric Motion: Type 2 167
8.1	Various Models for Transient Analysis 171
8.2	SDOF Spring-Mass-Damper System 176
8.3	Seal Model for a 2 DOF Vibration Model 177
8.4	Stiffness Force Integral 182
8.5	Damping Force Integral 182
8.6	Inertia Force Integral 183
9.1	Simulation Model 191
9.2	Rotor-Seal Model used for Simulation 191
10.1	Gradually Applied Load, 1780 N (400 lb), Disp. (y), Seal Force (Fy) 200
10.2	Gradually Applied Load, 5340 N (1200 lb), Disp. (y), Seal Force (Fy) 201
10.3	Gradually Applied Load, 8900 N (2000 lb), Disp. (y), Seal Force (Fy) 202
10.4	Steady State Seal Forces for Seal Unit 3-02, from Seal Code 205

FIGURE

Page

10.5	Steady State Seal Forces vs. Spring Forces, New Methods-1,2	205
10.6	Harmonic Load, 1780N (400lb) at 100Hz, Disp. (y), Seal Force (Fy) .	208
10.7	Harmonic Load, 3560N (800lb) at 100Hz, Disp. (y), seal Force (Fy) .	209
10.8	Harmonic Load, 5340N (1200lb) at 100Hz, Disp. (y), seal Force (Fy)	210
10.9	Harmonic Load (eccentric), 1340N (300lb), 100Hz, Disp. (y), Force (Fy)	211
10.10	High Frequency Load, 2225N (500lb) at 500Hz, Disp. (y), Seal Force (Fy)	214
10.11	High Frequency Load, 15570N (3500lb) at 500Hz, Disp. (y), Force (Fy)	215
10.12	High Frequency Load (eccentric), 4450N at 500Hz, Disp. (y), Force (Fy)	216
10.13	High Frequency Load, 17800N (4000lb) at 1000Hz Disp. (y), Force (Fy)	217
10.14	High Frequency Load, 35600N (8000lb) at 1000Hz, Disp. (y), Force (Fy)	218
10.15	Suddenly Applied Load, 1780N (400lb), Disp. (y), seal Force (Fy) . .	219
10.16	Suddenly Applied Load, 3560N (800lb), Disp. (y), Seal Force (Fy) . .	220
10.17	Suddenly Applied Load, 5340N (1200lb), Disp. (y), Seal Force (Fy) .	221
10.18	Impulse Load, 2225N-ms (500lb-ms), Disp. (y), Seal Force (Fy) . . .	224
10.19	Impulse Load, 4450N-ms (1000lb-ms), Disp. (y), Seal Force (Fy) . .	225
10.20	Impulse Load, 8000N-ms (1800lb-ms), Disp. (y), Seal Force (Fy) . .	226
10.21	Impulse Load (eccentric), 2225N-ms (500lb-ms), Disp. (y), Force (Fy)	227
10.22	Combination Loads, Disp. (y), Seal Force (Fy)	228
10.23	Limitations of Method-I: Discontinuities in Integrals	231
10.24	Limitations of Method-I: Dependence on Δt	231

NOMENCLATURE

c_0	nominal clearance (m)
c_i, c_e	inlet and exit clearances (m)
C_{xx}, C_{yy}	direct damping coefficients (N-s/m)
c_{xy}, c_{yx}	cross coupled damping coefficients (N-s/m)
$c(z, \beta)$	clearance function
$[C]$	damping matrix
e	eccentricity (m)
(e, ϕ)	displacement (eccentricity) of center of rotor
f_r, f_s	friction coefficients (Moody's or Hirs')
$F_{fluid-x}, F_{fluid-y}$	seal reaction force components (N)
f_{cxx}, f_{cyy}	direct damping forces (N)
f_{cxy}, f_{cyx}	cross coupled damping forces (N)
f_{kxx}, f_{kyy}	direct stiffness forces (N)
f_{kxy}, f_{kyx}	cross coupled stiffness forces (N)
f_{mxx}, f_{myy}	direct inertia forces (N)
f_{mxy}, f_{myx}	cross coupled inertia forces (N)
f	circular frequency (Hz)
F_x, F_y	X and Y components of seal force (N)
$F_x(t), F_y(t)$	components of time varying external load (N)
F_c	constant load applied to the rotor (N)
F_s	amplitude of sinusoidal load function (N)
h	fluid film thickness (m)
I	impulse function (N-s)
psr	pre-swirl ratio
K_{xx}, K_{yy}	direct stiffness coefficients (N/m)

k_{xy}, k_{yx}	cross coupled stiffness coefficients (N/m)
$[K]$	stiffness matrix
L	length of the seal (m)
M_{xx}, M_{yy}	direct mass coefficients (kg)
m_{xy}, m_{yx}	cross coupled mass coefficients (kg)
$[M]$	mass matrix
p_i	inlet pressure (Pa)
p_e	exit pressure (Pa)
$[Q]$	transformation matrix
R	radius of the rotor (m)
t_n	time period of the system (s)
t	time (s)
t_r	rise time of the applied load (s)
u	bulk flow axial velocity (m/s)
v	bulk flow circumferential velocity (m/s)
w	ωR , rotor surface velocity, (m/s)
(x, y)	displacement (eccentricity) of center of rotor (m)
(\dot{x}, \dot{y})	velocity of center of rotor (m/s)
(\ddot{x}, \ddot{y})	acceleration of center of rotor (m/s ²)
z, β	axial and circumferential coordinates
ρ	density (kg/m ³)
μ	dynamic viscosity (Pa-s)
ϵ	eccentricity ratio
ϕ	eccentricity angle (rad)
δ	ellipticity, $(c_x - c_y)/c_x$
$(\delta x, \delta y)$	small change in displacements

$(\delta \dot{x}, \delta \dot{y})$	small change in velocities (m/s)
$(\delta \ddot{x}, \delta \ddot{y})$	small change in accelerations (m/s ²)
$\Delta F_x, \Delta F_y$	X and Y components of incremental seal force (N)
Δt	time step for transient analysis (s)
ξ_i	inlet loss coefficient
ξ_e	exit pressure recovery coefficient
ω	angular frequency (rad/s)

CHAPTER I

INTRODUCTION

Annular seals are used in turbomachinery to reduce excessive leakage of the working fluid from high pressure side to the low pressure side. The schematic in Figure 1.1 shows a typical seal application. The working fluid is forced to leak from a high pressure region to the low pressure region through the stator-rotor interface and the function of a seal is to reduce this leakage. Even though, their main purpose is to inhibit leakage, the main interest in seals from a rotordynamic point of view arise from the fact that the fluid forces in a seal can have a strong influence on the dynamic characteristics of the turbomachine, directly affecting the performance of the machine. Depending on a number of parameters that go into the design of a seal, these fluid forces may act to stabilize the rotor system, or worse, work to destabilize the system.

Typical annular seal profiles are shown in Figure 1.2. Seals are classified based on the shape of the clearance profile. A seal with a constant clearance is a straight seal and that with a linearly varying profile is a tapered seal. A tapered seal may be either a convergent seal or a divergent seal depending on its slope relative to the direction of flow as shown in Figure 1.2.

1.1 Literature Survey

Extensive work has been done in the past two decades to understand the dynamic behavior of seals. Nguyen (1988), provides a complete overview of the work done by various researchers in this area in the past twenty years. Starting with Black's (1969) analysis of high-pressure seals, followed by Allaire's (1976) eccentric seal analysis and

Journal model is *Transactions of ASME Journal of Tribology*.

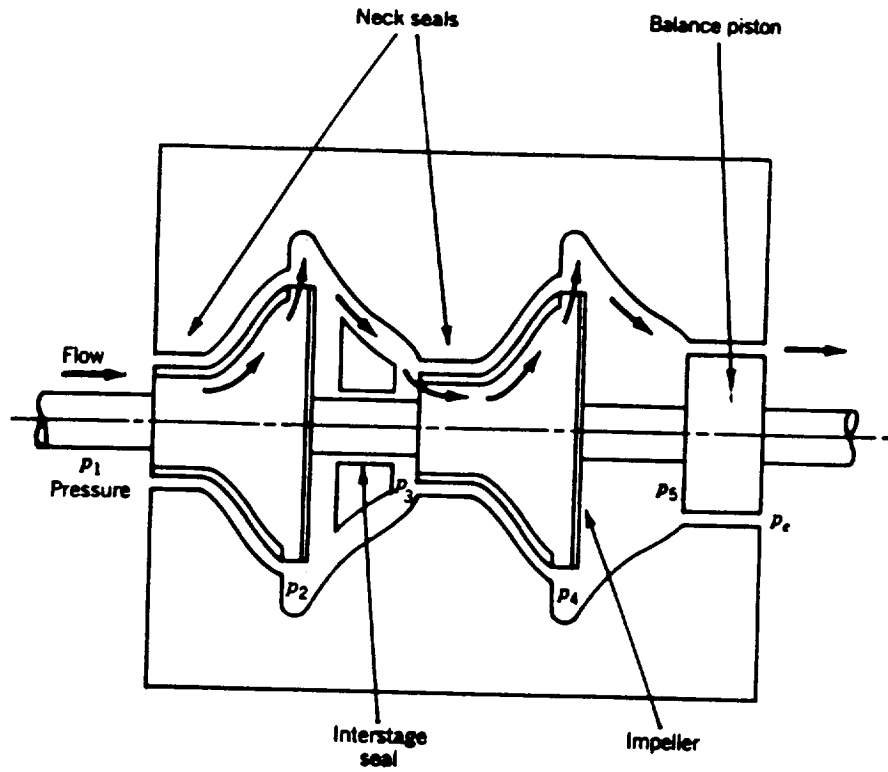


Figure 1.1 A Pump Annular Seal (Vance, 1991)

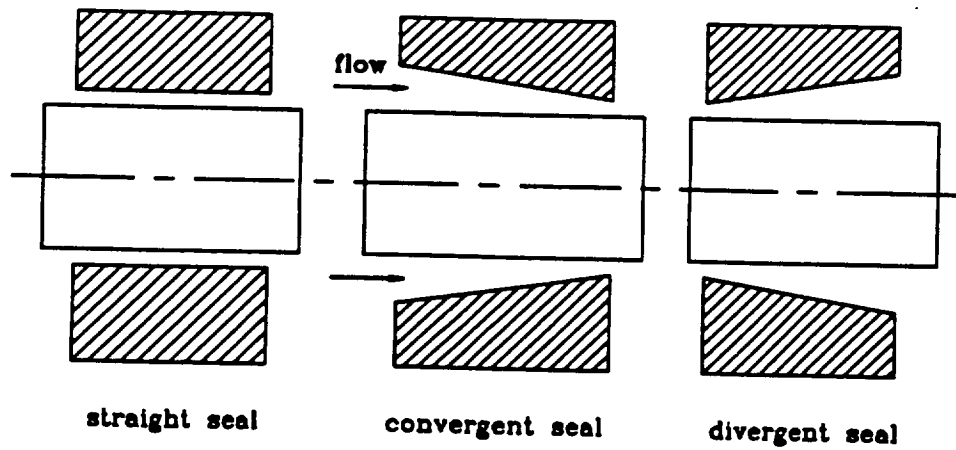


Figure 1.2 Typical Seal Profiles

Childs' (1985) Hirs' bulk flow analysis for tapered seals, there has been a steady improvement in the modeling of annular seals and the agreement of their predicted behavior with experimental results.

Of the recent work, Simon and Frene (1989) and later San Andres (1991) extended seal analysis to include variable fluid properties for cryogenic applications. Nelson and Nguyen (1988a,1988b) are generally credited with developing the first finite length eccentric solution for annular seals. A numerical solution is developed in terms of functions of *Fast Fourier Transforms* (FFT) which are used to compute the circumferential gradients of primary variables. The analysis agreed well with the experimental data. A improved formulation of this method is the basis for the current work. Yang *et al.* (1992) developed an ~~approximate~~ thermohydrodynamic (THD) analysis for cryogenic seals. This analysis includes an approximate steady state solution for a centered seal. San Andres *et al* (1992) provided a full set of governing equations for THD analysis based on a turbulent bulk flow model along with a numerical solution based on a finite difference (FDM) formulation.

Typically, an interstage seal of the Space Shuttle Main Engine High Pressure Oxygen Turbopump (SSME-ATD-HPOTP) is designed either as a straight or a tapered (convergent) seal over its entire length as shown in Figure 1.2. Tests of these seals after a period of operation have revealed a considerable change in their clearance profile from their original design clearance profile. Some of these distortions are due to assembly and operating interferences (Scharrer and Nunez, 1989) and others are due to mechanical and thermal stresses acting on the housing (Scharrer and Nelson, 1990) as the machine reaches and operates about its full power level (FPL).

The effect of seal distortions on rotordynamic coefficients was first considered by Sharrer and Nunez (1989). They reported that a 2-D, axisymmetric, finite element

analysis which considered the internal pressure distribution, and the boundary conditions due to assembly and operating interferences produced a clearance profile which was wavy and different from the nominal design tapered profile.

This distorted seal profile in the axial direction was fitted with a clearance function in the form of a polynomial as,

$$h(z) = a_1 + a_2z + a_3z^2 + a_4z^3 + a_5z^4 \quad (1.1)$$

where the coefficients a_1, a_2, \dots etc., are coefficients chosen to fit the distorted axial profile.

They adapted the analysis of a plain seal to the case of a wavy profile seal. They reported a marked change in the computed rotordynamic coefficients due to a change in the seal profile. San Andres (1991) repeated the above study using a variable fluid properties model and reported similar results.

Scharrer and Nelson (1990) treated this distortion problem using a partially tapered seal model. Instead of treating the distortions as a polynomial function, they tried to correct the predicted distortions by machining out the undesirable distortions at the design stage itself. The model they used to accomplish this is a seal with a taper on part of length of the seal. Using this model, they conducted a parametric study of various performance characteristics as a function of taper length to total length ratio (T/L). Based on this study they recommended optimum ratio of T/L for best performance of these distorted seals from a rotordynamic point of view.

Iwatsubo and Yang (1987) considered the effects of elastic deformation of the shaft and the seal housing due to high pressure difference, typical of a high pressure annular seal, and obtained dynamic coefficients based on this model. They reported that the direct stiffness is significantly changed when the elastic deformation is included. Childs (1987) studied the effects of variable radii and arbitrary clearance

function on fluid forces developed in pump impeller shrouds.

All the work reported in the literature on distortions in seals is limited to distortion along the length of the seal. Detailed thermo-elastic studies based on a finite element model of the entire turbopump have revealed that seal distortion is not limited to axial direction and a considerable distortion occurs along the circumference also.

An example predicted seal profile of an interstage seal of SSME-ATD-HPOTP from a thermo-elastic finite element study of the entire pump is shown in Figure 1.3. In this figure, the seal is stretched out 360°, and Z is the longitudinal axis of the seal. The seal, initially designed as a convergent seal, is severely distorted both in the axial direction as well as in the circumferential direction.

1.2 Dynamic Analysis of an Annular Seal

The main objective of this work is to develop a dynamic analysis for liquid annular seals with arbitrary profile and analyze a general distorted interstage seal of the SSME-ATD-HPOTP. The essentials of dynamic analysis of an annular seal are explained below.

The main objective of dynamic analysis of an annular seal is to estimate the coefficients of the *linearized force-motion model* of a seal shown in Eq 1.2, for a *small* motion of the rotor. The model shown in Eq. 1.2 is for a two degree of freedom (2-DOF) vibration model. There are more complex models available that include additional degrees of freedom, but the 2-DOF model in Eq. 1.2 is the most widely used one in seal literature to correlate theoretical and experimental data.

$$-\begin{Bmatrix} \Delta F_x \\ \Delta F_y \end{Bmatrix} = \begin{bmatrix} K_{xx} & k_{xy} \\ -k_{yx} & K_{yy} \end{bmatrix} \begin{Bmatrix} \delta x \\ \delta y \end{Bmatrix} + \begin{bmatrix} C_{xx} & c_{xy} \\ -c_{yx} & C_{yy} \end{bmatrix} \begin{Bmatrix} \delta \dot{x} \\ \delta \dot{y} \end{Bmatrix}$$

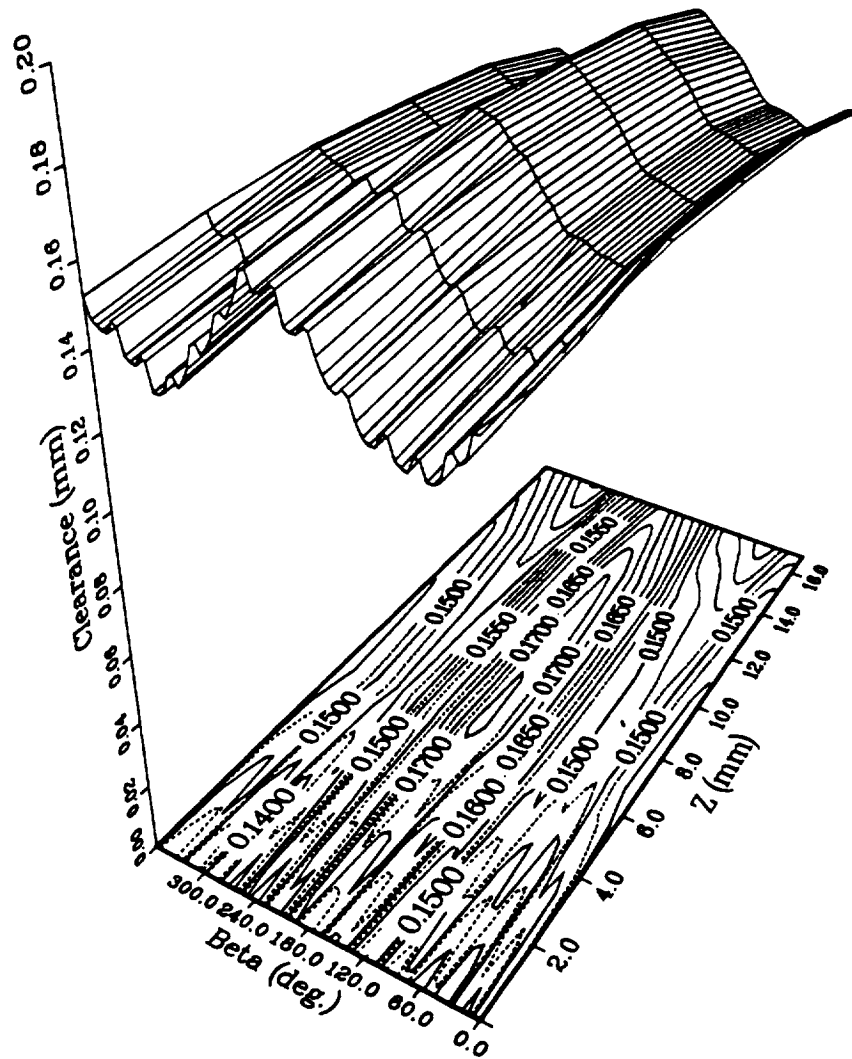


Figure 1.3 Predicted Clearance Profile for Seal, Unit 3-01

$$+ \begin{bmatrix} M_{xx} & m_{xy} \\ -m_{yx} & m_{yy} \end{bmatrix} \begin{Bmatrix} \delta \ddot{x} \\ \delta \ddot{y} \end{Bmatrix} \quad (1.2)$$

In this equation, $(\delta x, \delta y)$ are the displacements, $(\delta \dot{x}, \delta \dot{y})$ are the velocities and $(\delta \ddot{x}, \delta \ddot{y})$ are the accelerations in the X and Y directions respectively of the center of the rotor, relative to a static operating point (x, y) . The fluid force terms ΔF_x and ΔF_y are the incremental or perturbed fluid forces for a small motion of the rotor shaft about (x, y) . These force components, in general, vary as a function of rotor displacement, translational velocity and acceleration and are linear only for small orbital motion of the rotor.

In this model, K_{xx} , k_{xy} , k_{yx} , K_{yy} are the linearized stiffness coefficients, C_{xx} , c_{xy} , c_{yx} , C_{yy} are the linearized damping coefficients and M_{xx} , m_{xy} , m_{yx} and M_{yy} are the linearized added mass or inertia coefficients at the static operating point or eccentricity (x, y) .

In the linearized model, the terms $[K_{xx}\delta x]$ and $[K_{yy}\delta y]$ account for the incremental fluid reaction forces of the seal due to a small displacement of the rotor $(\delta x, \delta y)$. The term $[k_{xy}\delta y]$ is the cross coupled force in the X direction due to a displacement δy in the Y direction. Similarly, $[k_{yx}\delta x]$ is the cross coupled force in the Y direction due to a displacement δx in the X direction. These cross coupled forces arise out of circumferential velocity and are a source of instability in rotor systems. The terms $[C_{xx}\delta \dot{x}]$ and $[C_{yy}\delta \dot{y}]$ represent the incremental damping forces due to a small velocity change $(\delta \dot{x}, \delta \dot{y})$. Damping forces tend to have the opposite effect to that of cross coupled forces and their net effect is to add to the stability of the system. The terms $[M_{xx}\delta \ddot{x}]$ and $[M_{yy}\delta \ddot{y}]$ are the incremental fluid inertia forces due to a small change in acceleration $(\delta \ddot{x}, \delta \ddot{y})$. For a concentric seal, $K_{xx} = K_{yy}$, $k_{xy} = k_{yx}$ etc., reducing the number of coefficients from twelve to six. Typically, for an annular seal, the

important coefficients are direct stiffness, cross coupled stiffness, direct damping and direct mass. The contributions of other terms are negligible in most cases compared to these terms.

These coefficients are estimated by fitting the perturbed fluid forces ΔF_x and ΔF_y due to a small perturbed motion about a steady state position (x, y) to the linearized model in Eq. 1.2. These twelve coefficients together provide a dynamic model of the seal for a small motion of the rotor and this model may be used to predict the fluid forces acting on the rotor in vibration-response models and rotor stability analysis.

1.3 Current Work

The dynamic analysis developed in this work is based on a method originally proposed by Nelson and Nguyen (1988a, 1988b). They are credited (Childs, 1993) with developing the first finite length eccentric solution for annular seals. The original analysis showed good agreement with experimental results.

The original method proposed a method in which the governing nonlinear PDEs modeling the turbulent bulk flow in an annular seal are reduced to a set of ordinary differential equations by using an approximation scheme for computing the circumferential gradients of the primary variables. With this assumption, the order of the problem is reduced by one, i.e., from a 2-D to a 1-D problem and essentially the problem is reduced to solving a set of ordinary differential equations for which theory is well developed. This reduction in computational complexity by an order of magnitude is the main advantage of this method compared to a 2-D finite difference method (FDM) or finite element method (FEM) formulation of the same problem.

In the current work, the zeroth order and first order solutions of this original

analysis are improved to make the overall solution more accurate and computationally more efficient and eliminate some of the reported problems with the original method.

The original method used an innovative approximation scheme based on *Fast Fourier Transforms* (FFT) to compute the circumferential gradients of the zeroth order variables of the eccentric solution. The number of trigonometric functions included in the approximation is equal to the number of circumferential grid points. It has been reported (San Andres, 1991) that this method requires a considerable number of trigonometric functions for accurate solution at high eccentricities. Nguyen (1988) also reported problems with convergence at higher eccentricities in some cases, possibly due to the truncation error introduced by including only a finite number of functions. In addition, another disadvantage with trigonometric functions used in the original method is the very CPU intensive nature of their computation.

A simpler scheme based on cubic splines is found to be computationally more efficient since it does away with trigonometric functions and it also does not require as many circumferential grid points as the original method for a given accuracy tolerance. The increase in accuracy with cubic spline based approximation scheme also reflects in better convergence properties at higher eccentricities compared to the original method. This fact is verified by the successful analysis of cases with the new approach where the original method had failed.

This first order solution of the original analysis is modified by including a more exact solution that takes into account the variation of perturbed variables along the circumference. This improved analysis show better agreement with experimental results than earlier analysis, particularly at higher eccentricities. The new analysis developed treats these variables as general continuous functions and a completely new set of equations for dynamic analysis are derived based on this more general model. The original method was developed for Moody's friction model. In the current

work, a unified solution procedure that is valid for both Moody's and Hirs' models is developed.

Nguyen (1988) developed the original method for liquid seals with constant properties and gas seals. Since the main interest of the current work is analysis of liquid seals for cryogenic turbopumps, the improved method will be extended to include variable fluid properties and thermal effects.

Dynamic analysis based on the above improved method is developed for three different models.

1. Constant fluid properties.
2. Variable fluid properties
3. Thermal effects (energy equation) with variable fluid properties.

Arbitrarily varying seal profiles in both axial and circumferential directions are considered. The arbitrary seal profile may be either due to distortion as discussed earlier, or by design itself to enhance some optimum performance characteristics of the seal. An example case of an arbitrary profile, an elliptical seal with varying degrees of axial curvature, is analyzed in detail. An example film thickness analysis for this elliptical seal is presented.

A case study based on predicted clearances (6 axial planes, 68 clearances/plane) of an interstage seal of the SSME-ATD-HPOTP is presented. This predicted profile is obtained from a thermo-elastic finite element model of the entire turbopump. The results of distorted seal analysis are compared with those of a similar seal with average inlet and exit clearances.

Typically, seal coefficients are computed in a minimum film thickness coordinate system as a function of eccentricity ratio and then transformed into the user

defined coordinate system for actual application. Such a procedure is not valid for an arbitrary profile seal with a non-uniform cross section. This important feature of directional dependence of dynamic coefficients for arbitrary profile seals is illustrated with reference to an elliptical seal. A method for computing these coefficients directly in the rotor coordinate system is presented. Dynamic coefficients based on external specified load are introduced for seals for the first time to analyze seals that support a pre-load.

A number of cases from literature, both experimental and theoretical, are studied with reference to the analysis developed. In particular, results of current work are compared with the theoretical work of the following: Nelson and Nguyen (1988a,1988b), Childs and Kim (1985), Childs and Lindsey (1993), Sharrer and Nelson (1990), Scharer and Nunez (1989), and San Andres (1991,1992). In addition, theoretical predictions from current work are compared with a number of experimental results.

The other objective of this work is to study the effect of large rotor displacements of SSME-ATD-HPOTP on the dynamics of an annular seal and the resulting transient motion. Currently, the *linear model* of the annular seal employed at NASA Marshall Space Flight Center (MSFC) to estimate the seal forces during a transient motion of the turbopump rotor uses a set of 6 dynamic coefficients computed at zero ($\epsilon = 0$) eccentricity. This model, while valid for a *small* motion of the rotor about the centered position, may not be accurate for large off-center operation of the seal. One of the objectives of this study is to identify the magnitude of these deviations and establish limits of effectiveness of using such a model. This task is accomplished by solving the *bulk flow model* seal governing equations directly for transient seal forces for any given type of motion, including motion with large eccentricities.

This approach of solving governing equations directly for transient seal forces while being the most accurate, may not be practical for routine rotordynamic sim-

ulations. In fact, this is the primary reason for developing and studying approximate linear models and their widespread use in vibration-response and rotordynamic simulation studies. As an alternative, an innovative method is developed to model non-linearities in an annular seal based on dynamic coefficients computed at various static eccentricities in the seal clearance. This method, thoroughly tested for various types of transient motion, provides an accurate and computationally efficient means to model the effects of eccentric seal operation on the dynamics of the rotor system. The results from this new method compare well with bulk flow model results.

Typically, the dynamic coefficients are computed from the first order solution which is directly dependent on the zeroth order solution. Even though the zeroth order equations and associated boundary conditions are essentially the same for different analyses based on bulk flow model, for example Childs (1985), Nelson and Nguyen (1988a,b), San Andres (1991), and current analysis, there appears to be variations in how zeroth order and first order equations are formulated and solved. In the published literature on seals, it is assumed that the dynamic coefficients extracted from the first order solution automatically approximates accurately the dynamic behavior of the original governing equations for a small motion of the rotor. Two possible sources that may be cited for a discrepancy between these two approaches are, a) inaccurate formulation of the problem, b) error in implementation. In the present work, based on the transient analysis developed with original governing equations (no first order solution involved), an equivalence will be established, for the first time for seals, between the linearized coefficients based seal forces i.e., computing seal forces using coefficients in the linearized force-motion model of Eq. 1.2 versus the same forces as predicted by the original governing equations. If such an equivalence can be established, it proves that the dynamic coefficients being extracted from the dynamic analysis are indeed the correct coefficients which in turn validate the zeroth

and first order solutions. In other words, it is a check case for the entire analysis.

1.4 Original Contributions

The original contributions of the current research are summarized below.

1. Develop a dynamic analysis for arbitrary profile liquid annular seals based on an approach first proposed by Nelson and Nguyen (1988a, 1988b). The following modifications are incorporated into this analysis.
 - (a) Improved zeroth order solution.
 - (b) Improved first order solution.
2. Dynamic analysis for eccentric seals is developed for three different models based on the above method.
 - (a) Constant fluid properties.
 - (b) Variable fluid properties.
 - (c) Thermal effects (energy equation) with variable fluid properties (concentric case).
3. A unified solution procedure is presented for the following two friction models.
 - (a) Moody's Model
 - (b) Hirs' Model
4. Dynamic coefficients for seals based on external load specification.
5. Application of the new method to study the static and dynamic characteristics of an arbitrary profile seal, e.g., an elliptical seal with a varying axial curvature.

6. Study of directional dependence of dynamic coefficients for arbitrary profile seals.
7. Dynamic analysis of a general distorted interstage seal of SSME-ATD-HPOTP turbopump.
8. Transient analysis with an annular seal for large eccentric motion of the rotor.
 - (a) Transient analysis with bulk flow governing equations.
 - (b) Comparison of bulk flow model simulations with linear model (dynamic coefficients computed at concentric position) results.
 - (c) Study of equivalence between rotordynamic coefficients based transient motion and the same motion as predicted by the original governing equations.
 - (d) A new method to model non-linearities in an annular seal for transient analysis.
 - (e) Thorough testing of the new method for various types of transient motion and comparison with bulk flow model.

CHAPTER II

CONSTANT PROPERTIES MODEL

2.1 Bulk Flow Governing Equations

The bulk flow governing equations of turbulent fluid flow in an annular seal have been derived using several approaches. The following analysis is based on the work of Nelson (1984).

The primary variables of the bulk flow are the axial velocity $u(z, q)$, circumferential velocity $v(z, q)$ and pressure $p(z, q)$. The variation of these primary variables across the thin film is neglected. The axial and circumferential coordinates are z and q respectively. The radius of the rotor is R and the rotor angular velocity is ω rad/s.

The differential fluid volumes used to derive the bulk flow governing equations are shown in Figures 2.1–2.2. Mass conservation of fluid in the differential volume of Figure 2.1 yields,

$$\rho(v + \frac{\partial v}{\partial q} dq)(h + \frac{\partial h}{\partial q} dq)dz - \rho h v dz + \rho(u + \frac{\partial u}{\partial z} dz)(h + \frac{\partial h}{\partial z} dz)dq - \rho u h dq + \rho \frac{\partial h}{\partial t} dz dq = 0 \quad (2.1)$$

or,

$$u \frac{\partial h}{\partial z} + h \frac{\partial u}{\partial z} + v \frac{\partial h}{\partial q} + h \frac{\partial v}{\partial q} + \frac{\partial h}{\partial t} = 0 \quad (2.2)$$

Conservation of momentum in the axial direction for the fluid in the differential volume of Figure 2.2 may be expressed as,

$$(\rho h dz dq) \frac{Du}{Dt} = (-\tau_{sz} - \tau_{rz}) dz dq + p h dq - (p + \frac{\partial p}{\partial z} dz)(h + \frac{\partial h}{\partial z} dz) dq + p \frac{\partial h}{\partial z} dz dq \quad (2.3)$$

where The terms τ_{rz}, τ_{sz} are rotor and stator surface shear stresses in the axial direction. $\frac{Du}{Dt}$ is the total or material derivative of the axial velocity u and is defined

as,

$$\frac{Du}{Dt} = \left(\frac{\partial u}{\partial t} + u \frac{\partial u}{\partial z} + v \frac{\partial u}{\partial q} \right) \quad (2.4)$$

Simplifying the above expression yields,

$$-\frac{\partial p}{\partial z} = \rho \left(\frac{\partial u}{\partial t} + u \frac{\partial u}{\partial z} + v \frac{\partial u}{\partial q} \right) + \frac{1}{h} (\tau_{sz} + \tau_{rz}) \quad (2.5)$$

Similarly, conservation of momentum in the circumferential direction is expressed as,

$$(\rho h dz dq) \frac{Dv}{Dt} = (-\tau_{sq} - \tau_{rq}) dz dq + (p + \frac{\partial p}{\partial q} dq) (h + \frac{\partial h}{\partial q} dq) dz - p h dz \quad (2.6)$$

where τ_{rq}, τ_{sq} are the rotor and stator surface shear stresses and $\frac{Dv}{Dt}$ is the total derivative of circumferential velocity v defined as,

$$\frac{Dv}{Dt} = \left(\frac{\partial v}{\partial t} + u \frac{\partial v}{\partial z} + v \frac{\partial v}{\partial q} \right) \quad (2.7)$$

or,

$$-\frac{\partial p}{\partial q} = \rho \left(\frac{\partial v}{\partial t} + u \frac{\partial v}{\partial z} + v \frac{\partial v}{\partial q} \right) + \frac{1}{h} (\tau_{sq} + \tau_{rq}) \quad (2.8)$$

The shear stresses at the wall based on Moody friction factor are given by,

$$-(\tau_{sq} + \tau_{rq}) = \rho f_s \frac{v}{2} \sqrt{u^2 + v^2} + \rho f_r \frac{(v - w)}{2} \sqrt{u^2 + (v - w)^2} \quad (2.9)$$

$$-(\tau_{sz} + \tau_{rz}) = \rho f_s \frac{u}{2} \sqrt{u^2 + v^2} + \rho f_r \frac{u}{2} \sqrt{u^2 + (v - w)^2} \quad (2.10)$$

where,

- ρ density of fluid
- ω rotor rpm in rad/s
- w ωR , rotor surface velocity
- f_s stator friction factor
- f_r rotor friction factor

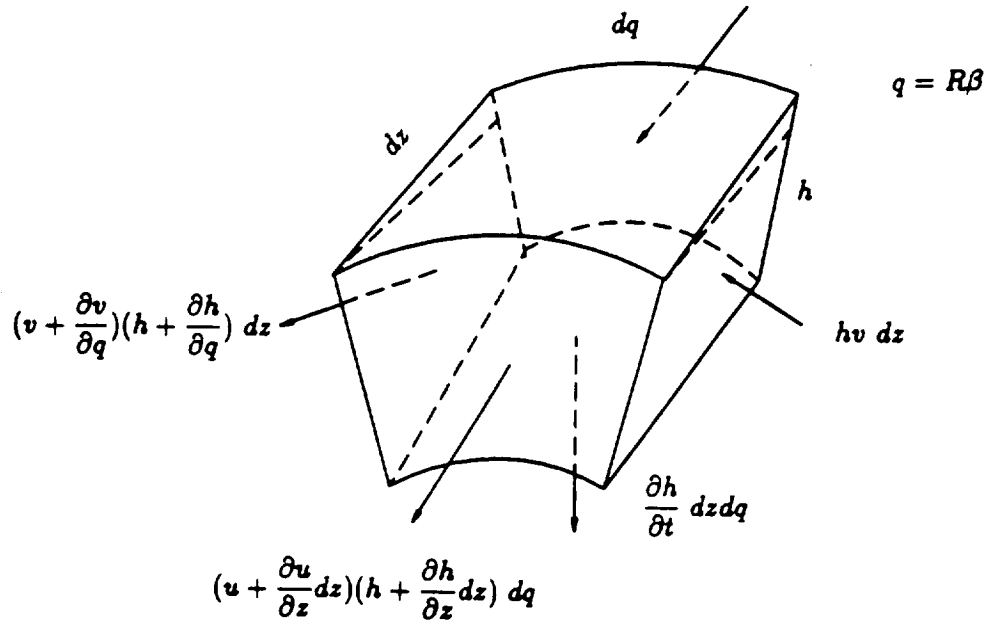


Figure 2.1 Differential Volume for Deriving the Continuity Equation

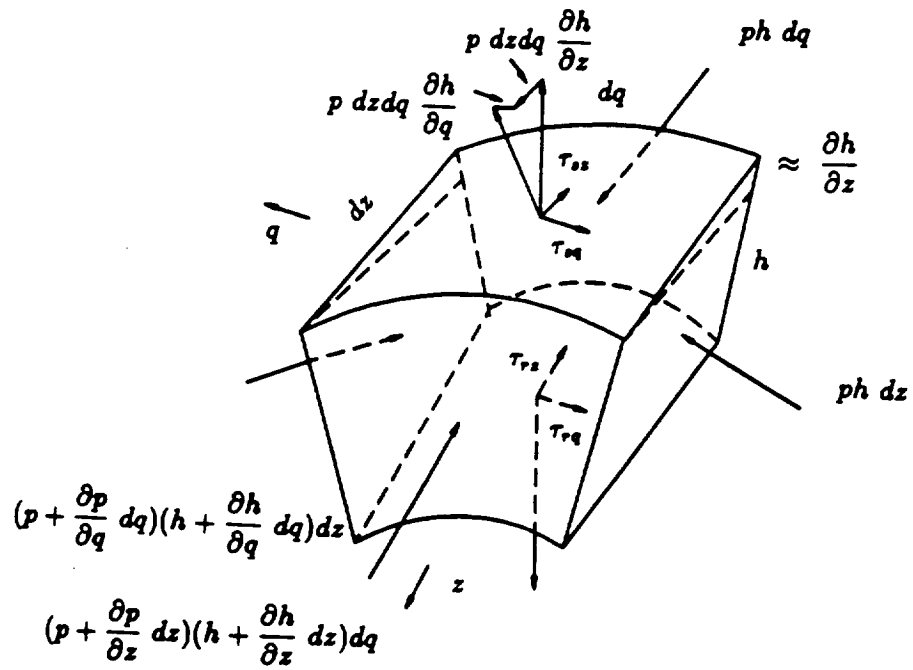


Figure 2.2 Differential Volume for Deriving the Momentum Equations

Using the transformation for the circumferential coordinate $q = R\beta$, in the Eqs. (2.2,2.5,2.8) yield the following bulk flow continuity, axial momentum and circumferential momentum equations for an incompressible fluid.

Continuity:

$$\frac{\partial(hu)}{\partial z} + \frac{1}{R} \frac{\partial(hv)}{\partial \beta} + \frac{\partial h}{\partial t} = 0 \quad (2.11)$$

Axial Momentum:

$$\begin{aligned} -\frac{h}{\rho} \frac{\partial p}{\partial z} = & h \left\{ \frac{\partial u}{\partial t} + \frac{v}{R} \frac{\partial u}{\partial \beta} + u \frac{\partial u}{\partial z} \right\} \\ & + f_s \frac{u}{2} \sqrt{u^2 + v^2} + f_r \frac{u}{2} \sqrt{u^2 + (v - w)^2} \end{aligned} \quad (2.12)$$

Circumferential Momentum:

$$\begin{aligned} -\frac{h}{\rho R} \frac{\partial p}{\partial \beta} = & h \left\{ \frac{\partial v}{\partial t} + \frac{v}{R} \frac{\partial v}{\partial \beta} + u \frac{\partial v}{\partial z} \right\} \\ & + f_s \frac{v}{2} \sqrt{u^2 + v^2} + f_r \frac{(v - w)}{2} \sqrt{u^2 + (v - w)^2} \end{aligned} \quad (2.13)$$

2.2 Friction Factors

Two friction models extensively used in seal analysis are the Moody's model and the Hirs' model. These two models differ in the way the roughness of the surface, both stator and rotor, are modeled. Of these two models, use of Moody's model is more prevalent because of a more realistic friction factor which is dependent on local Reynolds number, film thickness and surface roughness compared to the Hirs' model where the coefficients are for a fixed clearance and an average Reynolds number. However, considerable experimental and theoretical data exists for Hirs' model based analysis, for example Childs (1985), Sharrer and Nelson (1990) etc., making it attractive for comparative studies for any new analysis such as the current work.

Moody's Model:

$$f_s = \frac{0.0055}{4} \left\{ 1.0 + \left(10^4 \frac{e_s}{h} + 10^6 \frac{1}{R_s} \right)^{1/3} \right\} \quad (2.14)$$

$$f_r = \frac{0.0055}{4} \left\{ 1.0 + \left(10^4 \frac{e_r}{h} + 10^6 \frac{1}{R_r} \right)^{1/3} \right\} \quad (2.15)$$

$$R_s = \frac{2\rho h}{\mu} \sqrt{u^2 + v^2} \quad (2.16)$$

$$R_r = \frac{2\rho h}{\mu} \sqrt{u^2 + (v - w)^2} \quad (2.17)$$

where,

e_s stator pocket

e_r rotor pocket

h film thickness

c_s nominal radial clearance

R_s stator Reynold's number

R_r rotor Reynold's number

$\frac{e_s}{2c_s}$ stator relative roughness

$\frac{e_r}{2c_s}$ rotor relative roughness

Hirs' Model:

$$f_s = n_s R_s^{m_s} \quad (2.18)$$

$$f_r = n_r R_r^{m_r} \quad (2.19)$$

where n_s , m_s , n_r and m_r are Hirs' constants for stator and rotor respectively.

2.3 Film Thickness

The expression for film thickness $h(z, \beta)$ as a function of eccentricity is derived in the rotor (fixed) coordinate system, instead of a *minimum film thickness* coordinate system normally used in straight or tapered seal analysis. In a typical analysis with these seals, the minimum film thickness coordinate system is usually aligned with the X-axis of the rotor coordinate system and for eccentric operation, the dynamic coefficients are computed as a function of eccentricity along this axis. Although the dynamic coefficients can be rotationally transformed once they are evaluated at a given equilibrium position, the minimum film thickness system cannot be used with a seal that has a circumferentially varying clearance (which destroys axisymmetry). This same restriction applies to, for instance, modeling pressure dam bearings versus plain journal bearings. As a result of this asymmetry, the dynamic coefficients have to be computed directly in the rotor coordinate system for non-uniform profiles or if a minimum film thickness system is used, the orientation needs to be specified. This important feature of the directional dependence of dynamic coefficients for arbitrary profile seals will be further discussed with reference to an elliptical seal in Chapter V.

The seal geometry is, in general, defined by its clearance function $c(z, \beta)$. The clearance function of a seal defines the fluid film thickness when the rotor is at the centered or concentric position with respect to the seal. A constant c specifies a straight seal, a linear function in z defines a tapered seal and so on. For the purpose of this study, any profile other than a straight or a tapered profile is considered as an arbitrary profile. The film thickness, which varies with eccentricity, is derived as a function of $c(z, \beta)$ and the eccentricity vector (e, ϕ) . The angle ϕ , defined as the eccentricity angle, is the angle made by the eccentricity vector with respect to the fixed X-axis. The magnitude of the eccentricity vector is given by the eccentricity,

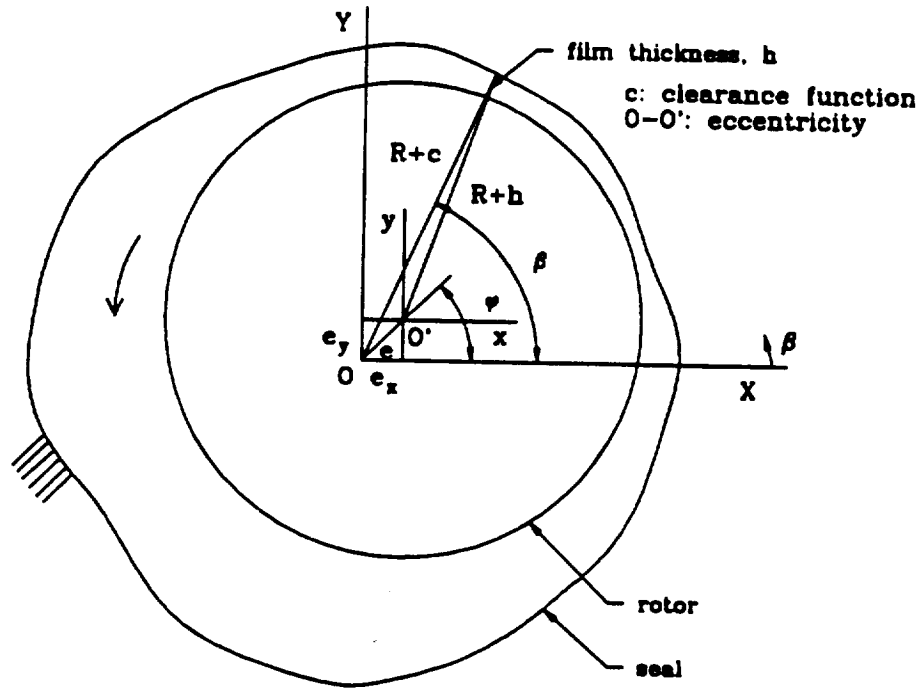


Figure 2.3 Diagram for Deriving General Seal Clearance Expression

e. The expression for the film thickness is given below with reference to Figure 2.3. In this figure, e_x , e_y are the offsets of the center of the rotor O' with respect to the center of the seal denoted by O . In this figure, ϕ is the eccentricity angle and β is the angular coordinate.

By the law of cosines,

$$(R + h)^2 = e^2 + (R + c)^2 - 2e(R + c)\cos(\beta - \phi) \quad (2.20)$$

or,

$$h(z, \beta) = \sqrt{e^2 + (R + c)^2 - 2e(R + c)\cos(\beta - \phi)} - R \quad (2.21)$$

substituting,

$$e\cos(\beta - \phi) = e_x\cos\beta + e_y\sin\beta \quad (2.22)$$

$$e_x = e\cos\phi \quad (2.23)$$

$$e_y = e \sin \phi \quad (2.24)$$

Eq. (2.21) may be rewritten as,

$$h(z, \beta) = \sqrt{(R+c)^2 - (e_x \sin \beta - e_y \cos \beta)^2} - (e_x \cos \beta + e_y \sin \beta) - R \quad (2.25)$$

and its gradients in β and z directions are,

$$\frac{\partial h}{\partial \beta} = \frac{(R+c) \frac{\partial c}{\partial \beta} - (e_x \sin \beta - e_y \cos \beta)(e_x \cos \beta + e_y \sin \beta)}{\sqrt{(R+c)^2 - (e_x \sin \beta - e_y \cos \beta)^2}} + (e_x \sin \beta - e_y \cos \beta) \quad (2.26)$$

$$\frac{\partial h}{\partial z} = \frac{(R+c) \frac{\partial c}{\partial z}}{\sqrt{(R+c)^2 - (e_x \sin \beta - e_y \cos \beta)^2}} \quad (2.27)$$

Besides specifying the film thickness in a fixed coordinate system, the above expression for film thickness has the following advantages over the more commonly used approximate form,

$$h(z, \beta) = c(z) - e_x \cos \beta - e_y \sin \beta \quad (2.28)$$

1. It models the curvature of the film thickness accurately. This is important, particularly, when analyzing a severely distorted seal or an arbitrary profile seal with a clearance function varying in the circumferential direction, such as an elliptical seal.
2. It specifies the film thickness in a fixed coordinate system which is essential for analyzing non-uniform profile seals as explained earlier. (examples to be discussed later).
3. The general expression in Eq. (2.25) is more accurate, mathematically, particularly at higher eccentricities than the approximate form in Eq. (2.28).

2.4 Solution Procedure

The general steps involved in the solution procedure are outlined in the flow chart (Nguyen, 1988) shown in Figure 2.4. These various steps are summarized below.

1. Derive the bulk flow governing equations.
2. Perform perturbations on the original governing equations to yield zeroth order and first order governing equations.
3. Form the appropriate boundary conditions at the inlet and the exit.
4. Solve the set of zeroth order equations subject to the boundary conditions at inlet and exit to obtain the zeroth order (steady state) solution of the primary variables, u_0 , v_0 , p_0 .
 - (a) Compute leakage.
 - (b) Compute steady state reactive seal forces.
 - (c) Compute frictional torque.
5. Perturb the zeroth order boundary conditions to obtain the first order boundary conditions.
6. Assume a harmonic solution form and use a *separation of variables* procedure to reduce the first order equations to a set of ordinary differential equations.
7. Solve for the first order variables, u_1 , v_1 , p_1 , subject to the first order boundary conditions.
8. Extract dynamic coefficients from the first order pressure field.

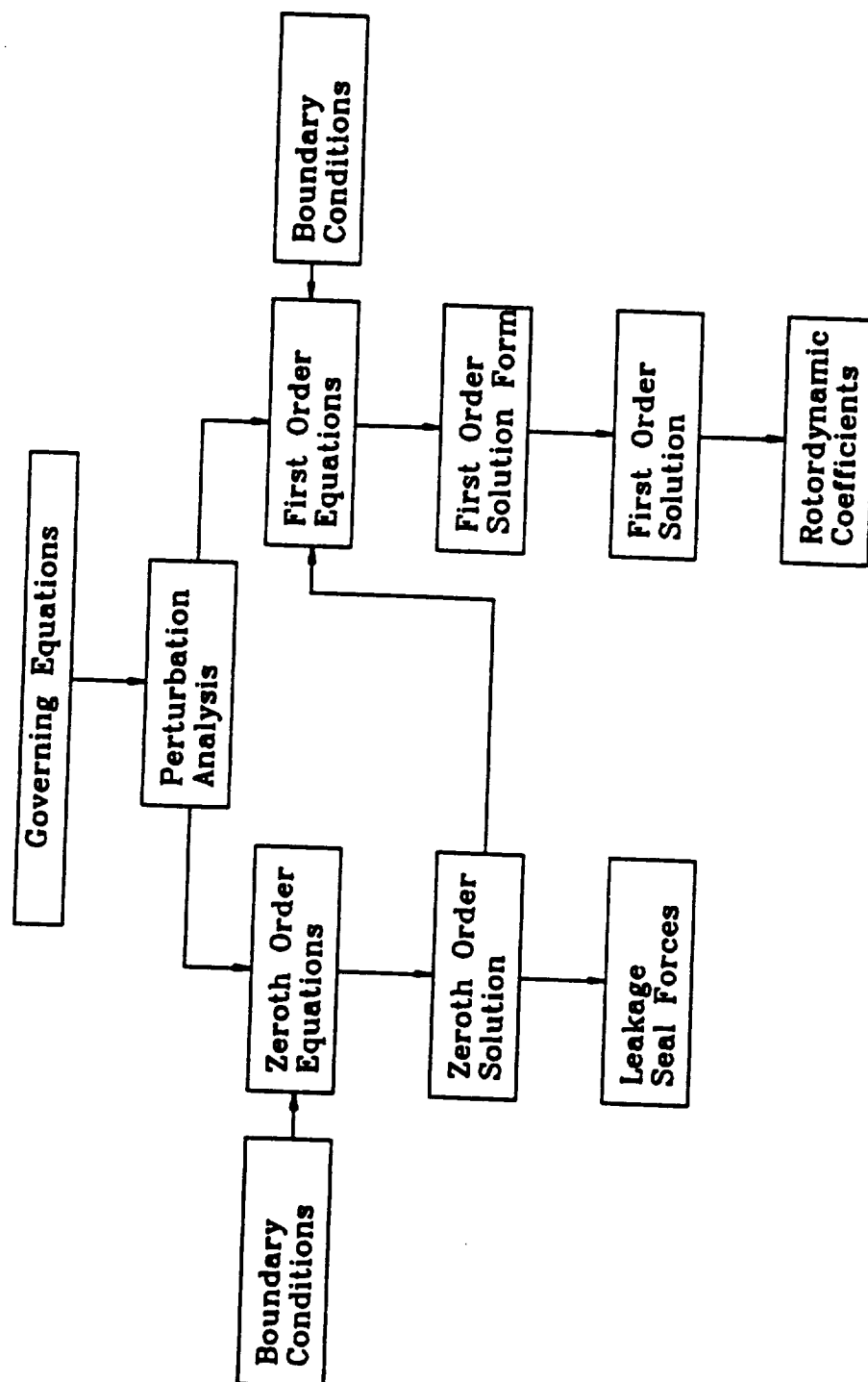


Figure 2.4 Flow Chart of Solution Procedure, Nguyen (1988)

2.5 Perturbation Analysis

In this section, the zeroth order and first order equations are derived using a perturbation analysis. The original bulk flow governing equations are perturbed about their steady state values to yield the zeroth order and first order governing equations. The zeroth order equations are also known as the steady state equations and they may also be obtained from the original governing equations by dropping the time dependent terms. The perturbed or first order equations of the governing equations Eqs. (2.11-2.13) are derived for a small motion of the rotor about a steady state eccentric position.

The assumed form for the dependent variables and film thickness for perturbation analysis are given as,

$$u(z, \beta, t) = u_0(z, \beta) + \epsilon u_1(z, \beta, t) \quad (2.29)$$

$$v(z, \beta, t) = v_0(z, \beta) + \epsilon v_1(z, \beta, t) \quad (2.30)$$

$$p(z, \beta, t) = p_0(z, \beta) + \epsilon p_1(z, \beta, t) \quad (2.31)$$

$$h(z, \beta, t) = h_0(z, \beta) + \epsilon h_1(z, \beta, t) \quad (2.32)$$

where ϵ is a small perturbation and u_0, v_0, p_0, h_0 are the zeroth order variables and u_1, v_1, p_1, h_1 are the corresponding first order variables. Substitution of these expressions into Eqs.(2.11-2.13) and neglecting second and higher order terms yields sets of zeroth order and first order equations of the form,

$$(\text{zeroth order equations}) + \epsilon(\text{first order equations}) = 0$$

2.5.1 Zeroth Order Equations

The zeroth order equations are essentially steady state equations and they may also be obtained by canceling out the time dependent terms in the original governing equations. The subscript 0 in the following zeroth order equations refer to zeroth order variables.

$$\frac{\partial(h_0 u_0)}{\partial z} + \frac{1}{R} \frac{\partial(h_0 v_0)}{\partial \beta} = 0 \quad (2.33)$$

$$\begin{aligned} -\frac{h_0}{\rho_0} \frac{\partial p_0}{\partial z} = & h_0 \left\{ \frac{v_0}{R} \frac{\partial u_0}{\partial \beta} + u_0 \frac{\partial u_0}{\partial z} \right\} \\ & + f_{s0} \frac{u_0}{2} \sqrt{u_0^2 + v_0^2} + f_{r0} \frac{u_0}{2} \sqrt{u_0^2 + (v_0 - w)^2} \end{aligned} \quad (2.34)$$

$$\begin{aligned} -\frac{h_0}{\rho_0 R} \frac{\partial p_0}{\partial \beta} = & h_0 \left\{ \frac{v_0}{R} \frac{\partial v_0}{\partial \beta} + u_0 \frac{\partial v_0}{\partial z} \right\} \\ & + f_{s0} \frac{v_0}{2} \sqrt{u_0^2 + v_0^2} + f_{r0} \frac{(v_0 - w)}{2} \sqrt{u_0^2 + (v_0 - w)^2} \end{aligned} \quad (2.35)$$

where the friction factors f_{r0} and f_{s0} are the friction factors.

The set of equations in Eqs. (2.33–2.35) are the zeroth order equations for a constant fluid properties model or an incompressible fluid.

2.5.2 First Order Equations

The first order equations are given by,

Continuity:

$$\begin{aligned} h_0 \frac{\partial u_0}{\partial z} + \frac{h_0}{R} \frac{\partial v_0}{\partial \beta} + \frac{\partial h_0}{\partial z} u_1 + \frac{1}{R} \frac{\partial h_0}{\partial \beta} v_1 = & -\frac{\partial h_0}{\partial t} - u_0 \frac{\partial h_0}{\partial z} - \frac{v_0}{R} \frac{\partial h_0}{\partial \beta} \\ & - \left(\frac{\partial u}{\partial z} + \frac{1}{R} \frac{\partial v}{\partial \beta} \right) h_1 \end{aligned} \quad (2.36)$$

Axial Momentum:

$$h_0 u_0 \frac{\partial u_0}{\partial z} + \frac{h_0}{\rho_0} \frac{\partial p_0}{\partial z} + \frac{h_0 v_0}{R} \frac{\partial u_0}{\partial \beta} + h_0 \frac{\partial u_0}{\partial t} + A_u u_1 + A_v v_1 = A_h h_1 \quad (2.37)$$

Circumferential Momentum:

$$h_0 u_0 \frac{\partial v_0}{\partial z} + \frac{h_0 v_0}{R} \frac{\partial v_0}{\partial \beta} + \frac{h_0}{\rho_0 R} \frac{\partial p_0}{\partial \beta} + h_0 \frac{\partial v_0}{\partial t} + B_u u_1 + B_v v_1 = B_h h_1 \quad (2.38)$$

where the coefficients A_u , A_v , A_h , B_u , B_v and B_h are functions of steady state variables u_0 , v_0 , p_0 and their axial and circumferential gradients and friction factors and their derivative terms. These coefficients for constant properties model are given in Appendix A.

It can be seen that the first order continuity and momentum equations do not change between the Moody's and Hirs' friction models and the friction factor model only affects the definition of the coefficients A_u , A_v ... etc.. These coefficients are derived in such a form such that the solution procedure is valid for any general friction model. Specific analyses for two particular models, a) Moody's model b) Hirs' model are developed based on this general format.

2.5.3 Linearization of Friction Factors

The friction factors f_s and f_r , for constant fluid properties, are implicit functions of u , v and h . The perturbation in the friction factor is obtained by a linearization process using Taylor's series expansion about the operating point. The following example analysis illustrates the steps involved in the linearization of friction factor f_s . Using Taylor's series expansion of f_s about the steady state variables, u_0 , v_0 and p_0 ,

$$\begin{aligned} f_s(u, v, h) = & f_{s0}|_{(u_0, v_0, h_0)} + \frac{\partial f_s}{\partial u}|_{(v_0, p_0)}(u - u_0) \\ & + \frac{\partial f_s}{\partial v}|_{(u_0, p_0)}(v - v_0) + \frac{\partial f_s}{\partial h}|_{(u_0, v_0)}(h - h_0) \end{aligned} \quad (2.39)$$

or,

$$f_s = f_{s0} + \frac{\partial f_s}{\partial u} \epsilon u_1 + \frac{\partial f_s}{\partial v} \epsilon v_1 + \frac{\partial f_s}{\partial h} \epsilon h_1 \quad (2.40)$$

The expressions, $\frac{\partial f_s}{\partial u}$, $\frac{\partial f_s}{\partial v}$, $\frac{\partial f_s}{\partial h}$ are derived for both Moody and Hirs friction factor models and are given in the Appendix D.

$$\frac{\partial f_s}{\partial u} = -g_{s0} \frac{u_0}{u_0^2 + v_0^2} \quad (2.41)$$

$$\frac{\partial f_s}{\partial v} = -g_{s0} \frac{v_0}{u_0^2 + v_0^2} \quad (2.42)$$

$$\frac{\partial f_s}{\partial h} = -\frac{h_{s0}}{h_0} \quad (2.43)$$

where,

$$g_{s0} = \frac{0.0055 \times 10^6}{12 R_{s0}} \left(10^4 \frac{e_s}{h_0} + 10^6 \frac{1}{R_{s0}} \right)^{-2/3} \quad (2.44)$$

$$h_{s0} = \frac{0.0055}{12} \left(10^4 \frac{e_s}{h_0} + 10^6 \frac{1}{R_{s0}} \right)^{1/3} \quad (2.45)$$

$$R_{s0} = \frac{2\rho_0 h_0}{\mu_0} \sqrt{u_0^2 + v_0^2} \quad (2.46)$$

For the case of a fluid with variable properties, there will be two additional terms, $\frac{\partial f_s}{\partial \rho}$, $\frac{\partial f_s}{\partial \mu}$.

2.6 Zeroth Order Boundary Conditions

The boundary conditions for the zeroth order or steady state equations are illustrated in Figure 2.5–2.6.

The fluid flow in an annular seal occurs from the high pressure side (inlet) to the low pressure side (exit) as shown in Figure 2.5. Just prior to the inlet ($z = 0$), the fluid has zero axial velocity and the fluid pressure is given by the supply pressure or reservoir pressure p_i . At the entrance of the seal a swirl is induced in the fluid by the eye of the impeller creating the tangential velocity of the fluid as shown in Figure 2.4.

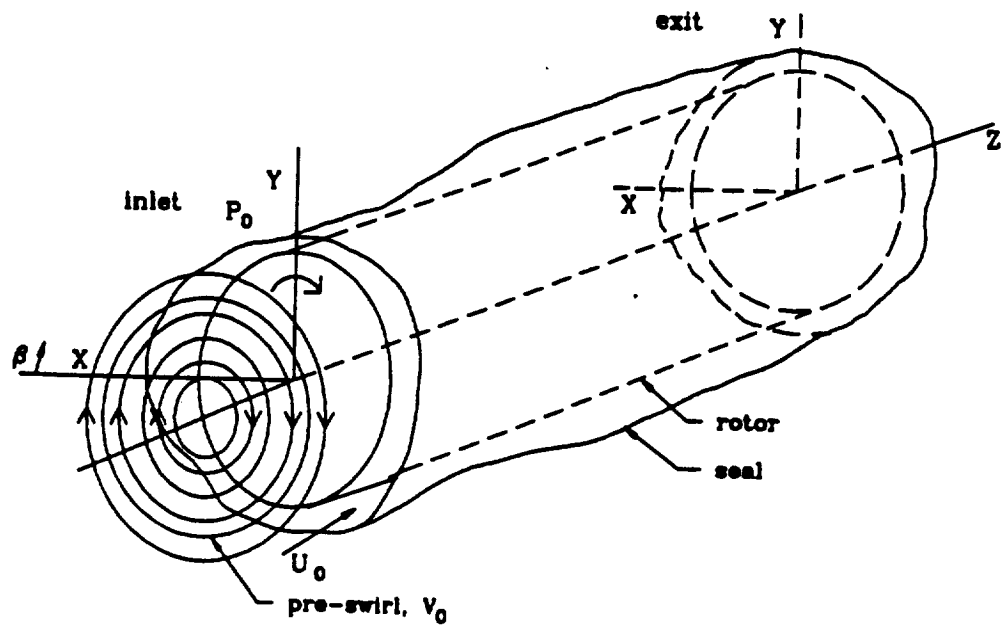


Figure 2.5 Boundary Conditions

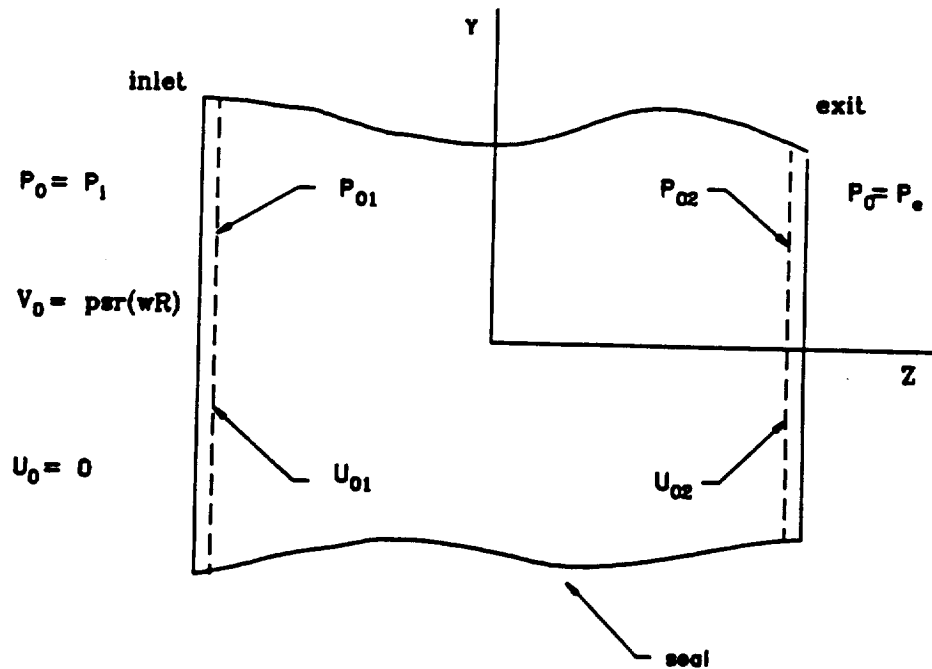


Figure 2.6 Zeroth Order Boundary Conditions

Generally, the magnitude of this tangential velocity is estimated as a percentage of the rotor surface speed and is specified by the *pre-swirl* ratio as, $v_0 = psr(\omega R)$, where R is the radius of the rotor, ω is the angular velocity in rad/s and psr is the pre-swirl ratio.

At the inlet, as the fluid enters the seal there is a loss in pressure with a corresponding increase in the acceleration of axial velocity, u . The relationship between these two variables is given by the Bernoulli's equation as,

$$p_i - p_{01}(0, \beta) = \frac{1}{2} \rho_0 u_{01}^2(0, \beta)(1 + \xi_i) \quad (2.47)$$

where, ξ_i is the inlet loss coefficient and p_{01} , u_{01} refer to the pressure and axial velocity right after inlet as shown in Figure 2.6.

The inlet or entrance loss factor, in general, is a function of geometry at the entrance as well as local Reynold's number (Nguyen, 1988). In the present work, as is the norm in seal literature, a constant value is assumed for this coefficient. In practice, one of the methods used to estimate the pre-swirl ratio and the inlet loss coefficient is by matching the theoretical flow rate with experimentally measured data. At present, there is no reliable way of predicting these two parameters and the empirical procedure used above typically gives rise to different sets of input data depending upon the seal analyst's objectives.

Right after the exit ($z = L$), the pressure is given by the low pressure, p_e . At the exit, a similar relation as given in Eq. (2.47) is used to relate the variables.

$$p_{02}(0, \beta) - p_e = \frac{1}{2} \rho_0 u_{02}^2(0, \beta)(1 - \xi_e) \quad (2.48)$$

where, ξ_e is the exit pressure recovery coefficient. Typical values for a worn and new seal are 0.7 and 0.85. In this analysis, the value of $\xi_e = 1.0$ is used, i.e, there is complete recovery of pressure.

The following is a summary of the boundary conditions for the zeroth order equations.

At the inlet:

axial velocity, u_0 :

prior to inlet:

$$u_0(0, \beta) = 0 \quad (2.49)$$

right after inlet:

$$u_0(0, \beta) = u_{01}(0, \beta) \quad (2.50)$$

circumferential velocity, v_0 :

$$v_0(0, \beta) = p s r \times \omega R \quad (2.51)$$

pressure, p_0 :

prior to inlet:

$$p_0(0, \beta) = p_i \quad (2.52)$$

right after inlet:

$$p_0(0, \beta) = p_{01}(0, \beta) \quad (2.53)$$

The pressures p_i , $p_{01}(0, \beta)$ and axial velocity $u_{01}(0, \beta)$ at the inlet are related by,

$$p_i - p_{01}(0, \beta) = \frac{1}{2} \rho_0 u_{01}^2(0, \beta) (1 + \xi_i) \quad (2.54)$$

At the exit, the exit pressure recovery coefficient is assumed to be 1, i.e.,

$$p_{02}(0, \beta) - p_e = \frac{\rho_0}{2} u_{02}^2(0, \beta) (1 - 1) \quad (2.55)$$

or,

$$p_{02}(0, \beta) = p_e \quad (2.56)$$

Let Δp be the total pressure drop across the seal.

$$\Delta p = p_i - p_e \quad (2.57)$$

Eq. (2.54) may be rewritten as,

$$p_{01}(0, \beta) = \Delta p + p_e - \frac{1}{2} \rho_0 u_{01}^2(0, \beta)(1 + \xi_i) \quad (2.58)$$

For the case of an incompressible fluid, the absolute pressure is not important and therefore the exit pressure may be set to zero, i.e.,

$$p_e = 0 \quad (2.59)$$

Eq. (2.58) may be rewritten as,

$$p_{01}(0, \beta) = \Delta p - \frac{1}{2} \rho_0 u_{01}^2(0, \beta)(1 + \xi_i) \quad (2.60)$$

or

$$u_{01}(0, \beta) = \sqrt{\frac{2}{\rho_0(1 + \xi_i)}(\Delta p - p_{01}(0, \beta))} \quad (2.61)$$

At the outset, $p_{01}(0, \beta)$ is unknown and must be solved iteratively by requiring that the pressure distribution at the seal exit satisfies the following condition.

$$p_{02} = 0 \quad (2.62)$$

subject to the constraints of Eqs. (2.51) and (2.54).

2.7 Solution Procedure for Zeroth Order Equations

The solution for zeroth order equations involves the direct integration of three coupled nonlinear partial differential equations subject to the boundary conditions given in the previous section. The current analysis uses a zeroth order solution procedure different

from the original method. The following is a brief comparison between Nelson and Nguyen's original approach and the one used in current work.

2.7.1 Comparison with Nelson and Nguyen Approach

The three steady state equations are arranged in the following fashion and integrated from inlet to the exit.

$$\begin{bmatrix} \frac{\partial u_0}{\partial z} \\ \frac{\partial v_0}{\partial z} \\ \frac{\partial p_0}{\partial z} \end{bmatrix} = \begin{bmatrix} F_u(u_0, v_0, p_0, \frac{\partial u_0}{\partial \beta}, \frac{\partial v_0}{\partial \beta}, \frac{\partial p_0}{\partial \beta}) \\ F_v(u_0, v_0, p_0, \frac{\partial u_0}{\partial \beta}, \frac{\partial v_0}{\partial \beta}, \frac{\partial p_0}{\partial \beta}) \\ F_p(u_0, v_0, p_0, \frac{\partial u_0}{\partial \beta}, \frac{\partial v_0}{\partial \beta}, \frac{\partial p_0}{\partial \beta}) \end{bmatrix} \quad (2.63)$$

The functions F_u , F_v , F_p , for a constant properties model, are given in *Appendix A*.

The original analysis of Nguyen (1988) proposed a method by which the coupled partial differential equations are reduced to coupled ordinary differential equations by approximating the circumferential gradients of the variables u_0 , v_0 and p_0 as shown in Eq. (2.63). At each axial step in the iterative procedure, the gradients with respect to β are computed based on the values of the variables at the previous step. An approximation scheme based on *Fast Fourier Transforms* (FFT) was used for this purpose. Assuming that velocity and pressure distributions are known at an axial step, the gradients of these variables, $\frac{\partial u_0}{\partial \beta}$, $\frac{\partial v_0}{\partial \beta}$, $\frac{\partial p_0}{\partial \beta}$, may be computed by specifying each of the known values as a finite-length complex Fourier series as given below.

$$u_0(z, \beta) = \text{Real}\{u_0 + 2 \int_{n=1}^{N-1} u_n(z) e^{in\beta}\} \quad (2.64)$$

$$v_0(z, \beta) = \text{Real}\{v_0 + 2 \int_{n=1}^{N-1} v_n(z) e^{in\beta}\} \quad (2.65)$$

$$p_0(z, \beta) = \text{Real}\{p_0 + 2 \int_{n=1}^{N-1} p_n(z) e^{in\beta}\} \quad (2.66)$$

where N is equal to one half the number of circumferential divisions. The above

expressions may then be used to compute the gradients as,

$$\frac{\partial u_0(z, \beta)}{\partial \beta} = \text{Real}\{2 \int_{n=1}^{N-1} i n u_n(z) e^{in\beta}\} \quad (2.67)$$

$$\frac{\partial v_0(z, \beta)}{\partial \beta} = \text{Real}\{2 \int_{n=1}^{N-1} i n v_n(z) e^{in\beta}\} \quad (2.68)$$

$$\frac{\partial p_0(z, \beta)}{\partial \beta} = \text{Real}\{2 \int_{n=1}^{N-1} i n p_n(z) e^{in\beta}\} \quad (2.69)$$

This methods suffers from the following drawbacks.

1. It requires too many functions for accurate solution at high eccentricities (San Andres, 1991).
2. Computation of trigonometric functions is a very CPU intensive procedure.
3. Convergence problems (Nguyen, 1988), possibly due to truncation error introduced by not including enough functions in the approximation scheme.
4. No reliable way to decide on the number of functions to be used.

In the present analysis, a simpler method based on cubic splines is implemented. This method is more accurate as no truncation error is involved as in the FFT method. Also, convergence at higher eccentricities is achieved with relatively fewer iterations than the FFT method. It is also computationally more efficient as it does not involve the computation of CPU intensive trigonometric functions. Also, the number of circumferential grid points may be varied, upto a limit, with out affecting the accuracy of the solution.

2.7.2 Iterative Solution for Zeroth Order Equations

Typically, an iterative procedure is used to solve for the pressure distribution. Figures 2.7–2.8 illustrate typical subdivisions in the axial and circumferential directions

for spline interpolation and numerical integration. The circumference is divided into segments of equal length both in the axial and the circumferential directions.

Let m be the number of axial grid points, while n is the number of circumferential grid points. Let the superscript j indicate a function evaluated at $\beta = \beta_j$. The coupled partial differential equations are reduced to a set of coupled ODE's, by moving all β -dependent terms to the right-hand side as shown in Eq. (2.63). At any given axial plane, cubic splines are used to fit $u_0^{(j)}$, $v_0^{(j)}$ and $p_0^{(j)}$ to compute the gradients $\frac{\partial u_0}{\partial \beta}^{(j)}$, $\frac{\partial v_0}{\partial \beta}^{(j)}$ and $\frac{\partial p_0}{\partial \beta}^{(j)}$ where $j = 1, 2, \dots, n$ the number of circumferential grid points. at that axial plane.

The set of differential equations in Eq. (2.63) are solved using *separation of variables* type assumption that at any *fixed* axial location, the gradients of the dependent variables u_0 , v_0 , p_0 are obtained by spline fitting these variables at that axial location as a function of the circumferential coordinate β .

Let Θ represent a cubic spline function operator which when applied to a set of function values yields a continuous piecewise cubic spline approximation in β of that function. In other words, given a set of grid values for $\beta = \beta_1, \beta_2, \dots, \beta_n$ at any axial location $z = z_k$,

$$u_0(z_k, \beta) = \Theta(\beta, u_0^{(j)}), \quad j = 1, 2, \dots, n \quad (2.70)$$

$$v_0(z_k, \beta) = \Theta(\beta, v_0^{(j)}), \quad j = 1, 2, \dots, n \quad (2.71)$$

$$p_0(z_k, \beta) = \Theta(\beta, p_0^{(j)}), \quad j = 1, 2, \dots, n \quad (2.72)$$

The circumferential gradients, $\frac{\partial u}{\partial \beta}$, $\frac{\partial v}{\partial \beta}$, $\frac{\partial p}{\partial \beta}$ are evaluated as,

$$\frac{\partial u_0}{\partial \beta}^{(j)} = \frac{\partial \Theta(\beta, u_0^{(j)})}{\partial \beta} \Big|_{\beta=\beta_j} \quad (2.73)$$

$$\frac{\partial v_0}{\partial \beta}^{(j)} = \frac{\partial \Theta(\beta, v_0^{(j)})}{\partial \beta} \Big|_{\beta=\beta_j} \quad (2.74)$$

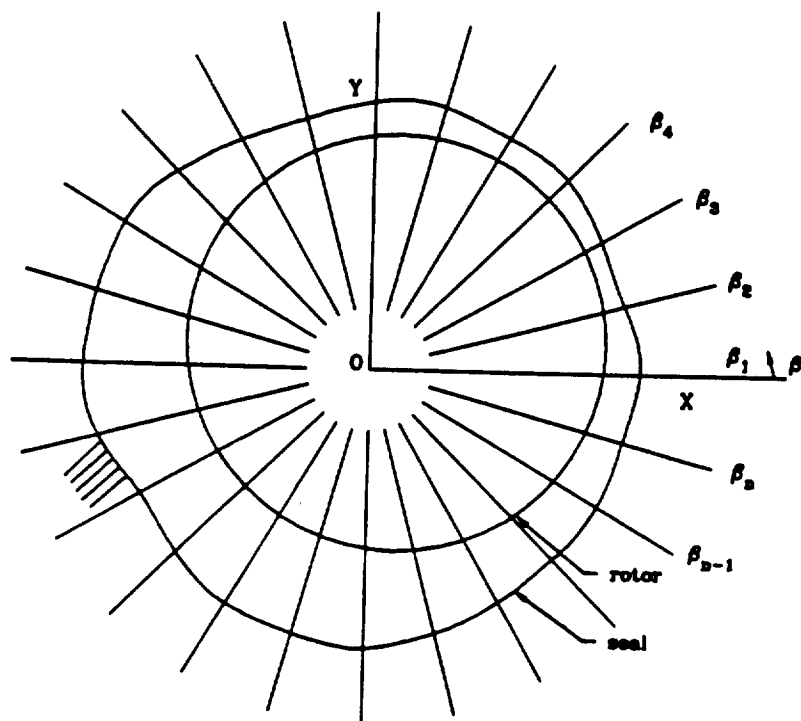


Figure 2.7 Circumferential Grid

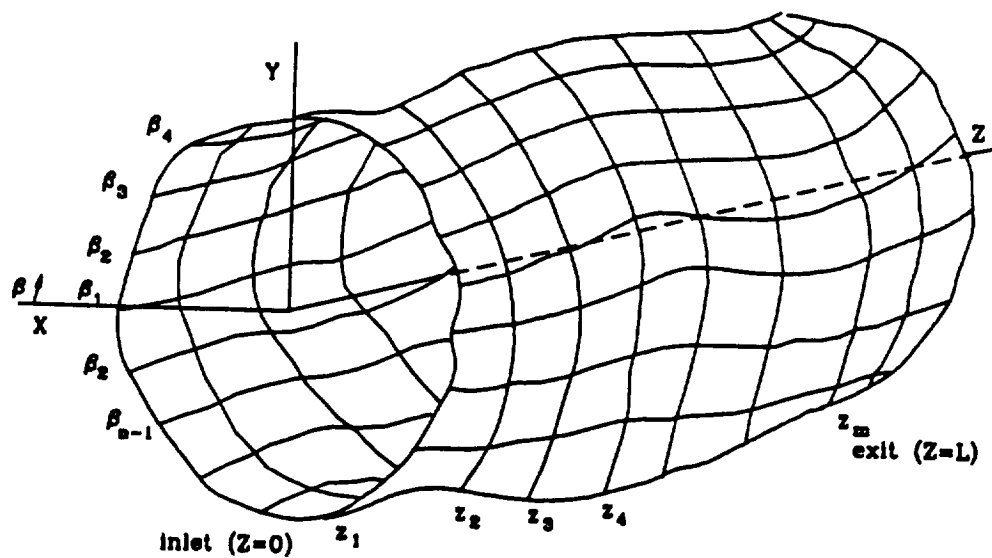


Figure 2.8 Grid for Numerical Integration

$$\frac{\partial p_0^{(j)}}{\partial \beta} = \frac{\partial \Theta(\beta, p_0^{(j)})}{\partial \beta} \Big|_{\beta=\beta_j} \quad (2.75)$$

The set of ODE's are solved subject to the boundary conditions

At the inlet, ($z = 0$),

circumferential velocity,

$$v_0^{(j)}(0, \beta_j) = \rho s r \times (\omega R), \quad j = 1, 2, \dots, n \quad (2.76)$$

pressure,

$$u_0^{(j)}(0, \beta_j) = \left\{ \frac{2}{\rho_0(1 + \xi_i)} (\Delta p - p_0^{(j)}(0, \beta_j)) \right\}^{1/2}, j = 1, 2, \dots, \quad (2.77)$$

At the exit, ($z = z_m$),

$$p_0^{(j)}(0, \beta_j) = 0, \quad j = 1, 2, \dots, n \quad (2.78)$$

In the parlance of numerical analysis, the above problem is classified as a “two point boundary value problem”, since the known boundary conditions exist at both ends of the boundary. In this study, this problem is solved using a multi-dimensional Newton-Raphson method known as “shooting method”. Nguyen (1988) reported using a similar method based on numerically computed gradients.

The problem may be specified in the following terms. It requires to find the n unknown inlet pressures, $p_0^{(1)}(z_1), p_0^{(2)}(z_1), \dots, p_0^{(n)}(z_1)$ subject to the condition that the n outlet pressures $p_0^{(1)}(z_m), p_0^{(2)}(z_m), \dots, p_0^{(n)}(z_m)$ are forced to be zero.

This may expressed as,

$$\begin{bmatrix} p_0^{(1)}\{z_m, p_0^{(1)}(z_1), p_0^{(2)}(z_1), \dots, p_0^{(n)}(z_1)\} \\ p_0^{(2)}\{z_m, p_0^{(1)}(z_1), p_0^{(2)}(z_1), \dots, p_0^{(n)}(z_1)\} \\ \vdots \\ p_0^{(n)}\{z_m, p_0^{(1)}(z_1), p_0^{(2)}(z_1), \dots, p_0^{(n)}(z_1)\} \end{bmatrix} = \begin{bmatrix} 0 \\ 0 \\ \vdots \\ 0 \end{bmatrix} \quad (2.79)$$

It may be noted that even though both $u_0^{(j)}$ and $v_0^{(j)}$ are unknown at the inlet, there are only n unknowns at z_1 due to the relationship given in Eq. (2.77).

The two point boundary value problem is now reduced to finding the n roots of the above equation. The numerical integration of the preceding differential equations may be considered as only a means of evaluating the functions $p_0^{(j)}(z_m)$ for any given set of guesses for the roots $p_0^{(1)}(z_1), p_0^{(2)}(z_1), \dots, p_0^{(n)}(z_1)$. As mentioned earlier, shooting method is an application of a multidimensional Newton-Raphson method for iterative search of roots $p_0^{(1)}(z_1), p_0^{(2)}(z_1), \dots, p_0^{(n)}(z_1)$ combined with a numerical integration based on evaluation of the exit pressures $p_0^{(j)}(z_m)$.

Dropping the subscript 0, let $p_k^{(j)}(z_1)$ represent the k -th guess for the set of inlet pressures $p_0^{(j)}(z_1)$ that satisfy the boundary condition of $p_0^{(j)}(z_m) = 0$ at the exit. Let the next guess be given by

$$p_{k+1}^{(j)}(z_1) = p_k^{(j)}(z_1) + \Delta p_k^{(j)}(z_1) \quad (2.80)$$

where $p_{k+1}^{(j)}(z_1)$ is the new guess. This may be expressed mathematically

$$\begin{pmatrix} \frac{\partial u_0^{(1)}}{\partial z} \\ \frac{\partial v_0^{(1)}}{\partial z} \\ \frac{\partial p_0^{(1)}}{\partial z} \\ \frac{\partial u_0^{(2)}}{\partial z} \\ \frac{\partial v_0^{(2)}}{\partial z} \\ \frac{\partial p_0^{(2)}}{\partial z} \\ \vdots \\ \frac{\partial u_0^{(n)}}{\partial z} \\ \frac{\partial v_0^{(n)}}{\partial z} \\ \frac{\partial p_0^{(n)}}{\partial z} \end{pmatrix} = \begin{pmatrix} F_u^1(u_0^{(1)}, v_0^{(1)}, \frac{\partial v_0^{(1)}}{\partial \beta}) \\ F_v^1(u_0^{(1)}, v_0^{(1)}, \frac{\partial v_0^{(1)}}{\partial \beta}, \frac{\partial p_0^{(1)}}{\partial \beta}) \\ F_p^1(u_0^{(1)}, v_0^{(1)}, \frac{\partial u_0^{(1)}}{\partial \beta}, \frac{\partial v_0^{(1)}}{\partial \beta}) \\ F_u^2(u_0^{(2)}, v_0^{(2)}, \frac{\partial v_0^{(2)}}{\partial \beta}) \\ F_v^2(u_0^{(2)}, v_0^{(2)}, \frac{\partial v_0^{(2)}}{\partial \beta}, \frac{\partial p_0^{(2)}}{\partial \beta}) \\ F_p^2(u_0^{(2)}, v_0^{(2)}, \frac{\partial u_0^{(2)}}{\partial \beta}, \frac{\partial v_0^{(2)}}{\partial \beta}) \\ \vdots \\ F_u^n(u_0^{(n)}, v_0^{(n)}, \frac{\partial v_0^{(n)}}{\partial \beta}) \\ F_v^n(u_0^{(n)}, v_0^{(n)}, \frac{\partial v_0^{(n)}}{\partial \beta}, \frac{\partial p_0^{(n)}}{\partial \beta}) \\ F_p^n(u_0^{(n)}, v_0^{(n)}, \frac{\partial u_0^{(n)}}{\partial \beta}, \frac{\partial v_0^{(n)}}{\partial \beta}) \end{pmatrix} \quad (2.81)$$

$$\begin{bmatrix} \alpha_{11}^k & \alpha_{12}^k & \cdots & \alpha_{1n}^k \\ \alpha_{21}^k & \alpha_{22}^k & \cdots & \alpha_{2n}^k \\ \vdots & \vdots & \ddots & \vdots \\ \alpha_{n1}^k & \alpha_{n2}^k & \cdots & \alpha_{nn}^k \end{bmatrix} \begin{pmatrix} \Delta p_k^{(1)}(z_1) \\ \Delta p_k^{(2)}(z_1) \\ \vdots \\ \Delta p_k^{(n)}(z_1) \end{pmatrix} = - \begin{pmatrix} p_k^{(1)}(z_m) \\ p_k^{(2)}(z_m) \\ \vdots \\ p_k^{(n)}(z_m) \end{pmatrix} \quad (2.82)$$

$$\alpha_{ij}^k = \frac{\partial p_0^{(i)}(z_m)}{\partial p_0^{(j)}(z_1)} \Big|_{p_k^{(j)}(z_1)} \quad (2.83)$$

The partial derivatives are computed numerically using a finite difference formula,

$$\begin{aligned} \frac{\partial p_0^{(i)}(z_m)}{\partial p_0^{(j)}(z_1)} &\approx \frac{1}{\Delta p_0^{(j)}(z_1)} \times \\ &[p_0^{(i)}\{z_m, p_0^{(1)}(z_1), \dots, p_0^{(j)}(z_1) + \Delta p_0^{(j)}(z_1), \dots, p_0^{(n)}(z_1)\} \\ &- p_0^{(i)}\{z_m, p_0^{(1)}(z_1), \dots, p_0^{(j)}(z_1), \dots, p_0^{(n)}(z_1)\}] \\ j &= 1, 2, \dots, n; \quad i = 1, 2, \dots, n \end{aligned} \quad (2.84)$$

It requires one complete numerical integration of the Eq. (2.81) to compute

$p_k^{(j)}(z_m)$ in Eq. (2.82) and an additional n integrations of Eq. (2.81) to obtain the derivatives in Eq. (2.83). These integrations may be performed by any standard integrators. Nguyen (1988) used the simple Euler's method for the above numerical integration. For this study, the following are used.

1. 4-5th order Runge-Kutta-Fehlberg Method.
2. Predictor-Corrector Method.
3. Adams' Method.

2.7.3 Cubic Spline Interpolation

Cubic splines are widely used in interpolation and surface fitting and a brief to introduction to splines is given in this section.

Let the dependent variable pressure p , along the circumference of the seal at a given axial location $z = z_m$ be specified by $p(z_m, \beta_j) = P(\beta_j)$, for $j = 1, 2, \dots, n$ corresponding to $\beta = \beta_1, \beta_2, \dots, \beta_n$, where n is the number of circumferential grid points.

In a given interval (β_j, β_{j+1}) , the dependent variable $P(\beta)$ is interpolated using a cubic polynomial function of the form given below.

$$P(\beta) = P_j + b_j(\beta - \beta_j) + c_j(\beta - \beta_j)^2 + d_j(\beta - \beta_j)^3, \quad \beta_j \leq \beta \leq \beta_{j+1} \quad (2.85)$$

The above equation may be rewritten in a more general form to facilitate the computation of the linear coefficients b_j, c_j, d_j . These coefficients are determined such that the above cubic polynomial is reduced to a cubic spline function, i.e., the function $P(\beta)$ and its derivative $P'(\beta)$ are continuous in (β_j, β_{j+1}) . In the following

equation " refers to the second derivative of the dependent variable.

$$P(\beta) = AP_j + BP_{j+1} + CP_j'' + DP_{j+1}'' \quad (2.86)$$

where,

$$A = \frac{\beta_{j+1} - \beta}{\beta_{j+1} - \beta_j} \quad (2.87)$$

$$B = \frac{\beta - \beta_j}{\beta_{j+1} - \beta_j} \quad (2.88)$$

$$C = \frac{1}{6}(A^3 - A)(\beta_{j+1} - \beta_j) \quad (2.89)$$

$$D = \frac{1}{6}(B^3 - B)(\beta_{j+1} - \beta_j) \quad (2.90)$$

The above formulation has the following important features.

1. The function $P(\beta)$ is continuous at β_j and β_{j+1} , i.e., at β_j in the interval (β_{j-1}, β_j) and at β_{j+1} in the interval (β_j, β_{j+1})
2. The function $P(\beta)$ has a continuous derivative at β_j and β_{j+1} , similar to the above condition.
3. The above two conditions give rise to four constraints which are used to determine four adjustable linear coefficients in terms of $P_j, P_{j+1}, P_j'', P_{j+1}''$.
4. Also, four is the number of parameters required to define a cubic polynomial in general.

The first and second derivative of the interpolating function is given by,

$$\begin{aligned} \frac{\partial p}{\partial \beta} &= \frac{P_{j+1} - P_j}{\beta_{j+1} - \beta_j} - \frac{3A^2 - 1}{6}(\beta_{j+1} - \beta_j)P_{j+1}'' \\ &\quad + \frac{3B^2 - 1}{6}(\beta_{j+1} - \beta_j)P_j'' \end{aligned} \quad (2.91)$$

$$\frac{\partial^2 p}{\partial \beta^2} = AP_j'' + BP_{j+1}'' \quad (2.92)$$

By imposing the condition of continuity in first derivative at node points, the following equation is obtained for $j = 2, 3, \dots, n-1$.

$$\frac{\beta_j - \beta_{j-1}}{6} P_{j-1}'' + \frac{\beta_{j+1} - \beta_{j-1}}{3} P_j'' + \frac{\beta_{j+1} - \beta_j}{6} P_{j+1}'' = \frac{P_{j+1} - P_j}{\beta_{j+1} - \beta_j} - \frac{P_j - P_{j-1}}{\beta_j - \beta_{j-1}} \quad (2.93)$$

This is a system of $n-2$ simultaneous linear equations involving n unknowns, $P_j'', j = 1, 2, \dots, n$. Two additional conditions are required to uniquely define the cubic spline. These two conditions may be provided in various ways based on the end conditions i.e., at β_1 and β_n .

Let $s_1(\beta)$ and $s_n(\beta)$ be two cubic polynomials that pass through the first and the last four data points. The two end conditions that complete the solution are defined by forcing these two cubics to have the same third derivative at the end points.

$$s'''(\beta_1) = P'''(\beta_1) \quad (2.94)$$

$$s'''(\beta_n) = P'''(\beta_n) \quad (2.95)$$

The Eq() may be rewritten in a more simplified form for actual computations.

$$\Delta\beta_j = \beta_{j+1} - \beta_j \quad (2.96)$$

$$\Delta_j = \frac{P_{j+1} - P_j}{\beta_{j+1} - \beta_j} \quad (2.97)$$

$$\Delta_j^{(2)} = \frac{\Delta_{j+1} - \Delta_j}{\beta_{j+2} - \beta_j} \quad (2.98)$$

$$\Delta_j^{(3)} = \frac{\Delta_{j+1}^{(2)} - \Delta_j^{(2)}}{\beta_{j+3} - \beta_j} \quad (2.99)$$

and the end conditions,

$$s'''(\beta_1) = 6\Delta_1^{(3)} \quad (2.100)$$

$$s'''(\beta_n) = 6\Delta_{n-3}^{(3)} \quad (2.101)$$

The quantities, $\Delta_j, 2\Delta_j^{(2)}, 6\Delta_j^{(3)}$ are approximations of the first, second and third derivatives respectively.

$$\begin{bmatrix} -\Delta\beta_1 & \Delta\beta_1 & 0 & 0 & \dots & 0 \\ \Delta\beta_1 & 2(\Delta\beta_1 + \Delta\beta_2) & \Delta\beta_2 & 0 & \vdots & 0 \\ 0 & \Delta\beta_2 & 2(\Delta\beta_2 + \Delta\beta_3) & \Delta\beta_3 & \vdots & 0 \\ \vdots & \ddots & \ddots & \ddots & \vdots & \vdots \\ \vdots & 0 & 0 & \Delta\beta_{n-2} & 2(\Delta\beta_{n-2} + \Delta\beta_{n-1}) & \Delta\beta_{n-1} \\ \dots & 0 & 0 & 0 & \Delta\beta_{n-1} & -\Delta\beta_{n-1} \end{bmatrix}$$

$$\times \begin{Bmatrix} P_1'' \\ P_2'' \\ P_3'' \\ \vdots \\ P_{n-1}'' \\ P_n'' \end{Bmatrix} = \begin{Bmatrix} \Delta\beta_1^2 \Delta_1^{(3)} \\ \Delta_2 - \Delta_1 \\ \Delta_3 - \Delta_2 \\ \vdots \\ \Delta_{n-1} - \Delta_{n-2} \\ -\Delta\beta_{n-1}^2 \Delta_{n-3}^{(3)} \end{Bmatrix} \quad (2.102)$$

The above system of equations has the following important characteristics.

1. The matrix is diagonal.
2. The matrix is symmetric.
3. The matrix is nonsingular and tridiagonal.
4. Efficient matrix reduction techniques available for solution.

The original cubic polynomial is given below along with the coefficients in terms of $P_j, P_{j+1}, P_j'', P_{j+1}''$.

Typically, the cubic spline is written in the following form.

In the interval (β_j, β_{j+1}) ,

$$P(\beta) = P_j + b_j(\beta - \beta_j) + c_j(\beta - \beta_j)^2 + d_j(\beta - \beta_j)^3, \quad \beta_j \leq \beta \leq \beta_{j+1} \quad (2.103)$$

$$b_j = \frac{P_{j+1} - P_j}{\Delta\beta_j} - \Delta\beta_j(P''_{j+1} + 2P''_j) \quad (2.104)$$

$$c_j = 3P''_j \quad (2.105)$$

$$d_j = \frac{P''_{j+1} - P''_j}{\Delta\beta_j} \quad (2.106)$$

The sets of coefficients are stored for the $n - 1$ intervals and the function values and its derivatives are computed whenever they are needed.

$$P'(\beta) = b_j + 2c_j(\beta - \beta_j) + 3d_j(\beta - \beta_j)^2, \quad (2.107)$$

$$P''(\beta) = 2c_j + 6d_j(\beta - \beta_j) \quad (2.108)$$

$$\beta_j \leq \beta \leq \beta_{j+1}$$

2.7.4 Leakage

The mass flow rate, dQ , through the differential element $h_0 R d\beta$ shown in Figure 2.9 is given by,

$$dQ = u_0(0, \beta) \rho_0 h_0(0, \beta) R d\beta \quad (2.109)$$

where,

$u_0(0, \beta)$ axial velocity at inlet

$h_0(0, \beta)$ film thickness at inlet

R radius of the rotor

ρ_0 density of fluid

The above expression is integrated around the circumference of the seal at the inlet to give the total mass flow rate or leakage, Q .

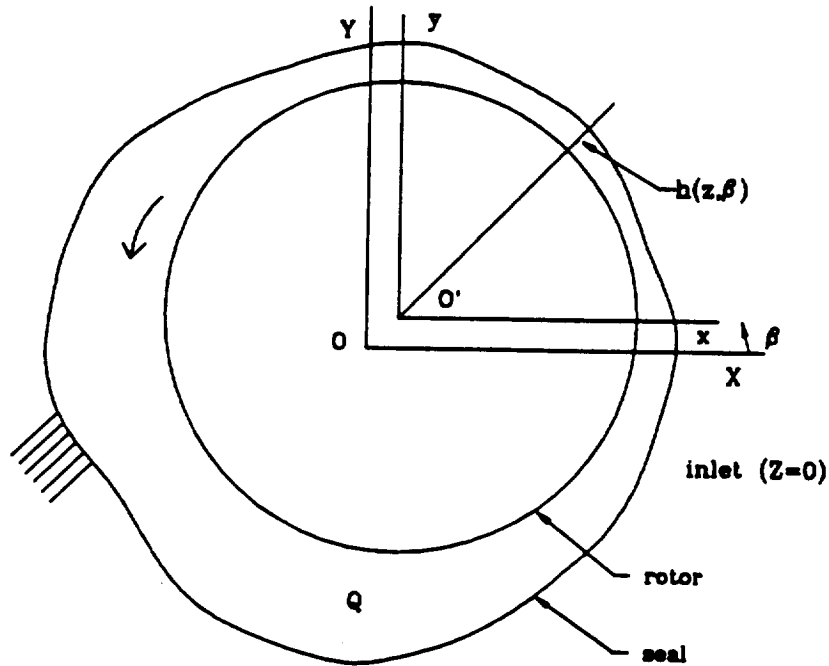


Figure 2.9 Leakage

$$Q = \int_0^{2\pi} u_0(0, \beta) \rho_0 h_0(0, \beta) R d\beta \quad (2.110)$$

2.7.5 Steady State Seal Forces

The reactive seal forces acting on a non-vibrating rotor are obtained by integrating the zeroth order pressure field, $p_0(z, \beta)$, around the rotor and along the length of the seal.

The X and Y components of force acting on the differential area element $Rd\beta dz$, shown in Figure 2.10, are given by,

$$-dF_x = p_0(z, \beta) \cos \beta R d\beta dz \quad (2.111)$$

$$-dF_y = p_0(z, \beta) \sin \beta R d\beta dz \quad (2.112)$$

Integrating the above force expressions over the entire surface area of the rotor

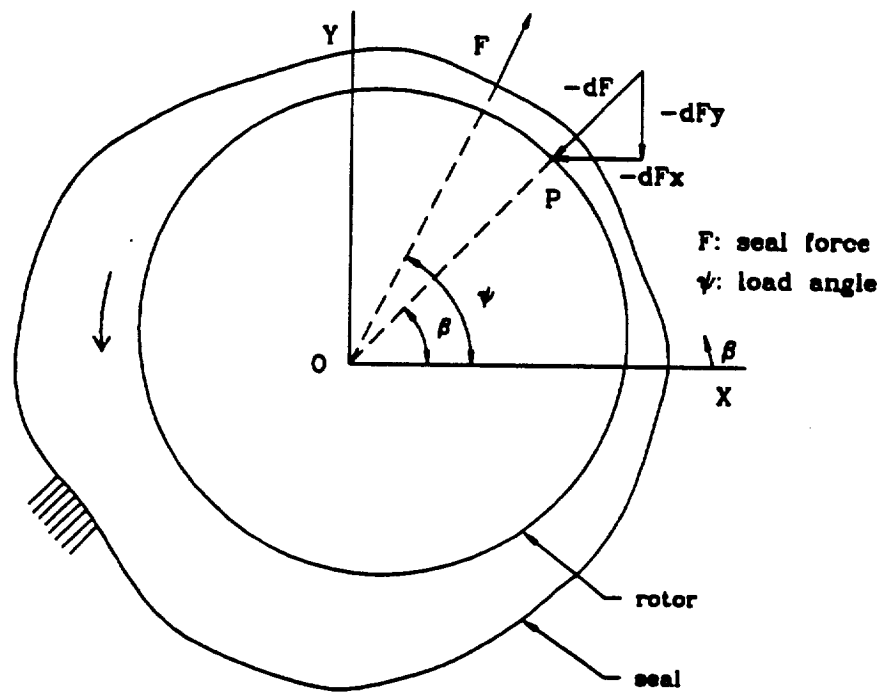


Figure 2.10 Steady State Seal Forces

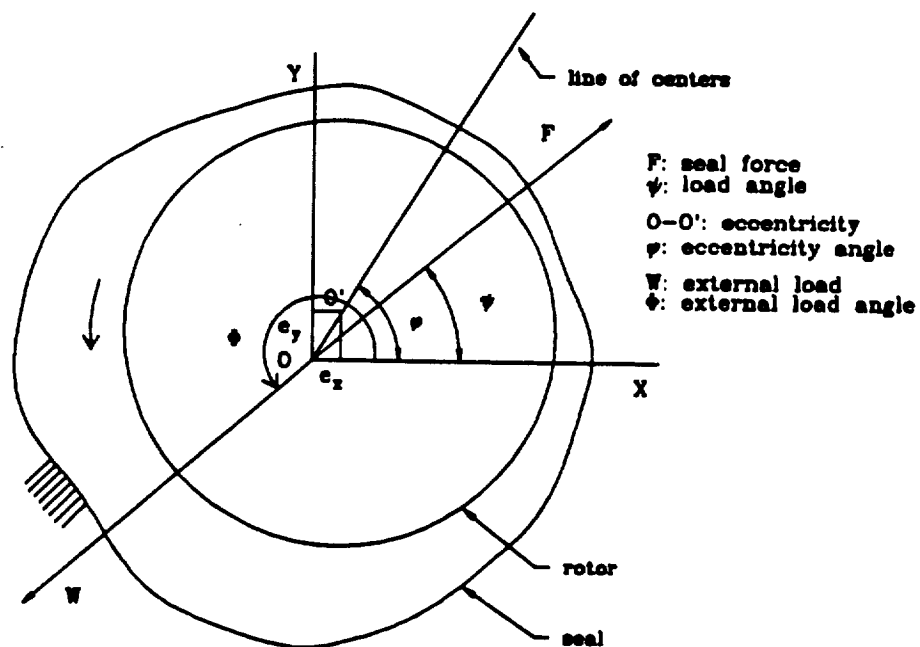


Figure 2.11 Force Geometry for Seal

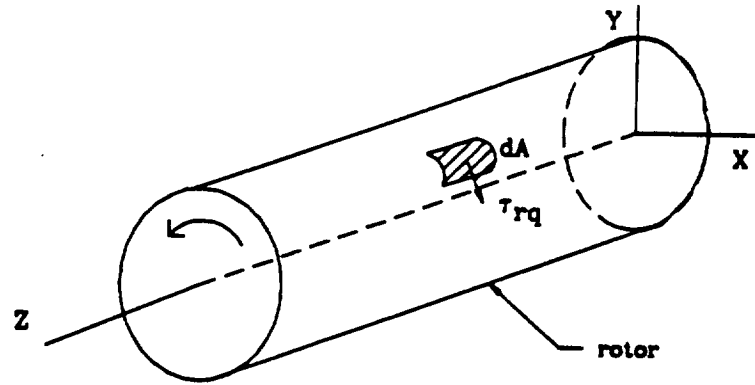


Figure 2.12 Frictional Torque

yields,

$$-F_x = \int_0^L \int_0^{2\pi} p_0(z, \beta) \cos \beta R d\beta dz \quad (2.113)$$

$$-F_y = \int_0^L \int_0^{2\pi} p_0(z, \beta) \sin \beta R d\beta dz \quad (2.114)$$

The angle made by the resultant seal force F with the X -axis is defined as the load angle and is given by,

$$\psi = \tan^{-1} \left(\frac{-F_y}{-F_x} \right) \quad (2.115)$$

$$F = \sqrt{F_x^2 + F_y^2} \quad (2.116)$$

The resultant seal force is also known as the load bearing capacity of the seal. This resultant seal force must balance against the external load (pre-load) applied by the rotor on the seal. The pre-load may vary in magnitude and direction as the pumps's speed or power-level changes.

2.7.6 Friction Loss

The friction loss or horse power loss computation is illustrated in Figure 2.12.

The frictional torque on a differential element $R d\beta dz$ due to friction at the rotor

surface is given as,

$$d\Gamma = R\tau_{rq}|_r R d\beta dz \quad (2.117)$$

$$-\tau_{rq}|_r = \frac{h}{2} \frac{\partial p}{\partial q} + \frac{\mu}{4h} \left\{ f_s \frac{v}{2} R_s - f_r \frac{(v-w)}{2} R_r \right\} \quad (2.118)$$

where $f_{r,0}$ is the rotor friction factor and $\tau_{rq}|_r$ is the shear stress at the rotor surface.

Total frictional torque, Γ , over the entire length of the rotor is given by,

$$\Gamma = - \int_0^L \int_0^{2\pi} \tau_{rq}|_r R^2 d\beta dz \quad (2.119)$$

and the power loss due to friction is (dropping the negative sign),

$$Power Loss = \Gamma \omega \quad (2.120)$$

where ω is the rotor rpm in rad/s.

2.8 First Order Boundary Conditions

The first order boundary conditions are obtained by perturbing the zeroth order boundary conditions of Eqs. (2.51,2.54,2.56).

$$p_1(0, \beta) = -(1 + \xi_i) \rho_0 u_0(0, \beta) u_1(0, \beta) \quad (2.121)$$

$$v_1(0, \beta) = 0 \quad (2.122)$$

$$p_1(L, \beta) = 0 \quad (2.123)$$

2.9 Solution Procedure for First Order Equations

The set of first order equations in Eqs. (2.36–2.38) are further reduced by employing a *separation of variables* technique for an assumed *small* motion of the vibrating rotor.

The assumed form of perturbations for the dependent variables and film thickness

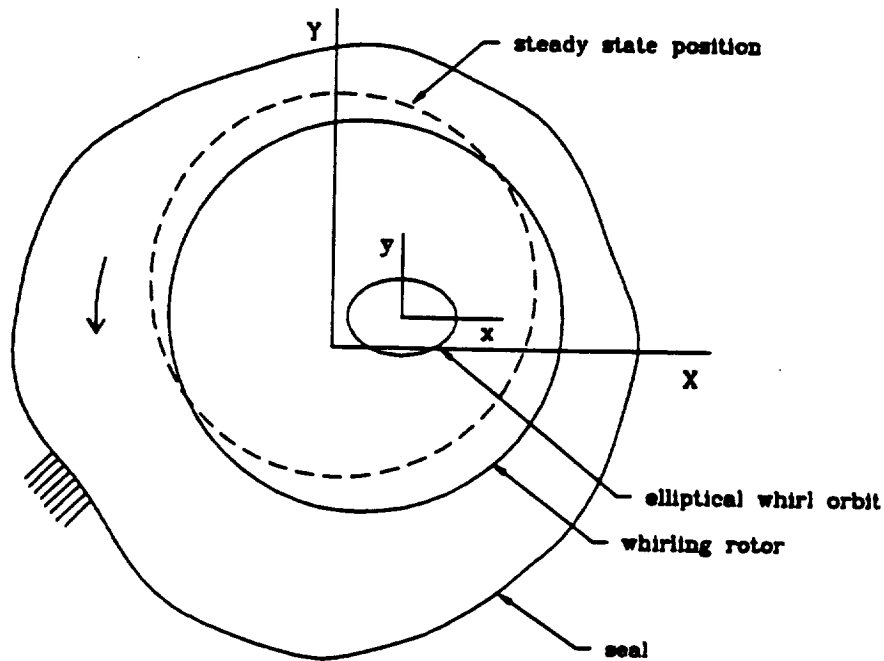


Figure 2.13 Elliptical Whirl Orbit

are,

$$u = u_0 + \epsilon u_1 \quad (2.124)$$

$$v = v_0 + \epsilon v_1 \quad (2.125)$$

$$p = p_0 + \epsilon p_1 \quad (2.126)$$

$$h = h_0 + \epsilon h_1 \quad (2.127)$$

The rotor is assumed to execute a whirling motion with an elliptical orbit as shown in Figure 2.13. The figure shows the steady state operating position of the rotor along with the vibrating (whirling) rotor. Let the semi-major and semi-minor axes of this perturbation ellipse be given by (\tilde{X}, \tilde{Y}) .

The perturbation ϵ may be considered to be a combination of two individual perturbations ϵ_x and ϵ_y . This assumption is the basis for eccentric seal analysis where the dependent variables vary in the circumferential direction as opposed to

the concentric case where they remain constant in the circumferential direction. The magnitudes of these perturbations are arbitrary since they do not form a part of the final solution. These perturbations are assumed to be *infinitesimally small* and is the basis for neglecting second and higher order terms in the perturbation analysis. These perturbations, ϵ_x and ϵ_y , are the non-dimensionalized axes of the whirling orbit as given below.

$$\epsilon u_1 = \frac{\bar{X}}{c_*} u_{1x} + \frac{\bar{Y}}{c_*} u_{1y} \quad (2.128)$$

$$\epsilon v_1 = \frac{\bar{X}}{c_*} v_{1x} + \frac{\bar{Y}}{c_*} v_{1y} \quad (2.129)$$

$$\epsilon p_1 = \frac{\bar{X}}{c_*} p_{1x} + \frac{\bar{Y}}{c_*} p_{1y} \quad (2.130)$$

$$\epsilon h_1 = \frac{\bar{X}}{c_*} h_{1x} + \frac{\bar{Y}}{c_*} h_{1y} \quad (2.131)$$

where c_* is some nominal clearance used to non-dimensionalize the perturbations.

Let the perturbations be redefined in the following non-dimensionalized form.

$$\Delta \epsilon_x = \frac{\bar{X}}{c_*} \quad (2.132)$$

$$\Delta \epsilon_y = \frac{\bar{Y}}{c_*} \quad (2.133)$$

Substituting Eqs. (2.132–2.133) in Eqs. (2.128–2.131) yields,

$$\epsilon u_1 = \Delta \epsilon_x u_{1x} + \Delta \epsilon_y u_{1y} \quad (2.134)$$

$$\epsilon v_1 = \Delta \epsilon_x v_{1x} + \Delta \epsilon_y v_{1y} \quad (2.135)$$

$$\epsilon p_1 = \Delta \epsilon_x p_{1x} + \Delta \epsilon_y p_{1y} \quad (2.136)$$

$$\epsilon h_1 = \Delta \epsilon_x h_{1x} + \Delta \epsilon_y h_{1y} \quad (2.137)$$

Assuming that the rotor whirls about its equilibrium position in an elliptical orbit whose center is located at (x_0, y_0) , then the position of the center of the vibrating

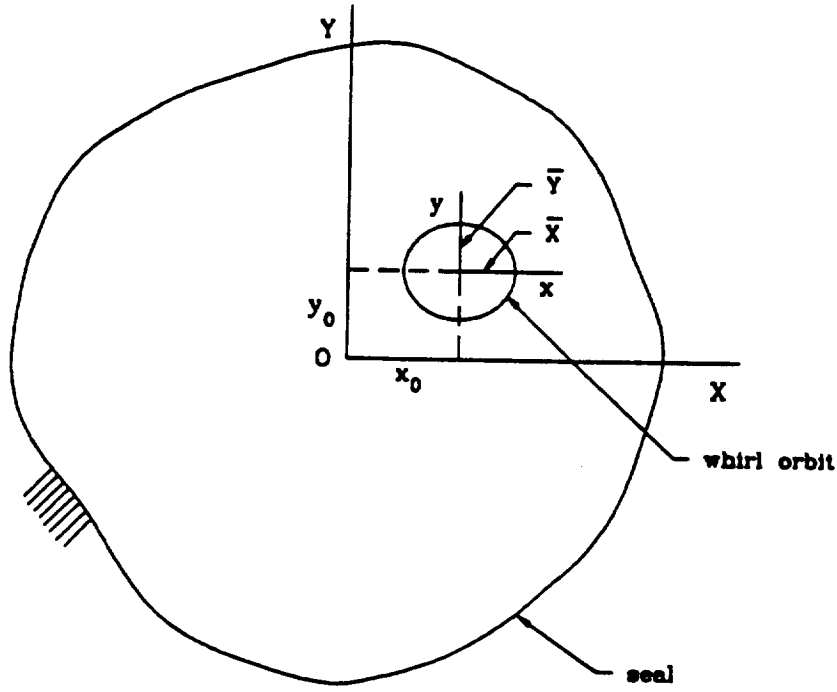


Figure 2.14 Perturbation Orbit

rotor relative to its static eccentric position is given by (Figure 2.14),

$$x - x_0 = \bar{X} \cos \omega t \quad (2.138)$$

$$y - y_0 = \bar{Y} \cos \omega t \quad (2.139)$$

Let $\alpha = \omega t$, where ω is the angular velocity of the rotor given in rad/s. The perturbed film thickness expression may be rewritten as,

$$h(z, \beta, t) = h_0(z, \beta) - (x - x_0) \cos \beta - (y - y_0) \sin \beta \quad (2.140)$$

or,

$$h(z, \beta, t) = h_0(z, \beta) + \epsilon h_1(z, \beta, t) \quad (2.141)$$

From the above equation, the perturbation in film thickness ϵh_1 is given as,

$$\epsilon h_1(z, \beta, t) = -\bar{X} \cos \alpha \cos \beta - \bar{Y} \sin \alpha \sin \beta \quad (2.142)$$

or

$$h_1 = -\frac{c_0}{\epsilon} \{ \Delta \epsilon_x \cos \alpha \cos \beta + \Delta \epsilon_y \sin \alpha \sin \beta \} \quad (2.143)$$

$$\frac{\partial h_1}{\partial \beta} = -\frac{c_0}{\epsilon} \{ -\Delta \epsilon_x \sin \alpha \sin \beta + \Delta \epsilon_y \sin \alpha \cos \beta \} \quad (2.144)$$

$$\frac{\partial h_1}{\partial t} = -\frac{\omega c_0}{\epsilon} \{ -\Delta \epsilon_x \sin \alpha \cos \beta + \Delta \epsilon_y \cos \alpha \sin \beta \} \quad (2.145)$$

The right hand side of the system of first order equations (Eqs. 2.36–2.38) consists of harmonic forcing functions h_0 , $\frac{\partial h_0}{\partial z}$, $\frac{\partial h_0}{\partial \beta}$, h_1 , $\frac{\partial h_1}{\partial \beta}$, and $\frac{\partial h_1}{\partial z}$. These functions are essentially harmonic functions from Eqs. (2.143–2.145). Based on this fact, the solution is assumed to be harmonic functions of α and β .

$$p_{1x} = a_1(z, \beta) \cos \alpha + a_2(z, \beta) \sin \alpha \quad (2.146)$$

$$u_{1x} = a_3(z, \beta) \cos \alpha + a_4(z, \beta) \sin \alpha \quad (2.147)$$

$$v_{1x} = a_5(z, \beta) \cos \alpha + a_6(z, \beta) \sin \alpha \quad (2.148)$$

$$p_{1y} = b_1(z, \beta) \cos \alpha + b_2(z, \beta) \sin \alpha \quad (2.149)$$

$$u_{1y} = b_3(z, \beta) \cos \alpha + b_4(z, \beta) \sin \alpha \quad (2.150)$$

$$v_{1y} = b_5(z, \beta) \cos \alpha + b_6(z, \beta) \sin \alpha \quad (2.151)$$

Using the above substitutions in the set of first order equations Eqs. (2.36–2.38) yields 12 coupled linear partial differential equations. This set of equations are given in Appendix A, for the constant properties model.

The solution procedure for the 12 linear PDE's is exactly the same as that of the zeroth order solution. The integration is performed with a 4–5th order Runge-Kutta method, predictor-corrector method and Adams methods. All the methods yield almost identical results, with the Runge-Kutta based method being the fastest.

2.9.1 Comparison with Nelson and Nguyen's Approach

The original analysis assumed the variables, a_i and b_i to be harmonic and separated them into two auxiliary functions of the form,

$$a_i(z, \beta) = f_i(z) \cos \beta + g_i(z) \sin \beta \quad (2.152)$$

where $f_i(z)$ and $g_i(z)$ are assumed not to vary with β . Nelson and Nguyen (1988a, 1988b) thereby apply a second separation of variables substitution to the first order differential equations. While the above form of assumed solution yields results that agree with available experimental results, an examination of the numerical values of the functions $f_i(z)$ and $g_i(z)$ revealed a β dependence, particularly at eccentricities above 0.5. The inclusion of the circumferential gradients of these variable should therefore improve the solution at higher eccentricities.

The a_i and b_i in the current analysis are totally general functions of z and β which thereby avoids the mathematical contradiction discussed above. Furthermore, in many cases the results of the current approach show better agreement with experimental results than the earlier results.

2.9.2 Boundary Conditions of Assumed Variables

The first order boundary conditions are expressed in the assumed solution variables are,

$$a_1(0, \beta) = -(1 + \xi_i) \rho a_3(0, \beta) \quad (2.153)$$

$$a_2(0, \beta) = -(1 + \xi_i) \rho a_4(0, \beta) \quad (2.154)$$

$$a_5(0, \beta) = 0 \quad (2.155)$$

$$a_6(0, \beta) = 0 \quad (2.156)$$

$$a_1(L, \beta) = 0 \quad (2.157)$$

$$a_2(L, \beta) = 0 \quad (2.158)$$

$$b_1(0, \beta) = -(1 + \xi_i) \rho b_3(0, \beta) \quad (2.159)$$

$$b_2(0, \beta) = -(1 + \xi_i) \rho b_4(0, \beta) \quad (2.160)$$

$$b_5(0, \beta) = 0 \quad (2.161)$$

$$b_6(0, \beta) = 0 \quad (2.162)$$

$$b_1(L, \beta) = 0 \quad (2.163)$$

$$b_2(L, \beta) = 0 \quad (2.164)$$

2.9.3 Solution of First Order Equations

The same solution procedure that is used for the zeroth order equations is used to solve the reduced first order equations given in *Appendix A* subject to the boundary conditions of Eqs. (2.153–2.164) for variables $a_i(z, \beta)$ and $b_i(z, \beta)$.

2.10 Determination of Dynamic Coefficients

In this section, dynamic coefficients are derived from first order pressure distribution $p_1(z, \beta, t)$. The following linearized force-motion model for a 2-DOF vibration is used to define the rotordynamic coefficients. In this equation, Δx and Δy define the displacement of the rotor relative to a static operating point and ΔF_x , ΔF_y are the components of the perturbed force due to first order pressure field, $p_1(z, \beta, t)$. The significance of each of the linearized coefficients have been explained in Chapter I.

$$-\begin{Bmatrix} \Delta F_x \\ \Delta F_y \end{Bmatrix} = \begin{bmatrix} K_{xx} & k_{xy} \\ -k_{yx} & K_{yy} \end{bmatrix} \begin{Bmatrix} \Delta x \\ \Delta y \end{Bmatrix} + \begin{bmatrix} C_{xx} & c_{xy} \\ -c_{yx} & C_{yy} \end{bmatrix} \begin{Bmatrix} \Delta \dot{x} \\ \Delta \dot{y} \end{Bmatrix}$$

$$+ \begin{bmatrix} M_{xx} & m_{xy} \\ -m_{yx} & m_{yy} \end{bmatrix} \begin{Bmatrix} \Delta \tilde{x} \\ \Delta \tilde{y} \end{Bmatrix} \quad (2.165)$$

The perturbed or incremental force components acting on the rotor due to a *small* motion about a static eccentric position (x, y) is given by integrating the first order pressure field,

$$-\Delta F_x = \int_0^L \int_0^{2\pi} \epsilon p_1 \cos \beta R d\beta dz \quad (2.166)$$

$$-\Delta F_y = \int_0^L \int_0^{2\pi} \epsilon p_1 \sin \beta R d\beta dz \quad (2.167)$$

The perturbation motion is described earlier by an elliptical orbit. The displacements, velocities and accelerations at any point on this elliptical orbit are given by,

$$\Delta x = \tilde{X} \cos \omega t \quad (2.168)$$

$$\Delta y = \tilde{Y} \sin \omega t \quad (2.169)$$

$$\Delta \dot{x} = -\omega \tilde{X} \sin \omega t \quad (2.170)$$

$$\Delta \dot{y} = -\omega \tilde{Y} \cos \omega t \quad (2.171)$$

$$\Delta \ddot{x} = -\omega^2 \tilde{X} \cos \omega t \quad (2.172)$$

$$\Delta \ddot{y} = -\omega^2 \tilde{Y} \sin \omega t \quad (2.173)$$

At $\omega t = 0$, $\sin \omega t = 0$, $\cos \omega t = 1$ and $\Delta y = \Delta \dot{x} = \Delta \ddot{y} = 0$. Substituting these values in Eq.(2.165),

$$-\frac{\Delta F_x}{c_e} = \Delta \epsilon_x \{-K_{xx} - M_{xx} \omega^2\} + \Delta \epsilon_y \{c_{xy} \omega\} \quad (2.174)$$

$$-\frac{\Delta F_y}{c_e} = \Delta \epsilon_x \{-k_{yx} + m_{yx} \omega^2\} + \Delta \epsilon_y \{C_{yy} \omega\} \quad (2.175)$$

At $\omega t = \frac{\pi}{2}$, $\sin \omega t = 1$, $\cos \omega t = 0$ and $\Delta x = \Delta \dot{y} = \Delta \ddot{x} = 0$. Substituting these values

in Eq.(2.165),

$$-\frac{\Delta F_x}{c_*} = \Delta \epsilon_x \{-C_{xx}\omega\} + \Delta \epsilon_y \{k_{xy} - m_{xy}\omega^2\} \quad (2.176)$$

$$-\frac{\Delta F_y}{c_*} = \Delta \epsilon_x \{c_{yx}\omega\} + \Delta \epsilon_y \{K_{yy} - M_{yy}\omega^2\} \quad (2.177)$$

From the following relationship between the first order pressure and the assumed variables, a_i and b_i ,

$$\epsilon p_1 = \Delta \epsilon_x p_{1x} + \Delta \epsilon_y p_{1y} \quad (2.178)$$

p_{1x} and p_{1y} may be expressed as,

$$p_{1x} = a_1 \cos \alpha + a_2 \sin \alpha \quad (2.179)$$

$$p_{1y} = b_1 \cos \alpha + b_2 \sin \alpha \quad (2.180)$$

Equating Eqs.(2.166–2.167 and Eqs.(2.174–2.177) and dropping the perturbations, the following relations for the dynamic coefficients are obtained.

$$K_{xx} - M_{xx}\omega^2 = \frac{1}{c_*} \int_0^L \int_0^{2\pi} a_1 \cos \beta R d\beta dz \quad (2.181)$$

$$c_{xy}\omega = \frac{1}{c_*} \int_0^L \int_0^{2\pi} b_1 \cos \beta R d\beta dz \quad (2.182)$$

$$-k_{yx} + m_{yx}\omega^2 = \frac{1}{c_*} \int_0^L \int_0^{2\pi} a_1 \sin \beta R d\beta dz \quad (2.183)$$

$$C_{yy}\omega = \frac{1}{c_*} \int_0^L \int_0^{2\pi} b_1 \sin \beta R d\beta dz \quad (2.184)$$

$$-C_{xx}\omega = \frac{1}{c_*} \int_0^L \int_0^{2\pi} a_2 \cos \beta R d\beta dz \quad (2.185)$$

$$k_{yx} - m_{xy}\omega^2 = \frac{1}{c_*} \int_0^L \int_0^{2\pi} b_2 \cos \beta R d\beta dz \quad (2.186)$$

$$c_{yx}\omega = \frac{1}{c_*} \int_0^L \int_0^{2\pi} a_2 \sin \beta R d\beta dz \quad (2.187)$$

$$K_{yy} - M_{yy}\omega^2 = \frac{1}{c_*} \int_0^L \int_0^{2\pi} b_2 \sin \beta R d\beta dz \quad (2.188)$$

These 8 equations must be evaluated for at least two whirl frequencies to obtain solutions for the 12 dynamic coefficients. A least squares approach is employed for this step. Typically, 2-4 whirl frequencies are used in a least squares scheme to compute these coefficients. Also, the dynamic coefficients for an annular seal are essentially independent of whirl frequencies. The 2-D integration performed numerically is an improvement over the average value approach employed by the Nelson and Nguyen (1988a, 1988b).

2.11 Dynamic Coefficients based on External Load Specification

Typically, for seals the dynamic coefficients are computed as a function of eccentricity. This assumes that the eccentric position of the shaft has been specified and the resultant reactive force due to the pressure distribution in the seal is to be determined. In some cases, it is possible to specify the angle at which external load is supported by the seal during the operation of the turbomachine. For example, unit 3-01, an experimental seal under design at NASA (results to be discussed later) supports the external load at a constant angle of 290° in the rotor coordinate system as shown in Figure 2.15.

The problem now is to determine the eccentric position given an external load F and its load angle Φ . This is accomplished by iteratively searching for an eccentric position e of the rotor which produces a pressure distribution $p_0(z, \beta)$ which when integrated over the entire seal balances the applied load in magnitude and direction. This iterative search is carried out using a modified 2-D Newton-Raphson method discussed below.

Power Level	Component Side Load						Resultant Static Load			
	PBI		MSI		Turbine		Ball Bearing		Roller Bearing	
	Load (lbf)	Phase (deg)	Load (lbf)	Phase (deg)	Load (lbf)	Phase (deg)	Load (lbf)	Phase (deg)	Load (lbf)	Phase (deg)
65%	82	158	290	291	200	270	130	91	325	87
80%	75	142	475	283	280	270	215	105	480	88
100%	125	125	670	285	300	270	275	114	585	100

Note: PBI is Preburner Impeller, MSI is Main Stage Impeller.

Table 19. Component Side Loads

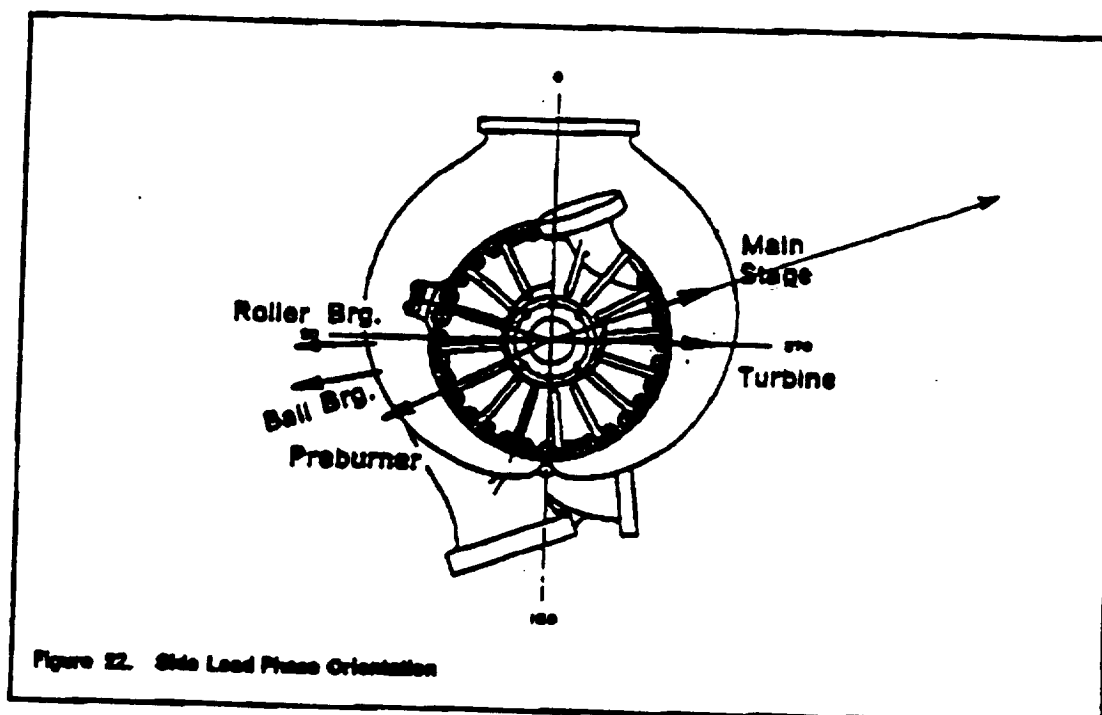


Figure 22. Side Load Phase Orientation

Figure 2.15 Example of External Load acting on a Seal

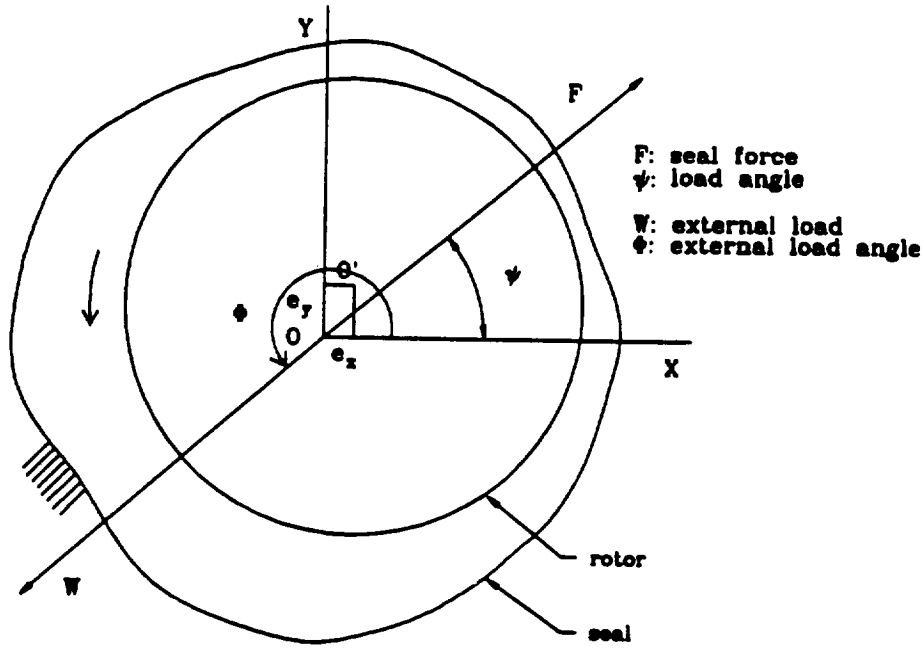


Figure 2.16 External Load and External Load Angle

2.11.1 Steady State Force Equilibrium Position

A modified 2-D Newton-Raphson method is used to locate the operating position. At the steady state equilibrium position,

Let F_x and F_y be the X and Y components of the seal force obtained by integrating the pressure field within the seal for a given rotor position (x, y) . Let \bar{F}_x and \bar{F}_y be the components of the external load.

$$f_x = \bar{F}_x + F_x \quad (2.189)$$

$$f_y = \bar{F}_y + F_y \quad (2.190)$$

where f_x and f_y are the residual forces in X and Y directions respectively. The problem reduces to finding (x, y) such that the residual forces f_x and f_y are zero. In other words, find a rotor eccentric position such that F_x is balanced by \bar{F}_x and F_y is

balanced \bar{F}_y .

The iterative search is described by,

$$x_{k+1} = x_k + \Delta x_k \quad (2.191)$$

$$y_{k+1} = y_k + \Delta y_k \quad (2.192)$$

and the increments Δx_k and Δy_k are computed from Eq. (2.193).

$$\begin{bmatrix} \frac{\partial F_x}{\partial x} & \frac{\partial F_x}{\partial y} \\ \frac{\partial F_y}{\partial x} & \frac{\partial F_y}{\partial y} \end{bmatrix} \begin{Bmatrix} \Delta x_k \\ \Delta y_k \end{Bmatrix} = \begin{Bmatrix} f_x \\ f_y \end{Bmatrix} \quad (2.193)$$

The derivatives in Eq. (2.193) are computed using a forward difference formula as,

$$\frac{\partial F_x}{\partial x} = \frac{F_x(x + \Delta x, y) - F_x(x, y)}{\Delta x} \quad (2.194)$$

$$\frac{\partial F_x}{\partial y} = \frac{F_x(x, y + \Delta y) - F_x(x, y)}{\Delta y} \quad (2.195)$$

$$\frac{\partial F_y}{\partial x} = \frac{F_y(x + \Delta x, y) - F_y(x, y)}{\Delta x} \quad (2.196)$$

$$\frac{\partial F_y}{\partial y} = \frac{F_y(x, y + \Delta y) - F_y(x, y)}{\Delta y} \quad (2.197)$$

The iterative search stops when the residual forces f_x and f_y are below some specified tolerance. Once, the eccentric position is determined, the computation of dynamic coefficients is carried out as before.

CHAPTER III

VARIABLE PROPERTIES MODEL

The effect of variable fluid properties as related to liquid seals for cryogenic applications was first investigated in some detail by Simon and Frene (1989). Their initial work did not include fluid inertia effects and the analysis was based on a simplified Reynolds equation. San Andres (1991) developed a seal analysis that included variable fluid properties as a function of local pressure and a mean temperature. He used the NIST 12 Database, MIPROPS (1986) to compute the fluid properties. This database is based on the 32-term *Modified Benedict-Webb-Ruben Equation of State*. Experimental and theoretical data is used to compute the coefficients of the terms in this equation of state and data is available for a number of fluids.

The working fluid in SSME turbopump is either liquid oxygen (LOX) or liquid hydrogen (LH2). Figure 3.1 shows the variation of density and viscosity of LOX a function of pressure. Typical inlet pressures for the turbopump are in the range of 20 Mpa and the exit pressures are in the 3 Mpa range.

For a typical seal, inlet and exit conditions are given below.

inlet pressure, p_i	19.0 Mpa
exit pressure, p_e	3.0 Mpa
mean temperature, T^*	90° K

For the above conditions, the fluid properties for LOX at inlet and exit are,

at inlet:

density, ρ_i	1179 kg/m ³ K
viscosity, μ_i	2.32×10^{-4} Pa-s

compressibility, $\frac{1}{\rho} \frac{\partial \rho}{\partial p} |_T$ 0.0014 1/MPa

at exit:

density, ρ_e 1148 kg/m³ K

viscosity, μ_e 2.01×10^{-4} Pa-s

compressibility, $\frac{1}{\rho} \frac{\partial \rho}{\partial p} |_T$ 0.0019 1/MPa

For the same conditions, the fluid properties for LH2 at inlet and exit are,

at inlet:

density, ρ_i 42.13 kg/m³ K

viscosity, μ_i 6.43×10^{-6} Pa-s

compressibility, $\frac{1}{\rho} \frac{\partial \rho}{\partial p} |_T$ 0.03335 1/MPa

at exit:

density, ρ_e 8.18 kg/m³ K

viscosity, μ_e 4.13×10^{-6} Pa-s

compressibility, $\frac{1}{\rho} \frac{\partial \rho}{\partial p} |_T$ 0.334 1/MPa

The change in density and viscosity for LOX is relatively small (about 2.6% and 12% respectively for the above case). However, for LH2, the change in density between inlet and exit is considerable and this will have a noticeable effect on the dynamic coefficients computed (San Andres, 1991). A similar change is also noticed in viscosity.

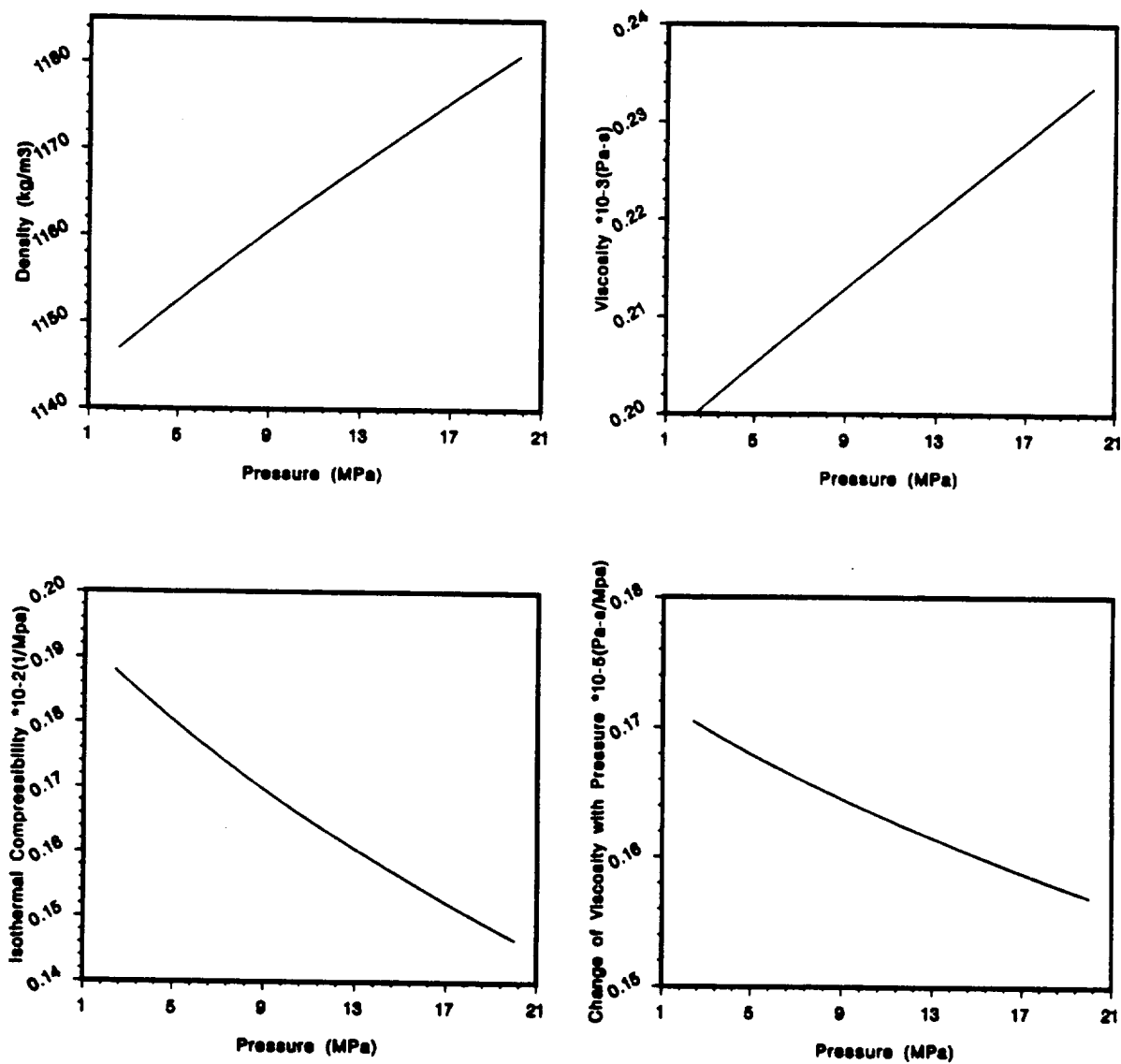


Figure 3.1 Properties of Liquid Oxygen at 90°K

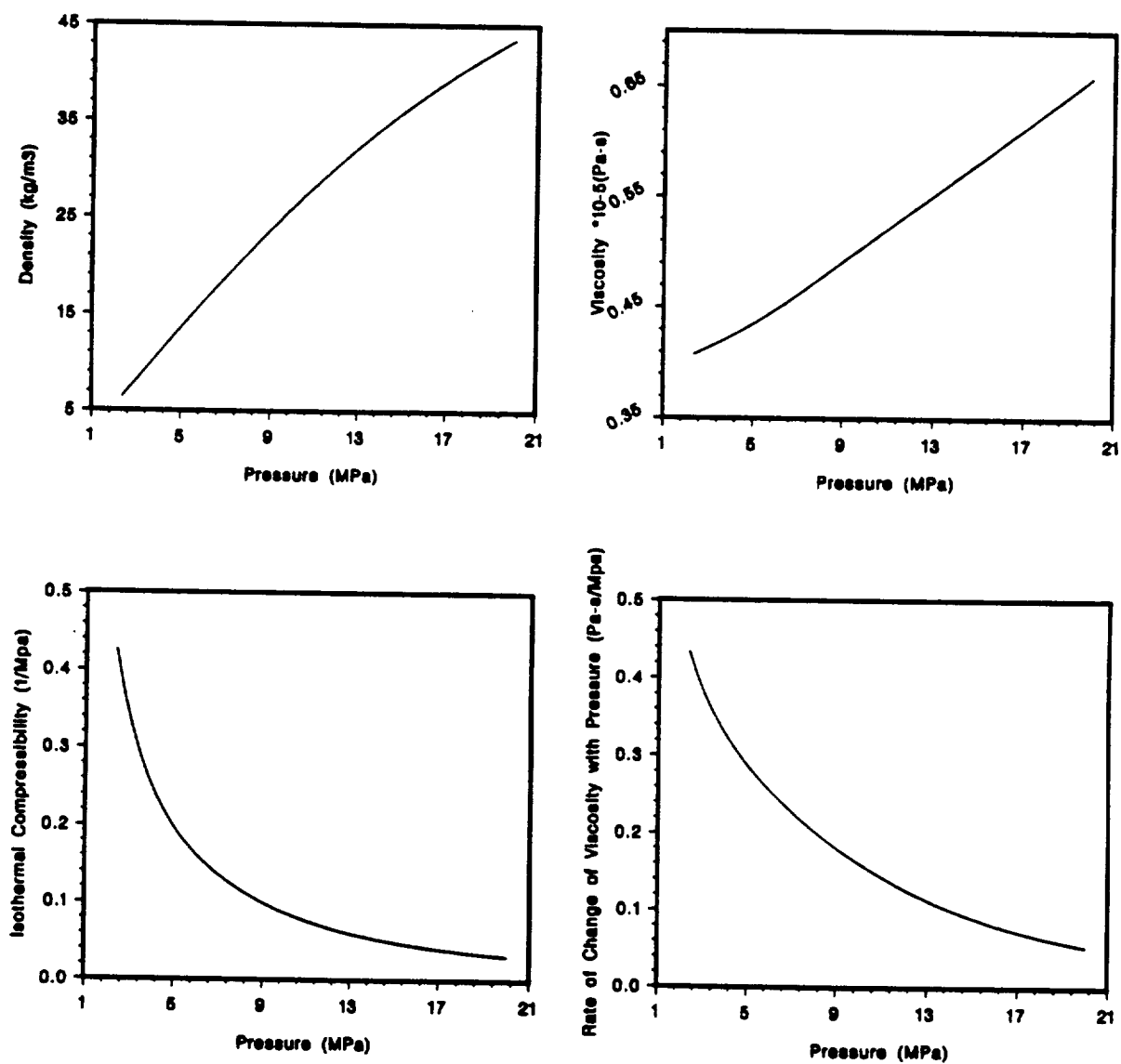


Figure 3.2 Properties of Liquid Hydrogen at 90°K

3.1 Thermophysical Properties Model

Even though the following analysis is valid for any liquid, the two fluids of interest in this research are the cryogenic fluids, liquid oxygen and liquid hydrogen. These are the two working fluids commonly used in the SSME turbopump.

The standard model generally used for representing the thermophysical properties of fluids is the "Modified Benedict-Webb-Ruben (MBWR)" equation of state. This particular model is widely used to correlate thermodynamic property data and a number of computer codes are available to tabulate the properties for various fluids based on this equation of state. The most important of these codes is *NIST Standard Reference Database 12*, published by National Institute of Standards and Technology. This code is available in source form and can be easily integrated into a seal code and this code in its source form is used in the present work.

The main advantages of a MBWR based fluid property model are,

1. Accurate data available for a number of fluids.
2. Easy adaptability to use in a seal code.
3. Correlation of experimental data from various sources.
4. Lends itself to analytical work.

3.2 MBWR Equation of State

The MBWR equation of state in the single phase region is a 32-term equation given below.

$$p = \rho RT + \rho^2(G(1)T + G(2)T^{1/2} + G(3) + G(4)/T + G(5)/T^2) +$$

$$\begin{aligned}
& \rho^3(G(6)T + G(7) + G(8)/T + G(9)/T^2) + \\
& \rho^4(G(10)T + G(11) + G(12)/T) + \rho^5(G(13)) + \\
& \rho^6(G(14)/T + G(15)/T^2) + \rho^7(G(16)/T) + \\
& \rho^8(G(17)/T + G(18)T^2) + \rho^9(G(19)/T^2) + \\
& \rho^3(G(20)/T^2 + G(21)/T^3) e^{\gamma\rho^2} + \\
& \rho^5(G(22)/T^2 + G(23)/T^4) e^{\gamma\rho^2} + \\
& \rho^7(G(24)/T^2 + G(25)/T^3) e^{\gamma\rho^2} + \\
& \rho^9(G(26)/T^2 + G(27)/T^4) e^{\gamma\rho^2} + \\
& \rho^{11}(G(28)/T^2 + G(29)/T^3) e^{\gamma\rho^2} + \\
& \rho^{13}(G(30)/T^2 + G(31)/T^3 + G(32)/T^4) e^{\gamma\rho^2}
\end{aligned} \tag{3.1}$$

where,

p pressure

ρ density

T absolute temperature

$\gamma = -\frac{1}{\rho_c^2}$, ρ_c density at T_{crit}

$G(i), i = 1, 2, \dots, 32$ linear coefficients

The linear coefficients $G(i)$ are computed using experimental and analytical data for various fluids.

The expression for viscosity is given as,

$$\mu = \mu_0(T) + \mu_1(T)\rho + \mu_2(\rho, T) \tag{3.2}$$

$$\mu_0 = \sum_{i=1}^9 G_\nu(i) T^{(4-i)/3} \tag{3.3}$$

$$\mu_1(T) = F_\nu(1) + F_\nu(2) \{F_\nu(3) - \ln(T/F_\nu(4))\}^2 \tag{3.4}$$

$$\mu_2(\rho, T) = e^{F(\rho, T)} - e^{G(T)} \quad (3.5)$$

$$\begin{aligned} F(\rho, T) = & E_\nu(1) + E_\nu(2)H(\rho) + E_\nu(3)\rho^{0.1} + \\ & E_\nu(4)H(\rho)/T^2 + E_\nu(5)\rho^{0.1}/T^{1.5} + \\ & E_\nu(6)/T + E_\nu(7)H(\rho)/T \end{aligned} \quad (3.6)$$

$$G(T) = E_\nu(1) + E_\nu(2)/T \quad (3.7)$$

$$H(\rho) = \rho^{0.5}(\rho - E_\nu(8))/E_\nu(8) \quad (3.8)$$

3.3 Bulk Flow Governing Equations

The bulk flow governing equations for compressible flow are given by Nelson (1985). The original equations are derived for gas seals and the same equations will be used for this analysis using MBWR equation of state.

Continuity:

$$\frac{\partial(\rho hu)}{\partial z} + \frac{1}{R} \frac{\partial(\rho hv)}{\partial \beta} + \frac{\partial(\rho h)}{\partial t} = 0 \quad (3.9)$$

Axial Momentum:

$$\begin{aligned} -\frac{h}{\rho} \frac{\partial p}{\partial z} = & h \left\{ \frac{\partial u}{\partial t} + \frac{v}{R} \frac{\partial u}{\partial \beta} + u \frac{\partial u}{\partial z} \right\} \\ & + f_s \frac{u}{2} \sqrt{u^2 + v^2} + f_r \frac{u}{2} \sqrt{u^2 + (v - w)^2} \end{aligned} \quad (3.10)$$

Circumferential Momentum:

$$\begin{aligned} -\frac{h}{\rho R} \frac{\partial p}{\partial \beta} = & h \left\{ \frac{\partial v}{\partial t} + \frac{v}{R} \frac{\partial v}{\partial \beta} + u \frac{\partial v}{\partial z} \right\} \\ & + f_s \frac{v}{2} \sqrt{u^2 + v^2} + f_r \frac{(v - w)}{2} \sqrt{u^2 + (v - w)^2} \end{aligned} \quad (3.11)$$

A comparison of the above governing equations with the case of constant properties model (Eqs. 2.13–2.15) reveals that these governing equations are essentially the same except for the continuity equation where the density term is retained within

the derivative. The momentum equations are the same, but with a variable density and viscosity.

3.4 Comparison with San Andres (1991)

San Andres (1991), presented an analysis for variable properties based on a finite difference formulation. The solution is based on a finite difference scheme that is based on a method of Launder and Leschziner (1978) and used a SIMPLEC algorithm of Van Doormal and Raithby (1984). In the current work, a completely different solution procedure will be used. The analysis developed for the constant properties case in the previous chapter will be extended to the case of variable properties.

3.5 Perturbation Analysis

In this section, the set of governing equations, Eqs. (3.9–3.11) are perturbed about their steady state values to obtain the zeroth and first order equations. The procedure is similar to the one outlined in Section 2.5.

The assumed form for the dependent variables, film thickness and the fluid properties for perturbation are given as,

$$u(z, \beta, t) = u_0(z, \beta) + \epsilon u_1(z, \beta, t) \quad (3.12)$$

$$v(z, \beta, t) = v_0(z, \beta) + \epsilon v_1(z, \beta, t) \quad (3.13)$$

$$p(z, \beta, t) = p_0(z, \beta) + \epsilon p_1(z, \beta, t) \quad (3.14)$$

$$h(z, \beta, t) = h_0(z, \beta) + \epsilon h_1(z, \beta, t) \quad (3.15)$$

$$\rho(z, \beta, t) = \rho_0(z, \beta) + \epsilon \rho_1(z, \beta, t) \quad (3.16)$$

$$\mu(z, \beta, t) = \mu_0(z, \beta) + \epsilon \mu_1(z, \beta, t) \quad (3.17)$$

where $u_0, v_0, p_0, h_0, \rho_0, \mu_0$ are the zeroth order variables and $u_1, v_1, p_1, h_1, \rho_1, \mu_1$

are the corresponding first order variables, and $\epsilon u_1, \epsilon v_1, \epsilon p_1, \epsilon h_1, \epsilon \rho_1, \epsilon \mu_1$ are the perturbations. The zeroth order variables, ρ_0 and μ_0 and the corresponding first order variables ρ_1, μ_1 are not independent and will be related to the primary variables u, v, p through the MBWR equation of state. Substitution of these expressions into Eqs. (3.9–3.11) and neglecting second and higher order terms yields the sets of zeroth order and first order equations.

$$(\text{zeroth order equations}) + \epsilon(\text{first order equations}) = 0$$

3.5.1 Zeroth Order Equations

The zeroth order equations are given by,

Continuity:

$$\frac{\partial(\rho_0 h_0 v_0)}{\partial z} + \frac{1}{R} \frac{\partial(\rho_0 h_0 v_0)}{\partial \beta} = 0 \quad (3.18)$$

Axial Momentum:

$$\begin{aligned} -\frac{h_0}{\rho_0} \frac{\partial p_0}{\partial z} = & h_0 \left\{ \frac{v_0}{R} \frac{\partial u_0}{\partial \beta} + u_0 \frac{\partial u_0}{\partial z} \right\} \\ & + f_{s0} \frac{u_0}{2} \sqrt{u_0^2 + v_0^2} + f_{r0} \frac{u_0}{2} \sqrt{u_0^2 + (v_0 - w)^2} \end{aligned} \quad (3.19)$$

Circumferential Momentum:

$$\begin{aligned} -\frac{h_0}{\rho_0 R} \frac{\partial p_0}{\partial \beta} = & h_0 \left\{ \frac{v_0}{R} \frac{\partial v_0}{\partial \beta} + u_0 \frac{\partial v_0}{\partial z} \right\} \\ & + f_{s0} \frac{v_0}{2} \sqrt{u_0^2 + v_0^2} + f_{r0} \frac{(v_0 - w)}{2} \sqrt{u_0^2 + (v_0 - w)^2} \end{aligned} \quad (3.20)$$

3.5.2 First Order Equations

The first order equations are given below.

Continuity:

$$\begin{aligned} \frac{\rho_0 v_0}{R} \frac{\partial h_1}{\partial \beta} + \frac{\rho_0 h_0}{R} \frac{\partial v_1}{\partial \beta} + \frac{v_0 h_0}{R} \frac{\partial \rho_1}{\partial \beta} + \rho_0 h_0 \frac{\partial u_1}{\partial z} + u_0 h_0 \frac{\partial \rho_1}{\partial z} \\ + A_u u_1 + A_v v_1 + A_\rho \rho_1 = -\rho_0 u_0 \frac{\partial h_1}{\partial z} - \rho_0 \frac{\partial h_1}{\partial t} - A_h h_1 \end{aligned} \quad (3.21)$$

Axial Momentum:

$$\begin{aligned} \frac{h_0 v_0}{R} \frac{\partial u_1}{\partial \beta} + h_0 u_0 \frac{\partial u_1}{\partial z} + h_0 \frac{\partial p_1}{\partial z} + h_0 \frac{\partial u_1}{\partial t} + B_u u_1 + B_v v_1 + B_\rho \rho_1 \\ + B_\mu \mu_1 = B_h h_1 \end{aligned} \quad (3.22)$$

Circumferential Momentum:

$$\begin{aligned} \frac{h_0 v_0}{R} \frac{\partial v_1}{\partial \beta} + \frac{h_0}{\rho_0} \frac{\partial p_1}{\partial \beta} + h_0 u_0 \frac{\partial v_1}{\partial z} h_0 \frac{\partial v_1}{\partial t} + C_u u_1 + C_v v_1 + C_\rho \rho_1 \\ + C_\mu \mu_1 = C_h h_1 \end{aligned} \quad (3.23)$$

where the coefficients A_u, A_v, \dots etc. are functions of steady state variables u_0, v_0, p_0 and their axial and circumferential gradients.

3.6 Zeroth Order Boundary Conditions

The boundary conditions are similar to the constant properties model, except for exit pressure term which is retained for the variable properties case, since the fluid properties vary with pressure. The boundary conditions for zeroth order equations are shown in Figure 2.6.

The following is a summary of the boundary conditions for the zeroth order equations.

At the inlet:

axial velocity, u_0 :

prior to inlet:

$$u_0(0, \beta) = 0 \quad (3.24)$$

right after inlet:

$$u_0(0, \beta) = u_{01}(0, \beta) \quad (3.25)$$

circumferential velocity, v_0 :

$$v_0(0, \beta) = p s r \times \omega R \quad (3.26)$$

pressure, p_0 :

prior to inlet:

$$p_0(0, \beta) = p_i \quad (3.27)$$

right after inlet:

$$p_0(0, \beta) = p_{01}(0, \beta) \quad (3.28)$$

The pressures p_i , $p_{01}(0, \beta)$ and axial velocity $u_{01}(0, \beta)$ at the inlet are related by,

$$p_i - p_{01}(0, \beta) = \frac{1}{2} \rho_0(0, \beta) u_{01}^2(0, \beta) (1 + \xi_i) \quad (3.29)$$

At the exit, the exit pressure recovery coefficient is assumed to be 1, i.e.,

$$p_{02}(0, \beta) - p_e = \frac{1}{2} \rho_0(0, \beta) u_{02}^2(0, \beta) (1 - 1) \quad (3.30)$$

or,

$$p_{02}(0, \beta) = p_e \quad (3.31)$$

Eq. (3.29) may be rewritten as,

$$p_{01}(0, \beta) = p_i - \frac{1}{2} \rho_0(0, \beta) u_{01}^2(0, \beta) (1 + \xi_i) \quad (3.32)$$

or

$$u_{01}(0, \beta) = \sqrt{\frac{2}{\rho_0(0, \beta) (1 + \xi_i)} (p_i - p_{01}(0, \beta))} \quad (3.33)$$

At the outset, $p_{01}(0, \beta)$ is unknown and must be solved iteratively by requiring that the pressure distribution at the seal exit satisfies the following condition.

$$p_{02}(L, \beta) = p_e \quad (3.34)$$

subject to the constraints of Eqs. (3.26, 3.29)

3.7 Reduction of Zeroth Order Equations

In the following analysis, the original zeroth order equations are reduced into a form suitable for the solution procedure developed in Chapter II.

The fluid properties are, in general, functions of local pressure and temperature as given below.

$$\rho = \rho(p, T) \quad (3.35)$$

$$\mu = \mu(p, T) \quad (3.36)$$

The dependent variables, pressure p and temperature T are functions of the axial and circumferential coordinates, (z, β) .

$$p = p(z, \beta) \quad (3.37)$$

$$T = T(z, \beta) \quad (3.38)$$

or Eqs. (3.35,3.36) may be rewritten as,

$$\rho = \rho(p(z, \beta), T(z, \beta)) \quad (3.39)$$

$$\mu = \mu(p(z, \beta), T(z, \beta)) \quad (3.40)$$

Using chain rule for differentiation, the terms $\frac{\partial \rho_0}{\partial \beta}$, $\frac{\partial \rho_0}{\partial z}$, $\frac{\partial \mu_0}{\partial \beta}$, $\frac{\partial \mu_0}{\partial z}$, which represent the changes in fluid properties with respect to axial and circumferential coordinates, are expressed (subscript 0 refers to zeroth order variables) as,

$$\frac{\partial \rho_0}{\partial z} = \frac{\partial \rho_0}{\partial p_0} \frac{\partial p_0}{\partial z} + \frac{\partial \rho_0}{\partial T_0} \frac{\partial T_0}{\partial z} \quad (3.41)$$

$$\frac{\partial \rho_0}{\partial \beta} = \frac{\partial \rho_0}{\partial p_0} \frac{\partial p_0}{\partial \beta} + \frac{\partial \rho_0}{\partial T_0} \frac{\partial T_0}{\partial \beta} \quad (3.42)$$

$$\frac{\partial \mu_0}{\partial z} = \frac{\partial \mu_0}{\partial p_0} \frac{\partial p_0}{\partial z} + \frac{\partial \mu_0}{\partial T_0} \frac{\partial T_0}{\partial z} \quad (3.43)$$

$$\frac{\partial \mu_0}{\partial \beta} = \frac{\partial \mu_0}{\partial p_0} \frac{\partial p_0}{\partial \beta} + \frac{\partial \mu_0}{\partial T_0} \frac{\partial T_0}{\partial \beta} \quad (3.44)$$

In the following analysis, fluid properties are assumed to be a function of the local pressure and a mean temperature, T^* .

$$\rho = \rho(p, T^*) \quad (3.45)$$

$$\mu = \mu(p, T^*) \quad (3.46)$$

In other words, the fluid flow is treated as an isothermal flow and the fluid properties, density and viscosity are assumed to vary as function of local pressure, $p(z, \beta)$, only. For a constant temperature field, the partial derivatives with respect to temperature T in Eqs. (3.41–3.44) vanish giving the following simplified expressions.

$$\frac{\partial \rho_0}{\partial z} = \frac{\partial \rho_0}{\partial p_0} \frac{\partial p_0}{\partial z} \quad (3.47)$$

$$\frac{\partial \rho_0}{\partial \beta} = \frac{\partial \rho_0}{\partial p_0} \frac{\partial p_0}{\partial \beta} \quad (3.48)$$

$$\frac{\partial \mu_0}{\partial z} = \frac{\partial \mu_0}{\partial p_0} \frac{\partial p_0}{\partial z} \quad (3.49)$$

$$\frac{\partial \mu_0}{\partial \beta} = \frac{\partial \mu_0}{\partial p_0} \frac{\partial p_0}{\partial \beta} \quad (3.50)$$

$\frac{\partial \rho_0}{\partial p_0}$ Rate of change of density with pressure

$\frac{\partial \mu_0}{\partial p_0}$ Rate of change of viscosity with pressure

$\frac{\partial p_0}{\partial z}$ Axial pressure gradient

$\frac{\partial p_0}{\partial \beta}$ Circumferential pressure gradient

The term $\frac{\partial \rho}{\partial p}$ is related to the compressibility of the fluid and is usually represented by the dimensionless parameter, isothermal compressibility, $\frac{1}{\rho} \frac{\partial \rho}{\partial p}|_T$. A larger isothermal compressibility signifies a more compressible fluid.

Using these relations, the Eqs. (3.18–3.20) may be rewritten as given in Appendix B, Eqs. (B.1–B.4). For constant properties, i.e., an incompressible fluid, $\rho_0, \mu_0 =$ constant, or, $\frac{\partial \rho_0}{\partial p_0} = \frac{\partial \mu_0}{\partial p_0} = 0$, and the Eqs. (B.1–B.4) reduce to the Eqs. (A.1–A.4) of the constant properties model.

As in the case of constant properties model, the reduced zeroth order equations may be rewritten with all β -dependent terms on the right-hand side as,

$$\begin{bmatrix} \frac{\partial u_0}{\partial z} \\ \frac{\partial v_0}{\partial z} \\ \frac{\partial p_0}{\partial z} \end{bmatrix} = \begin{bmatrix} F_u(u_0, v_0, p_0, \frac{\partial u_0}{\partial \beta}, \frac{\partial v_0}{\partial \beta}, \frac{\partial p_0}{\partial \beta}) \\ F_v(u_0, v_0, p_0, \frac{\partial u_0}{\partial \beta}, \frac{\partial v_0}{\partial \beta}, \frac{\partial p_0}{\partial \beta}) \\ F_p(u_0, v_0, p_0, \frac{\partial u_0}{\partial \beta}, \frac{\partial v_0}{\partial \beta}, \frac{\partial p_0}{\partial \beta}) \end{bmatrix} \quad (3.51)$$

The functions F_u, F_v, F_p for the variable properties model are given in Appendix B.

3.8 Solution Procedure for Zeroth Order Equations

The solution procedure for zeroth order solution is exactly the same as discussed in Section 2.7. The only difference is that the fluid properties and their dependent terms are updated at each grid point during numerical integration.

3.9 Reduction of First Order Equations

The original first order equations given in Eqs. (3.21–3.23) are reduced similar the zeroth order equations.

The first order variables in the first order equations, Eqs.(3.21–3.23) are u_1 , v_1 , p_1 , ρ_1 , μ_1 . Out of these variables only u_1 , v_1 , p_1 are primary variables. The remaining two variables ρ_1 , μ_1 are related to p_1 using the property relations based on the MBWR equation of state.

The relationship first order variables p_1 and ρ_1 is given by

$$p_1 = A_{\rho 1} \rho_1 \quad (3.52)$$

where,

$$A_{\rho 1} = \frac{\partial p}{\partial \rho} \quad (3.53)$$

The above relationship is obtained by perturbing the MBWR equation of state with respect to pressure and density and equating the terms on both sides. From a different perspective the ratio $\frac{p_1}{\rho_1}$ is a ratio of two infinitesimally small quantities, which is nothing but the derivative $\frac{\partial p}{\partial \rho}$.

In the expression for viscosity given in Eqs. (3.2–3.8), the relation between pressure and viscosity is not explicit. Let the first order variables μ_1 and ρ_1 be related as,

$$\mu_1 = B_{\mu 1} \rho_1 \quad (3.54)$$

where,

$$B_{\mu 1} = \frac{\partial \mu}{\partial \rho} \quad (3.55)$$

The first order variables p_1 and μ_1 are then related through,

$$p_1 = A_{\mu 1} \mu_1 \quad (3.56)$$

where,

$$A_{\mu 1} = A_{\rho 1} B_{\mu 1} \quad (3.57)$$

The terms $\frac{\partial \rho}{\partial \beta}$ and $\frac{\partial \mu}{\partial \rho}$ are obtained by differentiating Eqs. (3.1,3.2-3.8) with respect to density ρ and viscosity μ respectively and these expressions are given in Appendix F.

Using the relations Eqs. (3.52-3.57), the first order equations are rewritten in terms of the primary first order variables u_1 , v_1 and p_1 .

Continuity:

$$\begin{aligned} \frac{\rho_0 v_0}{R} \frac{\partial h_1}{\partial \beta} + \frac{\rho_0 h_0}{R} \frac{\partial v_1}{\partial \beta} + \frac{v_0 h_0}{R} \frac{\partial \rho_1}{\partial \beta} + \rho_0 h_0 \frac{\partial u_1}{\partial z} + u_0 h_0 \frac{\partial p_1}{\partial z} + h_0 A_{\rho 1} \frac{\partial p_1}{\partial t} \\ + A_u u_1 + A_v v_1 + A_p p_1 = -\rho_0 u_0 \frac{\partial h_1}{\partial z} - \rho_0 \frac{\partial h_1}{\partial t} - A_h h_1 \end{aligned} \quad (3.58)$$

Axial Momentum:

$$\begin{aligned} \frac{h_0 v_0}{R} \frac{\partial u_1}{\partial \beta} + h_0 u_0 \frac{\partial u_1}{\partial z} + \frac{h_0}{\rho_0} \frac{\partial p_1}{\partial z} + h_0 \frac{\partial u_1}{\partial t} + B_u u_1 + B_v v_1 + B_p p_1 \\ = B_h h_1 \end{aligned} \quad (3.59)$$

Circumferential Momentum:

$$\begin{aligned} \frac{h_0 v_0}{R} \frac{\partial v_1}{\partial \beta} + \frac{h_0}{\rho_0 R} \frac{\partial p_1}{\partial \beta} + h_0 u_0 \frac{\partial v_1}{\partial z} + h_0 \frac{\partial v_1}{\partial t} + C_u u_1 + C_v v_1 + C_p p_1 \\ = C_h h_1 \end{aligned} \quad (3.60)$$

The coefficients A_u, A_v, \dots for a variable properties model are defined in Appendix B.

3.10 First Order Boundary Conditions

Perturbing the zeroth order boundary conditions of Eqs. (3.26,3.29,3.34) yield the following first order boundary conditions.

At the inlet:

circumferential velocity, v_1 :

$$v_1(0, \beta) = 0 \quad (3.61)$$

pressure, p_1 :

$$p_1(0, \beta) = -\frac{1}{2}\{2\rho_0(0, \beta)u_0(0, \beta)u_1(0, \beta) + u_{01}^2(0, \beta)\rho_1(0, \beta)\} \quad (3.62)$$

At the exit:

pressure, p_1 :

$$p_1(0, \beta) = 0 \quad (3.63)$$

Using the relation between p_1 and ρ_1 , Eq. (3.62) may be rewritten as,

$$p_1(0, \beta) = -\frac{1}{\{1 + 0.5(1 + \xi_i)u_{01}^2(0, \beta)\frac{\partial \rho}{\partial p}\}}\{(1 + \xi_i)\rho_0(0, \beta)u_0(0, \beta)\}u_1(0, \beta) \quad (3.64)$$

3.11 Solution of First Order Equations

The same procedure developed for the constant properties model is used for this case. The set of first order equations in Eqs.(3.58-3.60) are further reduced by employing "separation of variables" technique for an assumed *small* motion of the vibrating rotor.

The right hand side of the system of first order equations consists of harmonic forcing functions $h_0, \frac{\partial h_0}{\partial x}, \frac{\partial h_0}{\partial \beta}, h_1, \frac{\partial h_1}{\partial \beta}, \frac{\partial h_1}{\partial x}$. Based on this fact, the solution is assumed

to be harmonic functions of α and β .

$$p_{1x} = a_1(z, \beta) \cos \alpha + a_2(z, \beta) \sin \alpha \quad (3.65)$$

$$u_{1x} = a_3(z, \beta) \cos \alpha + a_4(z, \beta) \sin \alpha \quad (3.66)$$

$$v_{1x} = a_5(z, \beta) \cos \alpha + a_6(z, \beta) \sin \alpha \quad (3.67)$$

$$p_{1y} = b_1(z, \beta) \cos \alpha + b_2(z, \beta) \sin \alpha \quad (3.68)$$

$$u_{1y} = b_3(z, \beta) \cos \alpha + b_4(z, \beta) \sin \alpha \quad (3.69)$$

$$v_{1y} = b_5(z, \beta) \cos \alpha + b_6(z, \beta) \sin \alpha \quad (3.70)$$

Using the above substitutions in the set of first order equations Eqs. (3.58–3.60) yields 12 coupled linear partial differential equations.

The first order boundary conditions expressed in the assumed solution variables are:

$$a_1(0, \beta) = -\frac{(1 + \xi_i) \rho_0(0, \beta) a_3(0, \beta)}{\{1 + 0.5(1 + \xi_i) u_{01}^2(0, \beta) \frac{\partial \rho}{\partial p}\}} \quad (3.71)$$

$$a_2(0, \beta) = -\frac{(1 + \xi_i) \rho_0(0, \beta) a_4(0, \beta)}{\{1 + 0.5(1 + \xi_i) u_{01}^2(0, \beta) \frac{\partial \rho}{\partial p}\}} \quad (3.72)$$

$$a_5(0, \beta) = 0 \quad (3.73)$$

$$a_6(0, \beta) = 0 \quad (3.74)$$

$$a_1(L, \beta) = 0 \quad (3.75)$$

$$a_2(L, \beta) = 0 \quad (3.76)$$

$$b_1(0, \beta) = -\frac{(1 + \xi_i) \rho_0(0, \beta) b_3(0, \beta)}{\{1 + 0.5(1 + \xi_i) u_{01}^2(0, \beta) \frac{\partial \rho}{\partial p}\}} \quad (3.77)$$

$$b_2(0, \beta) = -\frac{(1 + \xi_i) \rho_0(0, \beta) b_4(0, \beta)}{\{1 + 0.5(1 + \xi_i) u_{01}^2(0, \beta) \frac{\partial \rho}{\partial p}\}} \quad (3.78)$$

$$b_5(0, \beta) = 0 \quad (3.79)$$

$$b_6(0, \beta) = 0 \quad (3.80)$$

$$b_1(L, \beta) = 0 \quad (3.81)$$

$$b_2(L, \beta) = 0 \quad (3.82)$$

The solution procedure follows the same steps as explained in Chapter II.

CHAPTER IV

THERMAL EFFECTS MODEL

Yang *et al.* (1992) and San Andres *et al.* (1992) conducted a thorough investigation of thermohydrodynamic (THD) analysis for cryogenic seals. Yang developed an approximate THD analysis and provided steady state solution for the case of a centered seal. San Andres (1992) introduced a full set of bulk flow governing equations for THD analysis and investigated it with a finite difference based numerical solution. The results from their study show that for some cryogenic fluids temperature rise due to friction at the rotor surface may lead to a two phase flow, seriously affecting the performance of the turbomachine.

The goal of this work is to extend the solution procedure developed in previous chapters to a THD analysis. The governing equations used for this analysis are based on San Andres *et al.* (1992) and are given in Eqs. (4.1–4.4). In the analysis developed in this chapter, the zeroth order equations will be solved for the primary variables, u_0 , v_0 , p_0 and T_0 for a centered seal. The temperature distribution will then be used with the variable properties model developed in Chapter III to compute the dynamic coefficients. In other words, perturbation due to temperature are not included in the analysis. The goal is to show the viability of current analysis to handle thermal effects of the energy equation.

Continuity:

$$\frac{\partial}{\partial t}(\rho h) + \frac{\partial}{\partial z}(\rho h u) + \frac{\partial}{\partial q}(\rho h v) = 0 \quad (4.1)$$

Axial Momentum:

$$\frac{\partial}{\partial t}(\rho u h) + \frac{\partial}{\partial z}(\rho h u^2) + \frac{\partial}{\partial q}(\rho h u v) = -h \frac{\partial p}{\partial z} + \tau_{zv}|_0^h \quad (4.2)$$

Circumferential Momentum:

$$\frac{\partial}{\partial t}(\rho h v) + \frac{\partial}{\partial z}(\rho h u v) + \frac{\partial}{\partial q}(\rho h v^2) = -h \frac{\partial p}{\partial q} + \tau_{qv}|_0^h \quad (4.3)$$

Energy Equation:

$$C_p \left\{ \frac{\partial}{\partial t}(\rho h T) + \frac{\partial}{\partial z}(\rho h u T) + \frac{\partial}{\partial q}(\rho h v T) \right\} + Q_s = T \beta_v h \left\{ \frac{\partial p}{\partial t} + v \frac{\partial p}{\partial q} + u \frac{\partial p}{\partial z} \right\} \\ + \omega R(\tau_{qv}|_h) - v(\tau_{qv}|_0^h) - u(\tau_{zv}|_0^h) \quad (4.4)$$

where, $q = R\beta$ and the shear stress terms, τ_{zv} , τ_{qv} etc., are given as,

$$\tau_{zv}|_0^h = -\rho(f_s \frac{u}{2} \sqrt{u^2 + v^2} + f_r \frac{u}{2} \sqrt{u^2 + (v-w)^2}) \quad (4.5)$$

$$\tau_{qv}|_0^h = -\rho(f_s \frac{v}{2} \sqrt{u^2 + v^2} + f_r \frac{(v-w)}{2} \sqrt{u^2 + (v-w)^2}) \quad (4.6)$$

$$\tau_{qv}|_h = \frac{h}{2} \frac{\partial p}{\partial q} + \frac{\mu}{4h} \left\{ f_s \frac{v}{2} R_s - f_r \frac{(v-w)}{2} R_r \right\} \quad (4.7)$$

The heat transferred, Q_s is given by,

$$Q_s = 0 \quad (4.8)$$

$$= h_r(T - T_{rotor}) + h_s(T - T_{seal}) \quad (4.9)$$

Eq. (4.8) is for adiabatic case where there is no heat transfer, while Eq. (4.9) is for a general case. The stator and rotor Reynolds numbers are given as,

$$R_s = \frac{2\rho h}{\mu} \sqrt{u^2 + v^2} \quad (4.10)$$

$$R_r = \frac{2\rho h}{\mu} \sqrt{u^2 + (v-w)^2} \quad (4.11)$$

The heat transfer coefficients for rotor and stator are given by,

$$h_s(z, q) = \rho C_p \sqrt{u^2 + v^2} \left(\frac{f_s}{2} \right) \left(\frac{\mu C_p}{k} \right)^{-\frac{2}{3}} \quad (4.12)$$

$$h_r(z, q) = \rho C_p \sqrt{u^2 + (v-w)^2} \left(\frac{f_r}{2} \right) \left(\frac{\mu C_p}{k} \right)^{-\frac{2}{3}} \quad (4.13)$$

The fluid properties, density ρ and viscosity μ are assumed to be a function of local pressure and temperature. MWBR equation of state is used to represent the fluid properties.

The variation in fluid properties with respect to the axial and circumferential coordinates, $\frac{\partial \rho_0}{\partial \beta}$, $\frac{\partial \rho_0}{\partial z}$, $\frac{\partial \mu_0}{\partial \beta}$, $\frac{\partial \mu_0}{\partial z}$ are expressed as (Eq. 3.39–3.40),

$$\frac{\partial \rho_0}{\partial z} = \frac{\partial \rho_0}{\partial p_0} \frac{\partial p_0}{\partial z} + \frac{\partial \rho_0}{\partial T_0} \frac{\partial T_0}{\partial z} \quad (4.14)$$

$$\frac{\partial \rho_0}{\partial \beta} = \frac{\partial \rho_0}{\partial p_0} \frac{\partial p_0}{\partial \beta} + \frac{\partial \rho_0}{\partial T_0} \frac{\partial T_0}{\partial \beta} \quad (4.15)$$

$$\frac{\partial \mu_0}{\partial z} = \frac{\partial \mu_0}{\partial p_0} \frac{\partial p_0}{\partial z} + \frac{\partial \mu_0}{\partial T_0} \frac{\partial T_0}{\partial z} \quad (4.16)$$

$$\frac{\partial \mu_0}{\partial \beta} = \frac{\partial \mu_0}{\partial p_0} \frac{\partial p_0}{\partial \beta} + \frac{\partial \mu_0}{\partial T_0} \frac{\partial T_0}{\partial \beta} \quad (4.17)$$

where $\frac{\partial u_0}{\partial \beta}$, $\frac{\partial v_0}{\partial \beta}$, $\frac{\partial p_0}{\partial \beta}$, $\frac{\partial T_0}{\partial \beta}$ are the circumferential gradients of the primary variables, u , v , p , and T respectively.

Using these relations, Eqs. (4.1–4.4) may be rewritten as,

$$\begin{aligned} \rho \frac{\partial h}{\partial t} + \rho u \frac{\partial h}{\partial z} + \rho v \frac{\partial h}{\partial q} + \rho h \frac{\partial u}{\partial z} + \rho h \frac{\partial v}{\partial q} + \frac{\partial T}{\partial t} (h \frac{\partial \rho}{\partial T}) + \frac{\partial T}{\partial z} (h u \frac{\partial \rho}{\partial T}) \\ + \frac{\partial T}{\partial q} (h v \frac{\partial \rho}{\partial T}) + \frac{\partial p}{\partial t} (h \frac{\partial \rho}{\partial p}) + \frac{\partial p}{\partial z} (h u \frac{\partial \rho}{\partial p}) + \frac{\partial p}{\partial q} (h v \frac{\partial \rho}{\partial p}) = 0 \end{aligned} \quad (4.18)$$

$$\rho h \frac{\partial u}{\partial t} + \rho h u \frac{\partial u}{\partial z} + \rho h v \frac{\partial u}{\partial q} = -h \frac{\partial p}{\partial z} + \tau_{zu}|_0^h \quad (4.19)$$

$$\rho h \frac{\partial v}{\partial t} + \rho h \frac{\partial v}{\partial z} + \rho h v \frac{\partial v}{\partial q} = -h \frac{\partial p}{\partial q} + \tau_{qv}|_0^h \quad (4.20)$$

$$\begin{aligned} \rho C_p h \left\{ \frac{\partial T}{\partial t} + u \frac{\partial T}{\partial z} + v \frac{\partial T}{\partial q} \right\} + Q_s = T \beta_v h \left\{ \frac{\partial p}{\partial t} + v \frac{\partial p}{\partial q} + u \frac{\partial p}{\partial z} \right\} \\ + \omega R (\tau_{qv}|_h) - v (\tau_{qv}|_0^h) - u (\tau_{zu}|_0^h) \end{aligned} \quad (4.21)$$

where,

ρ density

μ	dynamic viscosity
$\frac{\partial \rho}{\partial p}$	rate of change of density with pressure
$\frac{\partial \rho}{\partial T}$	rate of change of density with absolute temperature
C_p	specific heat at constant pressure, $\frac{\partial H}{\partial T} _p$
β_v	volumetric expansion coefficient, $\frac{1}{v} \frac{\partial v}{\partial T} _p$
k	thermal conductivity of fluid
f_s	stator friction factor
f_r	rotor friction factor

4.1 Zeroth Order Equations

The zeroth order equations are obtained by dropping the time dependent terms in Eqs. (4.18–4.21).

The above equations may again be written in the following fashion.

$$\begin{bmatrix} \frac{\partial u_0}{\partial z} \\ \frac{\partial v_0}{\partial z} \\ \frac{\partial p_0}{\partial z} \\ \frac{\partial T_0}{\partial z} \end{bmatrix} = \begin{bmatrix} F_u(u_0, v_0, p_0, T_0, \frac{\partial u_0}{\partial \beta}, \frac{\partial v_0}{\partial \beta}, \frac{\partial p_0}{\partial \beta}, \frac{\partial T_0}{\partial \beta}) \\ F_v(u_0, v_0, p_0, T_0, \frac{\partial u_0}{\partial \beta}, \frac{\partial v_0}{\partial \beta}, \frac{\partial p_0}{\partial \beta}, \frac{\partial T_0}{\partial \beta}) \\ F_p(u_0, v_0, p_0, T_0, \frac{\partial u_0}{\partial \beta}, \frac{\partial v_0}{\partial \beta}, \frac{\partial p_0}{\partial \beta}, \frac{\partial T_0}{\partial \beta}) \\ F_T(u_0, v_0, p_0, T_0, \frac{\partial u_0}{\partial \beta}, \frac{\partial v_0}{\partial \beta}, \frac{\partial p_0}{\partial \beta}, \frac{\partial T_0}{\partial \beta}) \end{bmatrix} \quad (4.22)$$

The functions F_u, F_v, F_p, F_T are given in Appendix C.

4.2 Zeroth Order Boundary Conditions

The boundary conditions for the zeroth order or steady state equations is illustrated in Figure 4.1.

The following is a summary of the boundary conditions for the zeroth order equations.

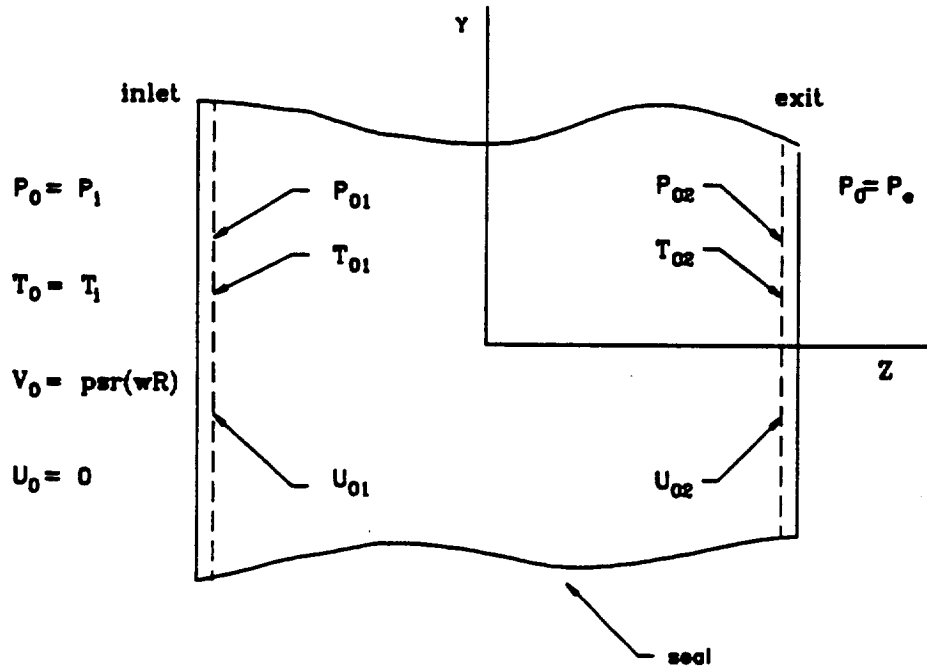


Figure 4.1 Zeroth Order Boundary Conditions

At the inlet:

axial velocity, u_0 :

prior to inlet:

$$u_0(0, \beta) = 0 \quad (4.23)$$

right after inlet:

$$u_0(0, \beta) = u_{01}(0, \beta) \quad (4.24)$$

circumferential velocity, v_0 :

$$v_0(0, \beta) = psr \times \omega R \quad (4.25)$$

pressure, p_0 :

prior to inlet:

$$p_0(0, \beta) = p_i \quad (4.26)$$

right after inlet:

$$p_0(0, \beta) = p_{01}(0, \beta) \quad (4.27)$$

temperature, T_0 :

prior to inlet:

$$T_0(0, \beta) = T_i \quad (4.28)$$

right after inlet:

$$T_0(0, \beta) = T_{01} \quad (4.29)$$

The pressures p_i , $p_{01}(0, \beta)$ and axial velocity $u_{01}(0, \beta)$ at the inlet are related by,

$$p_i - p_{01}(0, \beta) = \frac{1}{2} \rho_0(0, \beta) u_{01}^2(0, \beta) (1 + \xi_i) \quad (4.30)$$

$$T_0(0, \beta) = T_i - \frac{u_{01}^2(0, \beta)}{2C_{pi}} (1 + \xi_i) \left\{ 1 - \frac{\rho_0(0, \beta)}{\rho_i} (1 - T_i \beta_{wi}) \right\} \quad (4.31)$$

4.3 Solution Procedure for Zeroth Order Equations

The solution is based on an iterative procedure and the steps involved are explained below.

The continuity and momentum equations are solved using the solution procedure developed in previous chapters. At the outset, a nominal temperature distribution is assumed for the entire flow field. Typically, a constant temperature, T_i , temperature at inlet, is assumed. At the end of convergence of the continuity and momentum equations for a given temperature field, the energy equation is integrated using the updated variables u , v and p . from the previous iteration. At the end of one complete integration of energy equation, a new temperature distribution, $T_{new}(z, \beta)$, is available and it is used to update the fluid properties.

The set of continuity and momentum equations are again solved with the up-

dated properties until the solution converges. The new u , v , and p are then used in the integration of the energy equation to obtain a new updated temperature distribution. The cyclic procedure is repeated until two successive temperature distributions converge to a specified tolerance.

Typically, it takes about 6–8 iterations for the solution to converge.

4.4 Comparison of Current Analysis with San Andres *et al.*

San Andres *et al.* (1992), uses a finite difference scheme to solve the coupled, nonlinear PDEs of continuity, momentum and energy equations. The procedure they use is based on the forward marching solution of Launder and Leschziner (1978) and uses SIMPLEC algorithm of Van Doormal and Raithby (1984). The flow domain is divided into control volumes and governing equations are integrated on the control volumes to give sets of nonlinear algebraic difference equations for each primary variable. Then they implement an iterative procedure where the continuity and momentum equations are solved followed by the energy equation. The continuity and momentum equations are allowed to converge to an intermediate limit and then the energy equation is solved. Fluid properties are updated and the procedure is repeated until the solution converges.

The main advantage of the solution procedure used in the current work is its simplicity.

In the current work, an iterative procedure based on the direct integration of governing equations, is implemented. The problem is reduced to repeatedly solving a system of 3 ODEs until the temperature distribution converges.

San Andres *et al.* reported that their method requires about 20 iterations for the solution to converge. Current solution procedure takes about 6–8 iterations to

converge.

4.5 First Order Solution

The equations used for first order solution are the same as variables properties model. As mentioned earlier, the governing equations are not perturbed with respect to temperature T . The temperature distribution obtained from the zeroth order solution is used to update the properties as a function of local pressure and temperature and the dynamic coefficients are computed using the variable properties model of Chapter III.

CHAPTER V

ARBITRARY PROFILE SEALS

The typical seal geometry of an interstage seal of SSME turbopump has either a straight or a tapered (convergent) axial profile as shown in Figure 1.2. This nominal seal profile may be altered during the course of its operation, for example, as in the case of SSME interstage seals due to mechanical and thermal distortions. An example of predicted seal profile of an interstage seal is shown in Figure 1.3. Tests at NASA/MSFC reveal that seals initially designed with a large convergent taper have become divergent over a part of the length of the seal during the course of their operation changing the dynamic characteristics of that seals.

For the purpose of this study, an arbitrary profile seal is a seal whose geometry in axial and circumferential directions may vary in any specified fashion. For example, the distorted seal shown in Figure 1.3 would be an example of an arbitrary profile seal.

This change in the seal profile may be due to distortion such as in the interstage seals of SSME turbopump or by design itself in order to enhance some optimum dynamic characteristics of the seal. It has been known for a long time that convergent

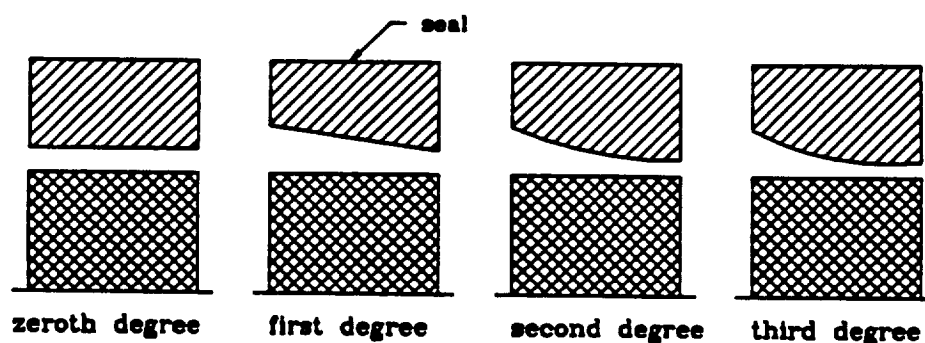


Figure 5.1 Examples of Seal Axial Profiles

seals provide a higher stiffness than a straight seal. It is also a fact that divergent seals under certain conditions lose stiffness with eccentricity. Generally, of all the variables that go into the design of an annular seal, the variable that can be easily modified is the profile of the seal whether it be a straight, tapered or more exotic shapes. As will be shown with reference to an elliptical seal, even a small change in seal profile can have a noticeable effect on the dynamic characteristics of the seal. The fact that dynamic coefficients can be varied with the profile may be used as a design criterion to build a seal with a set of optimum dynamic characteristics.

5.1 Example of an Arbitrary Profile Seal: Elliptical Seal

Annular seals initially designed with a circular cross section have been found to acquire, under load, an oval shape similar to an ellipse. Currently, investigations are being carried out to study the effect of such a change in profile on the flow rates and dynamic characteristics of these seals. This is the motivation behind the following study of an elliptical seal.

An elliptical seal is an annular seal with an elliptical cross-section as shown in Figure 5.3. The clearance function for this seal varies in the circumferential direction as opposed to a constant clearance for a typical straight or tapered seals with circular cross-sections. The degree of curvature of the elliptical seal compared to a circular seal is specified by the parameter *ellipticity*, δ as,

$$\delta = \frac{c_x - c_y}{c_x} \quad (5.1)$$

where c_x and c_y are radial clearances at semi-major and semi-minor axes respectively.

For $\delta = 0$, the seal is a circular seal and for $\delta = 1$ the stator contacts the rotor and for any value in between, i.e., $0 < \delta < 1$, the seal is an elliptical seal. Figure 5.4

illustrates an elliptical seal with various ellipticity factors.

The following different cases of axial profile are studied in detail for this elliptical seal.

1. Straight Profile
2. Linear Profile
3. Quadratic Profile

These axial profiles correspond to zeroth, first order and second curves shown in Figure 5.1.

The equation of an ellipse is given by,

$$x = a \cos \beta \quad (5.2)$$

$$y = b \sin \beta \quad (5.3)$$

where a and b are the semi-major and semi-minor axes respectively. At any angular position β along the circumference, the radius r of the ellipse is given by,

$$r(z, \beta) = \sqrt{(a \cos \beta)^2 + (b \sin \beta)^2} \quad (5.4)$$

and the clearance c at this location is given by,

$$c(z, \beta) = r(z, \beta) - R \quad (5.5)$$

where R is the radius of the rotor. If the semi-major and semi-minor axes of the ellipse vary in some functional form along the length of the seal, the clearance function of this seal is given by,

$$c(z, \beta) = \sqrt{(f_1(z) \cos \beta)^2 + (f_2(z) \sin \beta)^2} - R \quad (5.6)$$

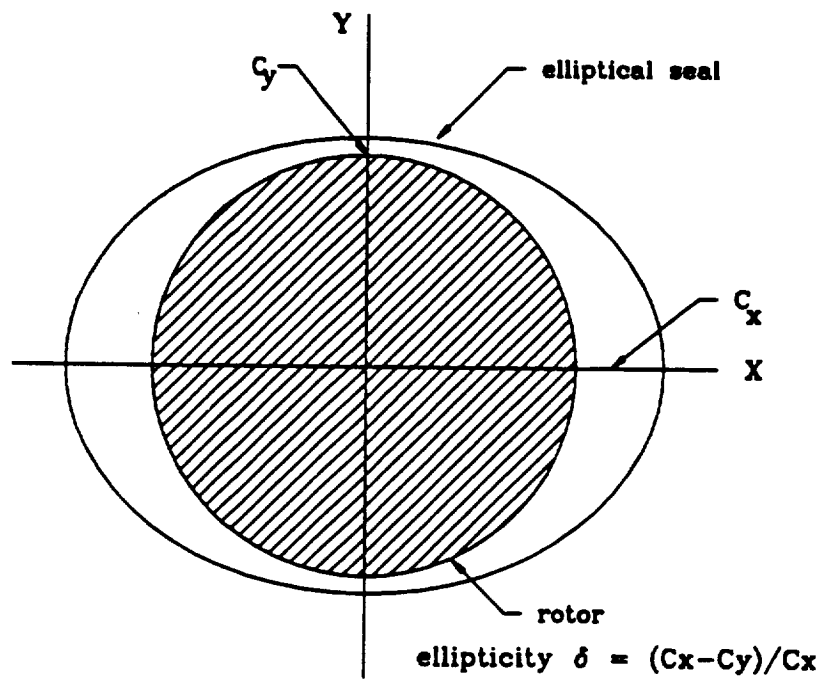
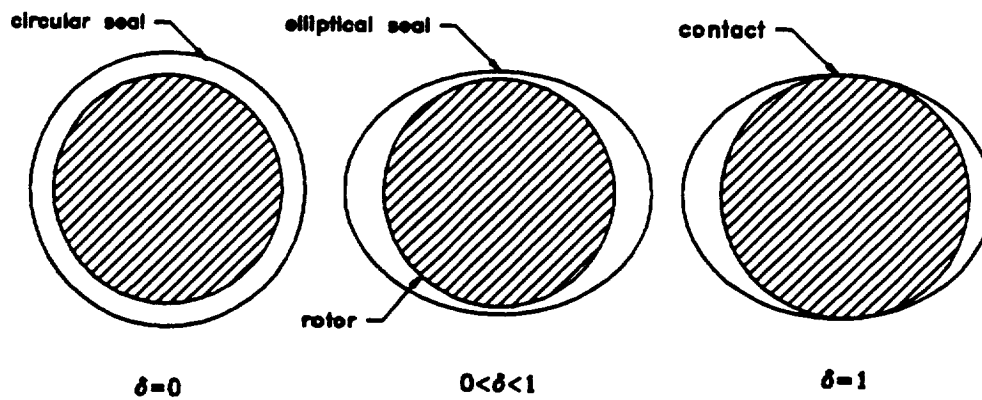


Figure 5.2 Elliptical Seal

Figure 5.3 Elliptical Seal with Various Ellipticity Factors, δ

where $f_1(z)$ and $f_2(z)$ are the semi-major and semi-minor axes variations along the z -axis of the ellipse. The function $f_1(z)$ for straight, linear and quadratic axial profiles are given below.

$$f_1(z) = a_1 \quad (5.7)$$

$$f_1(z) = a_1 + a_2 z \quad (5.8)$$

$$f_1(z) = a_1 + a_2 z + a_3 z^2 \quad (5.9)$$

$$f_2(z) = b_1 \quad (5.10)$$

$$f_2(z) = b_1 + b_2 z \quad (5.11)$$

$$f_2(z) = b_1 + b_2 z + b_3 z^2 \quad (5.12)$$

where $a_1, a_2, a_3, b_1, b_2, b_3$ are constants that define the curvature of the axial profile.

The curvature of the ellipse in the circumferential direction is varied using the parameter, ellipticity δ . The ellipticity of the seal is defined as (Figure 5.3), $c_x = c_i$ at inlet and $c_x = c_e$ at exit. Therefore, the clearance c_v is given by,

$$c_v = c_x(1 - \delta) \quad (5.13)$$

The Appendix E provides the functions $f_1(z)$ and $f_2(z)$ for straight, linear and quadratic axial profiles as a function of δ .

5.2 Results

Three different axial profiles are considered for the elliptical seal and their dynamic characteristics are studied with reference to similar seals with circular cross-sections. Results are provided for two cases.

1. Straight elliptical seal compared to a straight circular seal.

2. Elliptical seal with a linear axial profile compared to a similar seal with a curved (quadratic) profile.

5.2.1 Straight Elliptical Seal vs. Straight Circular Seal

The plots shown in Figures 5.4–5.7 are comparisons for a straight seal with two ellipticity factors. For, $\delta = 0$, the seal is a circular (straight). For, $\delta = 0.4$, the seal is an elliptical (straight) seal. The various coefficients are normalized with respect to straight circular seal ($\delta = 0$).

Figure 5.4 shows the variation of direct stiffness for both seals as a function of eccentricity ratio. Even though, both seals have roughly similar stiffness to start with, for straight elliptical seal, both K_{xx} and K_{yy} decrease with eccentricity. In other words, there is a loss in stiffness with eccentric operation.

The cross coupled stiffness in Figure 5.5 shows the opposite trend, i.e., they increase with eccentricity, almost exponentially. Such a large increase in cross coupled coefficients should be a cause for concern from a stability point of view.

Damping, shown in Figure 5.6, increases slightly with eccentricity but not to the extent of the circular seal. Leakage, shown in Figure 5.7, is smaller for elliptical seal.

In short, the elliptical seal compared with the circular seal shows the following trends as a function of eccentricity.

1. Loss in direct stiffness.
2. Large increase in cross coupled stiffness.
3. Relatively small increase in damping.
4. Reduction in leakage.

Except for the reduced leakage rate, all other comparisons point to the fact that

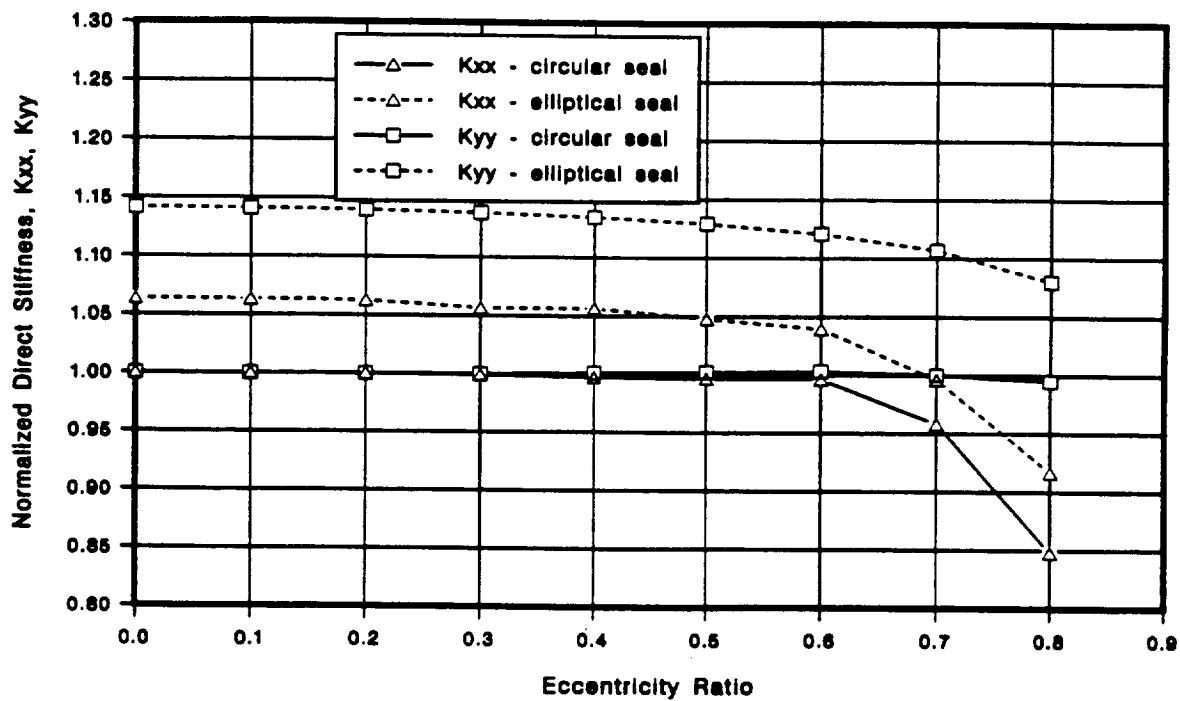


Figure 5.4 Normalized Direct Stiffness for Elliptical Seal (Straight), ($\delta=0$, $\delta=0.4$)

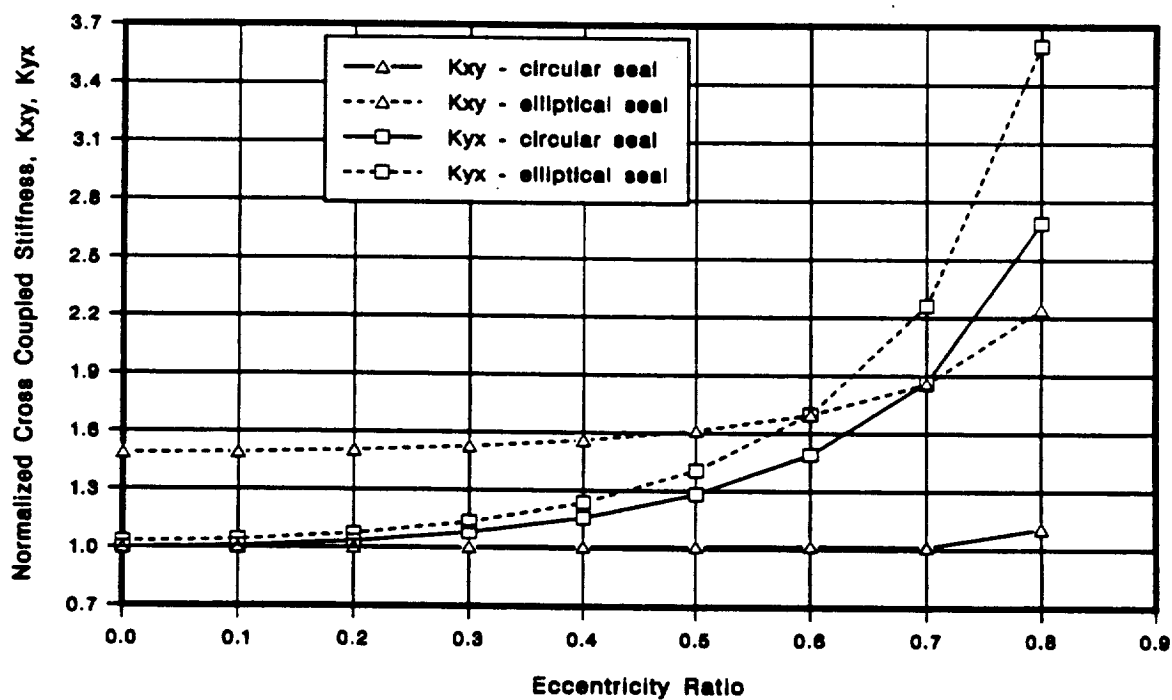


Figure 5.5 Normalized Cross Coupled Stiffness for Elliptical Seal (Straight), ($\delta=0$, $\delta=0.4$)

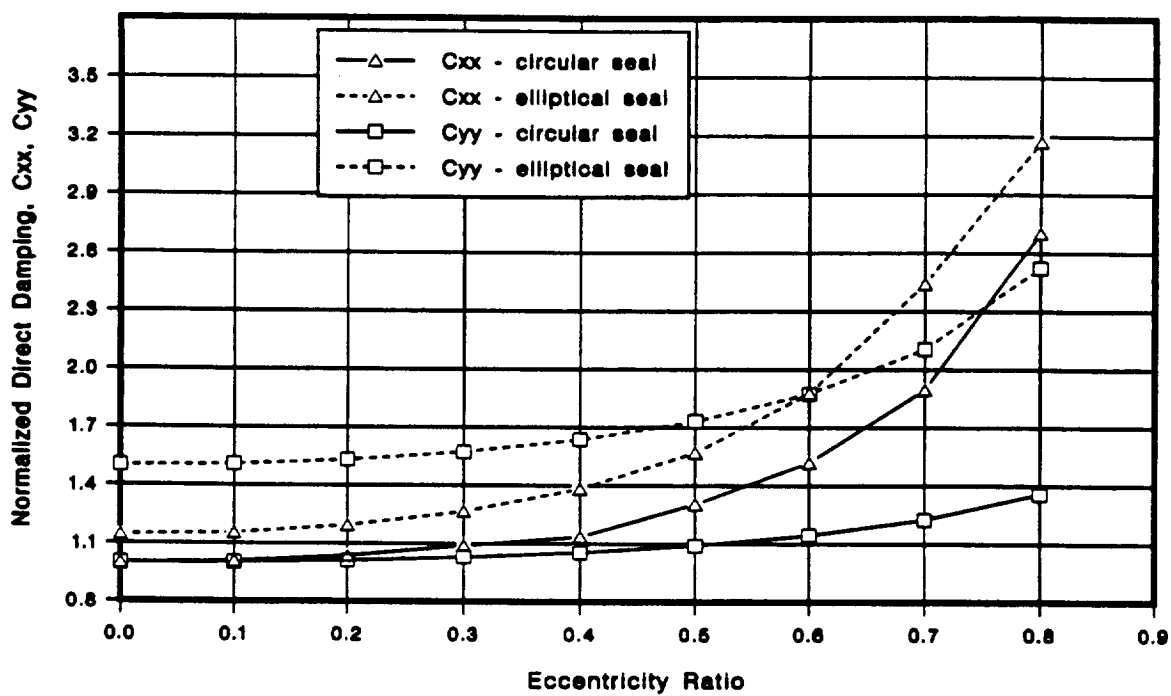


Figure 5.6 Normalized Direct Damping for Elliptical Seal (Straight), ($\delta=0$, $\delta=0.4$)

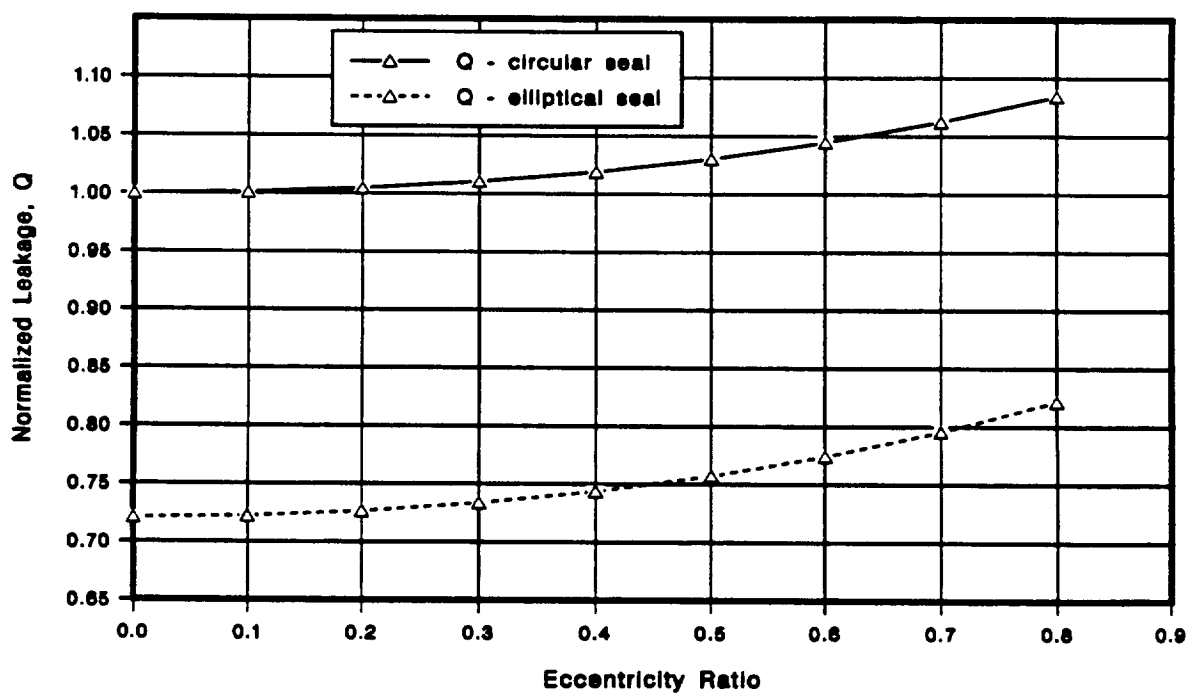


Figure 5.7 Normalized Leakage for Elliptical Seal (Straight), ($\delta=0$, $\delta=0.4$)

a straight elliptical seal is a bad design compared to a similar circular seal from a rotordynamic point of view.

5.2.2 Linear Profile vs. Curved Profile

The results shown in Figures 5.8–5.11, compare the results of an elliptical seal with a linear axial profile with a similar with a curved (quadratic) axial profile. The results are presented for a centered seal as a function of ellipticity, δ . The dynamic coefficients are normalized with respect to the coefficients for the linear profile case at $\delta = 0$. The values used for this normalization are $K_{xx} = 44975 \text{ kN/m}$ (256883 lb/in), $C_{xx} = 21.78 \text{ kN-s/m}$ (124.4 lb-s/in) and $k_{xy} = 15821 \text{ kN/m}$ (90364 lb/in).

For this study, the mid-point clearance of the quadratic profile is made 75% of $(c_i + c_e)/2$, i.e., 0.75 times the mid-point clearance of a linear profile with similar inlet and exit clearances.

The plot for direct stiffness in Figure 5.8 shows the effect of a change in profile on the direct stiffness. For the linear case, there is a complete loss of stiffness at around $\delta = 0.65$. The stiffness for the quadratic profile is almost twice that of the linear profile. Also, it retains its stiffness over a much wider range than the linear profile. The difference in the other coefficients, shown in Figures 5.9–5.10, are relatively small.

There is a drop of about 25% in leakage for the curved profile.

Based on these results, the following conclusions may be drawn.

1. Complete loss of stiffness for linear profile at $\delta = 0.65$.
2. The direct stiffness of curved profile is almost double that of linear profile.
3. There is a 25% reduction in leakage for curved profile.

This example illustrates the effect of seal profile on the dynamic coefficients. This example shows that and an arbitrary seal profile, other than a straight or tapered,

could possibly be used as a criterion in designing a seal for a set of optimum dynamic characteristics.

5.3 Case Study of a Distorted Seal of SSME-ATD-HPOTP

The predicted clearance profile of an interstage seal of the SSME-ATD-HPOTP turbopump is shown in Figure 1.3. The distorted clearance profile is obtained from a thermo-elastic finite element analysis of the turbopump. The clearances are obtained at six equidistant axial planes along the length of the seal with 68 clearances at each plane. The clearances along the circumference are located, roughly, at equal angular displacements.

The general procedure employed at NASA/MSFC with these distorted profiles is to compute the average inlet and exit clearances and used them as inlet and exit clearances of a tapered seal. In this study, rotordynamic coefficients of the distorted seal are compared with those computed using average clearances at inlet and outlet. The seal geometry and operating conditions at full power level (FPL) are given in Appendix G. The clearance function for this seal is approximated by fitting the clearance data with bi-cubic splines. This 2-D curve fitting enables the numerical computation of clearance, $c(z, \beta)$, and gradients $\frac{\partial c}{\partial \beta}$, $\frac{\partial c}{\partial z}$ at any given grid location (z, β) . According to the manufacturer's specifications, the side-load on this seal acts at a constant angle of 290° . The dynamic coefficients for this variable profile seal are computed as a function of side-load acting at this angle. The concept of external load based dynamic coefficients is discussed in section 2.10.

Figure 5.12 shows the the relation between seal forces and eccentricity. At zero load, distorted profile shows an eccentricity. No load operation requires the seal to be slightly off-centered due to the uneven distribution of fluid pressure in the distorted

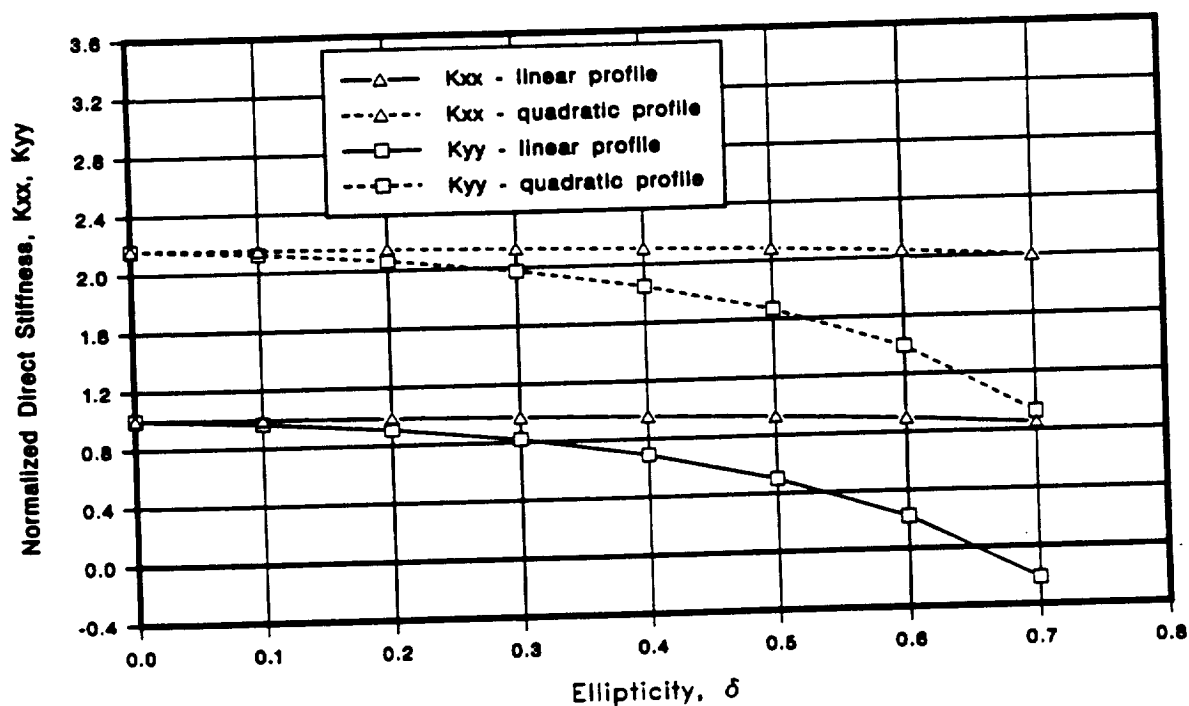


Figure 5.8 Normalized Direct Stiffness for Elliptical Seal (Curved)

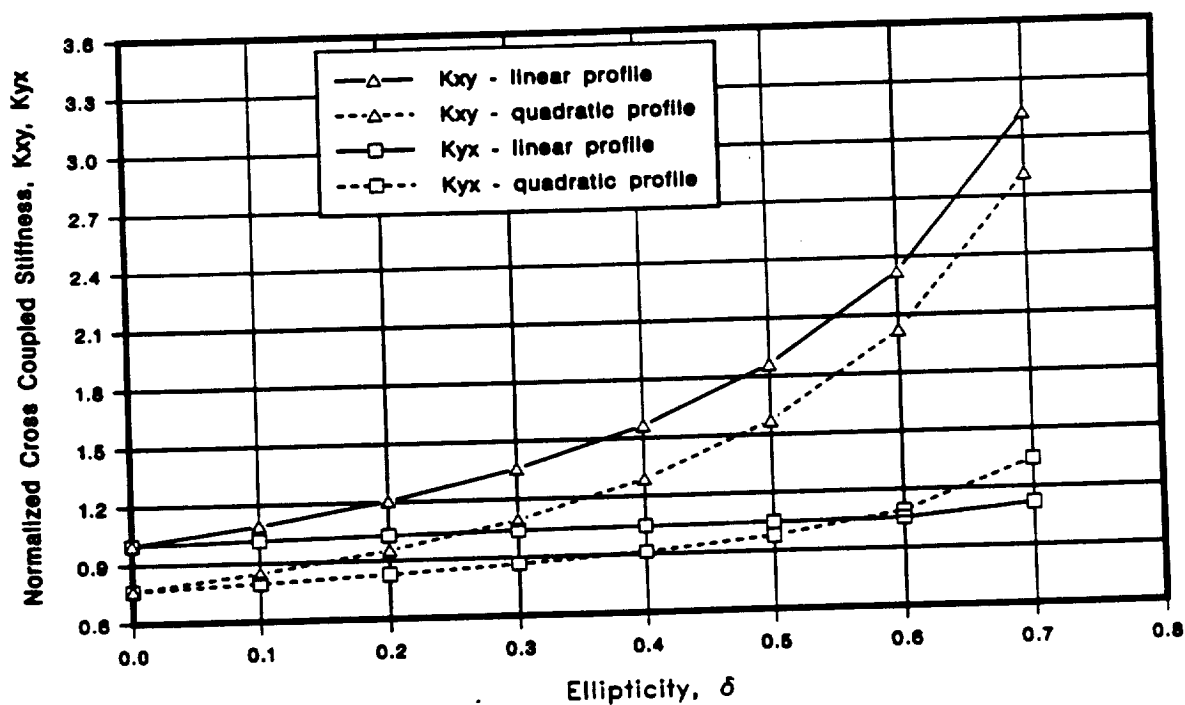


Figure 5.9 Normalized Cross Coupled Stiffness for Elliptical Seal (Curved)

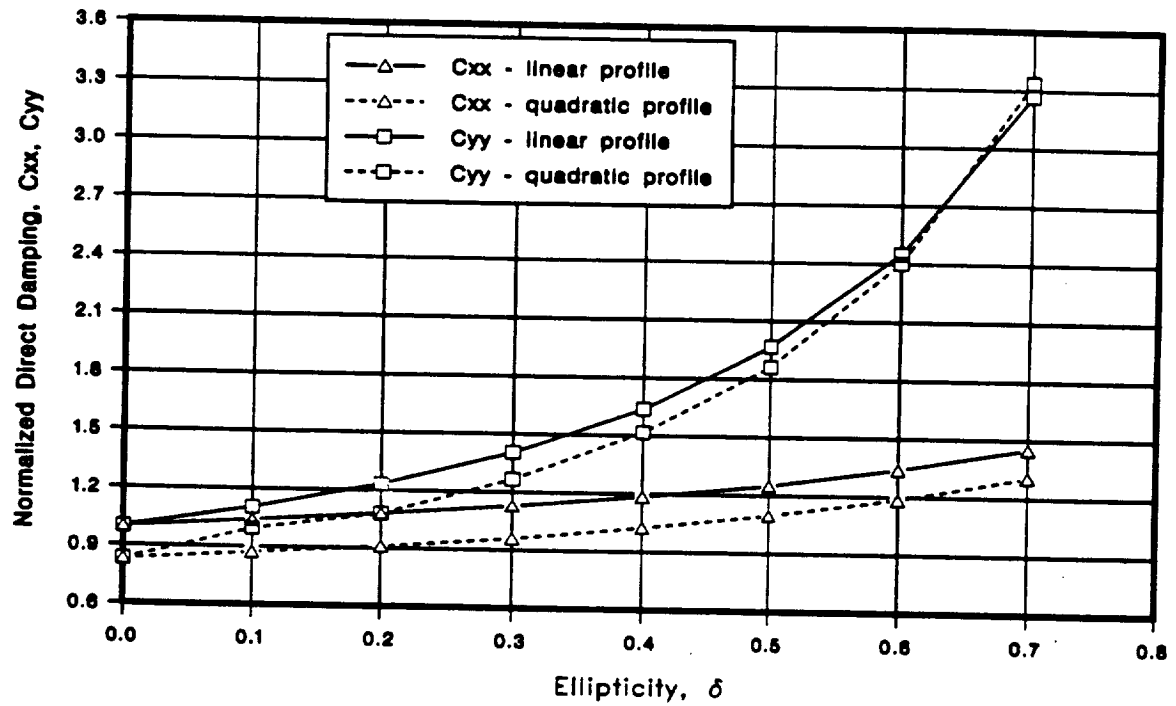


Figure 5.10 Normalized Direct Damping for Elliptical Seal (Curved)

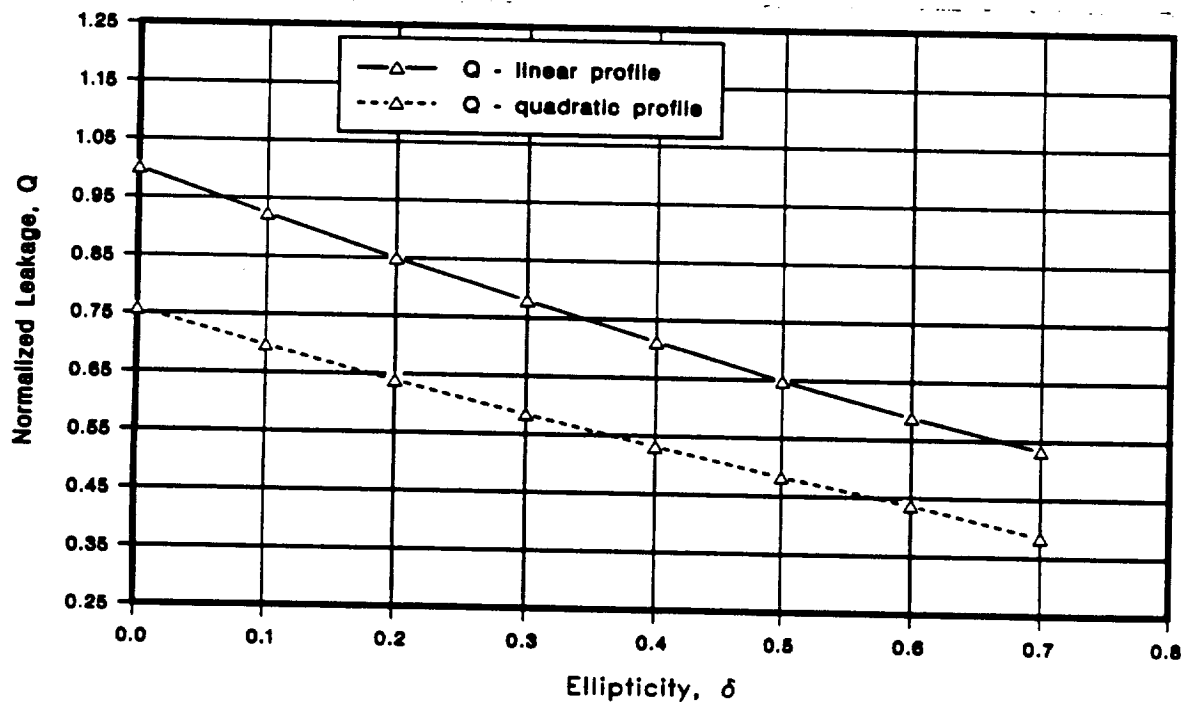


Figure 5.11 Normalized Leakage for Elliptical Seal (Curved)

seal. Leakage, for the average profile and the distorted profile, is shown in Figure 5.13. There is small increase in leakage for the distorted seal.

Figure 5.14 shows the variation of direct stiffness, K_{xx} , K_{yy} as a function of external load for both average and distorted profiles. The cross coupled stiffness shown in Figure 5.15 clearly shows the difference between the average clearances analysis and distorted seal analysis. There is an appreciable difference, particularly at high loads.

5.4 Directional Dependence of Dynamic Coefficients

Typically, as in the case of a plain journal bearing, the dynamic coefficients of an annular seal are computed in a minimum film thickness coordinate system (x', y') as shown in Figure 5.17. The seal represented in this figure is of a circular cross section, similar to a plain journal bearing. In this figure, (x, y) represents the global coordinate system fixed to the stator and is the coordinate system normally used in rotordynamic simulations. Therefore, the dynamic coefficients irrespective of the coordinate system in which they are computed should be transformed into this fixed coordinate system before they can be used in simulation studies.

For dynamic coefficients computed at eccentricities greater than zero, the eccentricity is varied along the x' -axis of the minimum film thickness system and the computed coefficients are then transformed into the fixed coordinate system using a transformation. For a seal with a circular cross section, dynamic coefficients computed at eccentricities greater than zero need to be transformed and those computed at zero eccentricity need no transformation.

In Figure 5.17, the angle of rotation between the minimum film thickness system and the fixed coordinate system is ϕ and is also known as the eccentricity angle as

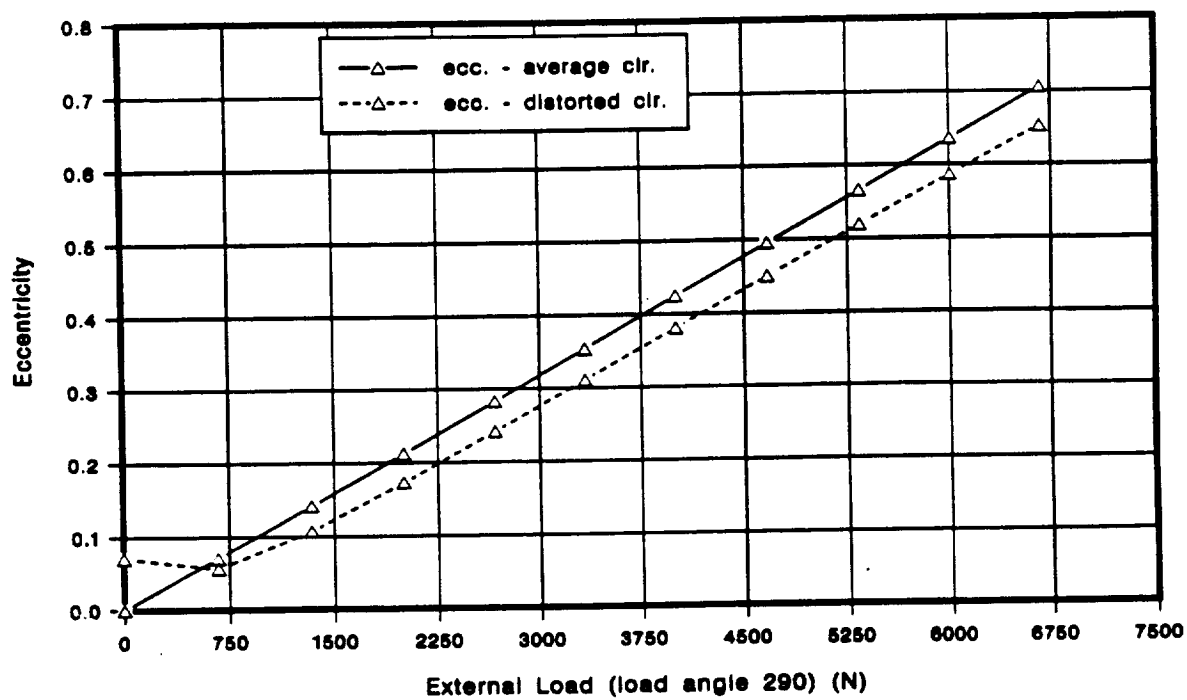


Figure 5.12 Load vs. Eccentricity for Distorted Seal, Unit 3-01

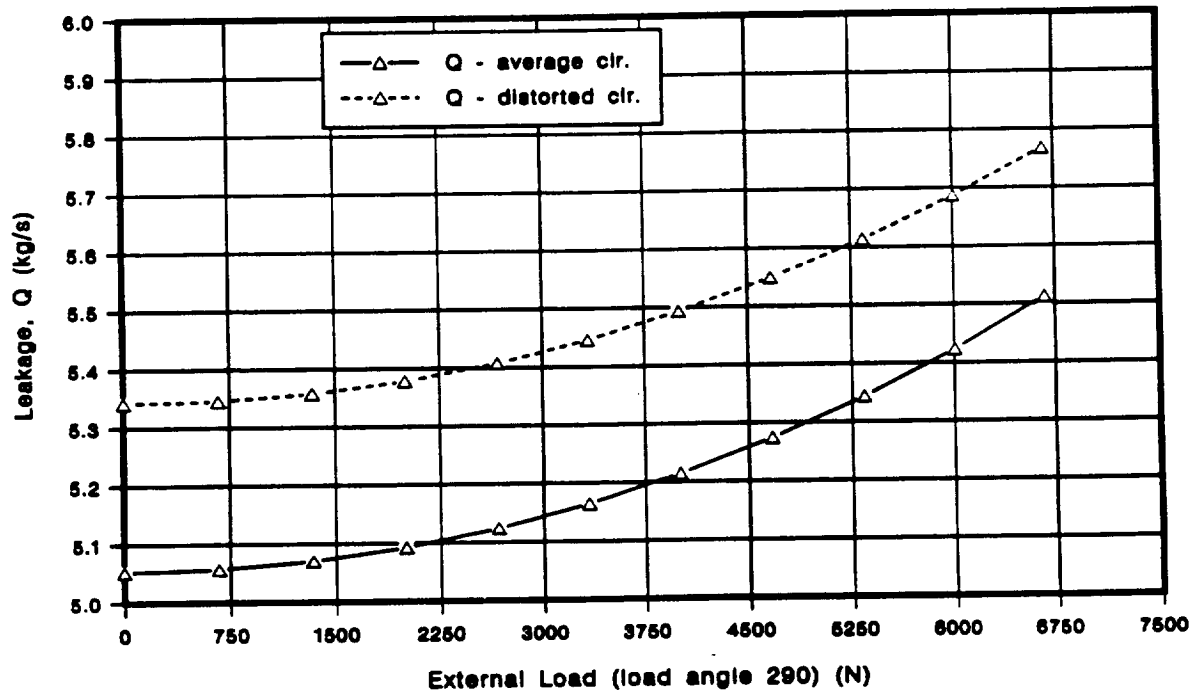


Figure 5.13 Leakage for Distorted Seal, Unit 3-01

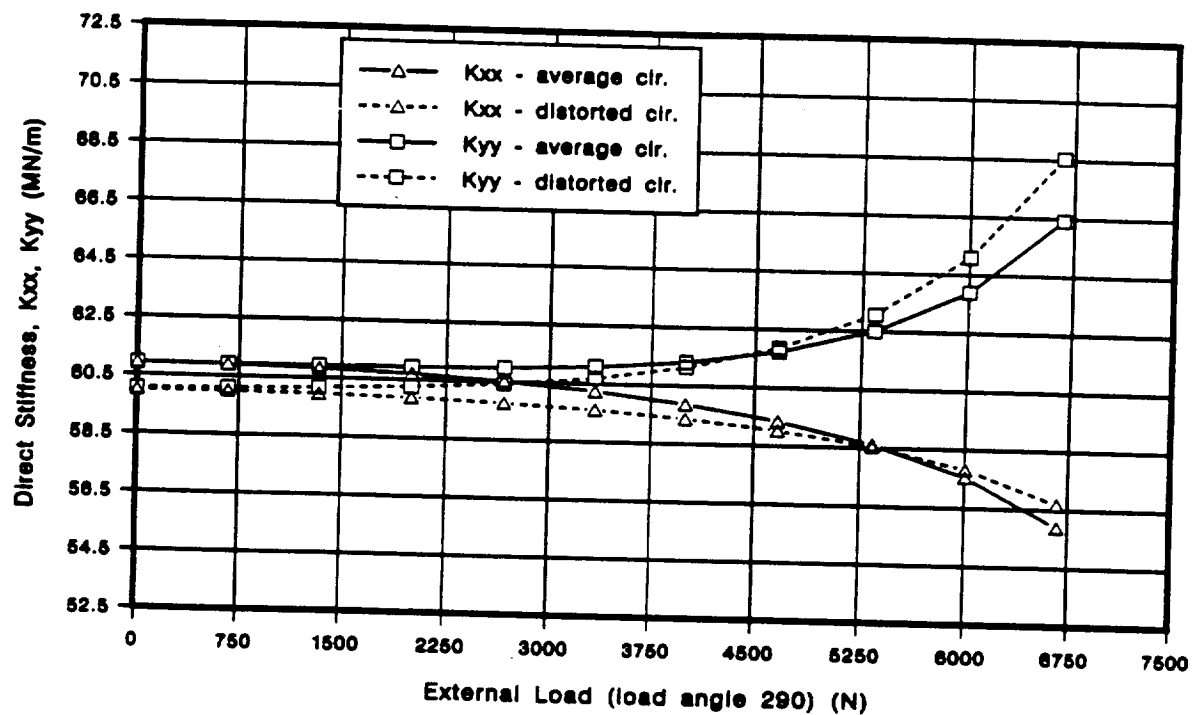


Figure 5.14 Direct Stiffness for Distorted Seal, Unit 3-01

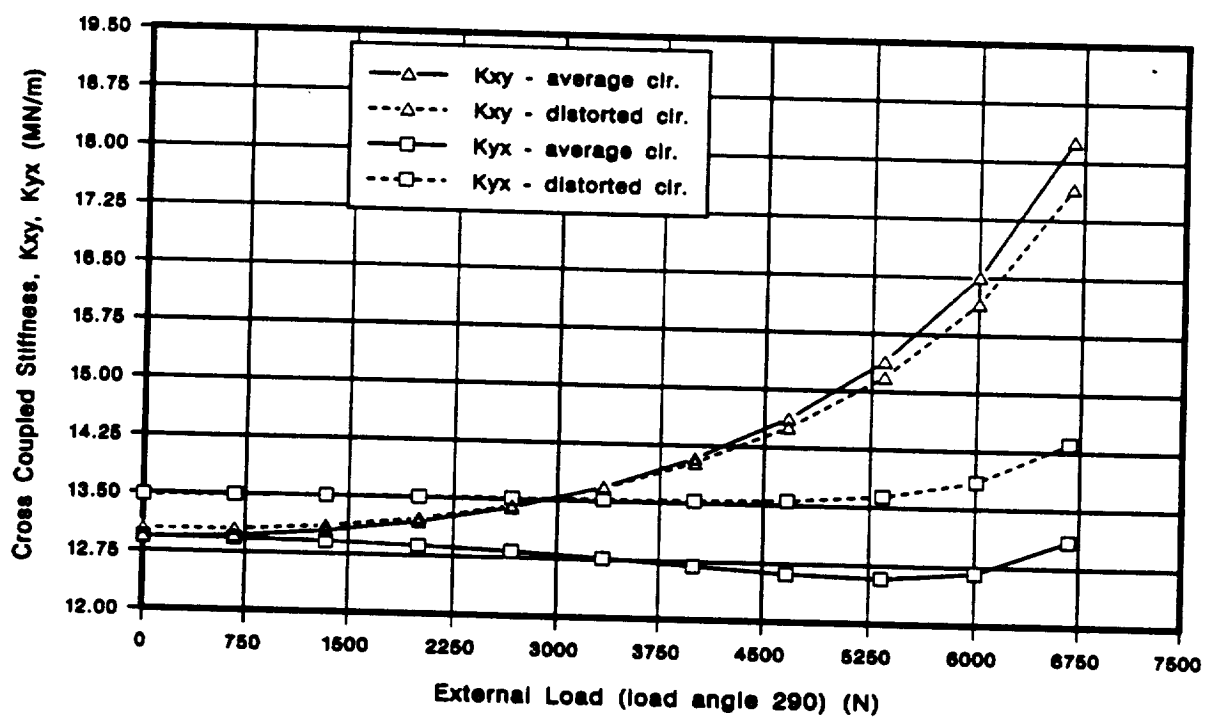


Figure 5.15 Cross Coupled Stiffness for Distorted Seal, Unit 3-01

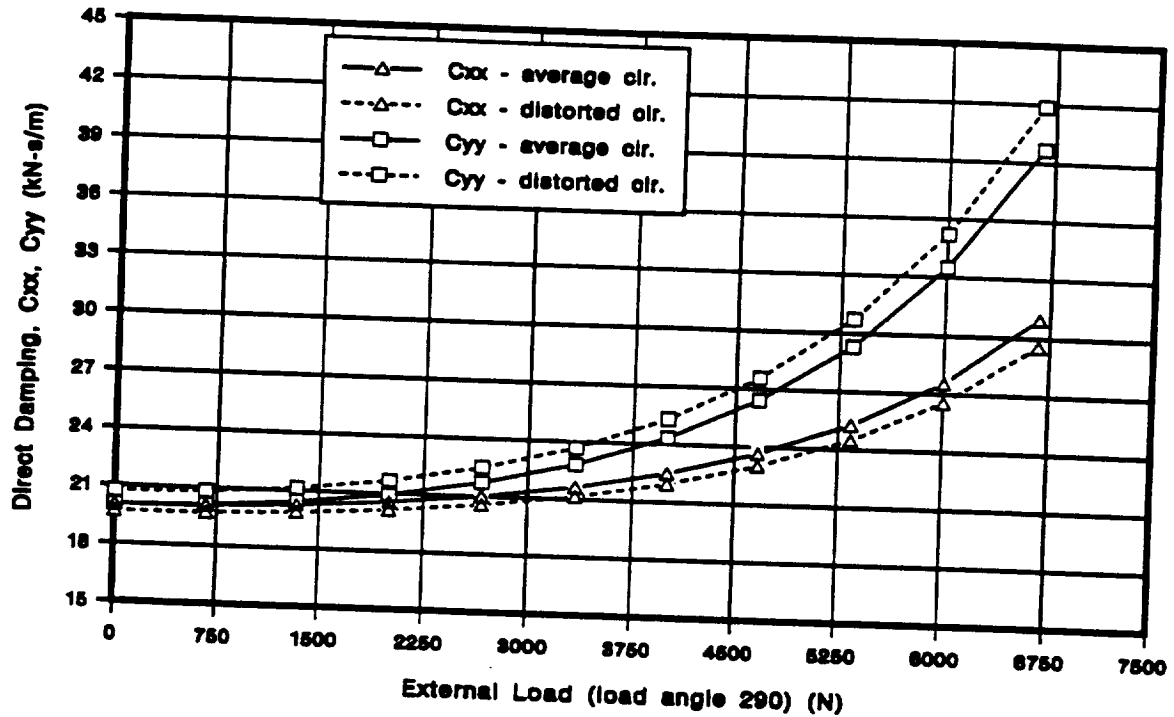


Figure 5.16 Direct Damping for Distorted Seal, Unit 3-01

it defines the eccentricity vector with respect to the fixed coordinate system. The points O and C refer to the center of seal and rotor respectively and the line passing through these two points is the line of centers.

The transformation of dynamic coefficients computed in a minimum film thickness system into fixed coordinate system is explained below.

Let $[Q]$ be the transformation matrix between the minimum film thickness system specified by (x', y') coordinate system and the global coordinate system represented by (x, y) . The angle of rotation between these two coordinate systems is ϕ , which is also the eccentricity angle as shown in Figure 5.18. Given a dynamic coefficient in (x', y') system, it is required to transform it into (x, y) coordinate system, which is the coordinate system normally used for simulations.

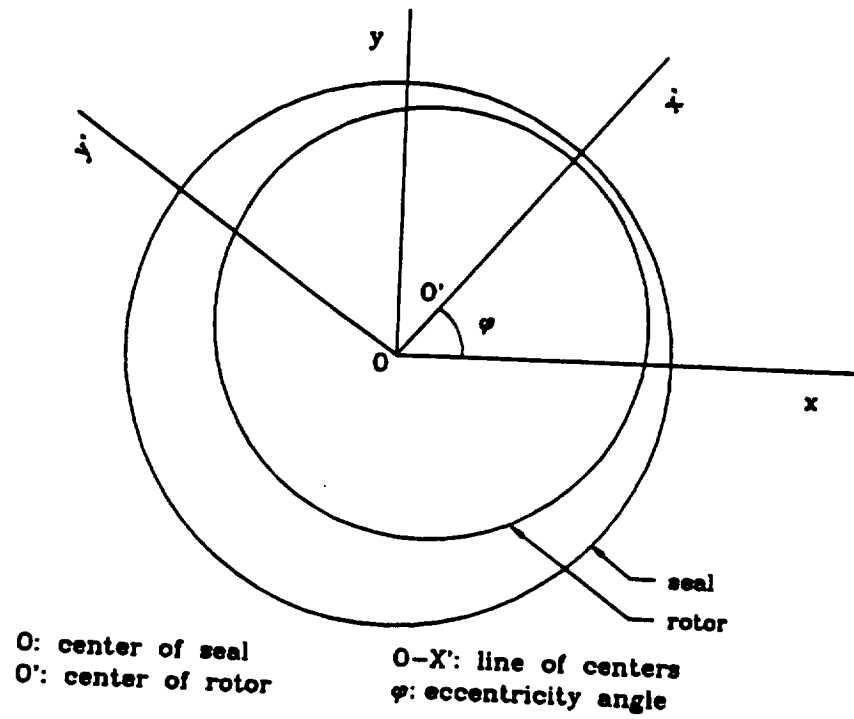


Figure 5.17 Definition of Angle of Line of Centers and Eccentricity Angle

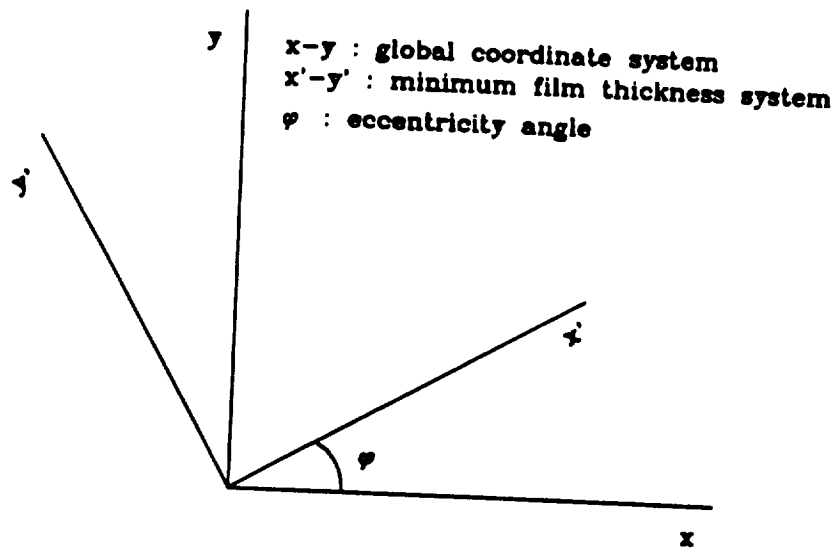


Figure 5.18 Rotor and Minimum Film Thickness Coordinate Systems

The transformation matrix $[Q]$ and its inverse $[Q]^{-1}$ is given below.

$$[Q] = \begin{bmatrix} \cos\phi & \sin\phi \\ -\sin\phi & \cos\phi \end{bmatrix} \quad (5.14)$$

$$[Q]^{-1} = \begin{bmatrix} \cos\phi & -\sin\phi \\ \sin\phi & \cos\phi \end{bmatrix} \quad (5.15)$$

Let the set of 12 dynamic coefficients at any given eccentricity e in the minimum film thickness coordinate system (x', y') be specified by the stiffness matrix $[K']$, damping matrix $[C']$ and the inertia matrix $[M']$.

$$[K'(e, 0)] = \begin{bmatrix} K'_{xx} & k'_{xy} \\ -k'_{yx} & K'_{yy} \end{bmatrix} \quad (5.16)$$

$$[C'(e, 0)] = \begin{bmatrix} C'_{xx} & c'_{xy} \\ -c'_{yx} & C'_{yy} \end{bmatrix} \quad (5.17)$$

$$[M'(e, 0)] = \begin{bmatrix} M'_{xx} & m'_{xy} \\ -m'_{yx} & M'_{yy} \end{bmatrix} \quad (5.18)$$

Let the set of 12 dynamic coefficients at the same eccentricity e as above, but in the global coordinate system (x, y) be given by the stiffness matrix $[K]$, damping matrix $[C]$ and the inertia matrix $[M]$.

$$[K(e, \phi)] = \begin{bmatrix} K_{xx} & k_{xy} \\ -k_{yx} & K_{yy} \end{bmatrix} \quad (5.19)$$

$$[C(e, \phi)] = \begin{bmatrix} C_{xx} & c_{xy} \\ -c_{yx} & C_{yy} \end{bmatrix} \quad (5.20)$$

$$[M(e, \phi)] = \begin{bmatrix} M_{xx} & m_{xy} \\ -m_{yx} & M_{yy} \end{bmatrix} \quad (5.21)$$

The two sets of dynamic coefficients are related by the following transformation.

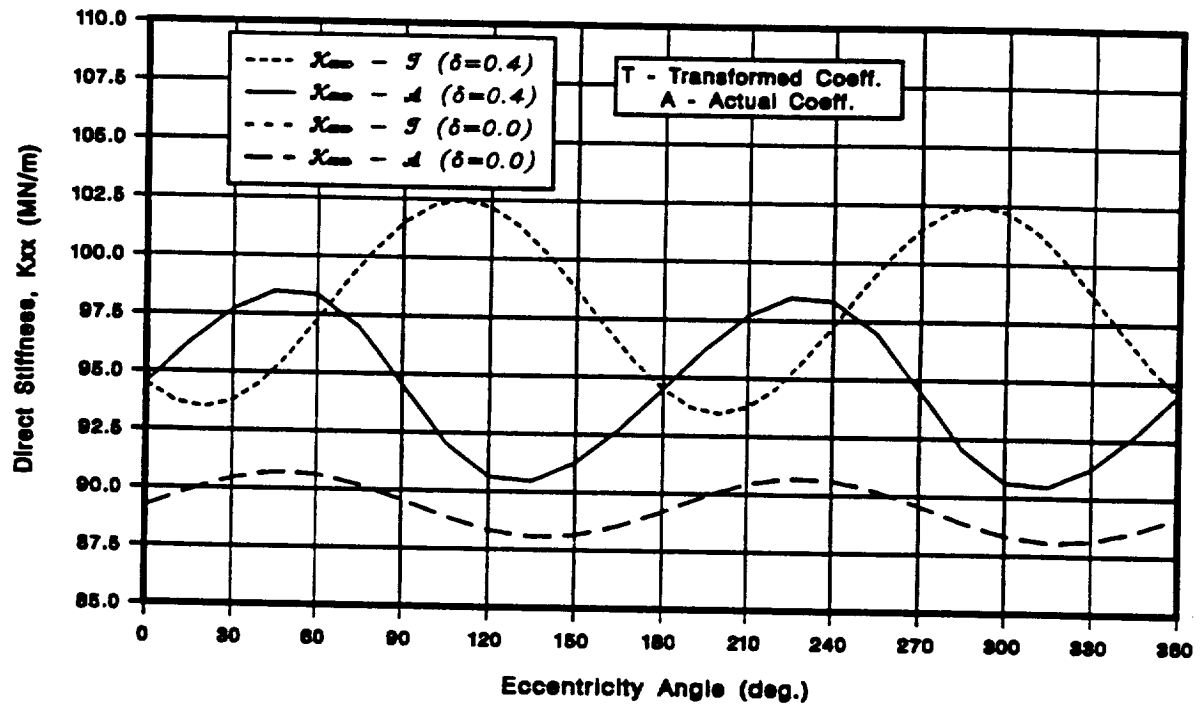
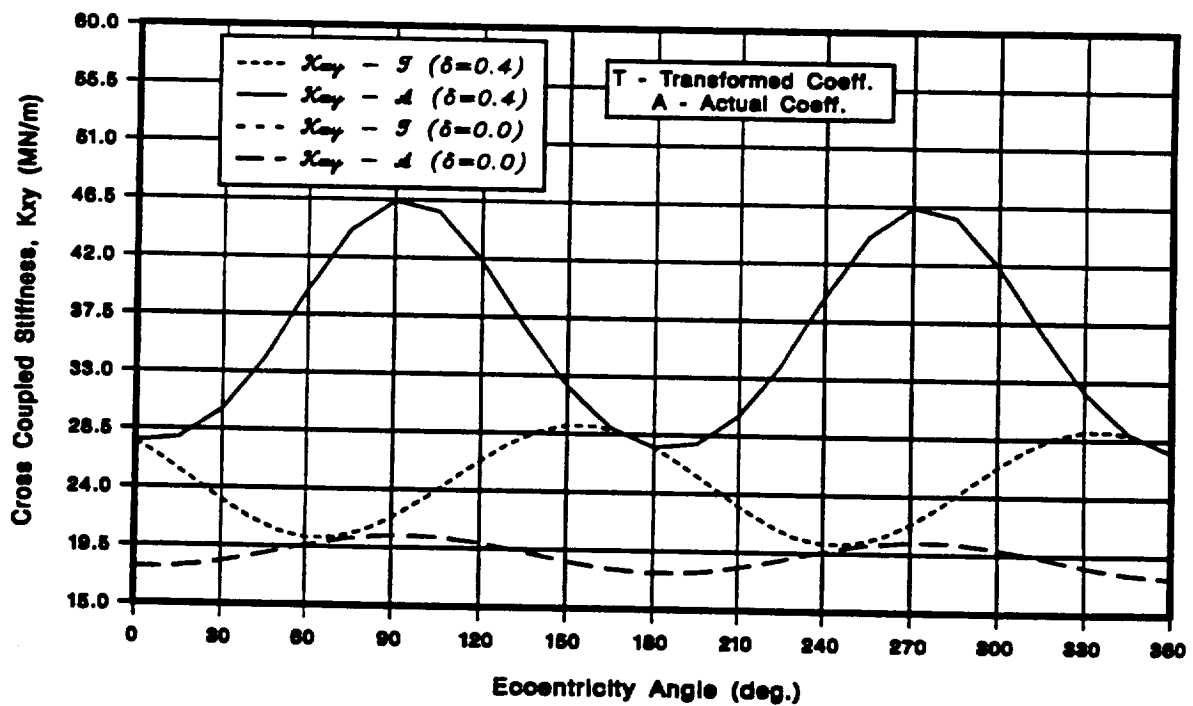
$$[K(e, \phi)] = [Q]^{-1}[K'(e, 0)][Q] \quad (5.22)$$

$$[C(e, \phi)] = [Q]^{-1}[C'(e, 0)][Q] \quad (5.23)$$

$$[M(e, \phi)] = [Q]^{-1}[M'(e, 0)][Q] \quad (5.24)$$

For a seal with a circular cross section, the coefficients computed in the minimum film thickness system will be the same irrespective of the eccentricity angle ϕ . In other words, coefficients computed at two different orientations ϕ_1 and at ϕ_2 in the minimum film thickness system will be the same. Typically, the (x', y') is aligned with (x, y) , i.e., $\phi = 0$, when these coefficients are computed. The results given in seal literature are usually computed in this fashion.

However, this procedure is no not valid with seals of non-circular cross sections, i.e., seals with circumferentially varying clearance functions. For these seals, the dynamic coefficients computed in the minimum film thickness vary with eccentricity angle and because of this the orientation of the (x', y') system with respect to (x, y) is important. One way to handle this is to compute these coefficient directly in the fixed coordinate system for a given eccentricity angle, or compute the coefficients in the minimum film thickness system and transform them using the transformations given in Eqs. (5.22–5.24).

Figure 5.19 Variation of K_{xx} for Elliptical SealFigure 5.20 Variation of k_{xy} for Elliptical Seal

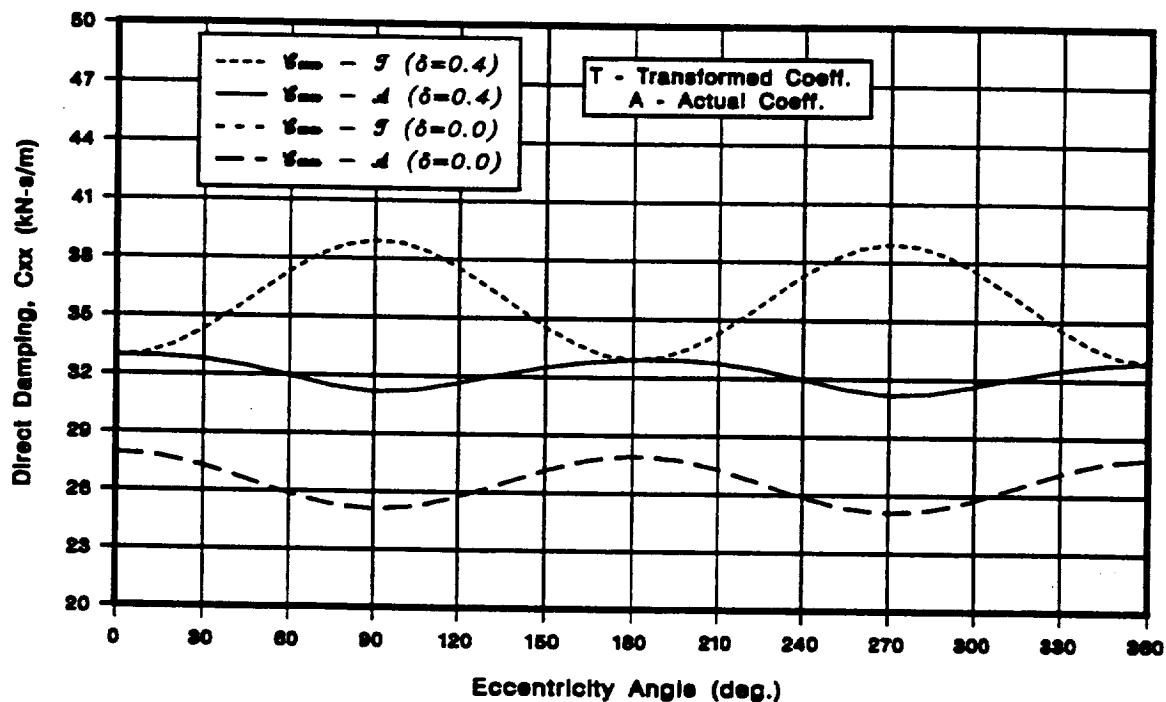


Figure 5.21 Variation of C_{xx} for Elliptical Seal

The following example illustrates the importance of orientation for arbitrary profile seals. Dynamic coefficients for a circular seal (ellipticity, $\delta = 0$) and an elliptical seal (ellipticity, $\delta = 0.4$), are computed using the two different approaches discussed earlier, for concentric position. Comparison plots for direct stiffness K_{xx} , cross coupled stiffness k_{xy} and direct damping C_{xx} computed using two approaches discussed above are shown in Figures 5.19–5.21.

In these figures, *Actual Coefficients* refer to coefficients computed directly in the fixed coordinate system (x, y) for a given eccentricity angle. The eccentricity angle is swept from 0 to 360° and these coefficients are computed at regular intervals. The *Transformed Coefficients* are coefficients computed in a minimum film thickness system aligned with fixed coordinate system, and then transformed for a given eccentricity angle using the transformations in Eqs (5.22–5.24).

For the $\delta = 0$ case, i.e., for a circular seal, there is no difference between the

two approaches. The transformed coefficients coincide with actual coefficients at all orientations, as expected. The same procedure repeated for an elliptical seal ($\delta = 0.4$), shows the differences between the two approaches. The transformed coefficients are entirely different from actual coefficients computed in the fixed coordinate system.

Therefore, for seals with non-circular cross sections, either the coefficients are to be computed in the fixed coordinate system at a given eccentricity angle, or if a minimum film thickness system is used, the actual eccentricity angle should be used to transform them into the fixed coordinate system. In other words, for these seals, dynamic coefficients should always be referred with respect to the orientation at which they are computed.

This the primary reason for using a fixed coordinate system for the analysis of arbitrary profile seals, for example, the distorted seal case and the elliptical seal case.

CHAPTER VI

RESULTS

In this chapter, current analysis is compared with both experimental and theoretical results from literature.

The following cases are studied in detail.

1. Childs and Lindsey (1993): This study presents experimental and theoretical results for high speed, short length, smooth, liquid annular seals with an axial taper. Experimental results are presented for both concentric and eccentric tests. Theoretical results for concentric case are based on Childs' (1993) code *MUDY*, while similar results for eccentric tests are based on San Andres' (1991) seal code *HSEAL*. The friction model is Moody's and constant properties are assumed.
2. Childs and Kim (1985): Theoretical and test results for a concentric seal based on Hirs' friction model and constant properties.
3. Scharrer and Nunez (1989): Theoretical results for a seal with a wavy (distorted) profile in the axial direction. The friction factor is based on Hirs' model and constant properties are used.
4. Scharrer and Nelson (1990): Theoretical results for a partially tapered annular seal. Results are for a concentric seal with Hirs' friction model and constant properties.
5. Jenssen (1970): Experimental results (seal forces) for smooth annular seals as a function of eccentricity.

6. Kanki and Kawakami (1984): Experimental results for long pump annular seals. Theoretical predictions of Nelson and Nguyen are included.
7. Falco *et al.* (1984): Experimental and theoretical results for plain annular seals. Theoretical predictions of Nelson and Nguyen are included.
8. Allaire *et al.* (1976): Theoretical results based on *short seal* assumption and a Blassius type friction model. Theoretical predictions of Nelson and Nguyen are included.
9. San Andres *et al.* (1992): Theoretical results for a cryogenic seal with Moody's friction model, Isothermal flow with variable properties.
10. San Andres *et al.* (1992): Theoretical results for a cryogenic seal with Moody's friction model, Adiabatic flow with variable properties.

6.1 Childs and Lindsey (1993)

The results discussed in this section are based on the combined experimental and theoretical work of Childs and Lindsey (1993). A summary of this work is presented below.

6.1.1 Work Summary

This work presents theoretical and experimental results for water lubricated, short length, smooth, liquid annular seals with an axial taper. Experiments are conducted with five different seal configurations at three different pressure differentials, 1.38 Mpa, 2.41 Mpa, and 3.45 Mpa. The experiments are repeated at three speeds 10200 rpm, 17400 rpm and 26400 rpm.

Table 6.1 Seal Geometry for Childs and Lindsey

seal no.	taper par. (q)	c_i (mm)	c_e (mm)	c_o (mm)
1, maximum divergent seal	-0.29	0.076	0.137	0.076
2, slightly divergent seal	-0.12	0.076	0.097	0.076
3, straight seal	0.00	0.076	0.076	0.076
4, slightly convergent seal	0.12	0.097	0.076	0.076
5, maximum convergent seal	0.29	0.137	0.076	0.076

In this study, the experimental results are compared with the theoretical prediction of Childs' (1993) computer code *MUDY* for concentric test results and with the predictions of San Andres' (1991) seal code *HSEAL* for eccentric test results. San Andres' analysis employs a finite difference based solution scheme while Childs uses direct integration. The friction model used is Moody's and constant fluid properties are assumed.

The taper ratio of a seal is specified by the taper parameter q which is defined as,

$$q = \frac{c_i - c_e}{c_i + c_e} \quad (6.1)$$

and for,

- $q = 0$ straight seal geometry
- $q > 0$ convergent seal geometry
- $q < 0$ divergent seal geometry

The five seal configurations used in the study are identified by their taper parameter q as given in Table 6.1.

It is assumed in this study that the pre-swirl ratio for a short annular seal is approximately equal to its whirl-frequency ratio. This ratio for each case is determined from the experimentally measured rotordynamic coefficients as,

$$WFR = \frac{k_{xy} - k_{yx}}{(C_{xx} + C_{yy})\omega} \quad (6.2)$$

and are tabulated for all cases. This data is included in *Appendix G*.

The seals are classified as smooth seals and the stator and rotor relative roughness is based on Moody friction model. The stator and rotor relative roughness, inlet loss coefficient, and exit pressure recovery coefficient are selected to match theoretical and experimental flow rates and the *best* set of values used in the theoretical predictions for all cases are given as,

inlet loss coefficient, ξ_i	0.1
exit pressure recovery coefficient, ξ_e	1.0
stator rel. roughness (Moody, smooth)	0.001
rotor rel. roughness (Moody, smooth)	0.001

Experimental results are provided for concentric and eccentric seal tests. For the concentric position runs, all five seal configurations are used. For the eccentric position runs, results are provided only for the straight seal ($q = 0$) and the slightly convergent seal ($q = 0.12$). The experimental results include measured flow rates and rotordynamic coefficients.

6.1.2 Comparative Study

The experimental and theoretical data included in this study present an excellent opportunity to compare the results of the present work with the analyses of Childs' and San Andres' since one of the problems associated with studies involving combined

experimental/theoretical data is a lack of consistent input data for theoretical predictions and each researcher typically chooses his or her own set of input data to match the experimental data. The objectives of this comparative study are two fold. One is to to compare the theoretical predictions of current analysis with experimental data and the other more important objective is to compare current analysis with Childs' and San Andres' analyses under similar assumed input data. This comparative study is significant in the sense that the results from the current analysis are being compared to the analyses of Childs and San Andres, who use solution procedures different from the current work, though all three analyses essentially use the same bulk flow governing equations, friction factor and boundary conditions.

In the following comparisons, the theoretical predictions are repeated based on the current analysis using exactly the same input parameters, i.e., same pre-swirl, inlet loss coefficient, exit pressure recovery coefficient, stator and rotor relative roughness, density and viscosity as reported by Lindsey (1993). The predictions from current analysis are repeated for both nominal clearances and measured clearances. Measured clearances are clearances measured under running conditions and take into account (Lindsey, 1993) the rotor growth and change in nominal seal clearance during the operation.

As will be evident from the comparative study to follow, the results based on nominal clearances (NCLR) are consistently closer to the experimental data than the results based on measured clearances (MCLR), suggesting possibly a need for refinement of the measurement system used for measuring these clearances.

In the plots shown for this study, *N* refers to results based on nominal clearances, and *M* refers to results based on measured clearances. Nominal clearances based results are available only for current analysis. For comparisons between various analyses, i.e, current analysis, Childs and San Andres, the results based on measured

clearances are used.

In the following study, results from current analysis are provided for all cases given below.

1. 5 seal configurations, taper par. q : -0.29, -0.12, 0.00, 0.12, 0.29
2. 3 pressure differentials, Δp : 1.38 Mpa, 2.41 Mpa, 3.45 Mpa
3. 3 rotor speeds, N : 10200 rpm, 17400 rpm, 24600 rpm
4. Concentric and eccentric tests.

6.1.3 Leakage, Concentric Tests

The leakage for concentric seal operation as a function of taper parameter q is given in Figure 6.1. As mentioned earlier, Lindsey uses Childs' code *MUDY* based on Moody's friction model, for theoretical predictions of concentric seal tests. These predictions from *MUDY* along with the predictions from the current analysis for both NCLR and MCLR are shown in this figure. As may be noted from this plot, there is a considerable difference between predictions based on MCLR and the experimental data. However, the leakage based on NCLR show very good agreement particularly for the convergent seal geometry where there is almost exact correlation with the experimental data for all speeds and pressure differentials. The maximum deviation is about 12% and it occurs for the maximum divergent case at 3.45 pressure differential and 24600 rpm case. This result is directly opposite to the results based on MCLR which are closest to experimental data for the maximum divergent case. In almost all cases, current analysis with MCLR predicts leakage which is slightly (about 10–15/Childs' predictions. One of the possible reasons for current analysis based on NCLR being much closer to the convergent seals' results compared to the divergent

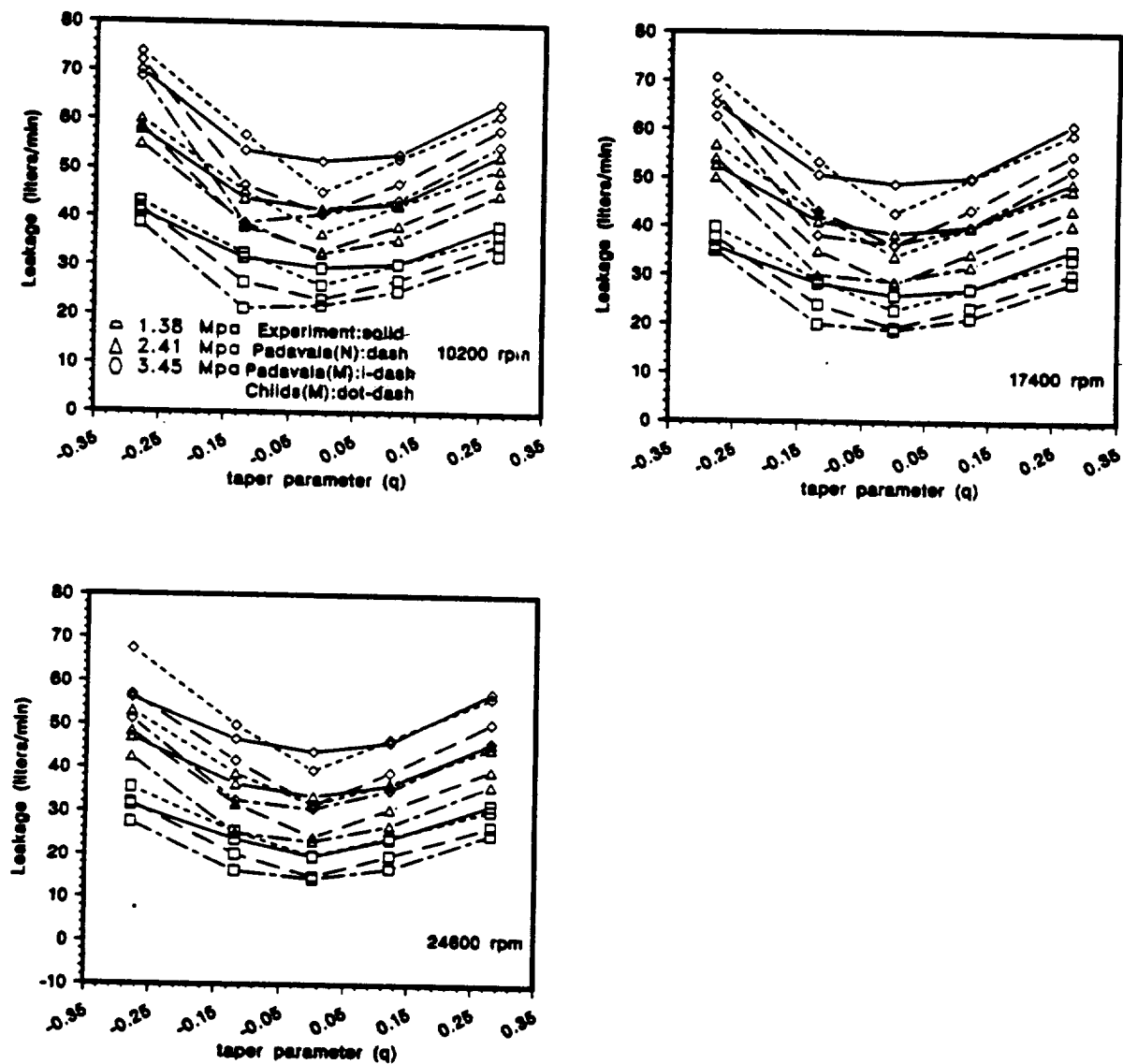


Figure 6.1 Leakage, Childs and Lindsey, Concentric Tests

seals' may be due to flow separation that is likely to occur in divergent seal geometries (Scharrer and Nelson, 1990) and bulk flow model used is not equipped to deal with that type of flow.

6.1.4 Dynamic Coefficients, Concentric Tests

The rotordynamic coefficients for the concentric tests are shown in Figure 6.2. for 10200 rpm case and in Figure 6.3 for the 17400 rpm case. The correlation between theoretical and experimental data for direct stiffness is, at best, average. However, the present analysis results based on NCLR show a much better correlation with experimental data than the MCLR based analysis. particularly for higher pressure differentials. Both current analysis (MCLR) and Childs agree well with the experimental data for the highly convergent case. Also, the theoretical predictions generally follow the trend of the experimental results, i.e., increase in stiffness with taper parameter q . The maximum deviation for direct stiffness occurs for the maximum divergent case and a possible reason is flow separation as mentioned earlier.

Both *MUDY* and current analysis predict similar damping and cross coupled stiffness. The added mass is severely under-predicted by both analyses, and Lindsey (1993) points out that this big difference may be due to unaccounted fluid inertia effects in the housing and piping system. In spite of the above reason, theoretical predictions typically under-predict mass coefficients.

Similar trends are noted for the dynamic coefficients of the 17400 rpm case except for the damping where the difference between theoretical and experimental data increase.

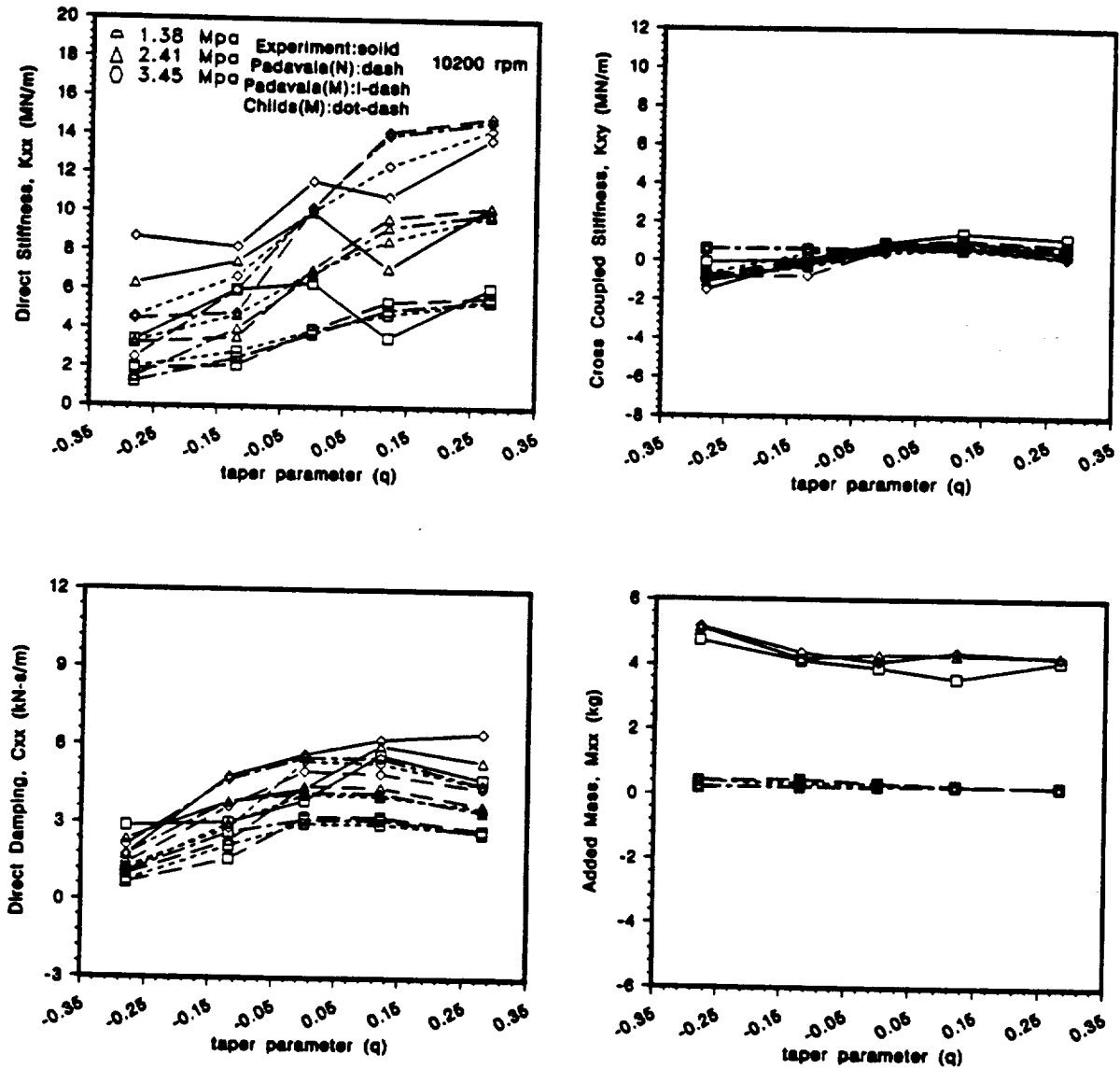


Figure 6.2 Dynamic Coefficients, Childs and Lindsey, Concentric (10200 rpm)

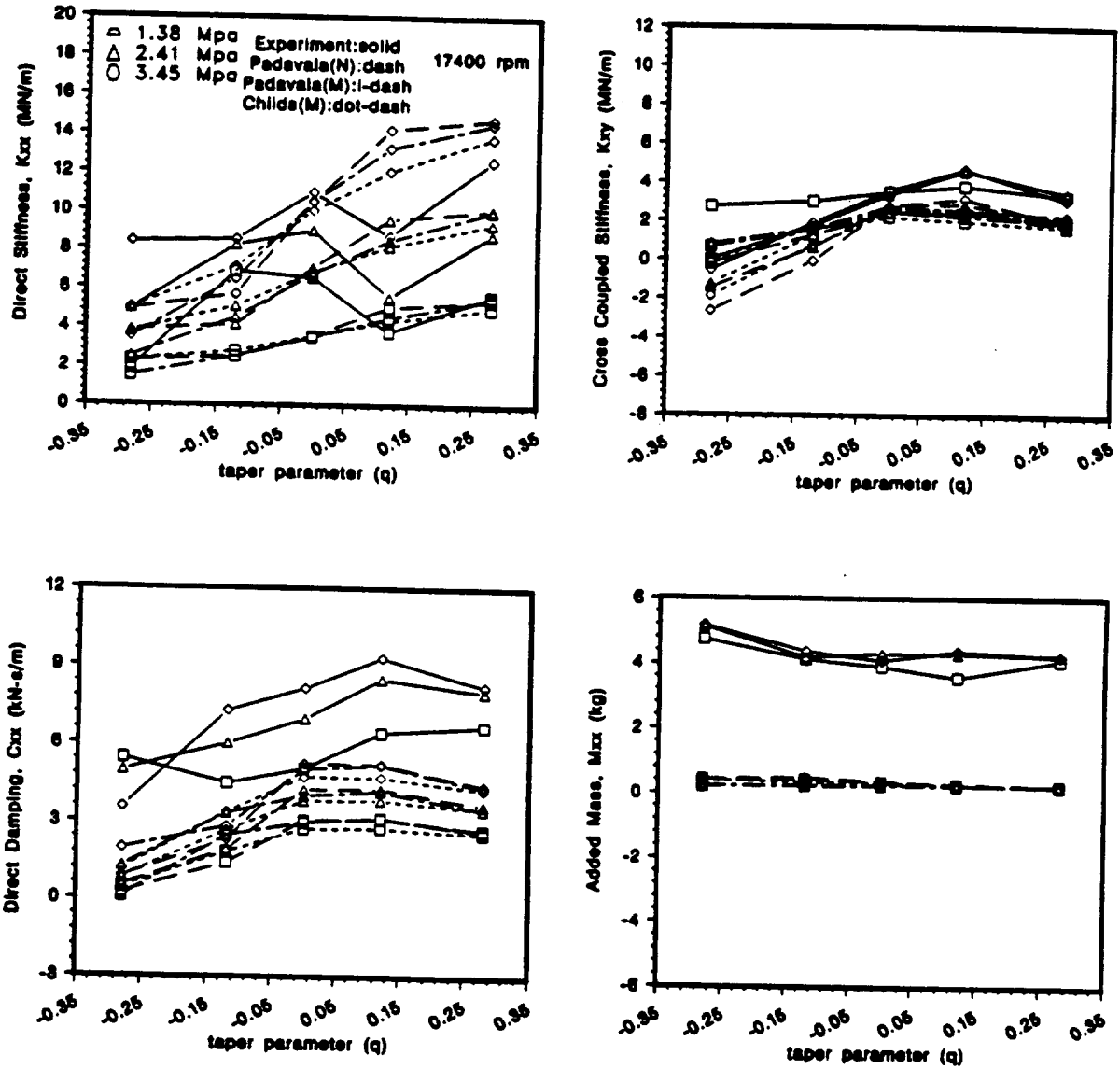


Figure 6.3 Dynamic Coefficients, Childs and Lindsey, Concentric (17400 rpm)

6.1.5 Leakage, Straight Seal, Eccentric Tests

For eccentric tests, experimental data is available only for two seal configurations; a straight seal ($q = 0$) and a slightly convergent seal ($q = 0.12$). The code used for theoretical predictions for eccentric seal analysis is *HSEAL*, developed by San Andres (1991) and is based on a finite difference formulation. The plots shown in Figure 6.4 correspond to the leakage of a straight seal operated at an eccentric position with eccentricity ratios varying from 0 to 0.5 and for three speeds. The prediction of the leakage rate by current analysis is typically 10–15% better than *HSEAL* predictions. However, the maximum difference between test data and current analysis based on NCLR is only about 10%.

The large deviations predicted by *HSEAL* are inexplicable and

6.1.6 Dynamic Coefficients, Straight Seal, Eccentric Tests

The plots in Figure 6.5 refer to the dynamic coefficients for the straight seal operated at various eccentricities. Predictions by both the current analysis and *HSEAL* are similar and follow the trends of the experimental data. Good comparison for direct damping and cross coupled stiffness for both analyses.

Similar trends are seen for the 17400 rpm case.

6.1.7 Leakage, Slightly Convergent Seal, Eccentric

The results in this section correspond to the leakage of the slightly convergent seal ($q = 0.12$). As noted earlier, there is excellent correlation between current analysis (NCLR) and measured flow rates for the convergent geometry seals (Figure 6.1). This very good correlation is repeated for the case of slightly convergent seal shown in Figure 6.7. Best comparison of flow rates for all seal configurations tested. These

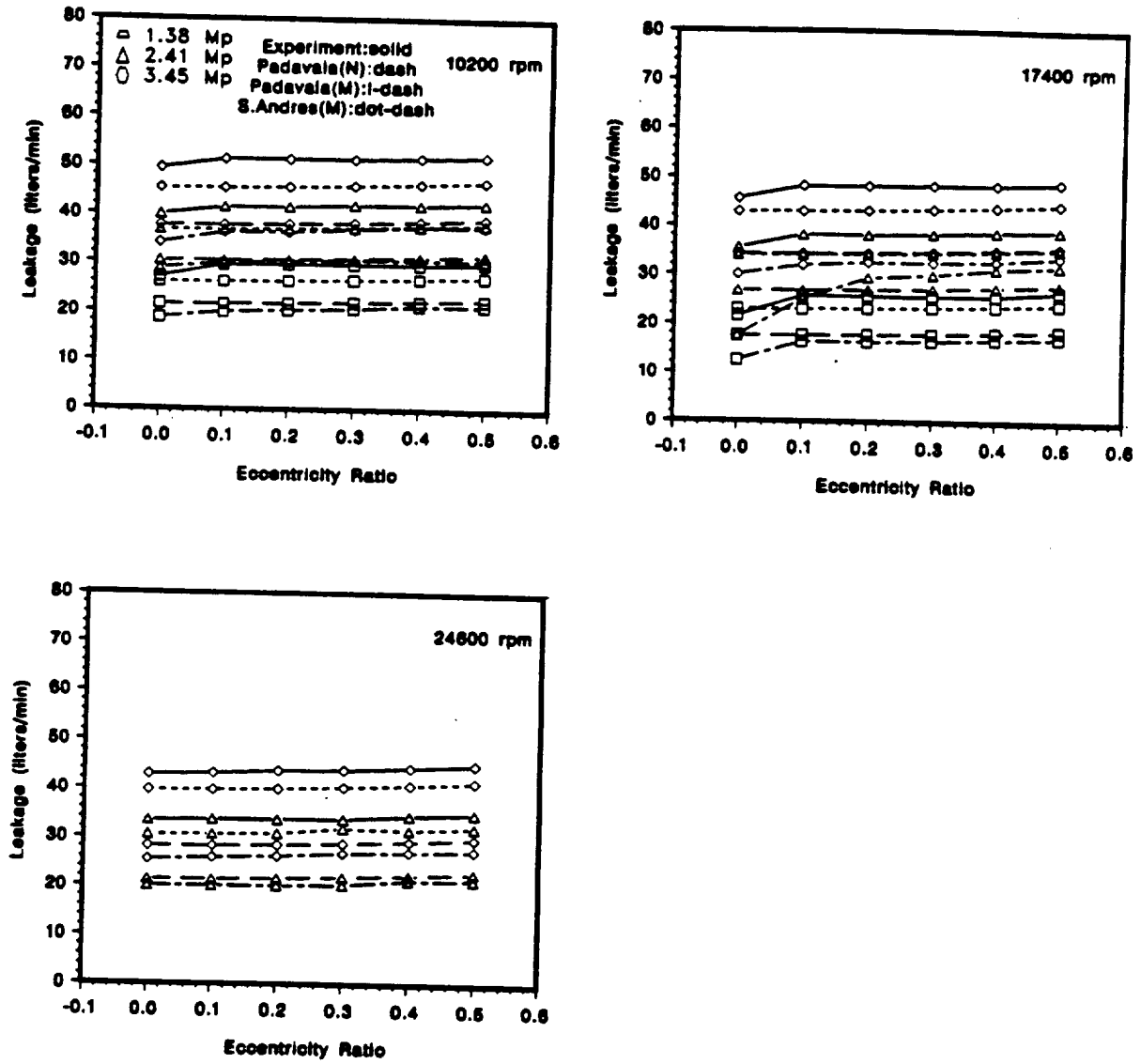


Figure 6.4 Leakage, Childs and Lindsey, Straight Seal, Eccentric Tests

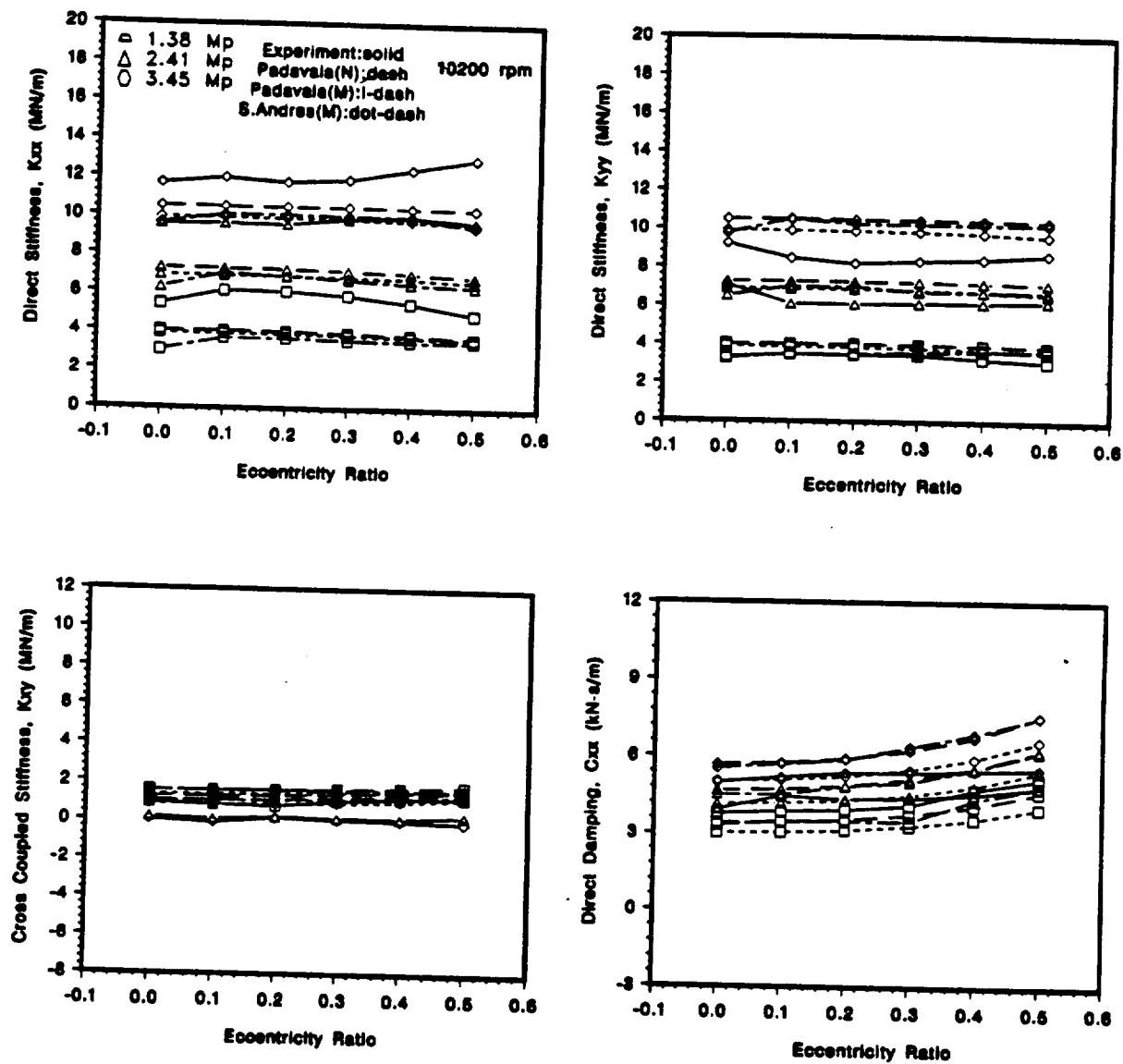


Figure 6.5 Dynamic Coefficients, Childs and Lindsey, Straight Seal, Eccentric (10200 rpm)

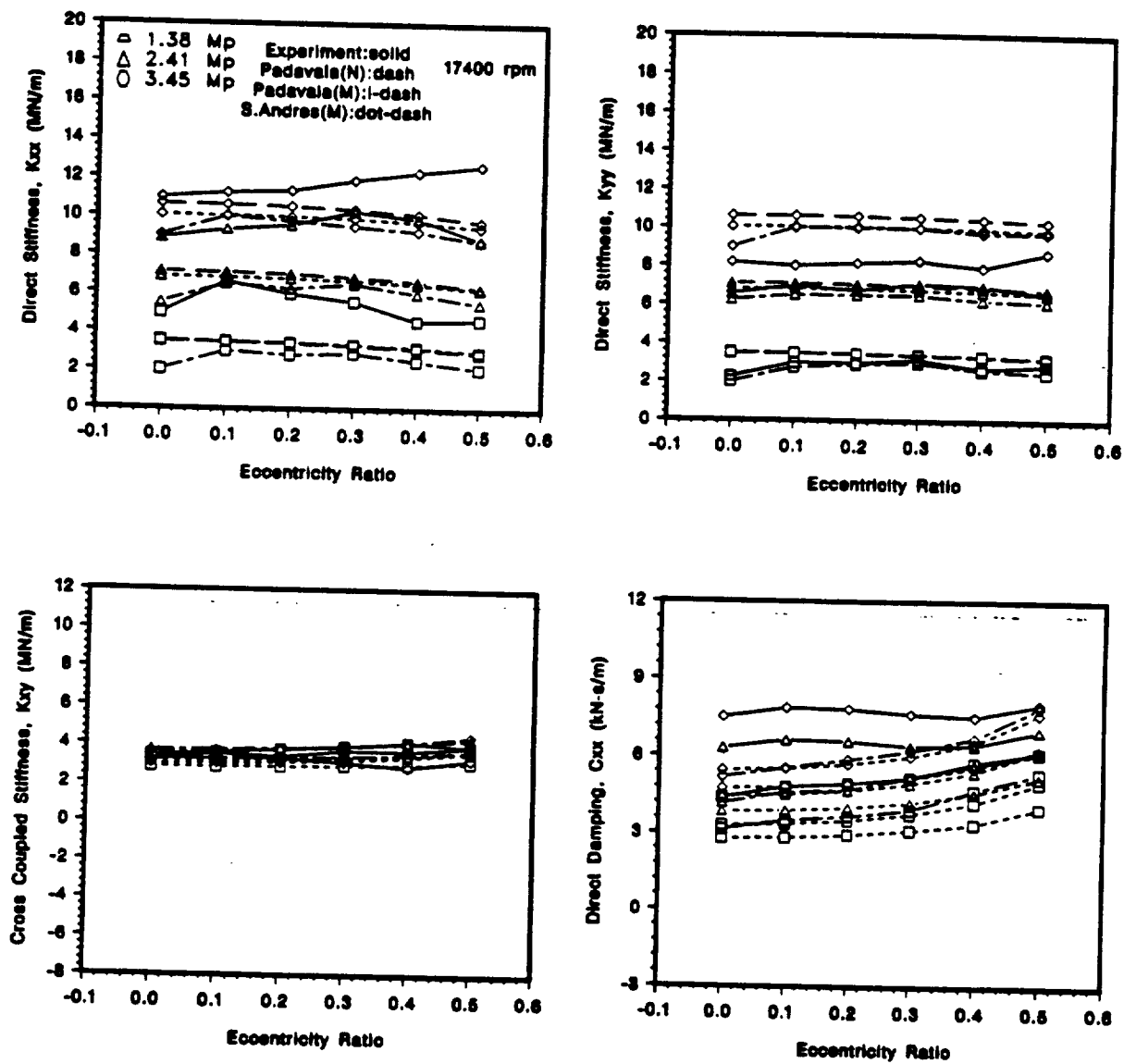


Figure 6.6 Dynamic Coefficients, Childs and Lindsey, Straight Seal, Eccentric (17400 rpm)

results based on nominal clearances point to the fact that possibly the measurement system employed to measure clearances during operation need to be refined.

There is considerable difference of more than 20% in leakage predictions between current analysis (MCLR) and San Andres' results, particularly for 17400 rpm and 24600 rpm cases.

6.1.8 Dynamic Coefficients, Convergent Seal, Eccentric Tests

The plots in Figure 6.8 and Figure 6.9 correspond to the dynamic coefficients for the slightly convergent seal configuration at 10200 rpm and 17400 rpm respectively. Excellent comparison of flow rates (NCL) translate into better correlation with dynamic coefficients, particularly for direct stiffness. For current analysis based on MCLR and San Andres report similar dynamic coefficients, with a slight variation in direct stiffness for the higher pressure differential case.

6.1.9 Conclusions

Lindsey makes the following conclusions based on the above study.

1. In general, results are consistent with theoretical predictions, except for flow rates.
2. Theory largely under predicts flow rates.
3. Flow rates comparison best for maximum divergent case
4. Direct Stiffness increases with taper parameter q .
5. Cross coupled stiffness predicted well by theory.
6. Damping decreases for $q < 0$ and $q > 0$.

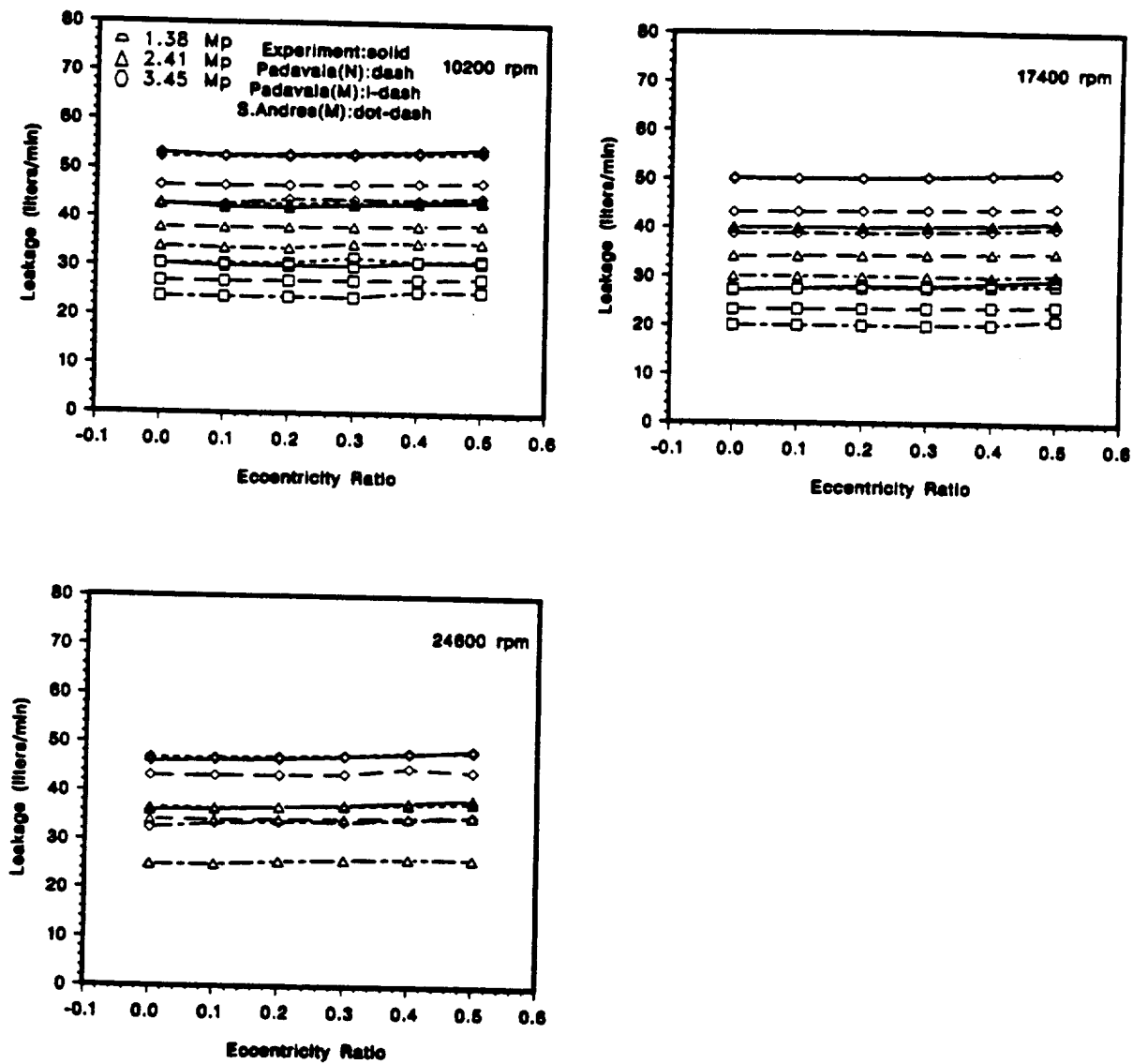


Figure 6.7 Leakage, Childs and Lindsey, Convergent Seal, Eccentric Tests

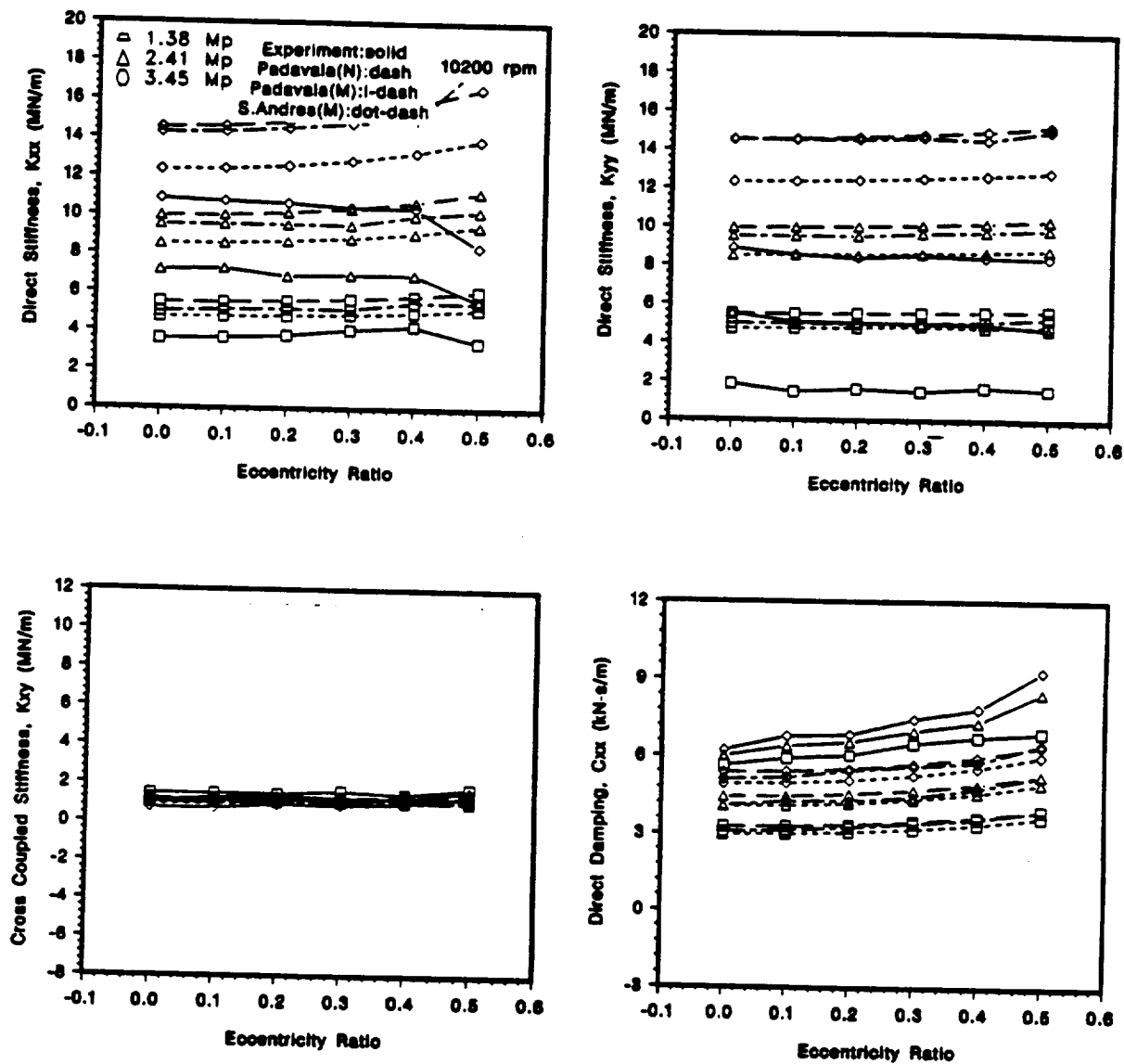


Figure 6.8 Dynamic Coefficients, Childs and Lindsey, Convergent Seal, Eccentric (10200 rpm)

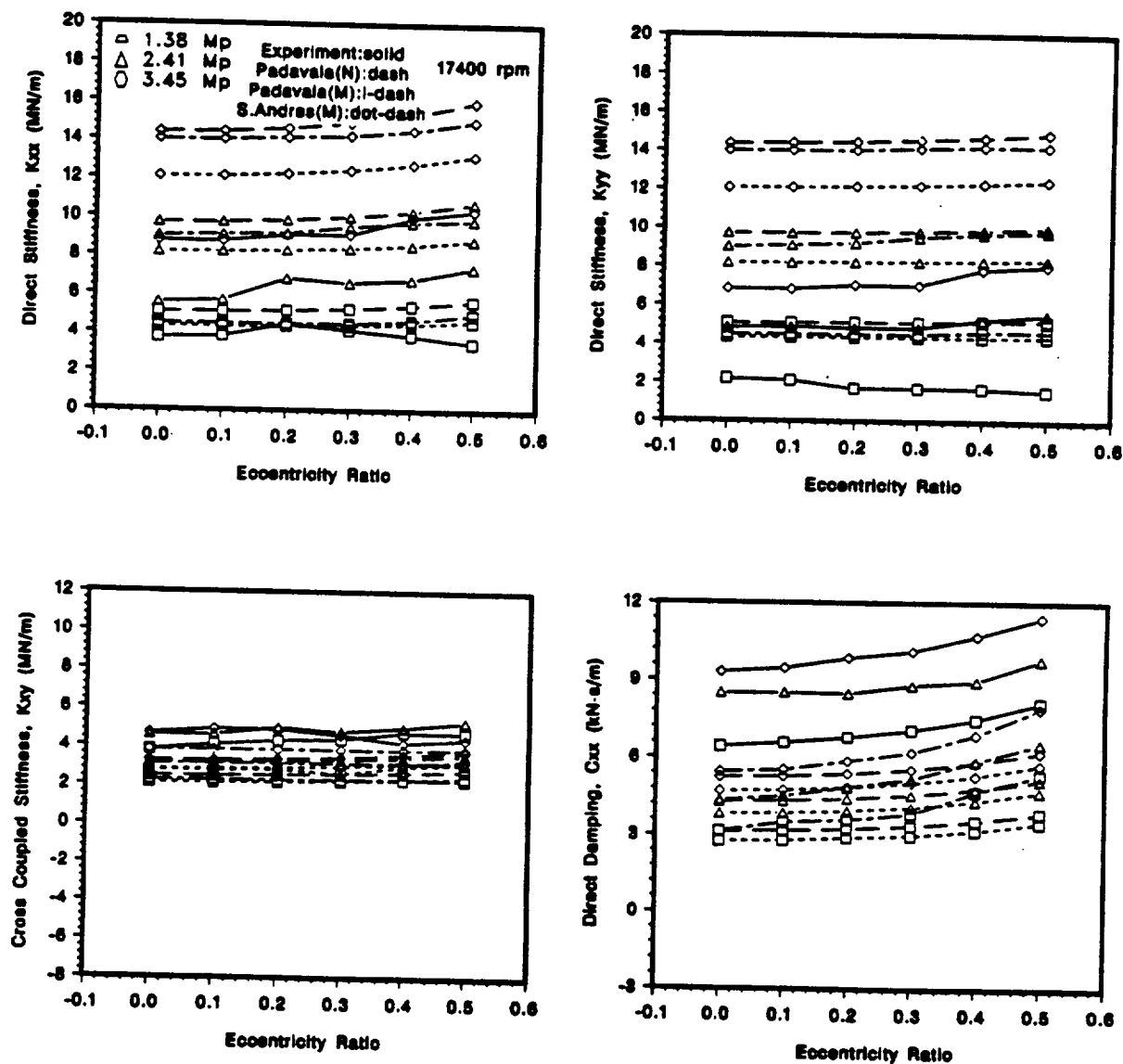


Figure 6.9 Dynamic Coefficients, Childs and Lindsey, Convergent Seal, Eccentric (17400 rpm)

7. Damping increases with eccentricity ratio.
8. For eccentric seals, the dynamic coefficients remain relatively constant upto an eccentricity ratio of 0.5.

Current analysis predictions based on nominal clearances for flow rates are much closer to measured flow rates than measured clearances based analyses. For convergent seal geometry, the flow rates almost match exactly. When measure clearances are used, current analysis shows a slightly better agreement (10–15%) than either *MUDY* or *HSEAL*. Comparison of all analyses in the case of direct stiffness is, at best, average. Current analysis based on NCLR gives a better correlation than the other analyses based on MCLR.

6.2 Childs and Kim (1985), Hirs Model

Childs and Kim [1985] presented an analytical and experimental study for rotordynamic coefficients of turbulent annular seals with different directionally-homogeneous surface roughness treatments for rotor and stator surfaces. The friction model is based on Hirs' model and constant properties are assumed and the analysis is for a concentric seal. The seal code based on the the analytical part of this study had been the mainstay of seal analysis work at NASA/MSFC for many years. MSFC provided this author with data for some test cases which were then compared with the results from the present analysis for Hirs' friction model. Results from one of the test cases is given in Table 6.2. The seal data for this example is given in *Appendix G*.

The results from current analysis for Hirs' friction model match well with the results of Childs and Kim (1985).

Table 6.2 Childs and Kim Check Case, Hirs' Model

<i>Data</i>	<i>Childs/Kim</i>	<i>Current Analysis</i>
K_{xx}	88.14 MN/m	88.14 MN/m
k_{xy}	11.11 MN/m	11.11 MN/m
C_{xx}	16.15 kN-s/m	16.14 kN-s/m
c_{xy}	0.419 kN-s/m	0.419 kN-s/m
M_{xx}	0.3215 kg	0.3214 kg
m_{xy}	-0.0024 kg	0.0005 kg
Q	7.959 kg/s	7.959 kg/s

6.3 Scharrer and Nunez (1989)

The effect of seal distortions on rotordynamic coefficients was first considered by Sharrer and Nunez (1989). They reported that a 2-D, axisymmetric, finite element analysis which considered the internal pressure distribution, and the boundary conditions due to assembly and operating interferences produced a clearance profile which was *wavy* and different from the nominal design tapered profile.

This distorted seal profile in the axial direction was fitted with a clearance function in the form of a polynomial as,

$$h(z) = a_1 + a_2z + a_3z^2 + a_4z^3 + a_5z^4 \quad (6.3)$$

where the coefficients a_1, a_2, \dots etc., are coefficients chosen to fit the distorted axial profile.

They adapted the analysis of a plain seal to the case of a wavy profile seal. They

Table 6.3 Scharrer and Nunez, Rough Wavy Seal Case

<i>Data</i>	<i>Scharrer/Nunez</i>	<i>Current Analysis</i>
K_{xx}	46.35 MN/m	57.30 MN/m
k_{xy}	52.02 MN/m	51.57 MN/m
C_{xx}	33.42 kN-s/m	33.65 kN-s/m
c_{xy}	1.49 kN-s/m	1.43 kN-s/m
M_{xx}	0.753 kg	0.772 kg
m_{xy}	0.026 kg	0.015 kg
Q	0.471 kg/s	0.462 kg/s

reported a marked change in the computed rotordynamic coefficients due to a change in the seal profile. These changes include, a) loss in direct stiffness b) increase in cross coupled stiffness c) increase in damping. The results for the case of rough wavy seal is given in Table 6.3. The direct stiffness between two analyses differ by about 20%.

6.4 Scharrer and Nelson (1990)

Scharrer and Nelson (1990) conducted a theoretical study of an annular seal with a partially tapered clearance. In this study, they investigated the axial distortion problem. They tried to correct the predicted distortions by machining out the undesirable distortions at the design stage itself. The model they used to accomplish this is a seal with a taper on part of length of the seal. Using this model, they conducted a parametric study of various performance characteristics as a function of taper length to total length ratio (T/L). Based on this study they recommended optimum ratio

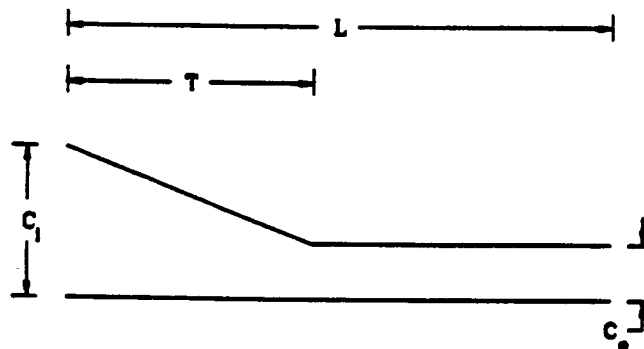


Figure 6.10 Scharrer and Nelson, A Partially Tapered Annular Seal

of T/L for best performance of these partially tapered seals from a rotordynamic analysis point of view.

They developed the analysis based on Hirs' turbulent lubrication equations (Hirs' friction model). In this analysis, the seal is assumed to have a taper only over a portion of the length of the seal and the rest of the seal is treated as a straight seal.

Figure 6.7 shows the details of a partially tapered seal. L is the total length and T is the taper length and c_i and c_e are inlet and exit clearances. The taper length/total length ratio is varied by varying the parameter, q given as,

$$q = T/L \quad (6.4)$$

The seal is a completely straight seal for $q = 0$ i.e., $c_i = c_e$ and a fully tapered seal for $q = 1.0$. This ratio is varied from 0 to 1 and its effect on leakage and rotordynamic coefficients is studied.

They analyzed two different seal configurations based on stator and rotor relative roughness.

1. Taper Smooth (varying q)
2. Taper Rough (varying q)

Table 6.4 Scharrer and Nelson, Partially Tapered Seals (Smooth), Taper=1.0

<i>Data</i>	<i>Scharrer/Nelson</i>	<i>Current Analysis</i>
K_{xx}	242.0 MN/m	215.0 MN/m
k_{xy}	65.5 MN/m	62.6 MN/m
C_{xx}	26.0 kN-s/m	24.8 kN-s/m
M_{xx}	0.66 kg	0.66 kg

For both the above cases, the inlet clearance to exit clearance ratio $\frac{c_i}{c_e}$ is maintained at 3. A portion of results from that study along with current analysis results are presented in Tables 6.4–6.9.

6.4.1 Smooth Seals

For the case of smooth seals, results are compared for three taper ratios;

1. taper ratio, $q = 1$, a fully tapered seal.
2. taper ratio, $q = 0.4$, a partially tapered seal.
3. taper ratio, $q = 0.0$, a fully straight seal.

Results given in Tables 6.4–6.6 show about 20% difference in K_{xx} and slightly smaller deviations for k_{xy} , for all cases.

6.4.2 Rough Seals

Similar results are reproduced for the case of rough seal for three different taper ratios. The results are shown in Tables 6.7–6.9. Again, as in the case of smooth seals,

Table 6.5 Scharrer and Nelson, Partially Tapered Seals (Smooth), Taper=0.4

<i>Data</i>	<i>Scharrer/Nelson</i>	<i>Current Analysis</i>
K_{zz}	220.0 MN/m	179.7 MN/m
k_{xy}	82.0 MN/m	75.26 MN/m
C_{zz}	32.0 kN-s/m	29.45 kN-s/m
M_{zz}	0.55 kg	0.55 kg

Table 6.6 Scharrer and Nelson, Partially Tapered Seals (Smooth), Taper=0.0

<i>Data</i>	<i>Scharrer/Nelson</i>	<i>Current Analysis</i>
K_{zz}	152.0 MN/m	159.0 MN/m
k_{xy}	102.5 MN/m	105.2 MN/m
C_{zz}	39.2 kN-s/m	40.1 kN-s/m
M_{zz}	1.02 kg	1.02 kg

Table 6.7 Scharrer and Nelson, Partially Tapered Seals (Rough), Taper=1.0

<i>Data</i>	<i>Scharrer/Nelson</i>	<i>Current Analysis</i>
K_{xx}	222.0 MN/m	194.0 MN/m
k_{xy}	61.0 MN/m	57.9 MN/m
C_{xx}	25.8 kN-s/m	24.3 kN-s/m
M_{xx}	0.66 kg	0.66 kg

there is difference of about 20% in direct stiffness. Both analyses use same governing equations with Hirs' friction model.

To explain this discrepancy, the results from this study are compared to Childs and Kim (1985) as all three analyses use the same governing equations based on Hirs' friction model and differing only in the solution procedure adopted. The results of this comparison are shown in Tables 6.10–6.11. These results show Scharrer and Nelson's analysis differs from Childs' and current analysis consistently. It is likely that Scharrer was using the same analysis that he and Nunez (1989) used for the wavy profile seal analysis where a similar discrepancy was also noted. The seal data for this study is included in Appendix G.

6.5 Jenssen (1970)

Jenssen (1970) investigated experimentally the load bearing capacity of smooth liquid annular seals at various eccentricities. The test data was collected for three pressure differentials, 0.344 Mpa, 1.034 Mpa, 1.724 Mpa and at three different speeds 3000 rpm, 5000 rpm and 7000 rpm. The seals used in the experiment are long seals ($L/D=1.025$) with water as the working fluid. He also presents theoretical predictions based on

Table 6.8 Scharrer and Nelson, Partially Tapered Seals (Rough), Taper=0.4

<i>Data</i>	<i>Scharrer/Nelson</i>	<i>Current Analysis</i>
K_{xx}	190.0 MN/m	170.2 MN/m
k_{xy}	68.0 MN/m	70.0 MN/m
C_{xx}	29.0 kN-s/m	29.0 kN-s/m
M_{xx}	0.67 kg	0.59 kg

Table 6.9 Scharrer and Nelson, Partially Tapered Seals (Rough), Taper=0.0

<i>Data</i>	<i>Scharrer/Nelson</i>	<i>Current Analysis</i>
K_{xx}	118.0 MN/m	121.0 MN/m
k_{xy}	87.5 MN/m	89.3 MN/m
C_{xx}	38.2 kN-s/m	38.6 kN-s/m
M_{xx}	1.08 kg	1.09 kg

Table 6.10 Scharrer and Nelson, Comparison with Childs and Kim, Taper=1.0, Rough

<i>Data</i>	<i>Scharrer/Nelson</i>	<i>Childs/Kim</i>	<i>Current Analysis</i>
K_{xx}	242.0 MN/m	215.7 MN/m	214.8 MN/m
k_{xy}	65.52 MN/m	62.74 MN/m	62.69 MN/m
C_{xx}	26.0 kN-s/m	24.8 kN-s/m	24.8 kN-s/m
c_{xy}	—	3.16 kN-s/m	3.16 kN-s/m
M_{xx}	0.66 kg	0.66 kg	0.66 kg
m_{xy}	—	0.0027 kg	-0.0041 kg
Q	—	9.568 kg/s	9.551 kg/s

Table 6.11 Scharrer and Nelson, Comparison with Childs and Kim, Taper=1.0, Rough

<i>Data</i>	<i>Scharrer/Nelson</i>	<i>Childs/Kim</i>	<i>Current Analysis</i>
K_{xx}	222.0 MN/m	194.6 MN/m	193.8 MN/m
k_{xy}	61.0 MN/m	58.1 MN/m	57.9 MN/m
C_{xx}	25.80 kN-s/m	24.36 kN-s/m	24.30 kN-s/m
c_{xy}	—	2.72 kN-s/m	2.72 kN-s/m
M_{xx}	0.66 kg	0.66 kg	0.66 kg
m_{xy}	—	-0.0042 kg	-0.0074 kg
Q	—	8.356 kg/s	8.346 kg/s

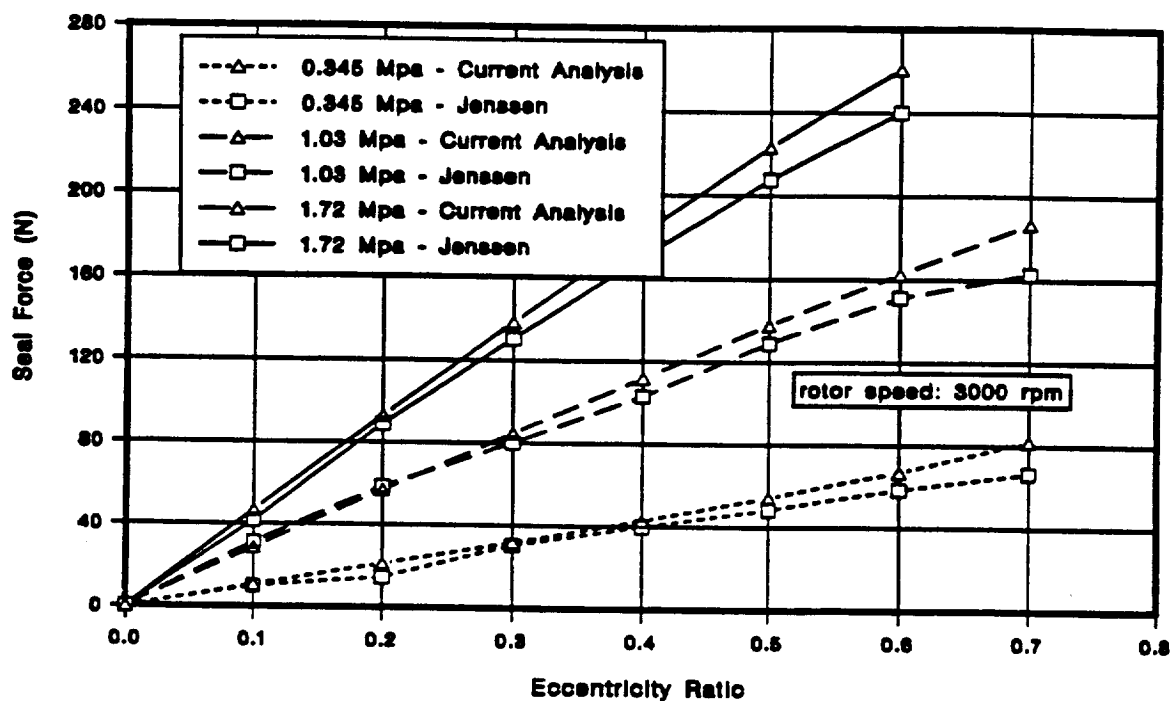


Figure 6.11 Seal Force at 3000 rpm, Jenssen

short seal assumption which are not shown here. The seal input data for this case is taken from Nguyen (1988) and is given in the Appendix G. Results from the current analysis along with the experimental data are given Figures 6.11–6.13, for the three rotor speeds.

The steady state seal forces are plotted as a function of eccentricity ratio and the predictions from the current analysis agree well with the experimental data for all pressure differentials and at all speeds.

6.6 Kanki and Kawakami (1984)

Kanki and Kawakami (1984) investigated the dynamic bearing effects of long pump annular seals as a function of eccentricity. Nguyen (1988), reported convergence problems at eccentricity ratios of above 0.4 with the original method as shown in the

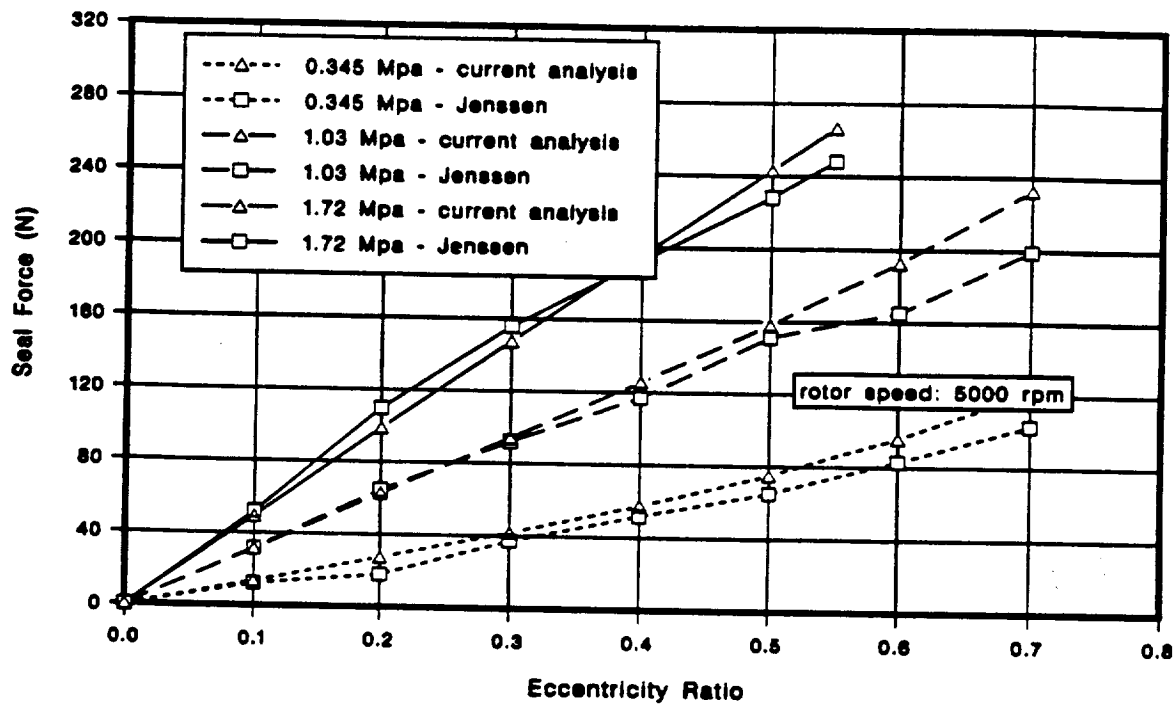


Figure 6.12 Seal Force at 5000 rpm, Jenssen

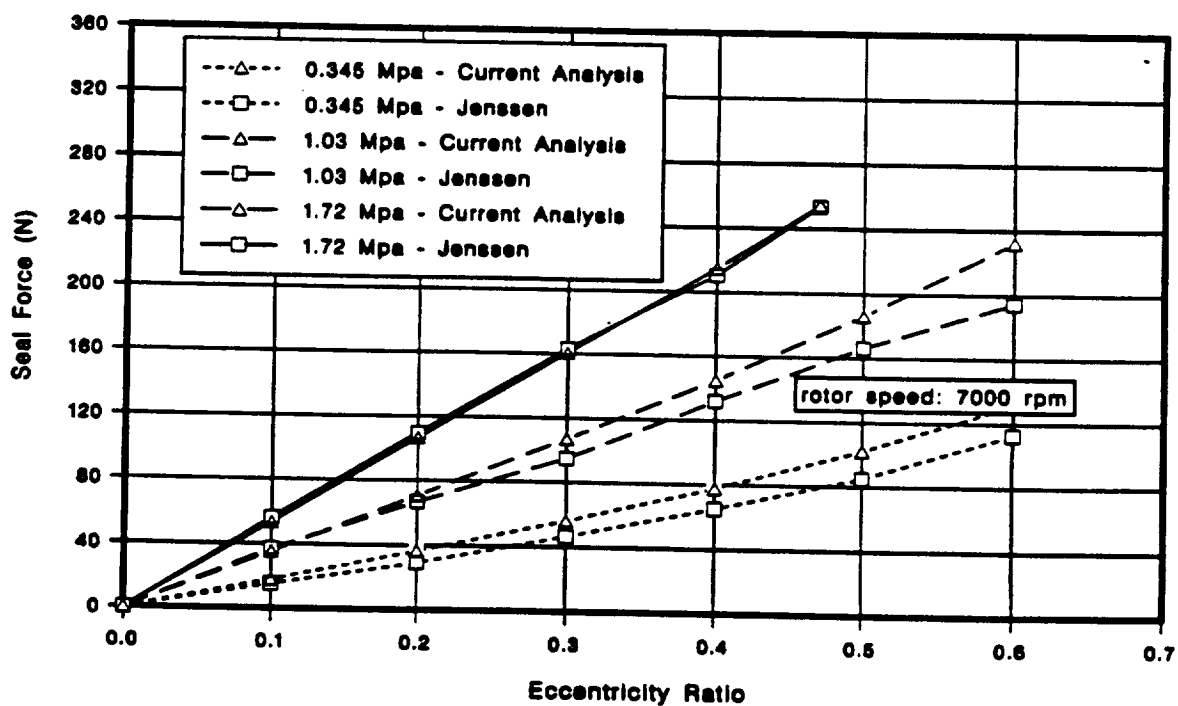


Figure 6.13 Seal Force at 7000 rpm, Jenssen

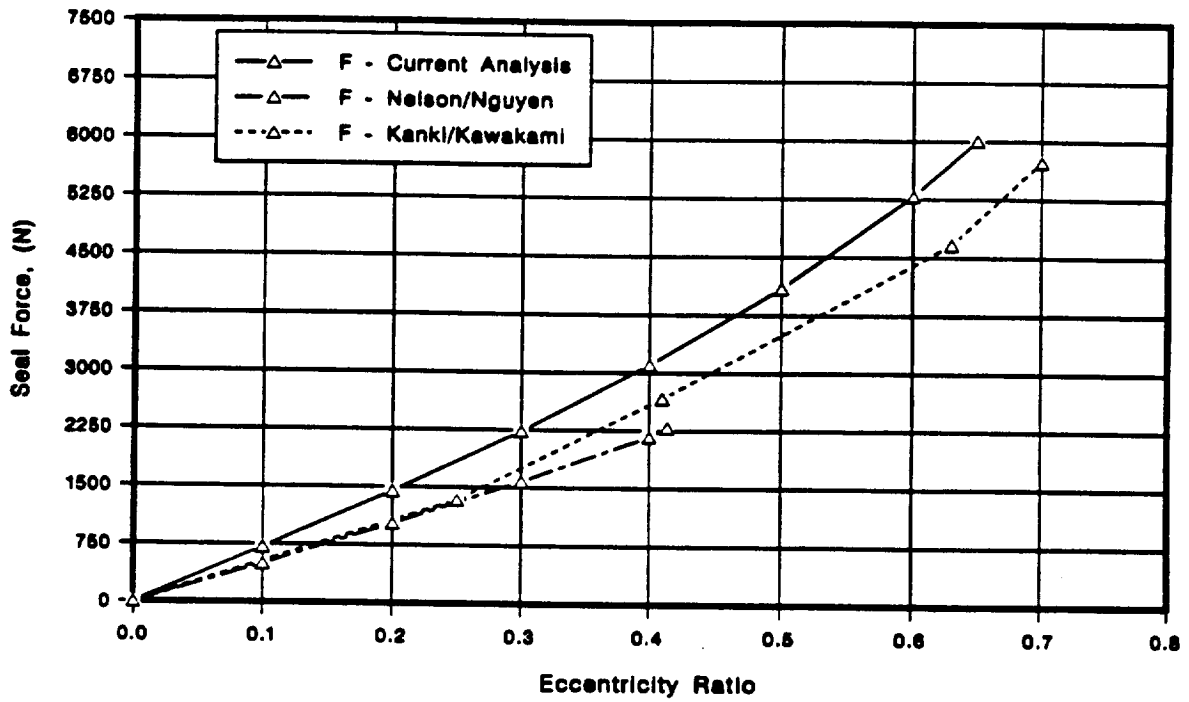
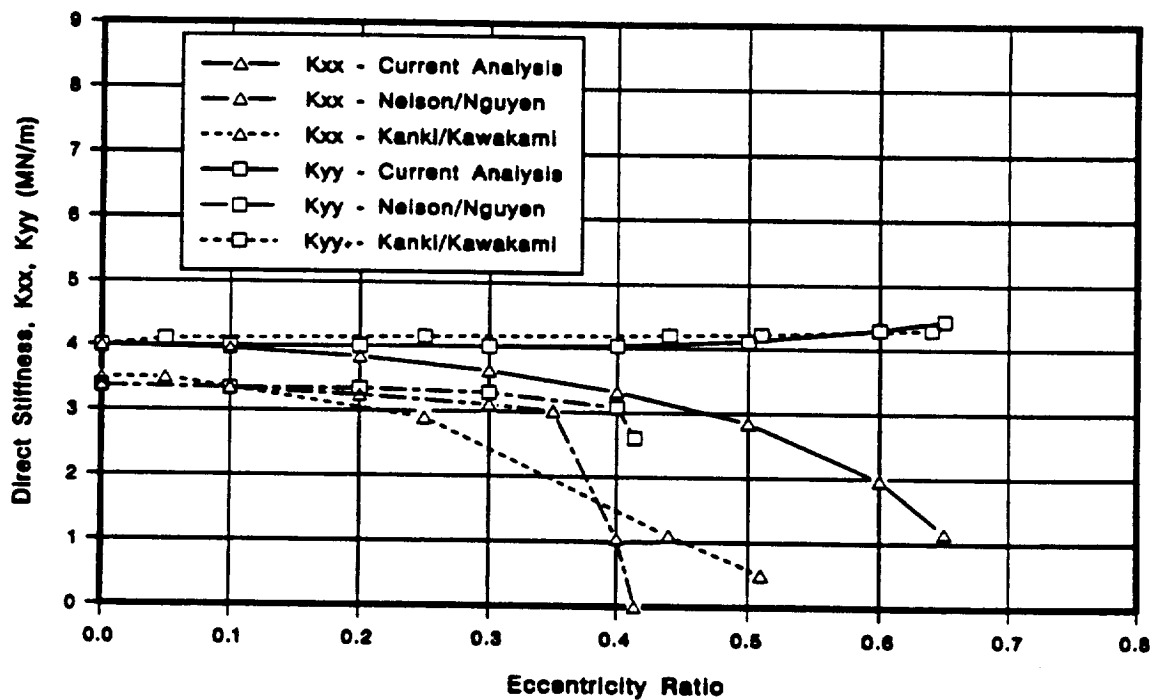
plots Figures 6.14–6.18. Beyond 0.4 eccentricity ratio, Nguyen's method has problems converging and he attributes this convergence problem to the onset of laminar flow and inability of the analysis to deal with negative direct stiffness. However, with the current analysis such a problem is not encountered. The test seal is a long smooth seal ($L/D=1.0$) and the working fluid is water.

The results for this case along with Nguyen's results are shown in Figures 6.14–6.18. It is true that the solution procedure has problems dealing with negative direct stiffness. However, this condition is rarely encountered in practical seal design and thus need not of major concern as far as the efficacy of this analysis is concerned.

Figure 6.14 shows the steady state seal force as a function of eccentricity. Nguyen (1988) results are only upto 0.4 due to numerical problems while the current analysis gives reasonably good results upto 0.65.

Nguyen's analysis predicts direct stiffness K_{yy} to decrease with eccentricity as shown in Figure 6.15. Current analysis predicts this direct stiffness in line with the test data, i.e., increase with eccentricity for K_{yy} and decrease with eccentricity for K_{xx} . Also, Nguyen's analysis runs into convergence problems around 0.4 eccentricity ratio. Current analysis encounters no such problems. There is reasonably good comparison for cross coupled stiffness, k_{xy} , k_{yx} , between current analysis and test data.

The main feature of the results presented in this case is the better convergence properties of the current analysis based on cubic splines compared to the original approach of Nelson and Nguyen based on *Fast Fourier Transforms* (FFT). Also, the results from current analysis agree with experimental data better than Nelson and Nguyen's analysis.

Figure 6.14 Seal Force, F , for Kanki and KawakamiFigure 6.15 Direct Stiffness, K_{xx} , K_{yy} for Kanki and Kawakami

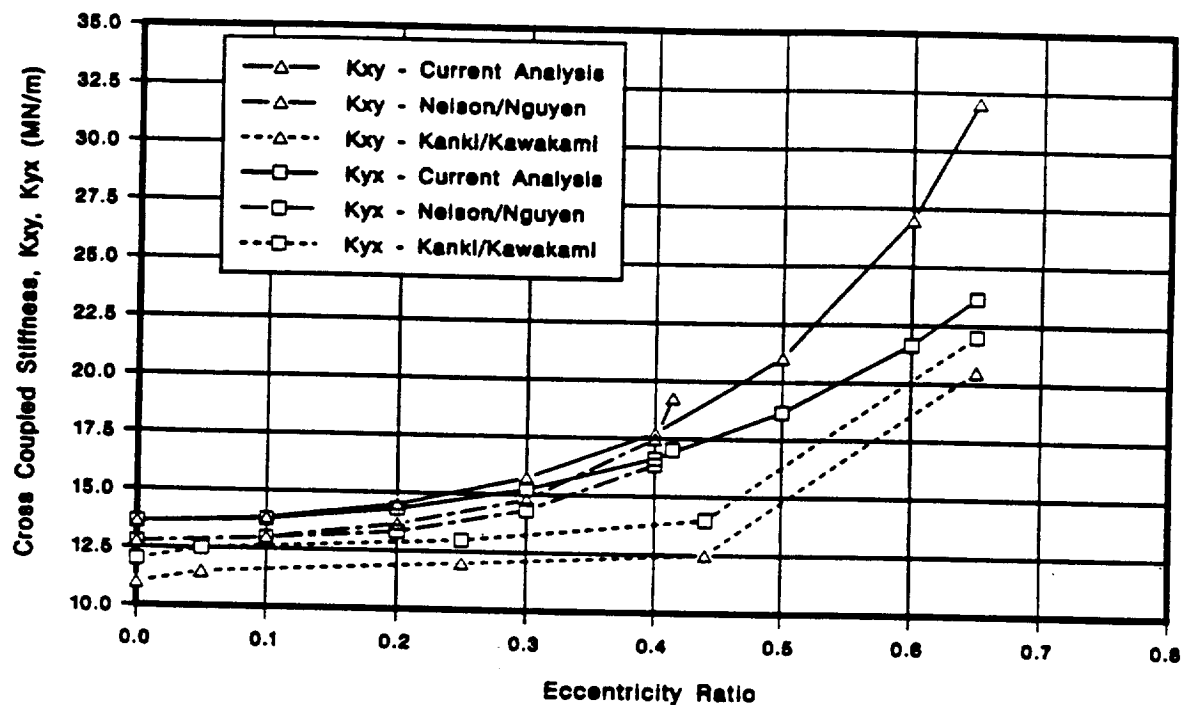


Figure 6.16 Cross Coupled Stiffness, k_{xy} , k_{yx} for Kanki and Kawakami

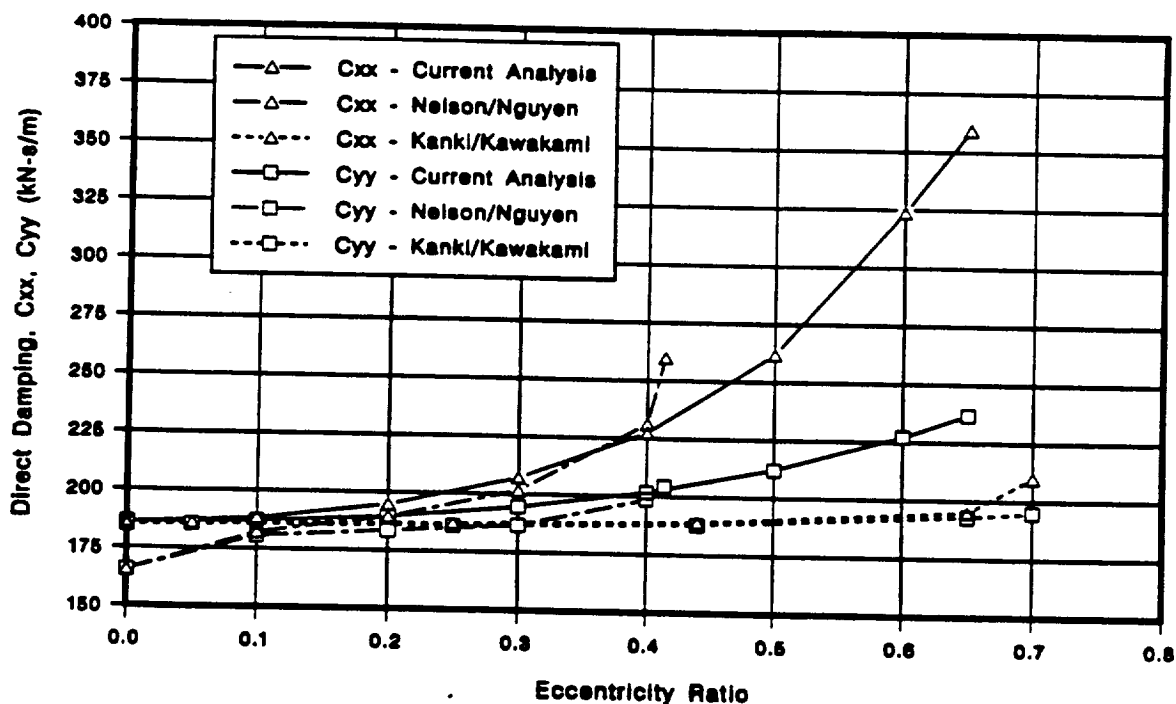


Figure 6.17 Direct Damping, C_{xx} , C_{yy} , for Kanki and Kawakami

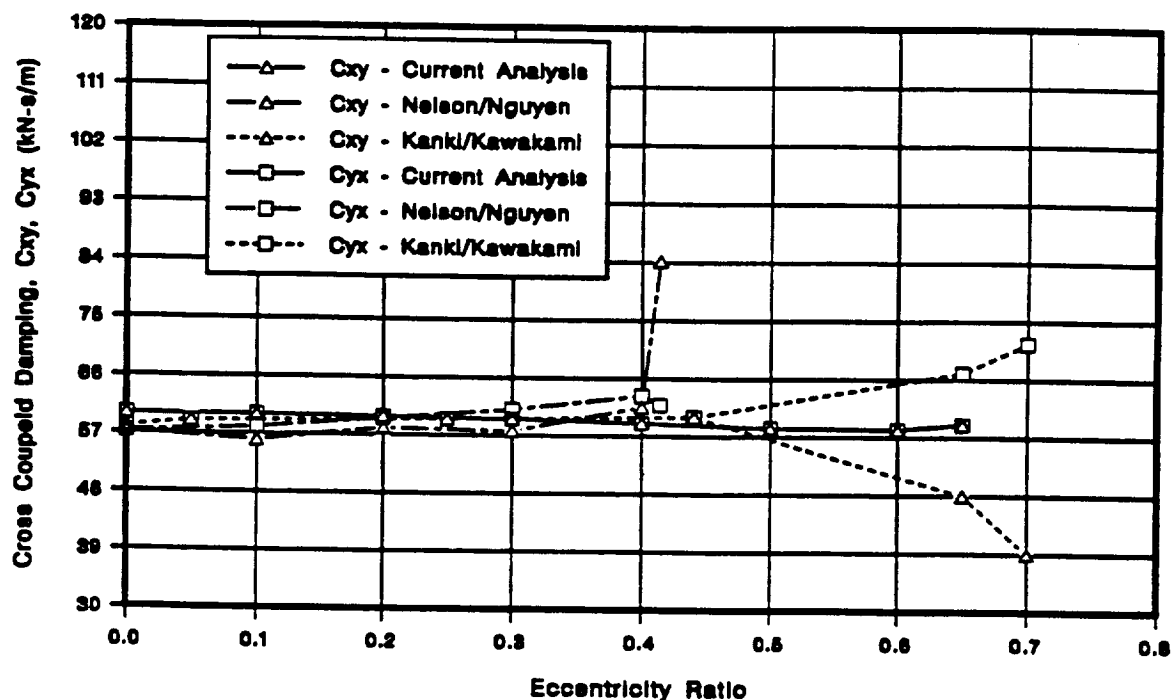


Figure 6.18 Cross Coupled Damping, c_{xy} , c_{yx} for Kanki and Kawakami

6.7 Falco *et al.* (1984)

In this combined experimental and theoretical work, Falco *et al.* investigated the effect of eccentricity on the dynamic coefficients of an annular seal. Their analytical work was based on a finite element model and they compared the analytical results with experimental test data. They compared their theoretical predictions with the various methods in use at that time and concluded that their finite element based analysis provided the best comparison with experimental data. Subsequently, Nguyen (1988) showed that the predictions from his analysis were in better agreement than Falco's theoretical results. In plots shown in Figures 6.22–6.26, Falco's experimental results along with Nguyen's predictions and current analysis results are given. The input data used is from Nguyen (1988) and is given in Appendix G. The results show good comparison with the original Nguyen's approach.

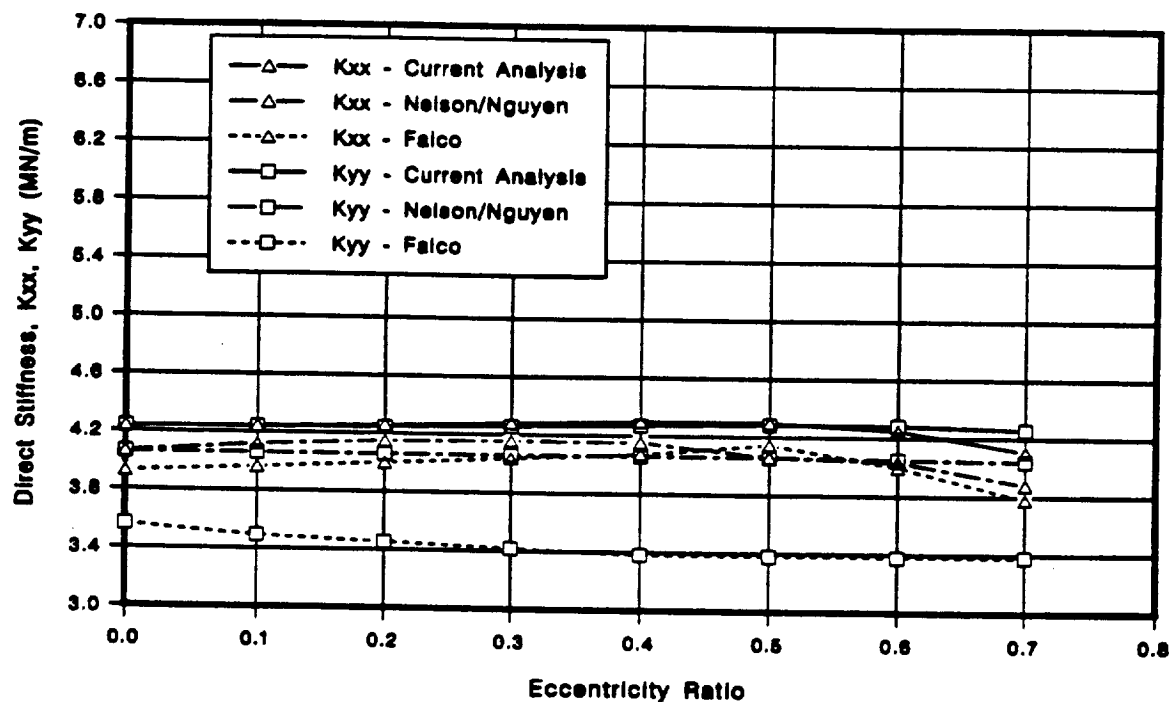


Figure 6.19 Direct Stiffness K_{xx} , K_{yy} , for Falco *et al.*

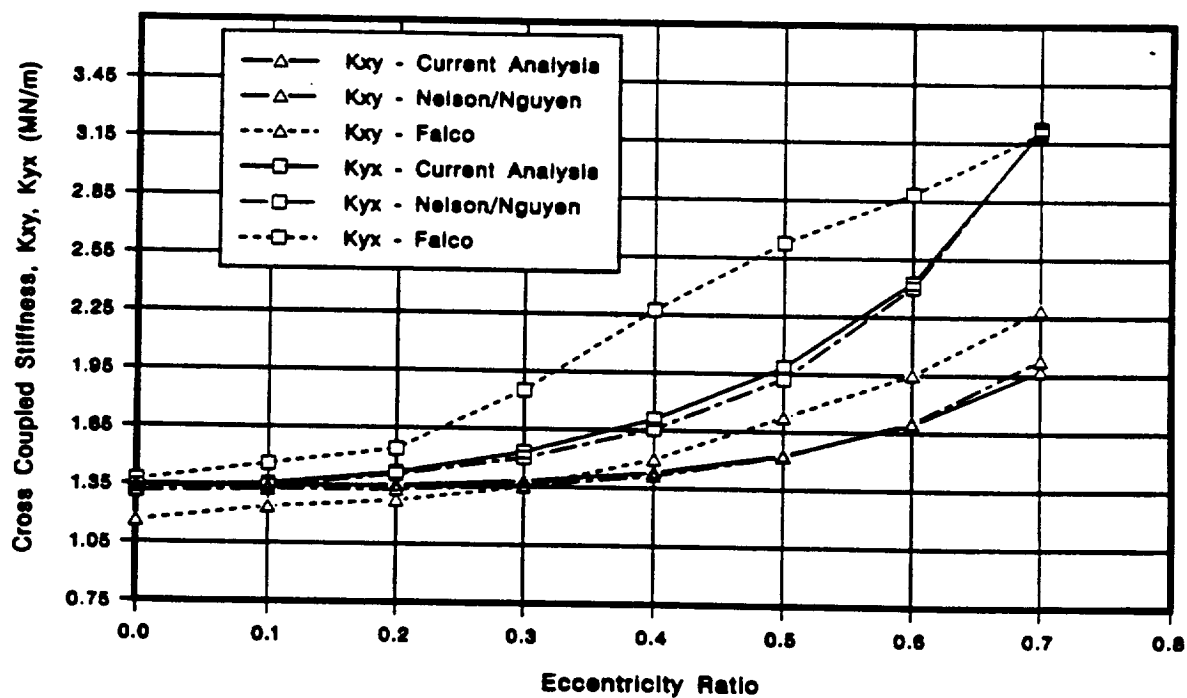


Figure 6.20 Cross Coupled Stiffness k_{xy} , k_{yx} for Falco *et al.*

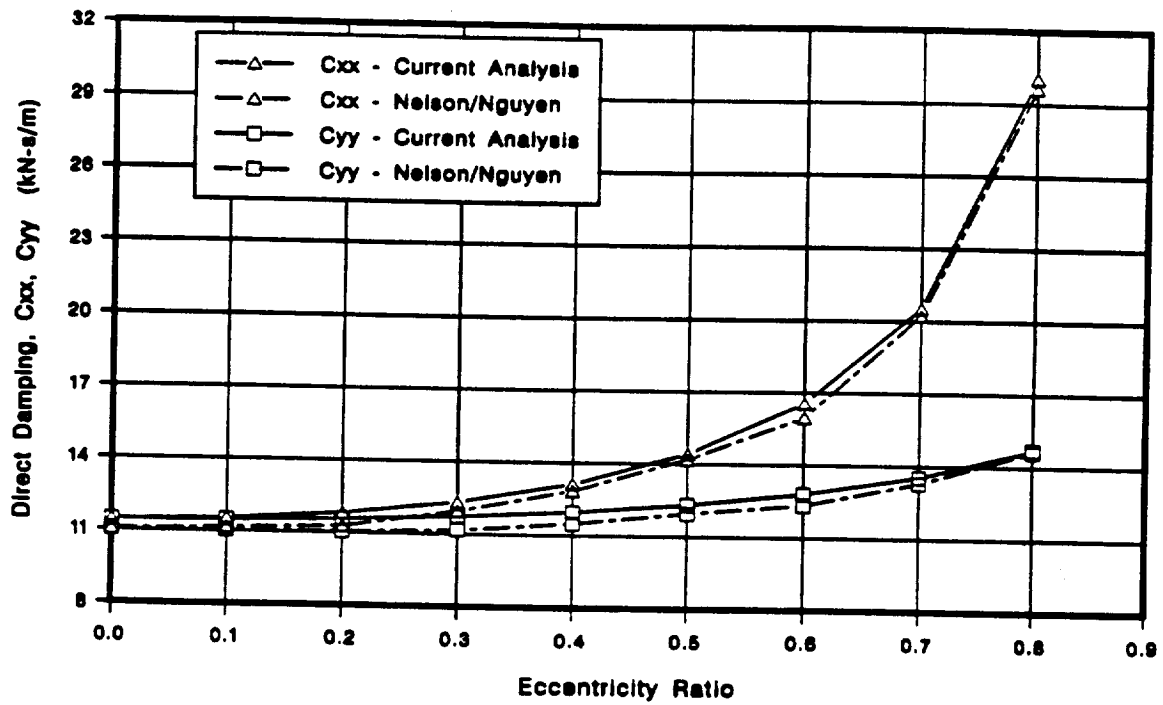


Figure 6.21 Direct Damping, C_{xx} , C_{yy} , for Falco *et al.*

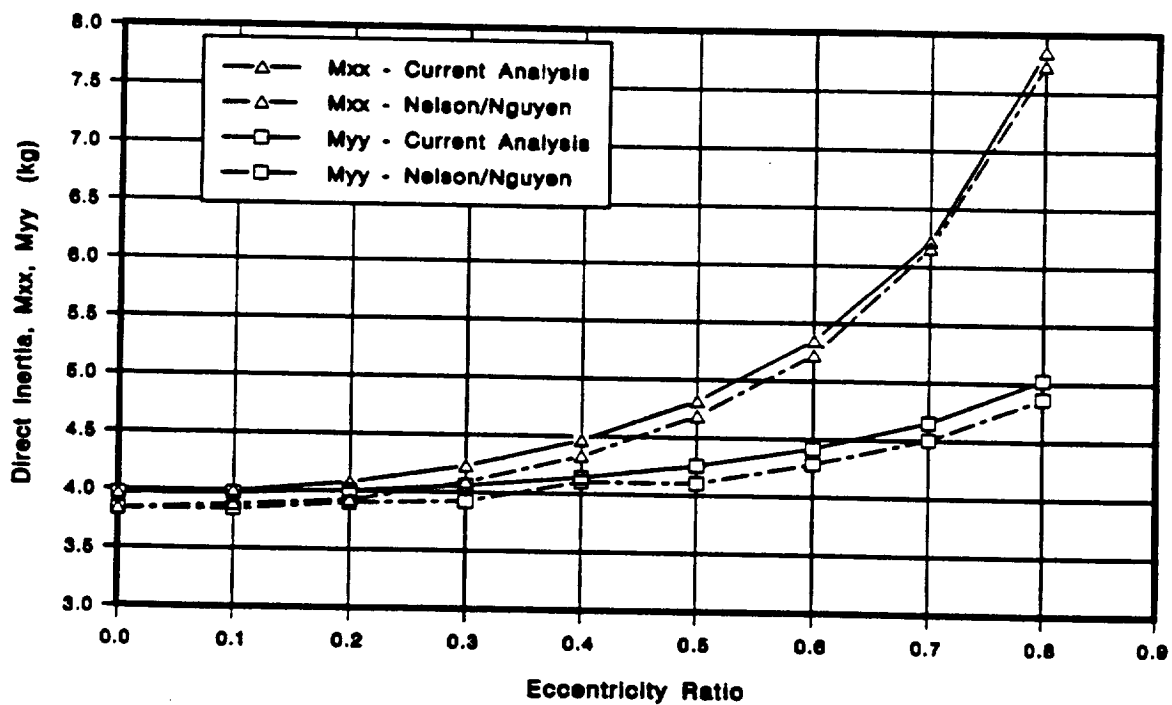


Figure 6.22 Direct Inertia, M_{xx} , M_{yy} for Falco *et al.*

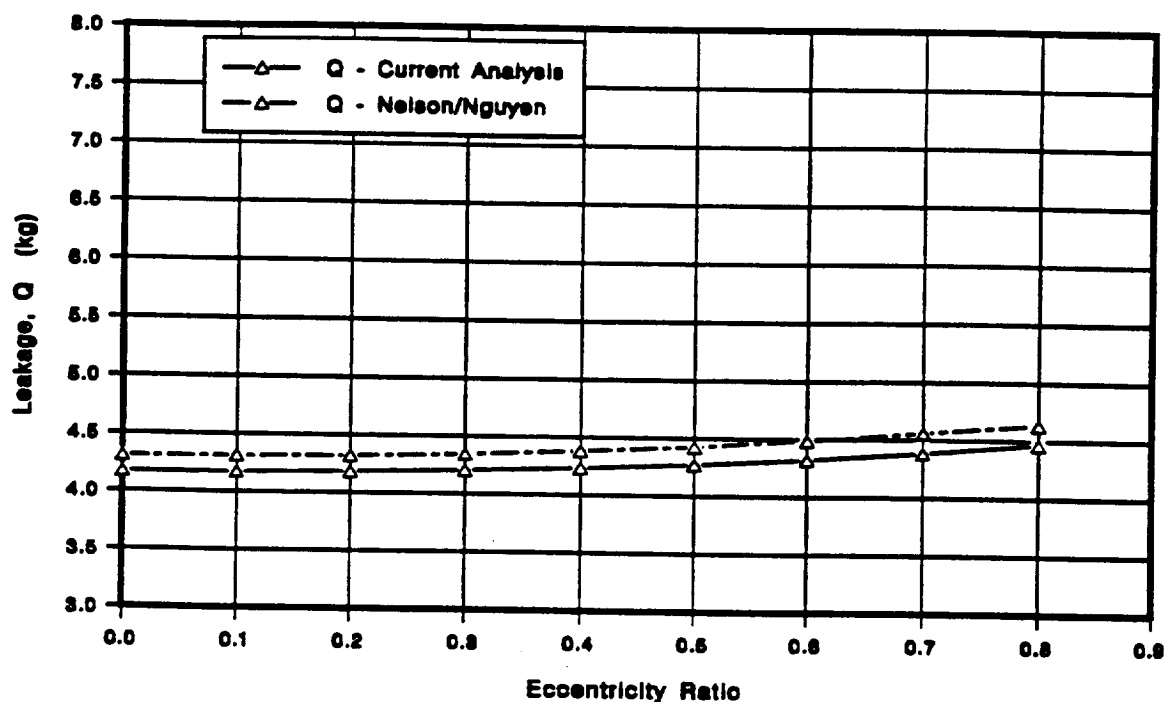


Figure 6.23 Leakage, Q , for Falco *et al.*

6.8 Allaire *et al.* (1976)

In this work, Allaire *et al.* investigated the effects of large eccentricity on the dynamic coefficients of interstage seal of Space Shuttle Main Engine High Pressure Fuel Turbopump (SSME-HPFTP). They used a solution approach using the *short* seal assumption (Couette flow) and a Blassius-type turbulent friction factor model. The results from current analysis along with Nelson and Nguyen predictions are given in Figures (6.19–6.21). The seal input data is taken from Nguyen (1988) and is included in the Appendix G.

6.9 Comparison of Variable Properties Model with Constant Properties Model

Results from a distorted seal analysis have been discussed in Chapter V. This exercise is repeated for the variable properties model developed in Chapter III. Comparisons

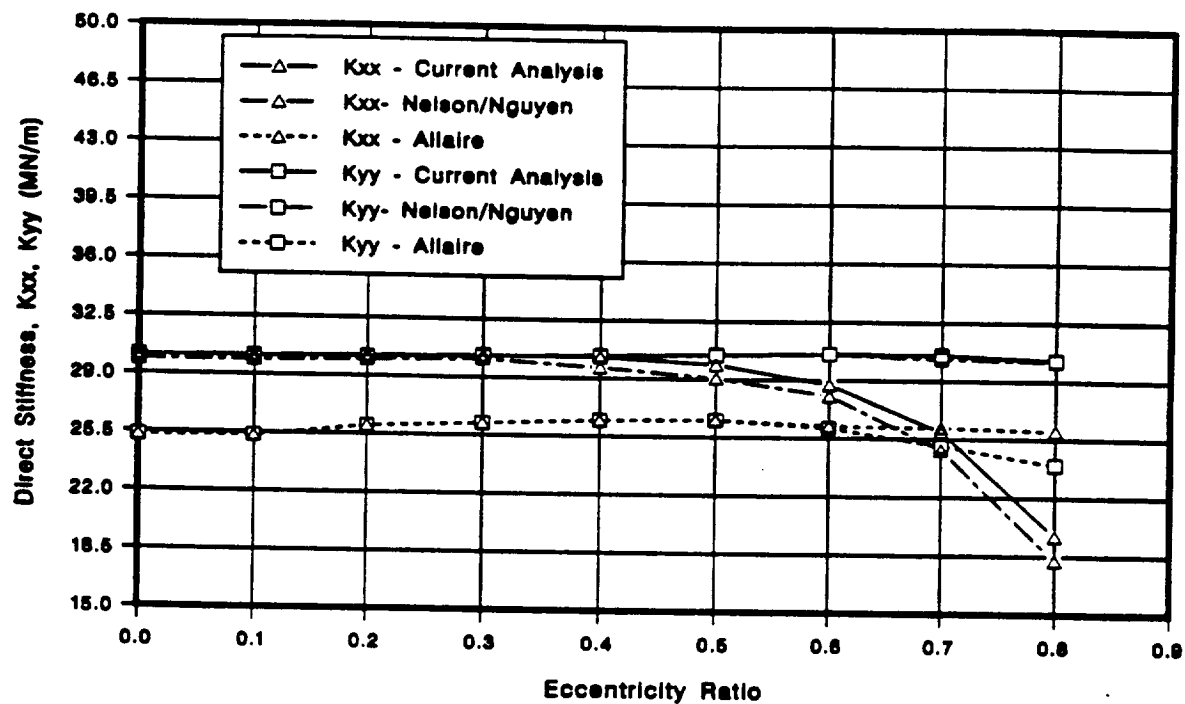


Figure 6.24 Direct Stiffness, K_{xx} , K_{yy} , for Allaire *et al.*

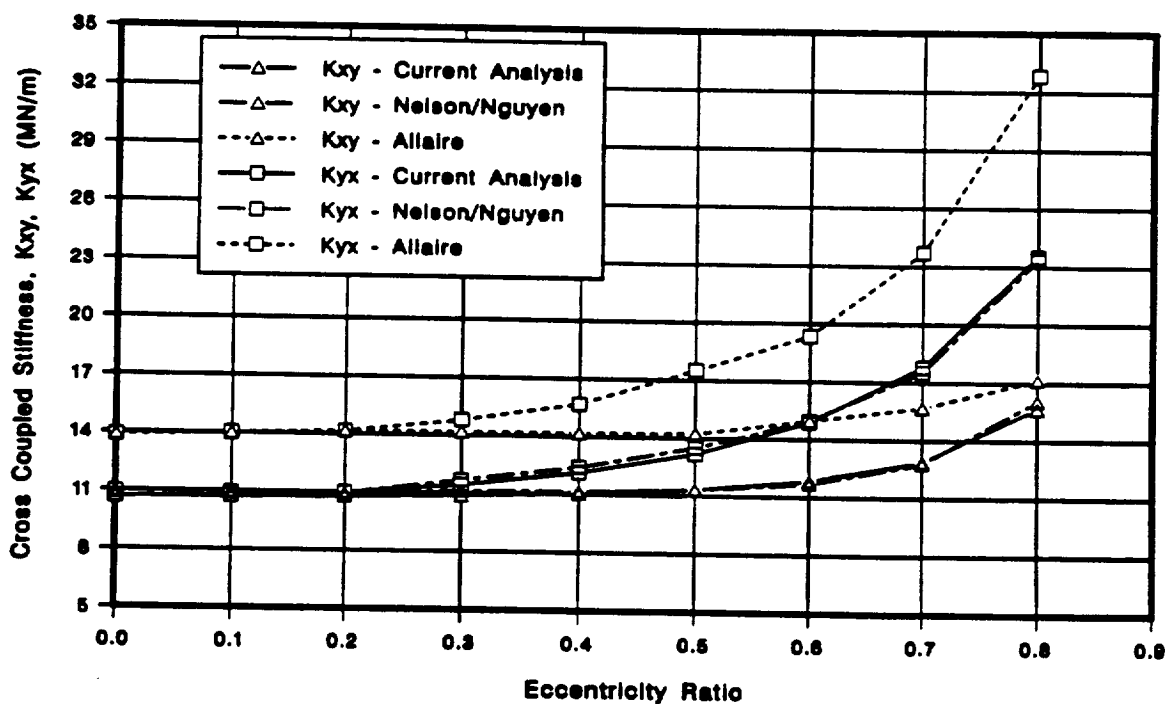


Figure 6.25 Cross Coupled Stiffness, k_{xy} , k_{yx} , for Allaire *et al.*

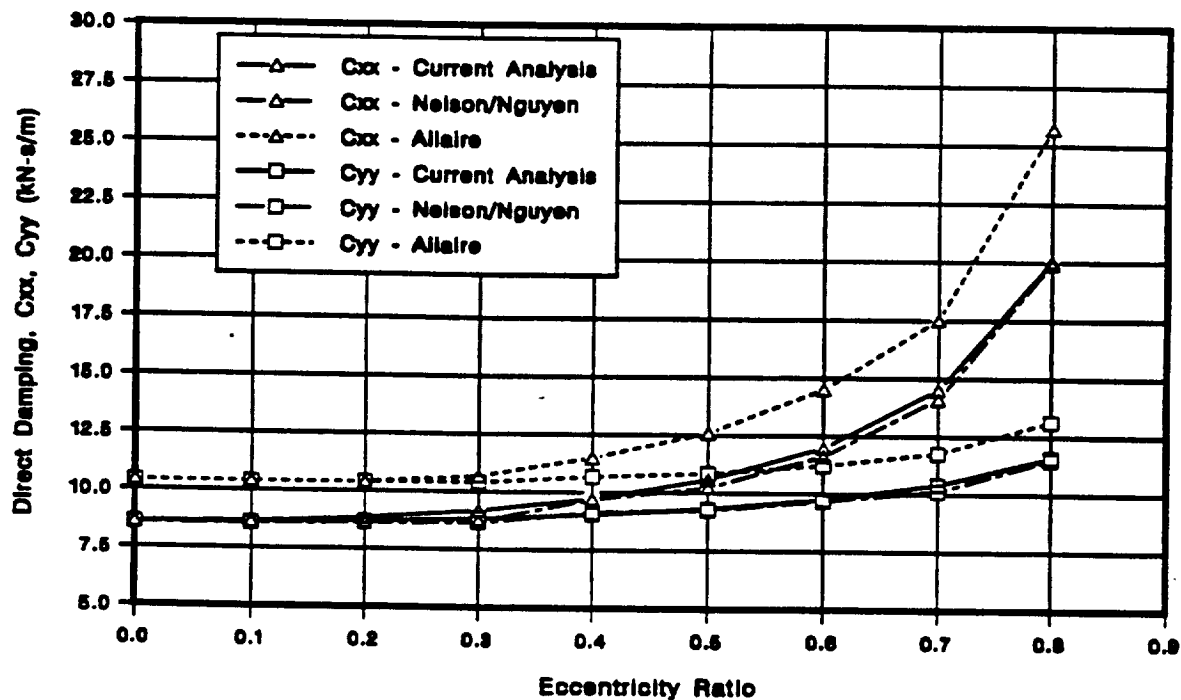


Figure 6.26 Direct Damping, C_{xx} , C_{yy} for Allaire *et al.*

made between the two models are shown in Figures 6.22–6.27.

The main difference between these two models is a reduction in direct stiffness for the variable properties case and its difference with eccentricity as shown in Figure 6.22. This may be explained by the inclusion of compressibility into the analysis, in effect making the *spring* softer. There is negligible difference in other coefficients.

Leakage, shown in Figure 6.27, is expectedly smaller for the variable properties model due to a decrease in density.

6.10 San Andres *et al.* (1992), Isothermal Case

San Andres *et al.* (1992) presented theoretical results for a straight seal with thermal effects and variable fluid properties. Two cases are considered.

1. Isothermal flow

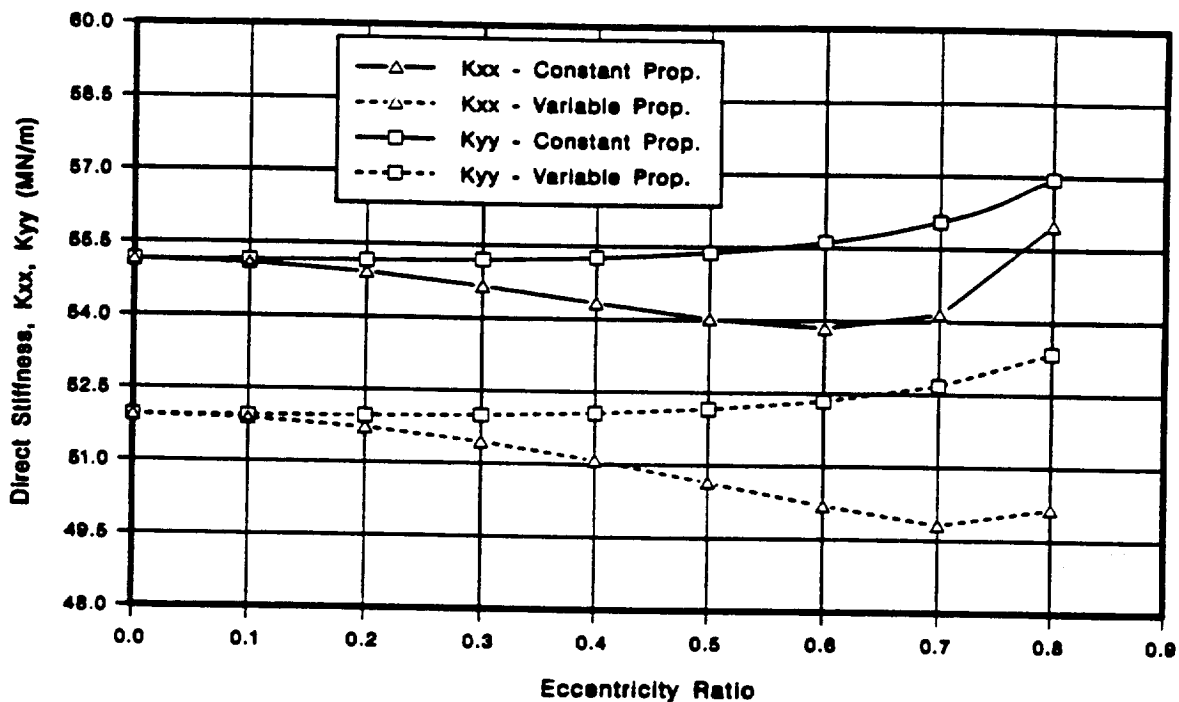


Figure 6.27 Direct Stiffness K_{xx} , K_{yy} , for Seal Unit 3-01

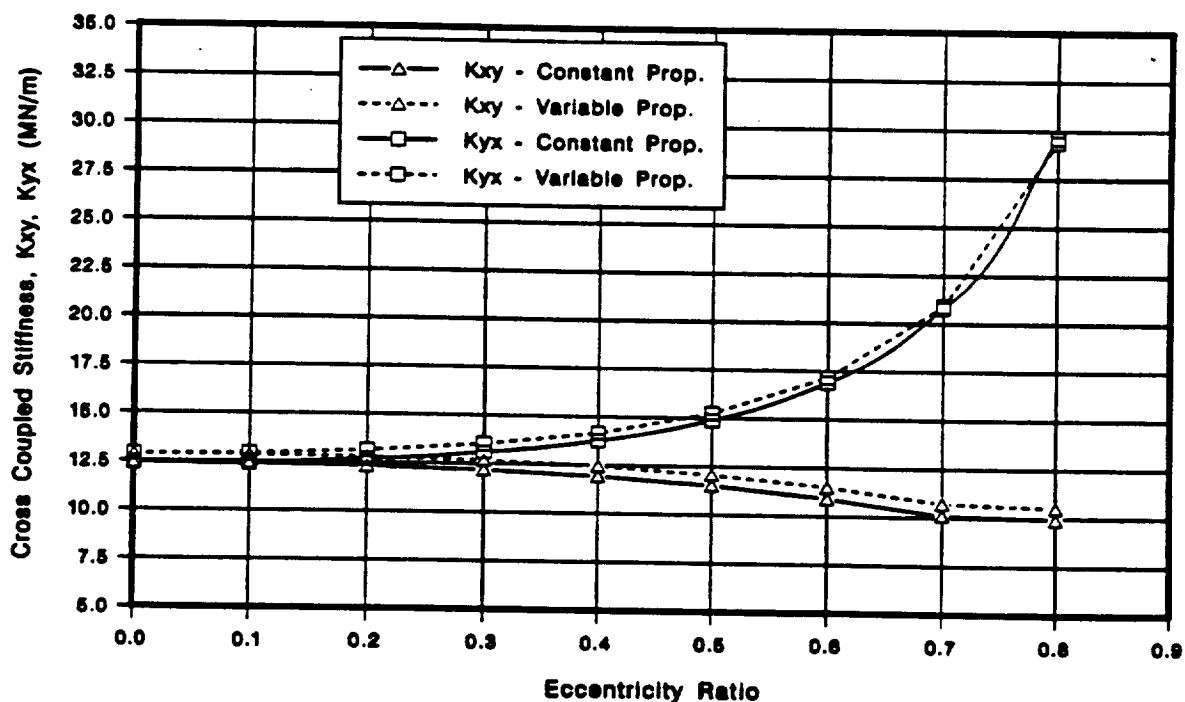


Figure 6.28 Cross Coupled Stiffness k_{xy} , k_{yx} , for Seal Unit 3-01

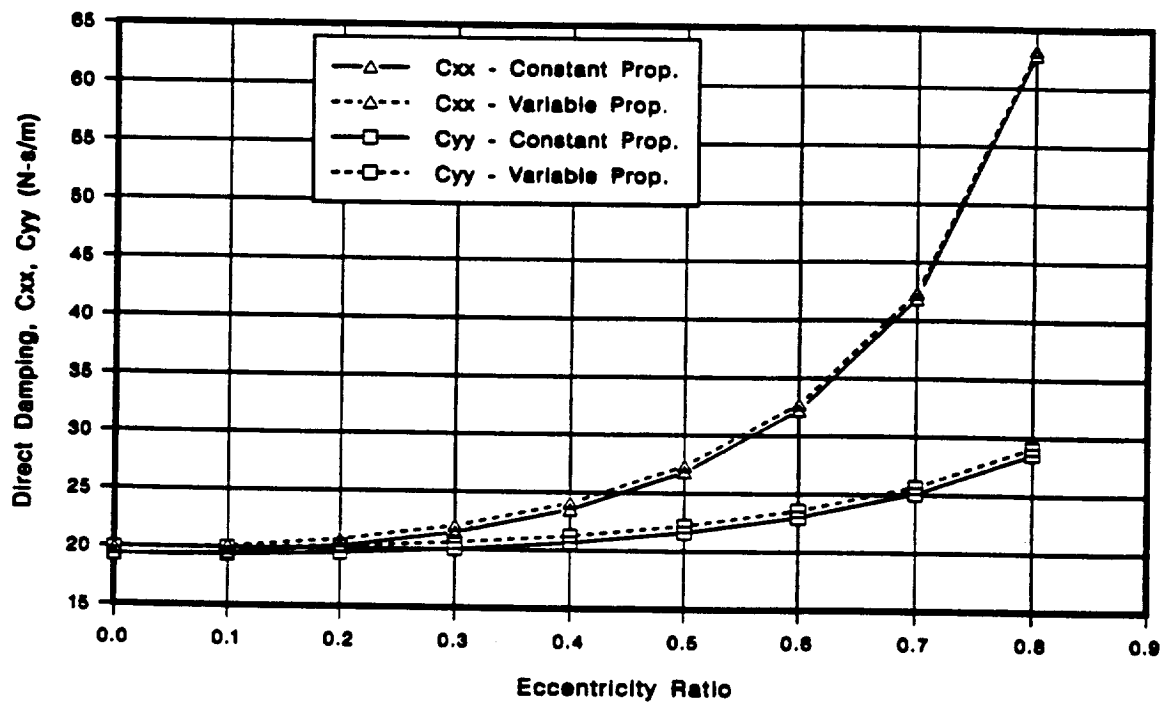


Figure 6.29 Direct Damping, C_{xx} , C_{yy} for Seal Unit 3-01

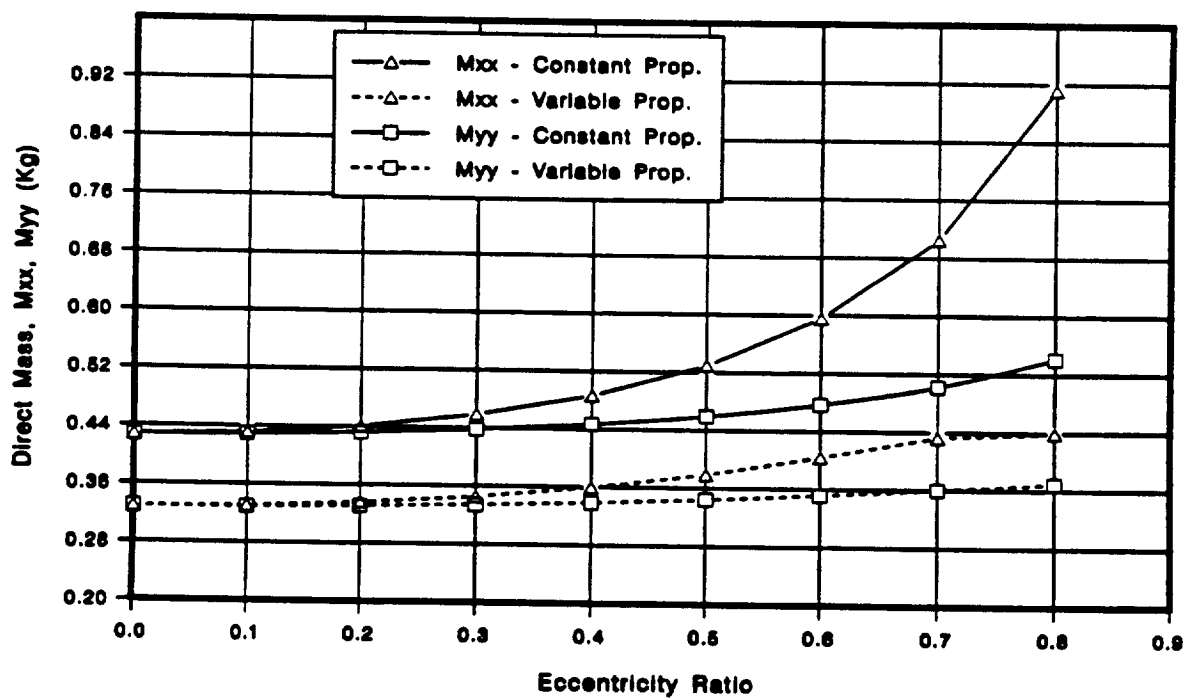


Figure 6.30 Direct Inertia, M_{xx} , M_{yy} for Seal Unit 3-01

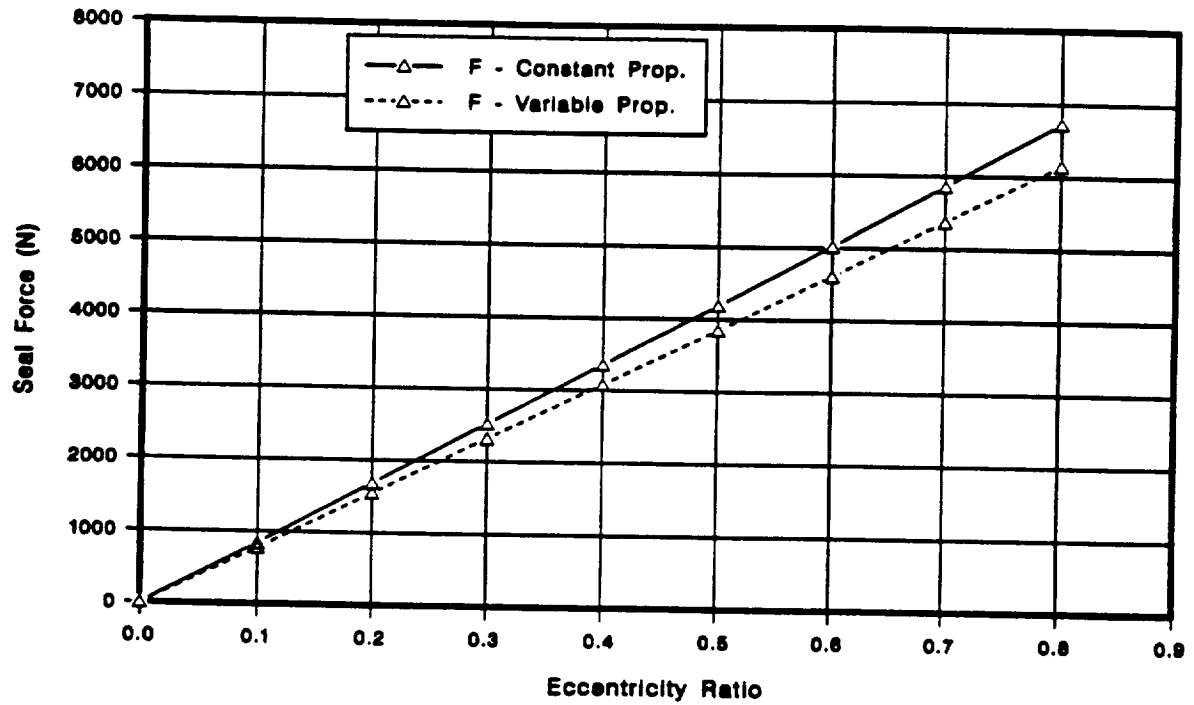


Figure 6.31 Seal Force, F, for Seal Unit 3-01

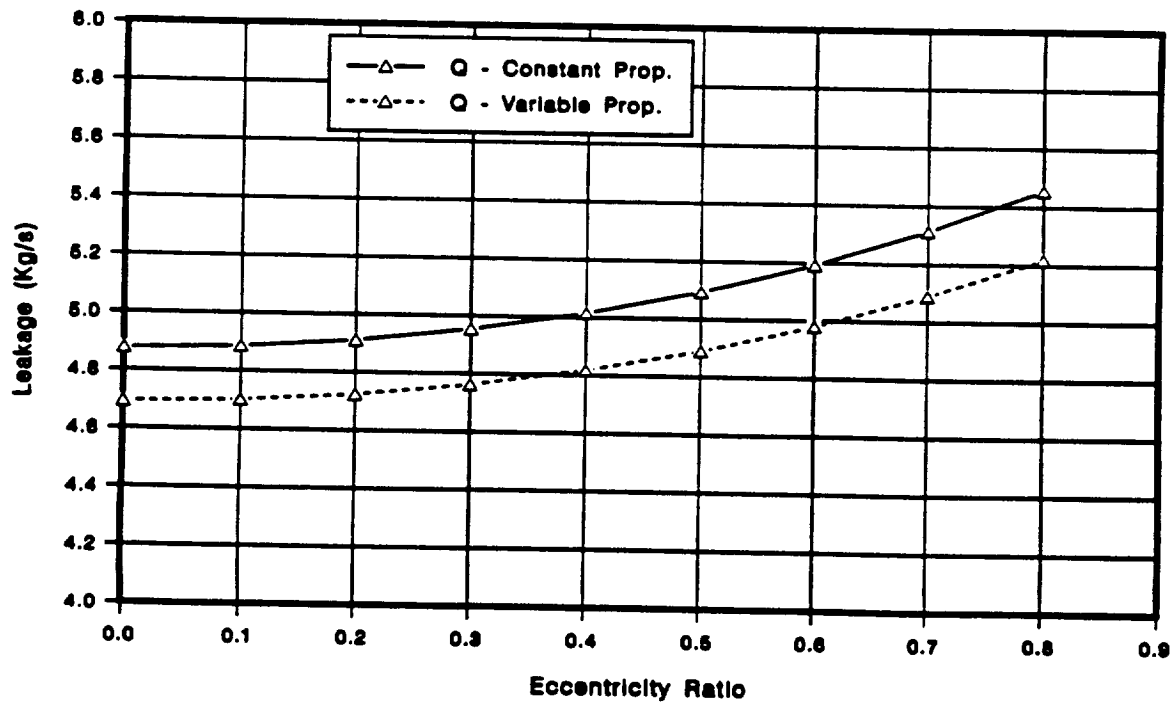


Figure 6.32 Leakage, Q, for Seal Unit 3-01

2. Adiabatic flow

The case of isothermal flow (constant temperature) is the same as the variable properties model discussed in Chapter III, i.e., fluid properties are assumed to be a function of local pressure and a mean temperature. The results for the isothermal case from current work are compared with San Andres' in Figures 6.28–6.33. Direct stiffness, shown in Figure 6.28, differs by about 20% and this difference is maintained at all eccentricities. Agreement for cross coupled stiffness, in Figure 6.29, is slightly better.

6.11 San Andres *et al.* (1992), Adiabatic Case

The same case considered in the previous example is repeated with the thermal effects model of Chapter IV. The results are shown in Figures (6.34–6.38). are for the adiabatic case ($Q_s = 0$, no heat transfer). The results are for concentric case and do not include perturbations in temperature as explained in Chapter IV.

The temperature rise across the seal is shown in Figure 6.34. San Andres points out that if this rise in temperature is big enough, the fluid may enter a two-phase region seriously affecting the performance of the turbomachine.

The frictional torque and flow rates shown in Figures 6.35, 6.36 roughly match. However, cross coupled stiffness, shown in Figure 6.37 is off by about 25%. Damping, both C_{xx} and c_{xy} , agree well.

6.12 Comparison of Current Analysis with Other Methods

The following general conclusions may be drawn based on the check cases discussed.

Comparison with Nelson and Nguyen:

Expectedly, all check cases with current analysis compare well with their theoretical

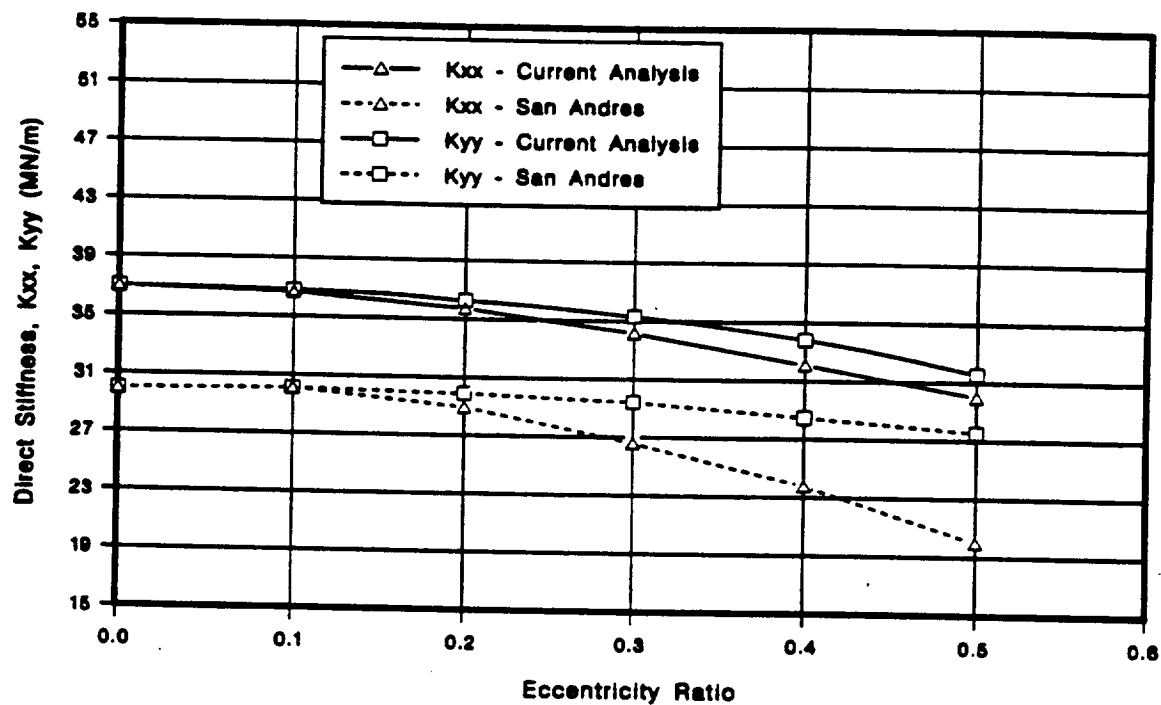


Figure 6.33 Direct Stiffness K_{xx} , K_{yy} , for San Andres, Isothermal

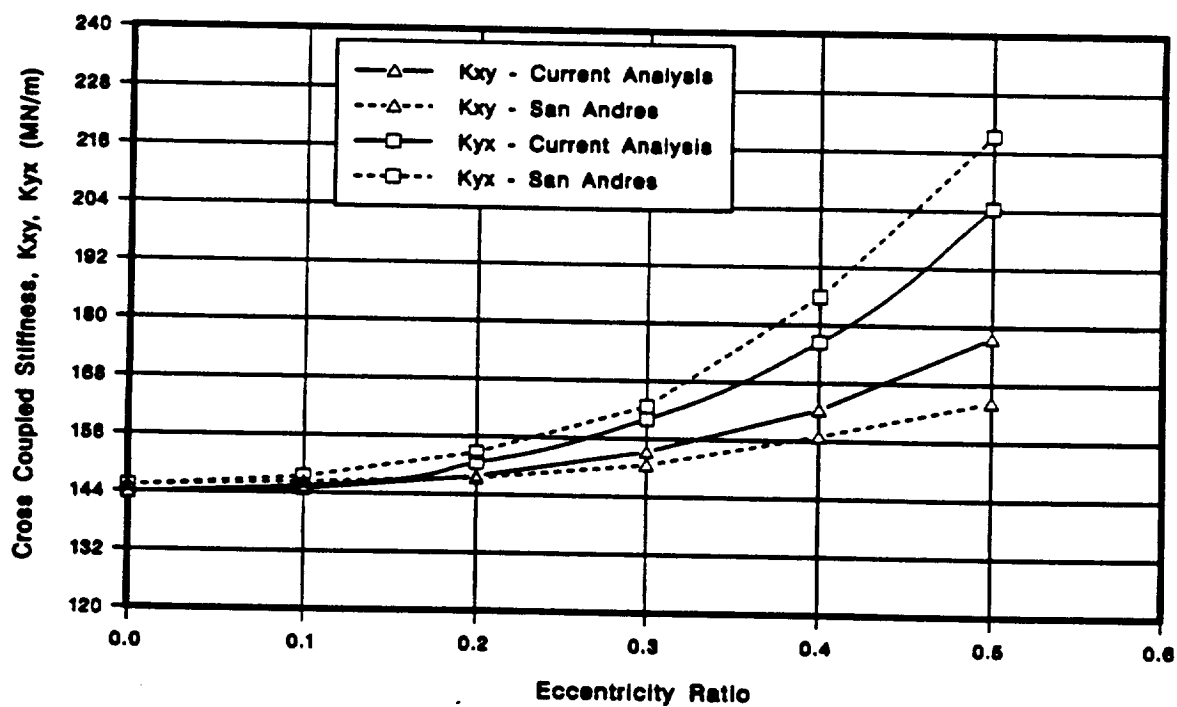


Figure 6.34 Cross Coupled Stiffness k_{xy} , k_{yx} , for San Andres, Isothermal

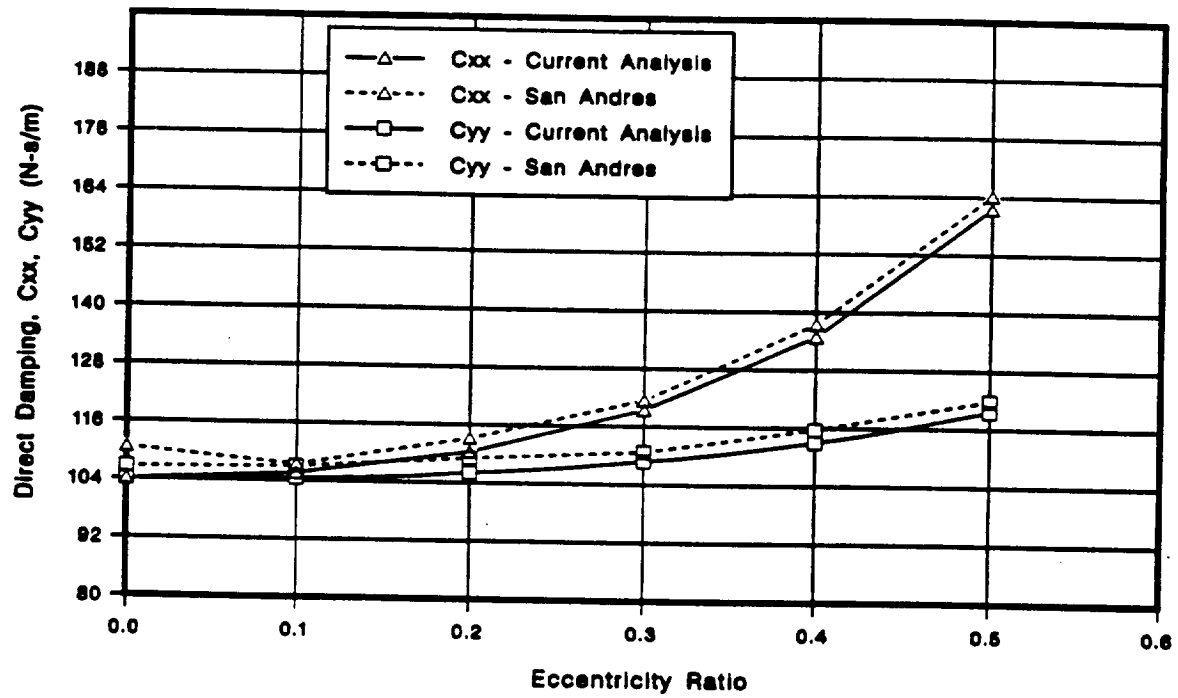


Figure 6.35 Direct Damping, C_{xx} , C_{yy} for San Andres, Isothermal

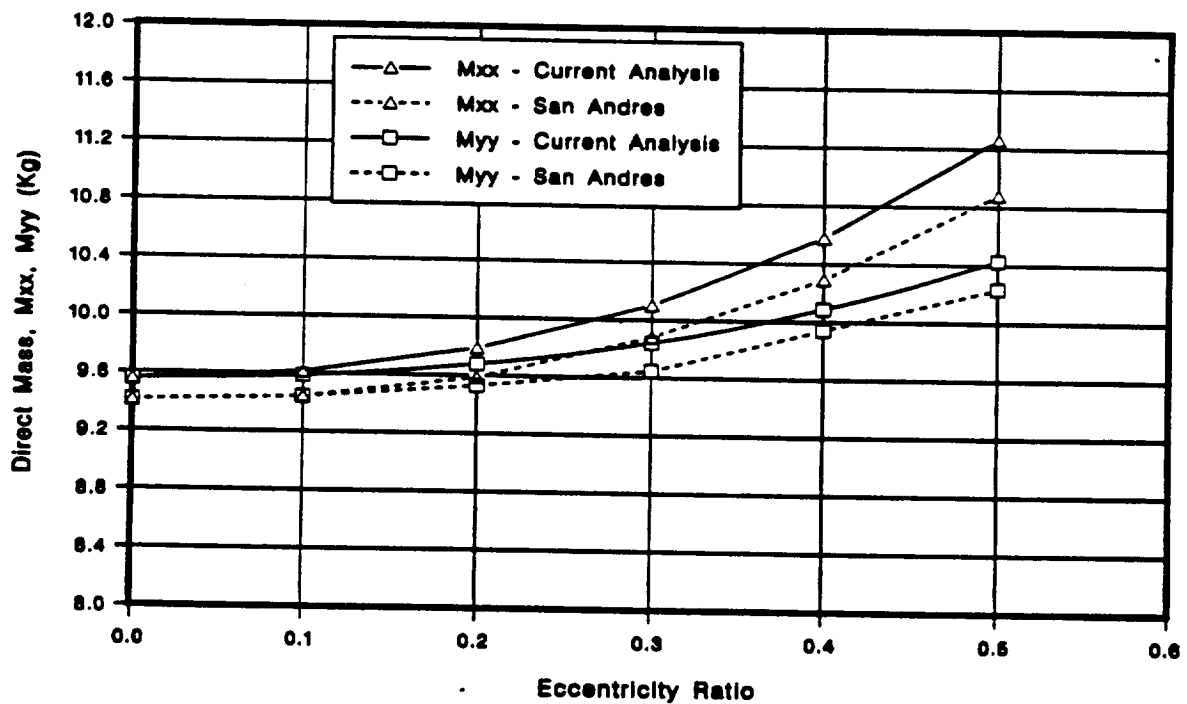


Figure 6.36 Direct Inertia, M_{xx} , M_{yy} for San Andres, Isothermal

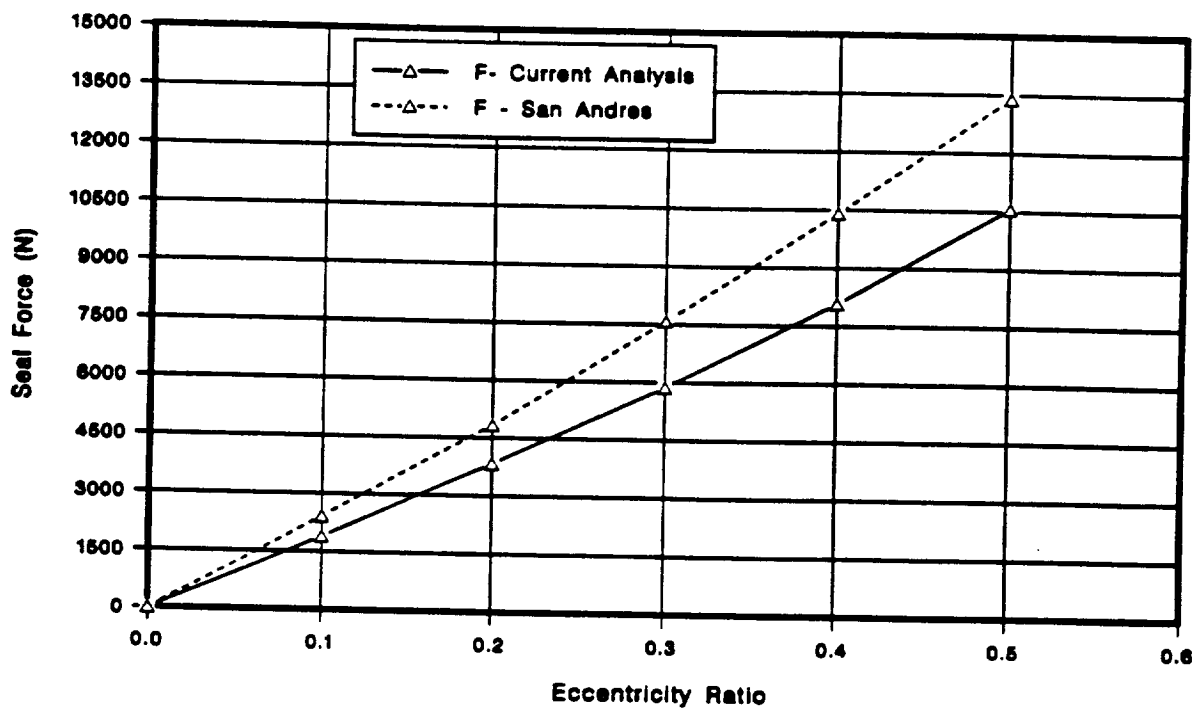


Figure 6.37 Seal Force, F, for San Andres, Isothermal

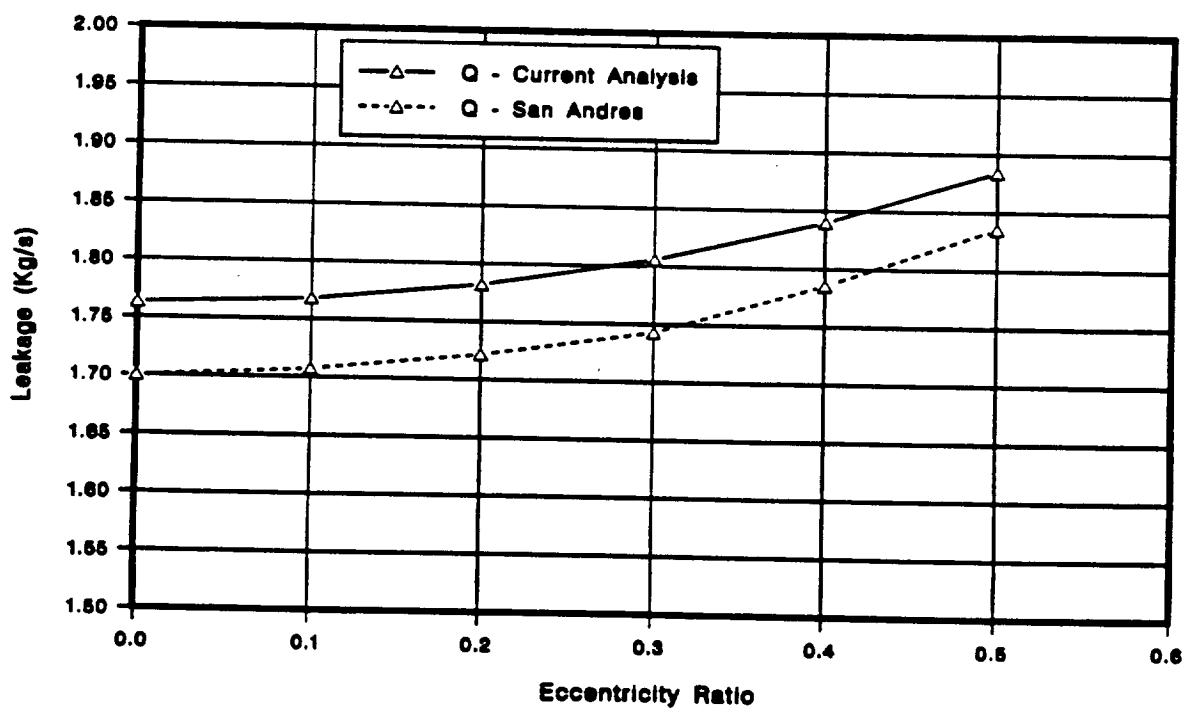


Figure 6.38 Leakage, Q, for San Andres, Isothermal

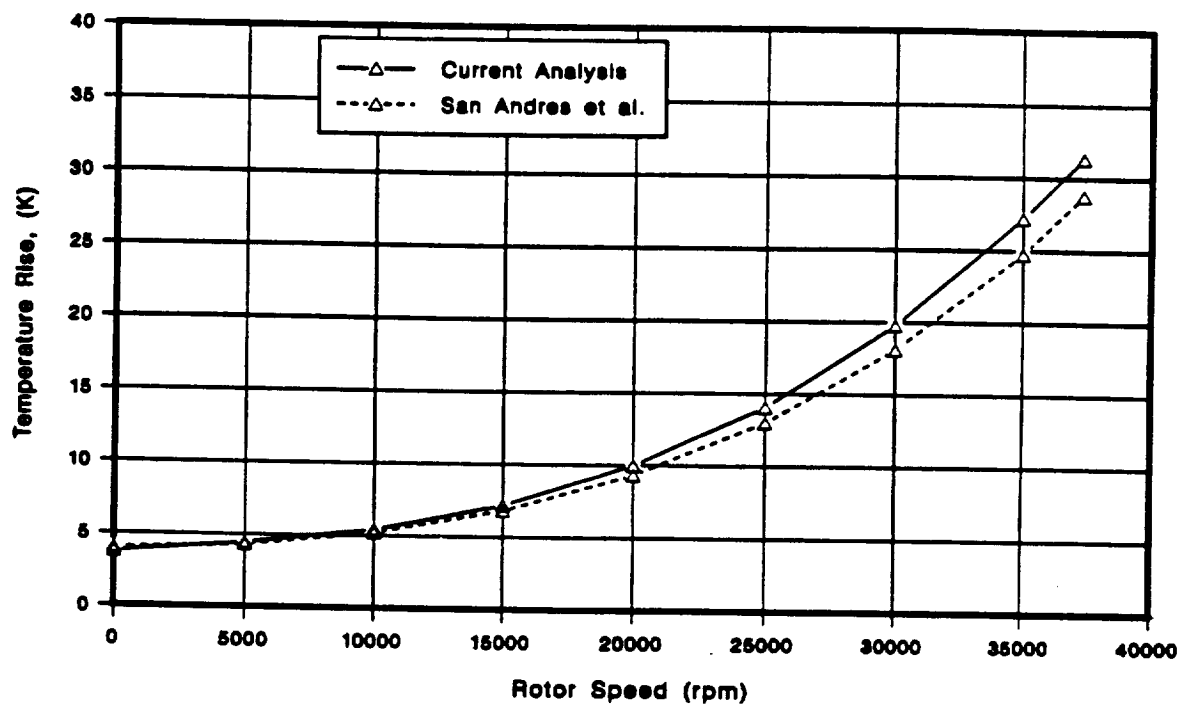


Figure 6.39 Temperature Rise, San Andres, Adiabatic

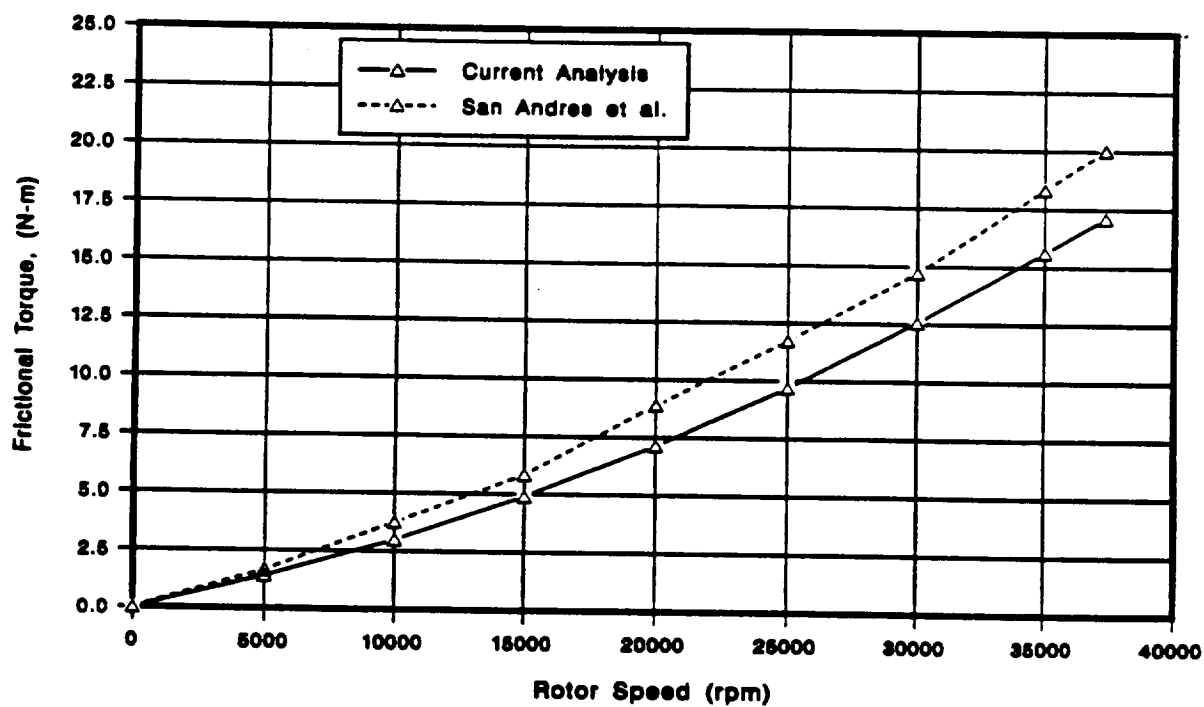


Figure 6.40 Frictional Torque, San Andres, Adiabatic

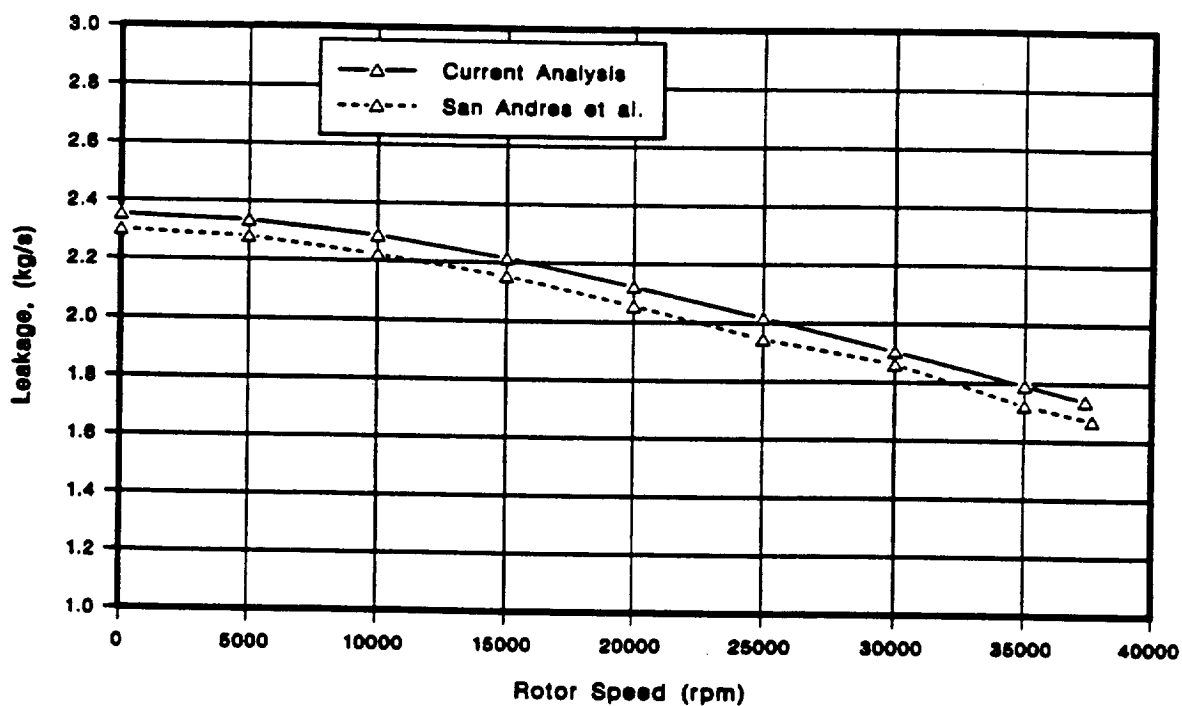


Figure 6.41 Leakage, San Andres, Adiabatic

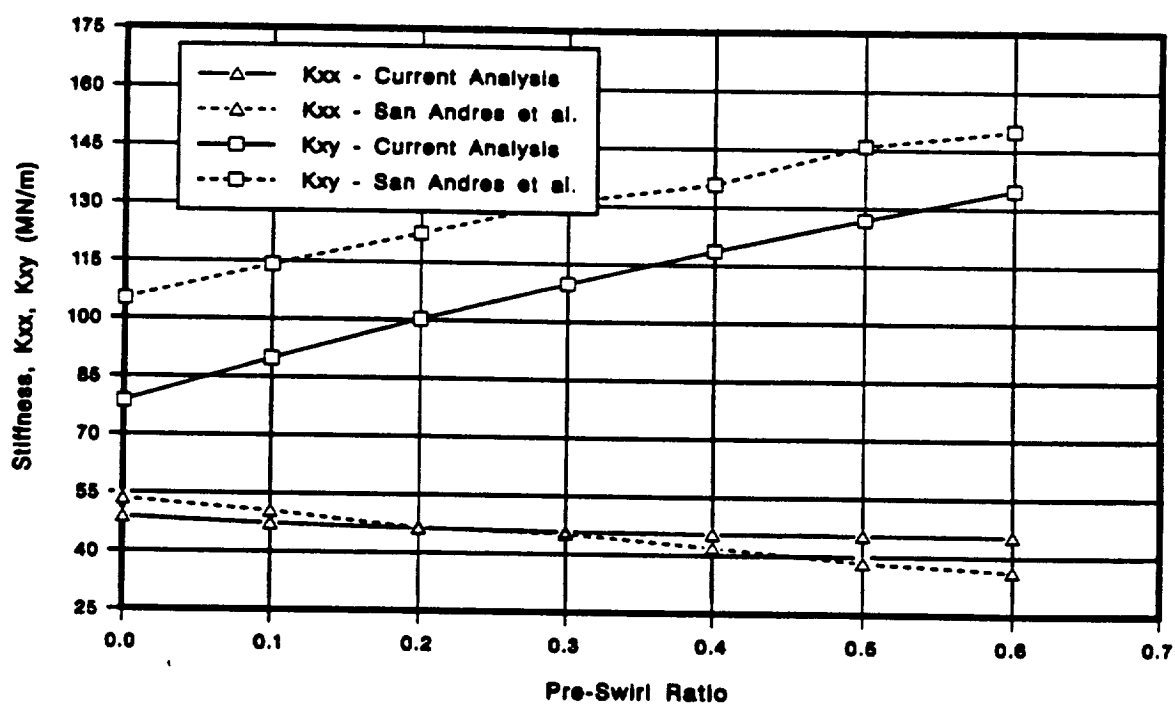


Figure 6.42 Stiffness, San Andres, Adiabatic

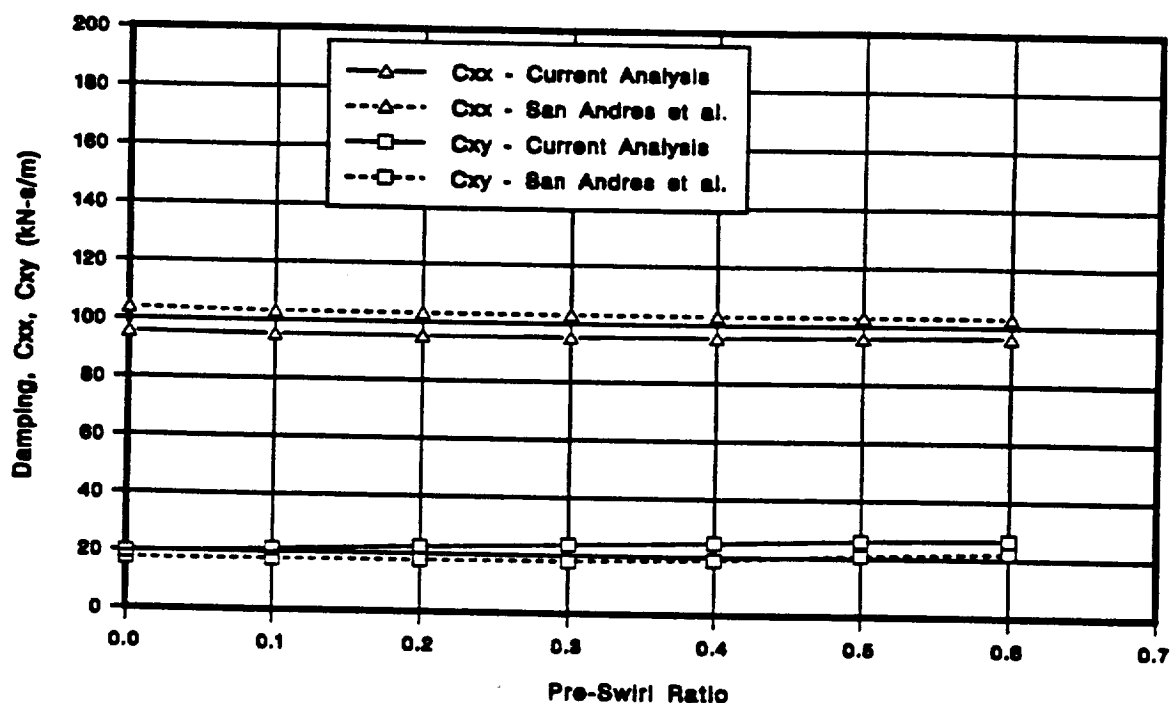


Figure 6.43 Damping, San Andres, Adiabatic

predictions. In some comparisons with the experimental data, the comparison with current analysis is better than their results. For check cases where their method had convergence problems and failed, current analysis gives good results.

Comparison with Childs:

The current analysis compares very well with Childs' Hirs' friction model based analysis (1985). For this friction model, current analysis matches Childs' analysis almost exactly. Similar comparison exists between current analysis and his more recent work based on Moody's model.

Comparison with Scharrer and Nelson:

There is some deviation between their analysis based on Hirs' friction model and the current analysis. A three-way comparative study between Childs' analysis, Scharrer and Nelson' work and the current analysis shows discrepancy in their results. While Childs and current analysis agree well consistently, their results for stiffness

coefficients are off by about 20%.

Comparison with San Andres:

There is some deviation between the current analysis and San Andres' Moody friction factor based eccentric analysis, both for constant properties and variable properties cases, particularly for stiffness coefficients. It appears as though these deviations vary from case to case. For example, for Childs and Lindsey (1993) experimental results, the difference in flow rates for convergent seals is considerably large. Same for direct stiffness at high pressure differentials. However, for other cases the differences are not of that order. It is difficult to speculate on the reasons for these deviations as both analyses use entirely different solution procedures.

However, for the current analysis an equivalence will be established between the dynamic coefficients based transient motion and the same motion based on original governing equations. For the second approach there is no first order solution involved. If these two approaches match consistently, it establishes, in the minimum, that there is no error in the linearized coefficients obtained from the dynamic analysis.

CHAPTER VII

TRANSIENT ANALYSIS

In simulating the dynamics of a rotor system with fluid bearings such as journal, tilt-pad bearings etc., or an annular seal in the present study, the dynamic effects of seals for a *small* motion of the rotor about an equilibrium position are usually modeled using a *linearized force-motion* model similar to the one shown in Eq. (7.1).

In this equation, $(\delta x, \delta y)$ are the displacements, $(\delta \dot{x}, \delta \dot{y})$ are the velocities and $(\delta \ddot{x}, \delta \ddot{y})$ are the accelerations in the X and Y directions respectively, relative to a static operating point (x, y) . The fluid force terms ΔF_x and ΔF_y are the incremental or perturbed fluid forces for a small motion of the rotor shaft about (x, y) . These force components, in general, vary as a function of rotor displacement, translational velocity and acceleration and are linear only for small orbital motion.

In this model, $K_{xx}, K_{yy}, k_{xy}, k_{yx}$ are the linearized stiffness coefficients, $C_{xx}, C_{yy}, c_{xy}, c_{yx}$ are the linearized damping coefficients and $M_{xx}, M_{yy}, m_{xy}, m_{yx}$ are the linearized added mass or inertia coefficients at the static operating point or eccentricity (x, y) .

$$\begin{aligned}
 - \begin{Bmatrix} \Delta F_x \\ \Delta F_y \end{Bmatrix} &= \begin{bmatrix} K_{xx} & k_{xy} \\ -k_{yx} & K_{yy} \end{bmatrix} \begin{Bmatrix} \delta x \\ \delta y \end{Bmatrix} + \begin{bmatrix} C_{xx} & c_{xy} \\ -c_{yx} & C_{yy} \end{bmatrix} \begin{Bmatrix} \delta \dot{x} \\ \delta \dot{y} \end{Bmatrix} \\
 &\quad + \begin{bmatrix} M_{xx} & m_{xy} \\ -m_{yx} & M_{yy} \end{bmatrix} \begin{Bmatrix} \delta \ddot{x} \\ \delta \ddot{y} \end{Bmatrix} \quad (7.1)
 \end{aligned}$$

In the linearized model, the terms $[K_{xx}\delta x]$ and $[K_{yy}\delta y]$ account for the incremental fluid reaction forces of the seal due to a small displacement of the rotor $(\delta x, \delta y)$. The term $[k_{xy}\delta y]$ is the cross coupled force in the X direction due to a displacement δy

in the Y direction. Similarly, $[k_{yx}\delta x]$ is the cross coupled force in the Y direction due to a displacement δx in the X direction. The terms $[C_{xx}\delta\dot{x}]$ and $[C_{yy}\delta\dot{y}]$ represent the incremental damping forces due to a small velocity change $(\delta\dot{x}, \delta\dot{y})$. Similarly, $[M_{xx}\delta\ddot{x}]$ and $[M_{yy}\delta\ddot{y}]$ are the incremental fluid inertia forces due to a small change in acceleration $(\delta\ddot{x}, \delta\ddot{y})$. For a concentric seal, $K_{xx} = K_{yy}$, $k_{xy} = k_{yx}$ etc., reducing the number of coefficients from twelve to six. Typically, for an annular seal, the important coefficients are direct stiffness, cross coupled stiffness, direct damping and direct or added mass. The contributions of other terms are negligible in most cases compared to these terms.

These twelve linearized coefficients are, in general, nonlinear functions of the static operating point (x, y) . The variations of direct stiffness K_{xx} , direct damping C_{xx} and cross coupled stiffness k_{xy} for various rotor operating positions for seal unit 3-02, an experimental seal under design at NASA/MSFC, are shown in Figures 7.2–7.4. These curves are obtained by the dividing the circumference of the seal into a number of segments as shown in Figure 7.1 and computing the coefficients as a function of eccentricity along each of the radii. For this seal, the coefficients remain constant upto an eccentricity ratio of 0.4. Beyond this limit, the coefficients start varying and this variation becomes much more pronounced as the eccentricity ratio exceeds 0.6. These curves are typical of a tapered seal and similar curves can be obtained for a straight seal.

In practice, usually a single set of dynamic coefficients computed at centered position is used to model the dynamic behavior of the seal i.e., to compute seal forces in rotordynamic simulations. This is based on the experimental and theoretical observations (Childs 1993) that generally there is little change in dynamic coefficients upto an eccentricity ratio of 0.4–0.5. In other words, for simulations involving motion with in this range the dynamic coefficients computed at zero eccentricity should be

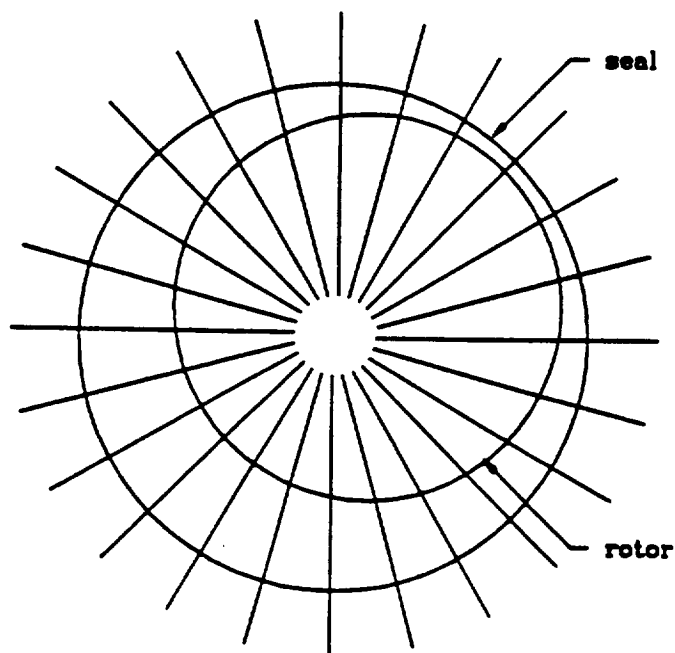


Figure 7.1 Circumferential Grid for Seal Coefficient Mapping

adequate to model the seal behavior. For example, at NASA/MSFC for the SSME turbopump simulations, dynamic coefficients used to model the interstage seal are computed at zero eccentricity.

It is assumed that this set of coefficients computed for a concentric seal would reliably predict the dynamic behavior of the seal over its entire range of operation, which may include motion with large eccentricities. This fact of large eccentric motion has been confirmed by the presence of destructive rubs in the SSME turbopump interstage seals.

This method of modeling a seal using a single set of coefficients is valid only if the dynamic coefficients remain invariant in the clearance space. For example, for the seal unit 3-02 (Figs. 7.2-7.4) the coefficients remain relatively constant as long as the operating point falls within a circle of radius of about 0.4 eccentricity ratio. As this limit is exceeded, the coefficients start varying and the variations are more rapid

at higher eccentricities.

In general, the above seal model (Eq. 7.1) consisting of 12 coefficients accurately approximates the dynamic behavior of the seal subject to a few limitations given below.

1. The model is valid only for a *small* motion in the immediate neighborhood of the static operating point at which the set of dynamic coefficients are computed, typically upto 0.4 eccentricity ratio. This is the basic assumption on which the linearized coefficients of the model are derived.
2. The dynamic coefficients derived at a given static operating position may not be accurate when used at a different operating point.
3. Even though these dynamic coefficients can be computed at various eccentricities, in general it is not possible to decide which set of coefficients to use when the rotor is moving around in the clearance space such as in a transient motion.

7.1 Objectives

The main objective of this work is to study the effect of large rotor displacements of SSME-ATD-HPOTP turbopump on the dynamics of the annular seal and the resulting transient motion.

For the purpose of this study, *large eccentric motion* is classified into two types as illustrated in Figures 7.5–7.6. Figure 7.5 shows the time-displacement curve for the center of a rotor executing a steady state motion with a large amplitude. The amplitude is of the order of radial clearance (in this case about 0.017 mm) and hence may be considered as a motion with large displacement.

The motion represented in Figure 7.6 is of the second type where the rotor is

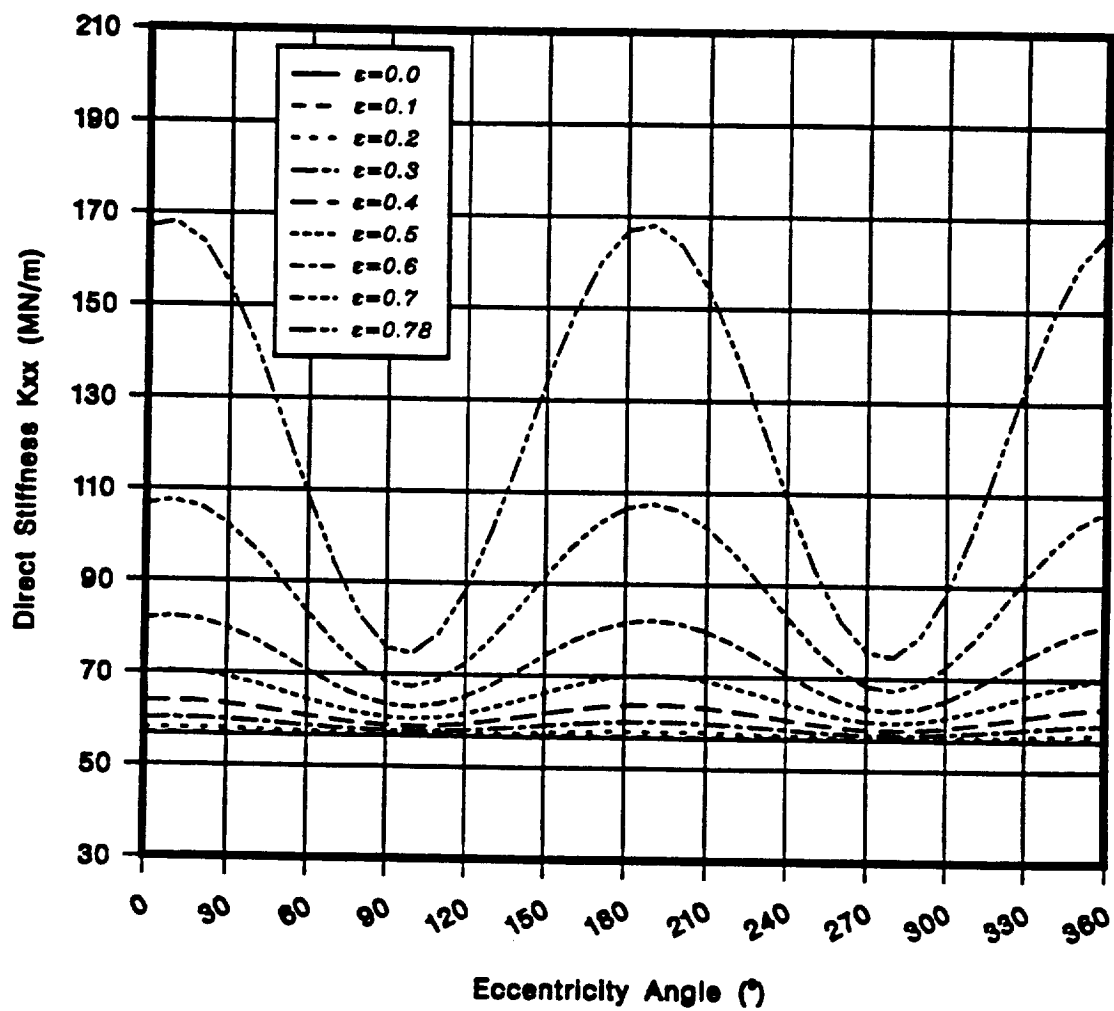


Figure 7.2 Variation of K_{xx} for unit 3-02 as a function of rotor position

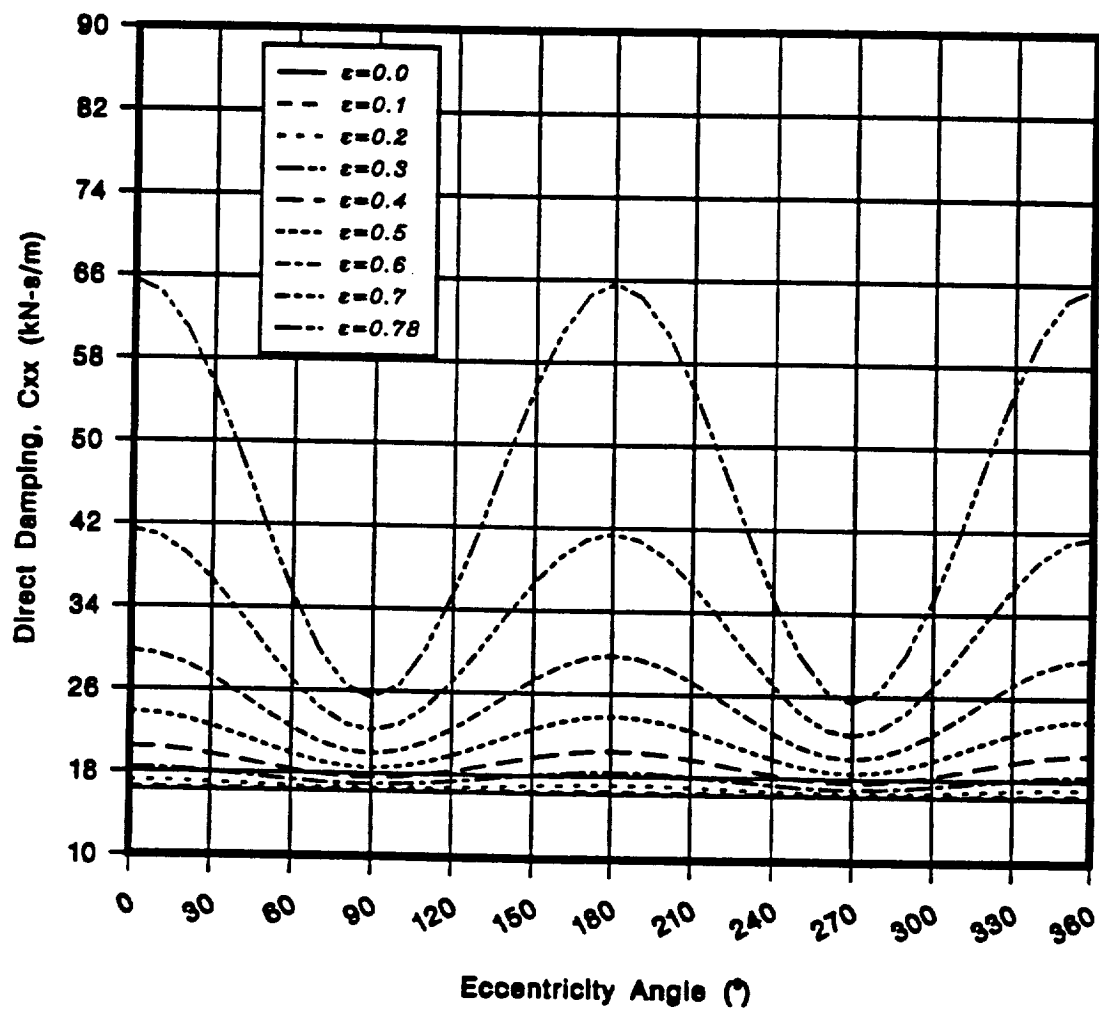


Figure 7.3 Variation of C_{xx} for unit 3-02 as a function of rotor position

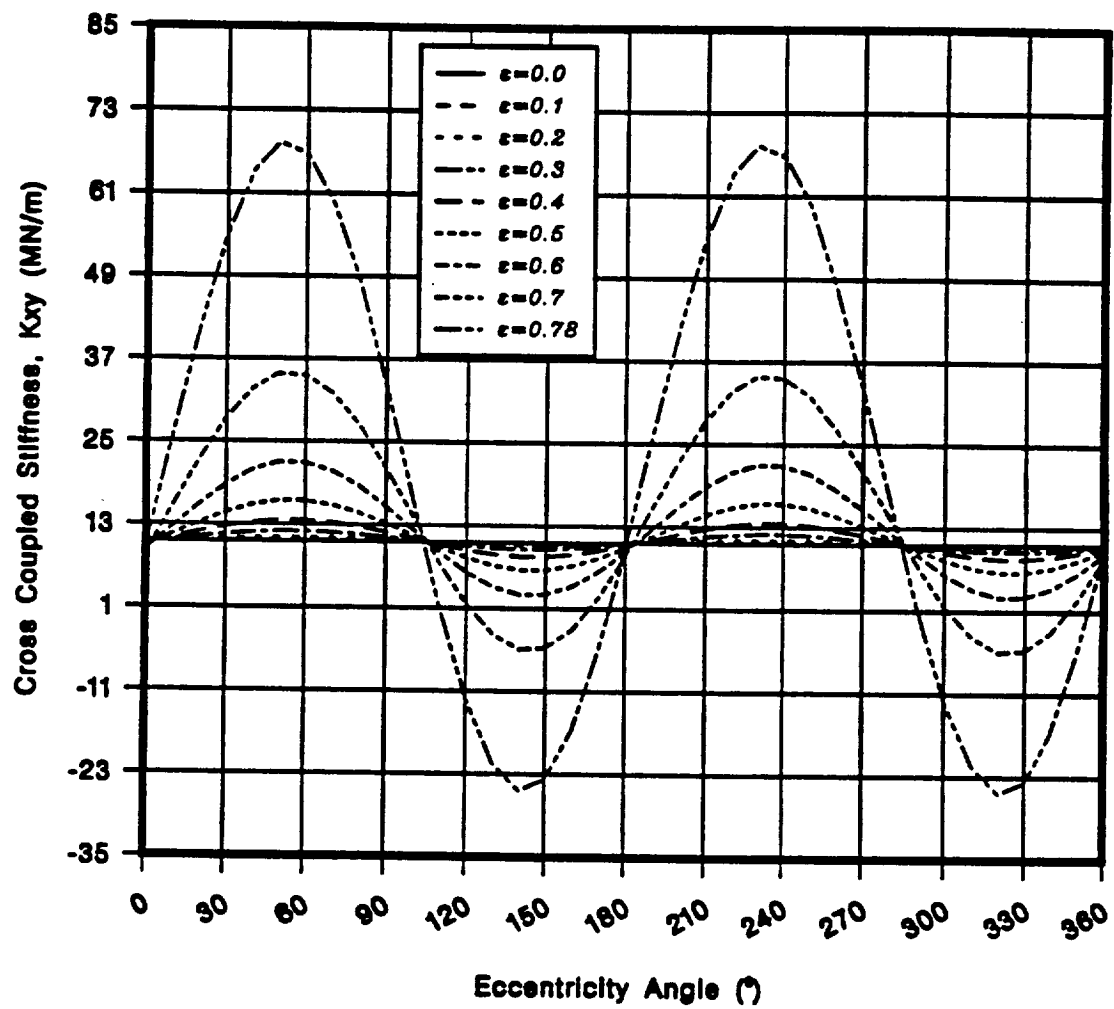


Figure 7.4 Variation of k_{xy} for unit 3-02 as a function of rotor position

displaced to a large static eccentric position ($\epsilon > 0.4$) while executing motion similar to type 1. The following study is not limited to these two types of motion and these are used only for the purpose of illustration. The analysis to be developed is valid for any type of general motion.

Results from the investigation of the first case should help in establishing the limits of accuracy of the linear force-motion model at a given static operating point. The basic underlying assumption of this model is that it is valid only for a small motion, typically for $\epsilon > 0.4$, about the operating point. The exact limits of this small motion are undefined. The study of second case is more important in the sense that the study focuses on deviations between the predictions using a single set of coefficients and the actual *bulk flow model* motion as the rotor moves through the clearance space in an arbitrary fashion.

For the purpose of this study, the model of seal represented by a single set of coefficients will be identified as *linear model* ($\epsilon = 0$). This model, while valid for a small motion about the centered position, may not be accurate for large off-center operation of the seal. This off-center motion includes both types of motion described earlier. One of the objectives of this study is to identify the magnitude of these deviations and examine the effect of these deviations on the overall stability of the rotor system and establish limits of effectiveness of using such a model. This task is accomplished by solving the bulk flow model seal governing equations directly for transient seal forces for any given type of motion, including motion involving large eccentricities. Results from this study confirm considerable differences, for large off-center operation, between the approximate *linear model* ($\epsilon = 0$) and the actual *bulk flow model*.

This approach of solving the governing equations directly for transient seal forces, while being the most accurate, may not be practical to be included in a rotordynamic

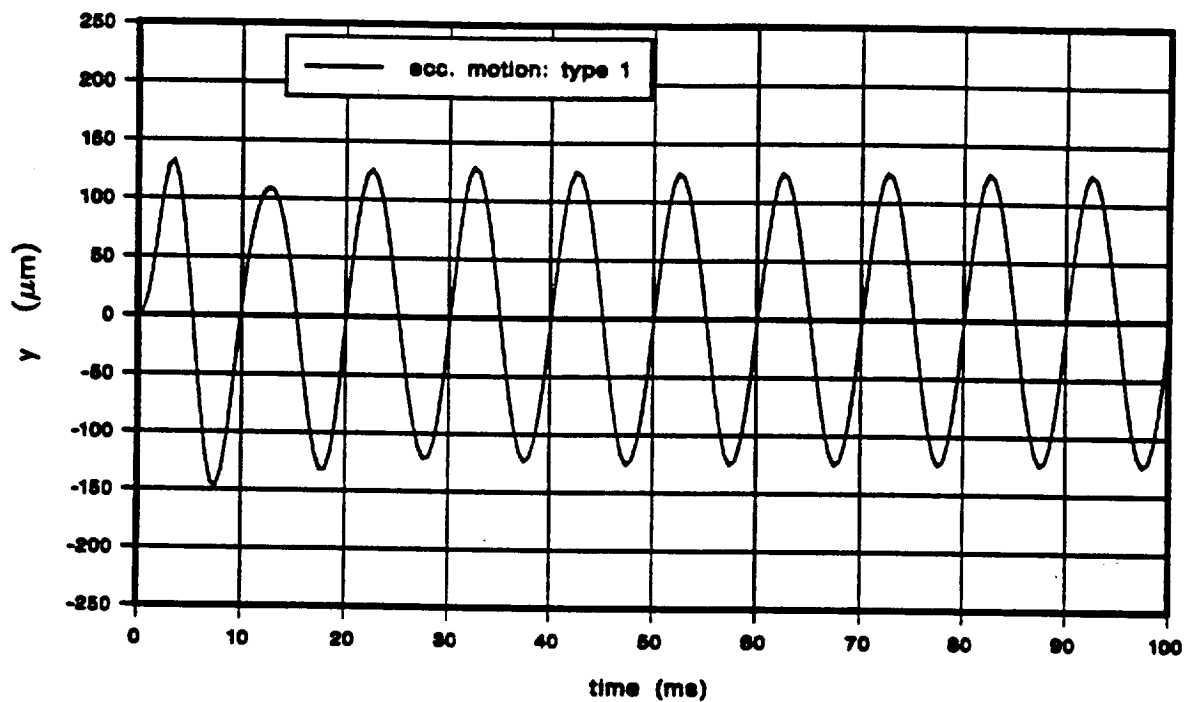


Figure 7.5 Eccentric Motion: Type 1

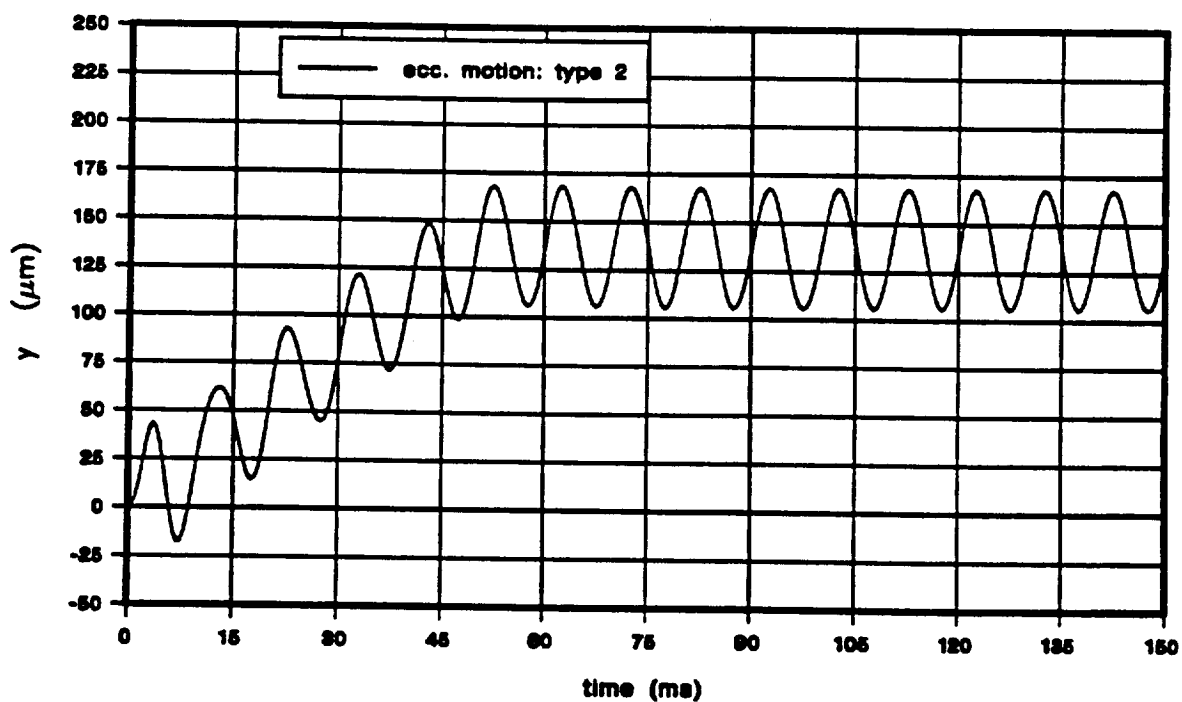


Figure 7.6 Eccentric Motion: Type 2

simulation code, mainly due to the large computing resources required to solve these equations at each time step. As a matter of fact, this is the primary reason for using approximate models such as the one shown in Eq. (7.1) in rotordynamic simulation codes. As an alternative, a general method is developed to model non-linearities in an annular seal based on dynamic coefficients computed at various static rotor operating positions in the seal clearance space. This method takes into consideration the time history of transient motion, i.e., displacement, velocity and acceleration profiles to compute the transient seal forces at any given instant of time. This method is extended for approximate displacement, velocity and acceleration profiles to yield a practical method that is accurate and easy to implement in a rotordynamic analysis code.

Results from these two methods compare well with those of the actual bulk flow model for large eccentric motion. These methods, thoroughly tested for various types of transient motion, provide an efficient and practical means for accurate simulation of the dynamic effects of an annular seal for any type of motion.

The following tasks are accomplished in this study.

1. Study the effect of large eccentric motion of the rotor on the dynamic behavior of a SSME-ATD-HPOTP annular seal using the bulk flow model seal governing equations.
2. Compare the results of the above study with those of the model currently in use at NASA/MSFC i.e., linear model ($\epsilon = 0$).
3. Develop a method that accurately simulates the dynamics of an annular seal for large eccentric motion of the rotor.
4. Thoroughly test the method for various types of transient motion using bulk

flow model results as benchmark.

5. Compare the results of various models and note their their relative merits and deficiencies.

CHAPTER VIII

VARIOUS SEAL MODELS FOR TRANSIENT ANALYSIS

In this chapter, the different models used to study the transient analysis with an annular seal are discussed. These various models differ in the way they compute the seal reaction forces for any specified motion of the rotor. The four different models used in this study are explained below.

1. Bulk Flow Model: This model uses a solution procedure based on the actual set of seal governing equations (Eqs. (2.1-2.3)) to compute for transient fluid forces at each time step based on a specified motion of the center of the rotor. The results of test cases with this model are used as a benchmark to compare the other approximate models.
2. Linear Model ($\epsilon = 0$): This model is based on the linear force-motion model of Eq. (7.1) and uses dynamic coefficients computed at zero eccentricity to compute the fluid forces. This is the model currently being used at NASA/MSFC for SSME turbopump rotordynamic simulations.
3. New Method-I: This model is based on a new method developed to compute the transient seal forces in a computationally efficient manner. This method makes use of time history of displacement, velocity and acceleration of the rotor to compute the seal forces.
4. New Method-II: This is a simplified extension of method-1 and it assumes approximate displacement, velocity and acceleration profiles to compute seal forces.

These various models are shown in flow chart in Figure 8.1.

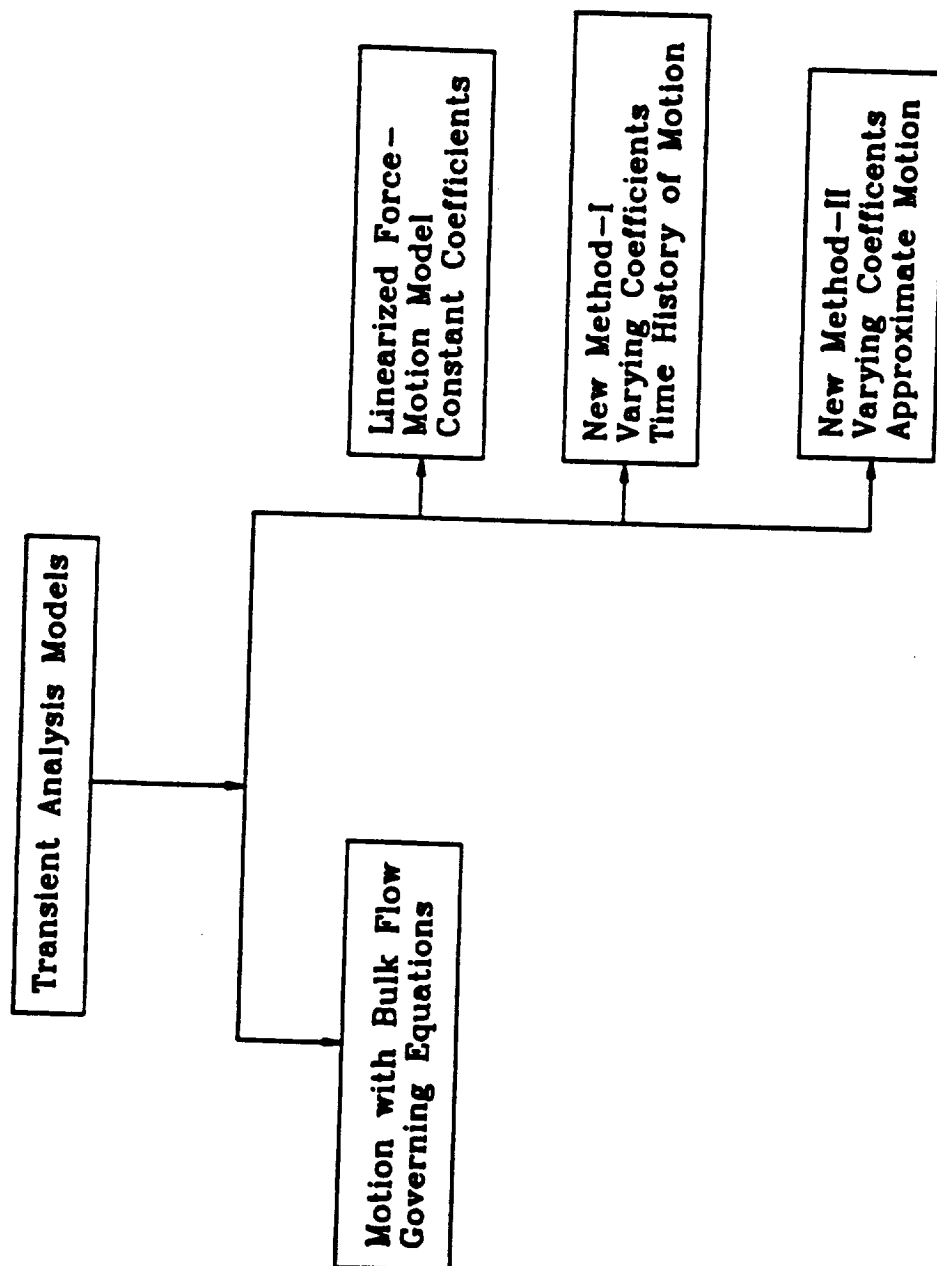


Figure 8.1 Various Models for Transient Analysis

In the following sections, each of the above models is discussed in more detail.

8.1 Transient Analysis with Bulk Flow Model

The linear force-motion model of seal shown in Eq. (7.1) approximates the behavior of the bulk flow model governing equations for a small motion of the rotor at the static operating point (x, y) . The coefficients in this model are obtained by perturbing the bulk flow model governing equations given in Eqs (2.1-2.3) at (x, y) and fitting the perturbed fluid forces to the linear model. While the linear model is valid only in the neighborhood of (x, y) , the governing equations are valid at any point in the clearance space. To study the deviations between the linear model at a given operating point and the actual bulk flow model, this set of governing equations are solved for the transient fluid forces directly. The Eqs. (2.1-2.3) are reproduced here for discussion.

Continuity:

$$\frac{\partial(hu)}{\partial z} + \frac{1}{R} \frac{\partial(hv)}{\partial \beta} + \frac{\partial h}{\partial t} = 0 \quad (8.1)$$

Axial Momentum:

$$\begin{aligned} -\frac{h}{\rho} \frac{\partial p}{\partial z} = & h \left\{ \frac{\partial u}{\partial t} + \frac{v}{R} \frac{\partial u}{\partial \beta} + u \frac{\partial u}{\partial z} \right\} \\ & + f_s \frac{u}{2} \sqrt{u^2 + v^2} + f_r \frac{u}{2} \sqrt{u^2 + (v - w)^2} \end{aligned} \quad (8.2)$$

Circumferential Momentum:

$$\begin{aligned} -\frac{h}{\rho R} \frac{\partial p}{\partial \beta} = & h \left\{ \frac{\partial v}{\partial t} + \frac{v}{R} \frac{\partial v}{\partial \beta} + u \frac{\partial v}{\partial z} \right\} \\ & + f_s \frac{v}{2} \sqrt{u^2 + v^2} + f_r \frac{(v - w)}{2} \sqrt{u^2 + (v - w)^2} \end{aligned} \quad (8.3)$$

The film thickness in the global coordinate system is given by (Eq. (2.29)) as,

$$h(z, \beta, t) = \sqrt{(R + c)^2 - (x \sin \beta - y \cos \beta)^2} - (x \cos \beta + y \sin \beta) - R \quad (8.4)$$

and its derivatives with respect to axial and circumferential coordinates are given by,

$$\frac{\partial h}{\partial z} = \frac{(R+c)\frac{\partial c}{\partial z}}{\sqrt{(R+c)^2 - (x\sin\beta - y\cos\beta)^2}} \quad (8.5)$$

$$\frac{\partial h}{\partial \beta} = \frac{(R+c)\frac{\partial c}{\partial \beta} - (x\sin\beta - y\cos\beta)(x\cos\beta + y\sin\beta)}{\sqrt{(R+c)^2 - (x\sin\beta - y\cos\beta)^2}} \quad (8.6)$$

$$\frac{\partial h}{\partial t} = \frac{-(x\sin\beta - y\cos\beta)(\dot{x}\sin\beta - \dot{y}\cos\beta)}{\sqrt{(R+c)^2 - (x\sin\beta - y\cos\beta)^2}} - (\dot{x}\cos\beta + \dot{y}\sin\beta) \quad (8.7)$$

The time derivatives $\frac{\partial u}{\partial t}$, $\frac{\partial v}{\partial t}$ and $\frac{\partial p}{\partial t}$ are approximated using a backward difference formula.

$$\frac{\partial u}{\partial t} \approx \frac{(u(t_2) - u(t_1))}{(t_2 - t_1)} \quad (8.8)$$

$$\frac{\partial v}{\partial t} \approx \frac{(v(t_2) - v(t_1))}{(t_2 - t_1)} \quad (8.9)$$

$$\frac{\partial p}{\partial t} \approx \frac{(p(t_2) - p(t_1))}{(t_2 - t_1)} \quad (8.10)$$

The displacement (x, y) is the displacement of the center of the rotor and (\dot{x}, \dot{y}) is the velocity of the center of rotor and (\ddot{x}, \ddot{y}) is the acceleration of the center of the rotor.

8.1.1 Transient Seal Forces with Bulk Flow Equations

The solution procedure to solve the above set of partial differential equations is similar to the procedure discussed in Chapter II. At each time step, Eqs. (8.1-8.3) are solved to subject to the the boundary conditions given in Eqs. (XX-XX). The variables $u(z, \beta, t)$, $v(z, \beta, t)$ and $p(z, \beta, t)$ are the time varying velocities and pressure. At each time step, the pressure distribution $p(z, \beta, t)$ is integrated along the length of the seal to compute the two components of the fluid force $F_{fluid-x}$ and

$F_{fluid-y}$.

$$- F_{fluid-x}(t) = \int_0^L \int_0^{2\pi} p(z, \beta, t) \cos\beta R d\beta dz \quad (8.11)$$

$$- F_{fluid-y}(t) = \int_0^L \int_0^{2\pi} p(z, \beta, t) \sin\beta R d\beta dz \quad (8.12)$$

The computation of these transient fluid forces is carried out in a continuous fashion from one time step to the next, with the current values of the variables acting as initial values for the next time step. Numerical integration with respect to time t is implemented using a fourth order Runge-Kutta integrator with adaptive step size. The following time step is used for the transient analysis.

$$\Delta t = \frac{t_n}{15} \quad (8.13)$$

where t_n is the time period of the system.

8.2 Transient Analysis with Linear Model ($\epsilon = 0$)

This is the model usually used to model the dynamic behavior of an annular seal (Eq. (7.1)). The dynamic coefficients used in the model refer to those computed at the steady state operating position of the rotor. While these linearized coefficients can be computed at various eccentricities, it is not possible to decide which set to use when the rotor is moving in the clearance space in an arbitrary fashion such as in a transient motion. In practice, the set of coefficients computed at zero eccentricity are used in the model to compute the seal forces. For example, at NASA/MSFC, SSME turbopump simulations use this model.

8.3 New Method-I

In this section, a general method is developed to simulate the dynamic behavior of an annular seal using dynamic coefficients computed at various static eccentricities

in the clearance space. The motivation for this endeavor is two fold.

- Firstly, there exists a need for a more accurate model to simulate the dynamic behavior of the seal for motion with $\epsilon > 0.4$ as predicted by the bulk flow model compared to linear model ($\epsilon = 0$). Large computing resources required to solve the set of governing equations, Eqs. (8.1–8.3), make bulk flow model approach impractical for routine rotordynamic simulations.
- Secondly, it requires a lot less effort to compute dynamic coefficients for a given seal unit and for a given set of operating conditions and the methodology for this process is well established.

Consider a single degree of freedom *spring-mass-damper* system shown in Figure 8.2. It is assumed that the stiffness (K), damping (C) and mass (M) vary only with displacement x and are independent of velocity and acceleration. This assumption follows from the case of an annular seal where the dynamic coefficients are essentially functions of eccentricity alone. Various restoring forces in the components of this system are considered below.

8.3.1 Stiffness Force

The incremental restoring stiffness force Δf_k in the spring due to an infinitesimal extension δx from x is given by,

$$\Delta f_k = -K(x)\delta x \quad (8.14)$$

where K is the spring stiffness.

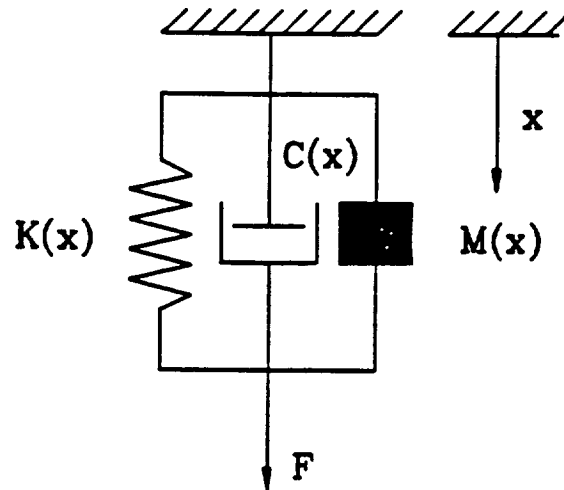


Figure 8.2 SDOF Spring-Mass-Damper System

8.3.2 Damping Force

The incremental restoring damping force Δf_c in a damper due to an infinitesimal change in velocity $\delta \dot{x}$ is given by,

$$\Delta f_c = -C(x)\delta \dot{x} \quad (8.15)$$

where C is the damping coefficient.

8.3.3 Inertia Force

Similarly, the incremental inertia restoring force Δf_m due to an infinitesimal change in acceleration $\delta \ddot{x}$ is given by,

$$\Delta f_m = -M(x)\delta \ddot{x} \quad (8.16)$$

where M is the inertia or mass coefficient.

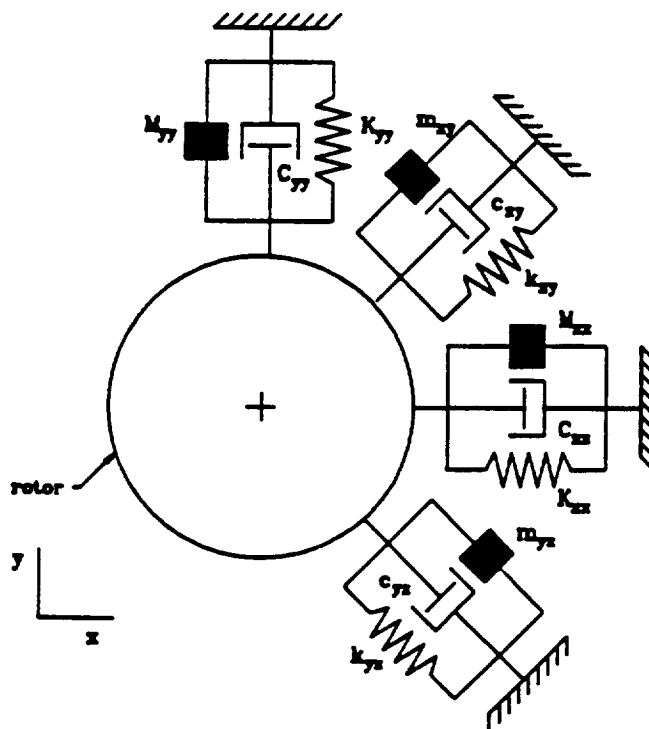


Figure 8.3 Seal Model for a 2 DOF Vibration Model

8.3.4 Theory

Consider the 2-DOF model of the seal in Figure 8.3 as represented by the 12 dynamic coefficients of the linear force-motion model of Eq. (7.1). at an eccentric position (x, y) . It is assumed that the stiffness, damping and inertia coefficients of this seal model are known at any static eccentricity (x, y) in the seal clearance space.

Let $K_{xx}(x, y)$, $k_{xy}(x, y)$, $k_{yx}(x, y)$ and $K_{yy}(x, y)$ be the stiffness coefficients, $C_{xx}(x, y)$, $c_{xy}(x, y)$, $c_{yx}(x, y)$, $C_{yy}(x, y)$ are the damping coefficients and $M_{xx}(x, y)$, $m_{xy}(x, y)$, $m_{yx}(x, y)$, $M_{yy}(x, y)$ are the inertia coefficients at eccentricity (x, y) .

An implicit assumption is made regarding the dependence of dynamic coefficients essentially on displacement and they are assumed to be almost independent of velocity and acceleration. This assumption will be verified in the following sections in comparison with original bulk flow governing equations.

The eccentricities or displacements of the center of rotor (x, y) are functions of time t and may be specified as $(x(t), y(t))$. Let $F_x(t_i)$ and $F_y(t_i)$ be the X and Y components of the fluid reaction force at any given time t_i . These two force components may be considered as a summation of 12 individual component forces due to the 12 dynamic coefficients of Eq. (7.1), as given below.

$$\begin{aligned} -F_x(t_i) &= f_{kxx}(t_i) + f_{kxy}(t_i) + f_{cxx}(t_i) + f_{cxy}(t_i) + f_{mxx}(t_i) + f_{mxy}(t_i) \\ -F_y(t_i) &= f_{kyx}(t_i) + f_{kyy}(t_i) + f_{cyx}(t_i) + f_{cyy}(t_i) + f_{myx}(t_i) + f_{myy}(t_i) \end{aligned} \quad (8.17)$$

Let at $t_{i+1} = t_i + \Delta t$, the incremental fluid force components in X and Y directions be $\Delta F_x(t_i)$ and $\Delta F_y(t_i)$ respectively.

$$\begin{aligned} F_x(t_i + \Delta t) &= F_x(t_i) + \Delta F_x(t_i) \\ F_y(t_i + \Delta t) &= F_y(t_i) + \Delta F_y(t_i) \end{aligned} \quad (8.18)$$

and the individual components of $\Delta F_x(t_i)$ and $\Delta F_y(t_i)$ are given below based on the linear-force motion model of Eq. (7.1)

$$\begin{aligned} -\Delta F_x(t_i) &= \Delta f_{kxx}(t_i) + \Delta f_{kxy}(t_i) + \Delta f_{cxx}(t_i) + \Delta f_{cxy}(t_i) + \Delta f_{mxx}(t_i) + \Delta f_{mxy}(t_i) \\ -\Delta F_y(t_i) &= \Delta f_{kyx}(t_i) + \Delta f_{kyy}(t_i) + \Delta f_{cyx}(t_i) + \Delta f_{cyy}(t_i) + \Delta f_{myx}(t_i) + \Delta f_{myy}(t_i) \end{aligned} \quad (8.19)$$

The infinitesimal change in displacement $(\delta x_i, \delta y_i)$ is given by,

$$\begin{aligned} \delta x_i &= x(t_i + \Delta t) - x(t_i) \\ \delta y_i &= y(t_i + \Delta t) - y(t_i) \end{aligned} \quad (8.20)$$

The infinitesimal change in velocity $(\delta \dot{x}_i, \delta \dot{y}_i)$ is given by,

$$\begin{aligned}\delta \dot{x}_i &= \dot{x}(t_i + \Delta t) - \dot{x}(t_i) \\ \delta \dot{y}_i &= \dot{y}(t_i + \Delta t) - \dot{y}(t_i)\end{aligned}\quad (8.21)$$

Similarly, the infinitesimal change in acceleration $(\delta \ddot{x}_i, \delta \ddot{y}_i)$ is given by,

$$\begin{aligned}\delta \ddot{x}_i &= \ddot{x}(t_i + \Delta t) - \ddot{x}(t_i) \\ \delta \ddot{y}_i &= \ddot{y}(t_i + \Delta t) - \ddot{y}(t_i)\end{aligned}\quad (8.22)$$

From Eq. (7.1), the incremental fluid forces in terms of their individual components are,

$$\Delta f_{k_{xx}}(t_i) = K_{xx}(x(t_i), y(t_i)) \delta x_i \quad (8.23)$$

$$\Delta f_{k_{xy}}(t_i) = k_{xy}(x(t_i), y(t_i)) \delta y_i \quad (8.24)$$

$$\Delta f_{k_{yx}}(t_i) = k_{yx}(x(t_i), y(t_i)) \delta x_i \quad (8.25)$$

$$\Delta f_{k_{yy}}(t_i) = K_{yy}(x(t_i), y(t_i)) \delta y_i \quad (8.26)$$

$$\Delta f_{c_{xx}}(t_i) = C_{xx}(x(t_i), y(t_i)) \delta \dot{x}_i \quad (8.27)$$

$$\Delta f_{c_{xy}}(t_i) = c_{xy}(x(t_i), y(t_i)) \delta \dot{y}_i \quad (8.28)$$

$$\Delta f_{c_{yx}}(t_i) = c_{yx}(x(t_i), y(t_i)) \delta \dot{x}_i \quad (8.29)$$

$$\Delta f_{c_{yy}}(t_i) = C_{yy}(x(t_i), y(t_i)) \delta \dot{y}_i \quad (8.30)$$

$$\Delta f_{m_{xx}}(t_i) = M_{xx}(x(t_i), y(t_i)) \delta \ddot{x}_i \quad (8.31)$$

$$\Delta f_{m_{xy}}(t_i) = m_{xy}(x(t_i), y(t_i)) \delta \ddot{y}_i \quad (8.32)$$

$$\Delta f_{m_{yx}}(t_i) = m_{yx}(x(t_i), y(t_i)) \delta \ddot{x}_i \quad (8.33)$$

$$\Delta f_{m_{yy}}(t_i) = M_{yy}(x(t_i), y(t_i)) \delta \ddot{y}_i \quad (8.34)$$

At time t_{i+1} , after n intervals of Δt , the incremental fluid force components at each time step may be added in the following manner to obtain the total force components.

$$f_{kxz}(t_{i+1}) = \sum_{i=1}^n K_{xz}(x_i, y_i) \delta x_i \quad (8.35)$$

$$f_{kxy}(t_{i+1}) = \sum_{i=1}^n k_{xy}(x_i, y_i) \delta y_i \quad (8.36)$$

$$f_{kyx}(t_{i+1}) = \sum_{i=1}^n k_{yx}(x_i, y_i) \delta x_i \quad (8.37)$$

$$f_{kyy}(t_{i+1}) = \sum_{i=1}^n K_{yy}(x_i, y_i) \delta y_i \quad (8.38)$$

$$f_{czz}(t_{i+1}) = \sum_{i=1}^n C_{zz}(x_i, y_i) \delta \dot{x}_i \quad (8.39)$$

$$f_{cxy}(t_{i+1}) = \sum_{i=1}^n c_{xy}(x_i, y_i) \delta \dot{y}_i \quad (8.40)$$

$$f_{cyx}(t_{i+1}) = \sum_{i=1}^n c_{yx}(x_i, y_i) \delta \dot{x}_i \quad (8.41)$$

$$f_{cyy}(t_{i+1}) = \sum_{i=1}^n C_{yy}(x_i, y_i) \delta \dot{y}_i \quad (8.42)$$

$$f_{mxx}(t_{i+1}) = \sum_{i=1}^n M_{xx}(x_i, y_i) \delta \ddot{x}_i \quad (8.43)$$

$$f_{mxy}(t_{i+1}) = \sum_{i=1}^n m_{xy}(x_i, y_i) \delta \ddot{y}_i \quad (8.44)$$

$$f_{myx}(t_{i+1}) = \sum_{i=1}^n m_{yx}(x_i, y_i) \delta \ddot{x}_i \quad (8.45)$$

$$f_{myy}(t_{i+1}) = \sum_{i=1}^n M_{yy}(x_i, y_i) \delta \ddot{y}_i \quad (8.46)$$

For infinitesimal quantities Δt , $(\delta x, \delta y)$, $(\delta \dot{x}, \delta \dot{y})$ and $(\delta \ddot{x}, \delta \ddot{y})$, the summation may be replaced by integration giving the following expressions.

$$f_{kxz}(t) = \int_0^{x(t)} K_{xz}(x, y) dx \quad (8.47)$$

$$f_{kxy}(t) = \int_0^{y(t)} k_{xy}(x, y) dy \quad (8.48)$$

$$f_{kyx}(t) = \int_0^{x(t)} k_{yx}(x, y) dx \quad (8.49)$$

$$f_{kyy}(t) = \int_0^{y(t)} K_{yy}(x, y) dy \quad (8.50)$$

$$f_{czz}(t) = \int_0^{\dot{z}(t)} C_{zz}(x, y) d\dot{z} \quad (8.51)$$

$$f_{cxy}(t) = \int_0^{\dot{y}(t)} c_{xy}(x, y) d\dot{y} \quad (8.52)$$

$$f_{cyx}(t) = \int_0^{\dot{x}(t)} c_{yx}(x, y) d\dot{x} \quad (8.53)$$

$$f_{cyy}(t) = \int_0^{\dot{y}(t)} C_{yy}(x, y) d\dot{y} \quad (8.54)$$

$$f_{mzz}(t) = \int_0^{\ddot{z}(t)} M_{zz}(x, y) d\ddot{z} \quad (8.55)$$

$$f_{mxy}(t) = \int_0^{\ddot{y}(t)} m_{xy}(x, y) d\ddot{y} \quad (8.56)$$

$$f_{myx}(t) = \int_0^{\ddot{x}(t)} m_{yx}(x, y) d\ddot{x} \quad (8.57)$$

$$f_{cyy}(t) = \int_0^{\ddot{y}(t)} M_{yy}(x, y) d\ddot{y} \quad (8.58)$$

These integrals for the case of a single DOF spring-mass-damper system are shown in Figures 8.4–8.6.

8.3.5 Evaluation of Integrals

Computation of each of the Integrals in Eqs. (8.51–8.61) requires the time history of displacement, velocity and acceleration of the rotor center as a function of time t . Since each of these curves may have any number of cycles, the following valid assumptions are made to reduce summation errors assuming no hysteresis loss.

When the displacement $x(t)$ is zero the following terms are set to zero and the

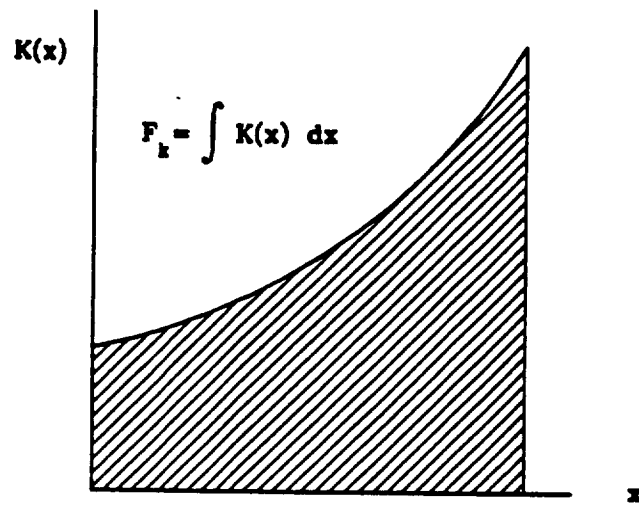


Figure 8.4 Stiffness Force Integral

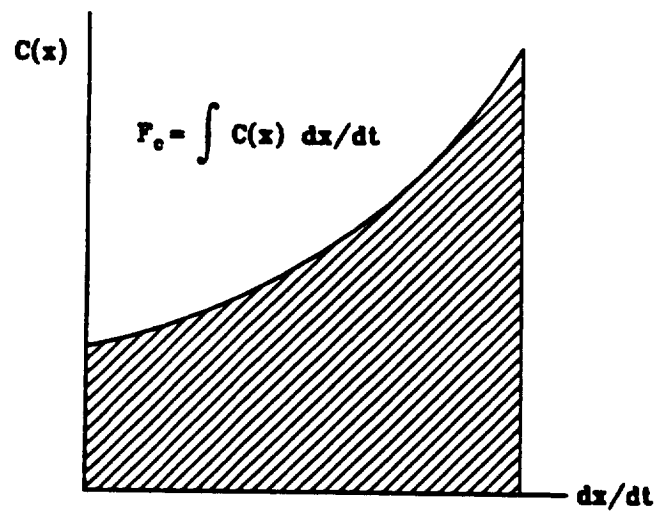


Figure 8.5 Damping Force Integral

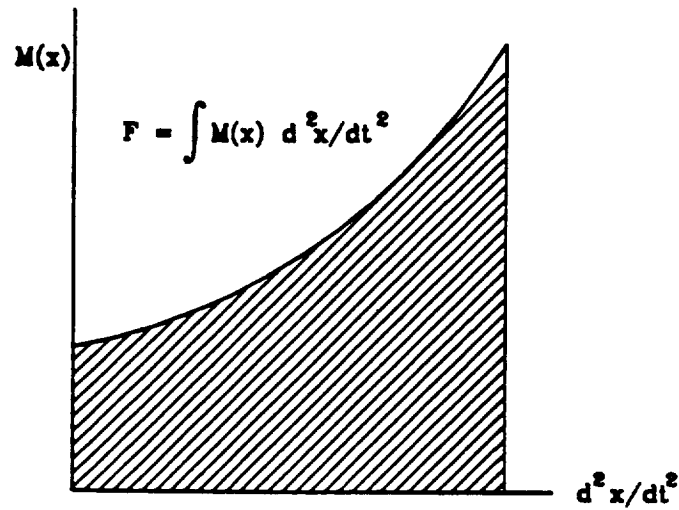


Figure 8.6 Inertia Force Integral

integration or summation starts from that instant.

$$\begin{aligned} f_{kxz}(x(t) = 0) &= 0 \\ f_{kyz}(x(t) = 0) &= 0 \end{aligned} \quad (8.59)$$

Similarly, when $y(t)$ is zero the following terms are set to zero.

$$\begin{aligned} f_{kzy}(y(t) = 0) &= 0 \\ f_{kyz}(y(t) = 0) &= 0 \end{aligned} \quad (8.60)$$

Similar assumptions are made with respect to damping and inertia forces. At $\dot{x}(t)$ equal to zero the following terms are set to zero.

$$\begin{aligned} f_{cex}(\dot{x}(t) = 0) &= 0 \\ f_{cye}(\dot{x}(t) = 0) &= 0 \end{aligned} \quad (8.61)$$

and at $\dot{y}(t)$ equal to zero the following terms are set to zero.

$$f_{cxy}(\dot{y}(t) = 0) = 0$$

$$f_{cv}(\dot{y}(t) = 0) = 0 \quad (8.62)$$

At $\tilde{x}(t)$ equal to zero the following terms are set to zero.

$$\begin{aligned} f_{mx}(\tilde{x}(t) = 0) &= 0 \\ f_{myx}(\tilde{x}(t) = 0) &= 0 \end{aligned} \quad (8.63)$$

and at $\tilde{y}(t)$ equal to zero the following terms are set to zero.

$$\begin{aligned} f_{my}(\tilde{y}(t) = 0) &= 0 \\ f_{myv}(\tilde{y}(t) = 0) &= 0 \end{aligned} \quad (8.64)$$

The effect of these initializations is to reduce the accumulation of errors as the integration is performed along the displacement, velocity and acceleration curves. In practice, zero values are never realized and a change in the sign of a variable is considered for the above initializations.

8.3.6 Summation vs. Integration

In the simulations with this model, the summation approach is used. The time step Δt is made very small so that the summation approaches the integration process.

$$\Delta t = \frac{t_n}{500} \quad (8.65)$$

where t_n is the time period of the displacement curve.

8.3.7 Limitations of Method-I

The method developed in this section requires the evaluation of 12 integrals of Eqs. (8.51–8.61). For a general motion, integrating each of these integrals involves two highly fluctuating functions. The integrand, which is a dynamic coefficient varying

with displacement, and the limit of integration which is either the displacement, velocity or acceleration curve. Since closed form solutions are unlikely, one has to resort to numerical integration to evaluate these integrals. The accumulation of errors over a period of time due to approximate summation or integration schemes as well as due to inherent approximate nature of the model may lead to inaccurate results if care is not taken to limit these errors. The parameter Δt is critical for the accuracy of this model if summation scheme is used.

A number of cases using the above method are included in the simulations.

8.4 New Method-II

In this section, the method-1 is simplified to make the computation of the Integrals in Eqs. (8.51–3.61) easier and more accurate.

The method-1 developed in the previous section has the following drawbacks.

- Difficult to integrate complicated displacement, velocity and acceleration profiles.
- Accumulation of modeling and integration errors as time progresses.
- Very small time step needed to maintain reasonable accuracy for summation.

In order to simplify the computation of these Integrals a few assumptions are made regarding the displacement, velocity and acceleration profiles. The main assumption, to be verified, is that the previous time history of the motion has little or no effect on the current state of motion for the bulk flow model used. Assuming that the above statement is valid, the actual displacement, velocity and acceleration curves may be replaced by approximate curves that are easier to integrate.

The following assumptions are made regarding the displacement, velocity and acceleration at any given instant of time.

1. The time history of displacement is neglected and only the current displacement is used in the computations. The displacement is assumed to increase from zero to the current value in a linear fashion gradually, and independent of time.
2. The time history of velocity prior to the current time step is neglected and the velocity is assumed to be linear with respect to displacement, i.e., velocity is initially zero when the displacement is zero and increases to the current value as a linear function of displacement while retaining its direction.
3. A similar assumption is made about acceleration, i.e., acceleration is zero initially and attains its current value in magnitude and direction as a linear function of displacement.

as a function of the time-displacement curve.

8.4.1 Theory

As in the previous case, the incremental fluid forces at any given operating point are given by Eq. (7.1). At any given time t_i , let the eccentricity or operating position of the rotor be given by (e_i, ϕ_i) or (x_i, y_i) , velocity by (v_i, γ_i) or (\dot{x}_i, \dot{y}_i) and acceleration by (a_i, η_i) or (\ddot{x}_i, \ddot{y}_i) .

The displacement is assumed to increase from $(0, 0)$ to (x_i, y_i) linearly. At any point along this path, the displacements are given by,

$$\begin{aligned} x &= e \cos \phi_i \\ y &= e \sin \phi_i \end{aligned} \tag{8.66}$$

where,

$$\begin{aligned} e &= \sqrt{x^2 + y^2} \\ e_i &= \sqrt{x_i^2 + y_i^2} \\ \tan \phi_i &= \frac{y_i}{x_i} \end{aligned} \quad (8.67)$$

and velocity as a function of displacement is given by,

$$\begin{aligned} \dot{x} &= v \cos \gamma_i \\ \dot{y} &= v \sin \gamma_i \end{aligned} \quad (8.68)$$

where,

$$\begin{aligned} v_i &= \sqrt{\dot{x}_i^2 + \dot{y}_i^2} \\ \tan \gamma_i &= \frac{\dot{y}_i}{\dot{x}_i} \\ v &= \frac{v_i}{e_i} e \end{aligned} \quad (8.69)$$

and acceleration is given as a function of displacement as,

$$\begin{aligned} \ddot{x} &= a \cos \eta_i \\ \ddot{y} &= a \sin \eta_i \end{aligned} \quad (8.70)$$

where,

$$\begin{aligned} a_i &= \sqrt{\ddot{x}_i^2 + \ddot{y}_i^2} \\ \tan \eta_i &= \frac{\ddot{y}_i}{\ddot{x}_i} \\ a &= \frac{a_i}{e_i} e \end{aligned} \quad (8.71)$$

The velocity profile may be rewritten as,

$$\begin{aligned}\dot{x} &= \left(\frac{\dot{x}_i}{x_i}\right) x \\ \dot{y} &= \left(\frac{\dot{y}_i}{y_i}\right) y\end{aligned}\quad (8.72)$$

i.e., the velocity is assumed to increase from (0,0) to the current value (\dot{x}_i, \dot{y}_i) as a linear function of the displacement curve. Similarly, acceleration increases from (0,0) to its current value (\ddot{x}_i, \ddot{y}_i) as a linear function of displacement.

$$\begin{aligned}\ddot{x} &= \left(\frac{\ddot{x}_i}{x_i}\right) x \\ \ddot{y} &= \left(\frac{\ddot{y}_i}{y_i}\right) y\end{aligned}\quad (8.73)$$

Using the above assumptions, the Eqs. (8.47–8.58) may be rewritten as,

$$f_{kxx}(t_i) = \int_0^{x_i} K_{xx}(x, y) dx \quad (8.74)$$

$$f_{kxy}(t_i) = \int_0^{y_i} k_{xy}(x, y) dy \quad (8.75)$$

$$f_{kyx}(t_i) = \int_0^{x_i} k_{yx}(x, y) dx \quad (8.76)$$

$$f_{kyy}(t_i) = \int_0^{y_i} K_{yy}(x, y) dy \quad (8.77)$$

$$f_{cxx}(t_i) = \int_0^{x_i} C_{xx}(x, y) \left(\frac{\dot{x}_i}{x_i}\right) dx \quad (8.78)$$

$$f_{cxy}(t_i) = \int_0^{y_i} c_{xy}(x, y) \left(\frac{\dot{y}_i}{y_i}\right) dy \quad (8.79)$$

$$f_{cyx}(t_i) = \int_0^{x_i} c_{yx}(x, y) \left(\frac{\dot{x}_i}{x_i}\right) dx \quad (8.80)$$

$$f_{cyy}(t_i) = \int_0^{y_i} C_{yy}(x, y) \left(\frac{\dot{y}_i}{y_i}\right) dy \quad (8.81)$$

$$f_{mxx}(t_i) = \int_0^{x_i} M_{xx}(x, y) \left(\frac{\ddot{x}_i}{x_i}\right) dx \quad (8.82)$$

$$f_{mxy}(t_i) = \int_0^{y_i} m_{xy}(x, y) \left(\frac{\ddot{y}_i}{y_i}\right) dy \quad (8.83)$$

$$f_{m_{yx}}(t_i) = \int_0^{x_i} m_{yx}(x, y) \left(\frac{\ddot{x}_i}{x_i} \right) dx \quad (8.84)$$

$$f_{m_{yy}}(t_i) = \int_0^{y_i} M_{yy}(x, y) \left(\frac{\ddot{y}_i}{y_i} \right) dy \quad (8.85)$$

The integration limits of the above integrals are much simpler as the velocity and acceleration profiles are replaced by equivalent displacement profile which is a simple function. These Integrals can be easily computed using any of the various numerical integration schemes available. Two methods, one based on Simpson's rule and other based on adaptive quadrature integration are used in this study.

As compared to the original method, this simplified method has the following advantages.

- Total fluid reaction force is computed at each time step instead of incremental summation and this eliminates the problem of accumulation of errors.
- Integrals are easier to compute.
- The method is valid for any type of motion.

CHAPTER IX

IMPLEMENTATION

Simulations involving various types of transient motion are used to study the various approaches discussed in the previous chapter. The model used is a modified Jeffcott rotor and is shown in Figure 9.1. It consists of a rotor floating in an annular seal and is released from rest at time $t = 0$. Various types of known varying loads are applied to the rotor and the resulting motion is studied using the following four different models.

1. Bulk Flow Model: This simulation is done by solving the actual set of seal governing equations for transient fluid forces at each time step. The results from this study are used as a benchmark to compare the results of the other models.
2. Linear Model ($\epsilon = 0$): This simulation is done using the dynamic coefficients computed at zero eccentricity, to compute the fluid forces. This is the model currently in use at NASA/MSFC.
3. New Method-I: This simulation is done using the method described in section 8.1.
4. New Method-II: This is the simplified extension of method-1 and it assumes approximate displacement, velocity and acceleration profiles to compute seal forces.

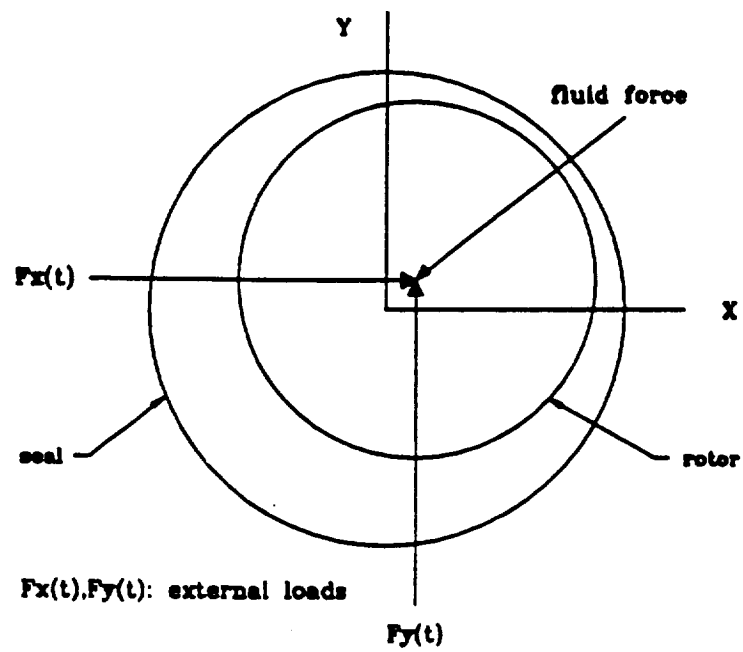


Figure 9.1 Simulation Model

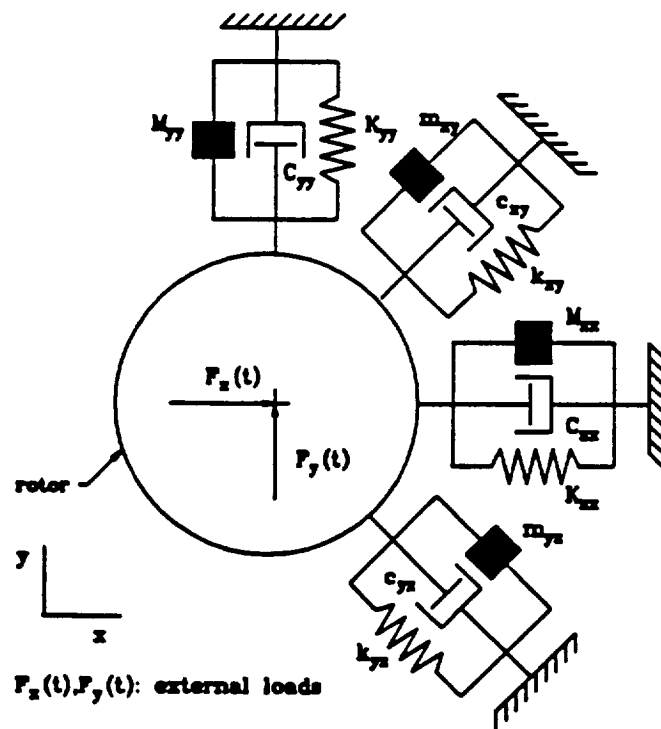


Figure 9.2 Rotor-Seal Model used for Simulation

9.1 Simulation Model

The equations of motion for the system used for simulation are given by,

$$\begin{aligned} m\ddot{x}(t) &= F_x(t) + F_{fluid-x}(t) \\ m\ddot{y}(t) &= F_y(t) + F_{fluid-y}(t) \end{aligned} \quad (9.1)$$

where $x(t)$ and $y(t)$ are the rotor displacements from centered position and m is the mass of the rotor. The terms $F_x(t)$ and $F_y(t)$ are the two components of the applied external load, and $F_{fluid-x}(t)$ and $F_{fluid-y}(t)$ are the fluid reaction forces computed using one of the four methods mentioned above.

This set of second order differential equations are reduced to a set of first order ordinary differential equations which are then integrated using a fourth order Runge-Kutta integrator with adaptive step size.

$$\begin{aligned} q_1(t) &= x(t) \\ q_2(t) &= \dot{x}(t) \\ q_3(t) &= y(t) \\ q_4(t) &= \dot{y}(t) \end{aligned} \quad (9.2)$$

$$\begin{aligned} \dot{q}_1(t) &= q_2(t) \\ m\dot{q}_2(t) &= F_x(t) + F_{fluid-x}(t) \\ \dot{q}_3(t) &= q_4(t) \\ m\dot{q}_4(t) &= F_y(t) + F_{fluid-y}(t) \end{aligned} \quad (9.3)$$

The initial conditions are given below.

$$q_1(t=0) = 0$$

$$\begin{aligned}
q_2(t=0) &= 0 \\
q_3(t=0) &= 0 \\
q_4(t=0) &= 0
\end{aligned}
\tag{9.4}$$

At each time step in the above integration process, a routine which computes the fluid force is called. The input to the routine is the current displacement, velocity and acceleration of the rotor center. The output is the the X and Y components of the fluid force. The mass of the rotor used in simulations is 45.4 kg (100lb).

9.2 Time Step for Transient Analysis

In the simulations carried out with various models, the following time step is used.

$$\Delta t = \frac{t_n}{15} \tag{9.5}$$

For the *method-1*, the following time step is used.

$$\Delta t = \frac{t_n}{500} \tag{9.6}$$

About 15–20 cycles of motion is studied for each simulation.

9.3 Fluid Inertia Coefficients

The model used to estimate the seal forces has four inertia coefficients M_{xx} , m_{xy} , m_{yx} and M_{yy} to account for the fluid inertia forces. Of these m_{xy} and m_{yx} are almost zero. Strictly speaking, the coefficients M_{xx} and M_{yy} have to be added to the rotor mass in the above simulation model. These fluid inertia forces are relatively small compared to the other terms even at high frequencies. To simplify the computations these inertia coefficients are retained in the linear model and the acceleration at the

previous time step is used to compute these forces. This approach is checked by including the fluid inertia coefficients in the rotor mass and comparing the results. The results indicate practically no change in the results even at very high frequencies.

9.4 Computation of Fluid Forces

In the simulations with bulk flow model, the fluid forces are computed by solving the set of equations Eqs. (8.1-8.3) for the pressure distribution $p(z, \beta, t)$ which is then integrated along the length of the seal to obtain the transient fluid forces. This process is implemented in a continuous fashion from one time step to the next.

For linear model ($\epsilon = 0$), the set of coefficients for zero eccentricity are used for computing the seal forces. These coefficients are obtained from seal code *TAMUSEAL-III*.

For new method-1 and new method-2, the following procedure is implemented. These two methods assume the availability of the 12 dynamic coefficients as continuous functions of the displacement (x, y) . Let these functions be specified by g_{kxz} , g_{kxy} , g_{kyx} etc., as shown below.

$$\begin{aligned}
 g_{kxz}(x, y) &= K_{xz}(x, y) \\
 g_{kxy}(x, y) &= k_{xy}(x, y) \\
 g_{kyx}(x, y) &= k_{yx}(x, y) \\
 g_{kyy}(x, y) &= K_{yy}(x, y)
 \end{aligned} \tag{9.7}$$

$$\begin{aligned}
 g_{czz}(x, y) &= C_{zz}(x, y) \\
 g_{czy}(x, y) &= c_{zy}(x, y) \\
 g_{cye}(x, y) &= c_{ye}(x, y)
 \end{aligned}$$

$$g_{c_{yy}}(x, y) = C_{yy}(x, y) \quad (9.8)$$

$$\begin{aligned} g_{m_{xx}}(x, y) &= M_{xx}(x, y) \\ g_{m_{xy}}(x, y) &= m_{xy}(x, y) \\ g_{m_{yx}}(x, y) &= m_{yx}(x, y) \\ g_{m_{yy}}(x, y) &= M_{yy}(x, y) \end{aligned} \quad (9.9)$$

These curves plotted as a function of eccentricity e are smooth curves with gradually varying slopes. They have no discontinuities or abrupt changes in function values. This property of continuous and smooth variation as a function of eccentricity enables these curves to be easily fitted with cubic splines using only a few sets of data. These splines can then be interpolated to compute coefficients at any given eccentricity.

A number of sets of dynamic coefficients at various eccentricity ratios starting from 0 to 0.8 are computed using the seal code *TAMUSEAL-III*. About 10–12 sets of dynamic coefficients at 0.05–0.1 eccentricity ratio increments are sufficient for accurate interpolation of these coefficients for intermediate values. The increment is made smaller for the higher eccentricity region as the coefficients vary more rapidly in that region. The data in Table 9.1 is the data used for all the simulations cases.

These sets of coefficients are obtained at an eccentricity angle of zero, i.e., along the X -axis. Using a transformation, it is possible to compute these coefficients at any eccentricity (x, y) using the eccentricity angle ϕ . This transformation method has been discussed in detail in section 5.4. The same procedure is employed to compute dynamic coefficients in the global coordinate system as required in the simulation model of Eq. 9.1.

9.5 Splines of Coefficients

About 12 sets of dynamic coefficients computed at various eccentricities and at zero eccentricity angle are fitted with cubic splines. This enables the computation of the dynamic coefficients in a pseudo-continuous fashion. For the case of a *distorted seal* or a seal with a non-circular cross section a 2-D table will be required. The seal parameters for seal unit 3-02 as given in *Appendix E*. A summary of these coefficients at various eccentricities is given in Table 9.1.

9.6 Transient Analysis Simulation Code: TRANSEAL

The four different models described earlier are implemented in the transient analysis simulation code *TRANSEAL*. The input to this code is the dynamic coefficients at various eccentricities, seal parameters and time step Δt . The output consists of the fluid forces, the 12 individual force components, displacements, velocities and accelerations at each time step.

Table 9.1 Table of Dynamic Coefficients for Seal Unit 3-02

ϵ	K_{ss}	k_{sy}	k_{sp}	K_{sv}	C_{ss}	c_{sy}	c_{sp}	C_{sv}	M_{ss}	m_{sy}	m_{sp}	M_{sv}
	lb/in	lb/in	lb/in	lb/in	lb-s/in	lb-s/in	lb-s/in	lb-s/in	lb-s ² /in	lb-s ² /in	lb-s ² /in	lb-s ² /in
.00	.323158E6	.60221E5	.60221E5	.323158E6	.934E2	.149E1	.149E2	.931E2	.219E-2	.385E-4	.385E-4	.219E-2
.05	.323603E6	.60221E5	.60317E5	.323331E6	.934E2	.149E1	.150E1	.932E2	.219E-2	.385E-4	.385E-4	.219E-2
.10	.325070E6	.60143E5	.60611E5	.323853E6	.943E2	.150E1	.151E1	.935E2	.221E-2	.387E-4	.385E-4	.219E-2
.15	.327556E6	.60037E5	.60611E5	.324741E6	.959E2	.151E2	.153E1	.941E2	.223E-2	.389E-4	.385E-4	.220E-2
.20	.331223E6	.59869E5	.61856E5	.326029E6	.981E2	.152E1	.156E1	.948E2	.227E-2	.393E-4	.386E-4	.222E-2
.25	.336285E6	.59623E5	.62872E5	.327758E6	.101E3	.154E1	.153E1	.958E2	.232E-2	.397E-4	.386E-4	.223E-2
.30	.343054E6	.59273E5	.64222E5	.323000E6	.105E3	.157E1	.165E1	.971E2	.239E-2	.400E-4	.386E-4	.225E-2
.36	.354073E6	.58674E5	.66411E5	.333483E6	.111E3	.161E1	.171E1	.990E2	.249E-2	.406E-4	.386E-4	.229E-2
.40	.363700E6	.58138E5	.68323E5	.336394E6	.117E3	.164E1	.178E1	.101E3	.258E-2	.408E-4	.386E-4	.231E-2
.46	.382810E6	.57083E5	.72144E5	.341871E6	.126E3	.172E1	.190E1	.104E3	.275E-2	.407E-4	.384E-4	.236E-2
.50	.399743E6	.56186E5	.75574E5	.346450E6	.136E3	.178E1	.199E1	.106E3	.289E-2	.401E-4	.382E-4	.240E-2
.55	.427589E6	.54826E5	.81334E5	.353534E6	.150E3	.189E1	.215E1	.109E3	.313E-2	.384E-4	.379E-4	.246E-2
.60	.466192E6	.53208E5	.89564E5	.362619E6	.170E3	.205E1	.236E1	.114E3	.344E-2	.350E-4	.374E-4	.253E-2
.65	.521888E6	.54826E5	.81334E5	.358702E6	.197E3	.229E1	.265E1	.119E3	.388E-2	.282E-4	.372E-4	.262E-2
.70	.608533E6	.49885E5	.12119E6	.390551E6	.237E3	.273E1	.305E1	.127E3	.455E-2	.160E-4	.384E-4	.273E-2
.75	.766823E6	.50528E5	.15467E6	.413505E6	.304E3	.367E1	.356E1	.137E3	.563E-2	-.62E-4	.455E-4	.291E-2
.78	.952857E6	.56073E5	.18905E6	.433172E6	.375E3	.489E1	.386E1	.145E3	.672E-2	-.14E-4	.573E-4	.304E-2

CHAPTER X

RESULTS

To study each of the models described in the earlier chapters, various types of known varying loads are applied to a rotor in an annular seal and the resulting transient motion is studied. The loads applied to the rotor are divided into the following six categories.

1. Gradually applied loads (ramp function)
2. Harmonic loads (sinusoidal function)
3. High frequency loads (sinusoidal function)
4. Suddenly applied loads (step function)
5. Impulse or shock loads (impulse function)
6. Combination of the above loads.

10.1 Gradually Applied Loads (Ramp Function)

In this test case, a series of loads 1780N (400lb), 5340N (1200lb) and 8900N (2000lb) are applied to the rotor in a vertically downward direction in a gradual manner. The loads follow a ramp function while increasing from a zero load at $t = 0$ to the maximum load at $t = 0.05s$. In practice, this type of load results from side loads. Each of these cases are repeated for the four models and the results are plotted as comparison plots. For each case two plots are shown: the first plot includes the time-displacement curve $y(t)$ while the second plot shows the y-component of the computed seal force $F_y(t)$ as a function of time.

The steady-state values of displacement y marked on the plots are obtained separately from a seal code based on the dynamic analysis developed earlier. This seal code solves the set of steady-state bulk flow seal governing equations to compute these values. These expected steady state displacement values are included for the purpose of comparison.

The comparison plots for this case are shown in Figures 10.1–10.3.

The external forcing function for this case is given below.

$$\begin{aligned} F_v(t) &= -(20t) F_c \quad (0 < t \leq 0.05s) \\ &= -F_c \quad (t > 0.05s) \\ F_s(t) &= 0 \end{aligned} \tag{10.1}$$

where F_c is the constant load.

The results for all the three approximate methods show good agreement with the bulk flow model for smaller load 1780N (400lb). For higher loads 5340N (1200lb) and 8900N (2000lb), as the eccentricity ratio exceeds 0.4, the linear model ($\epsilon = 0$) starts deviating from the actual model and this deviation increases as the eccentricity increases. The displacement plot in Figure 10.3 for the 8900N (2000lb) case clearly shows the difference between these two models. Also, note the almost exact matching of the results of the two new methods with those of the bulk flow model for all cases.

The plots for the fluid forces in Figures. 10.1–10.3 are all identical because the rise time t_r is much larger than the time period t_n of the system. Therefore, the seal reaction forces track the external load exactly in magnitude and without any phase shift.

The following important conclusions can be drawn from these results.

1. The transient motion using bulk flow model converges to the expected steady

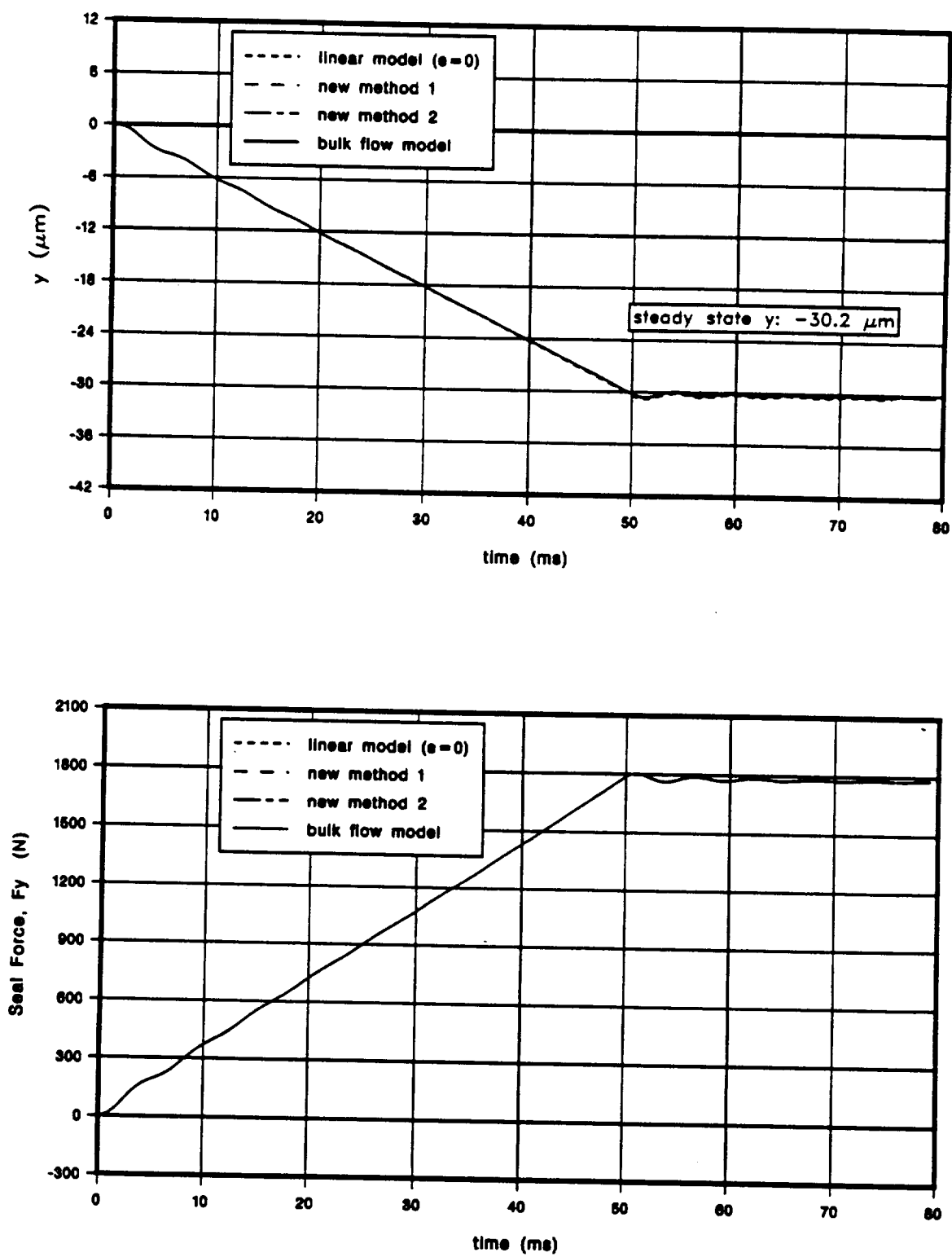


Figure 10.1 Gradually Applied Load, 1780 N (400 lb), Disp. (y), Seal Force (F_y)

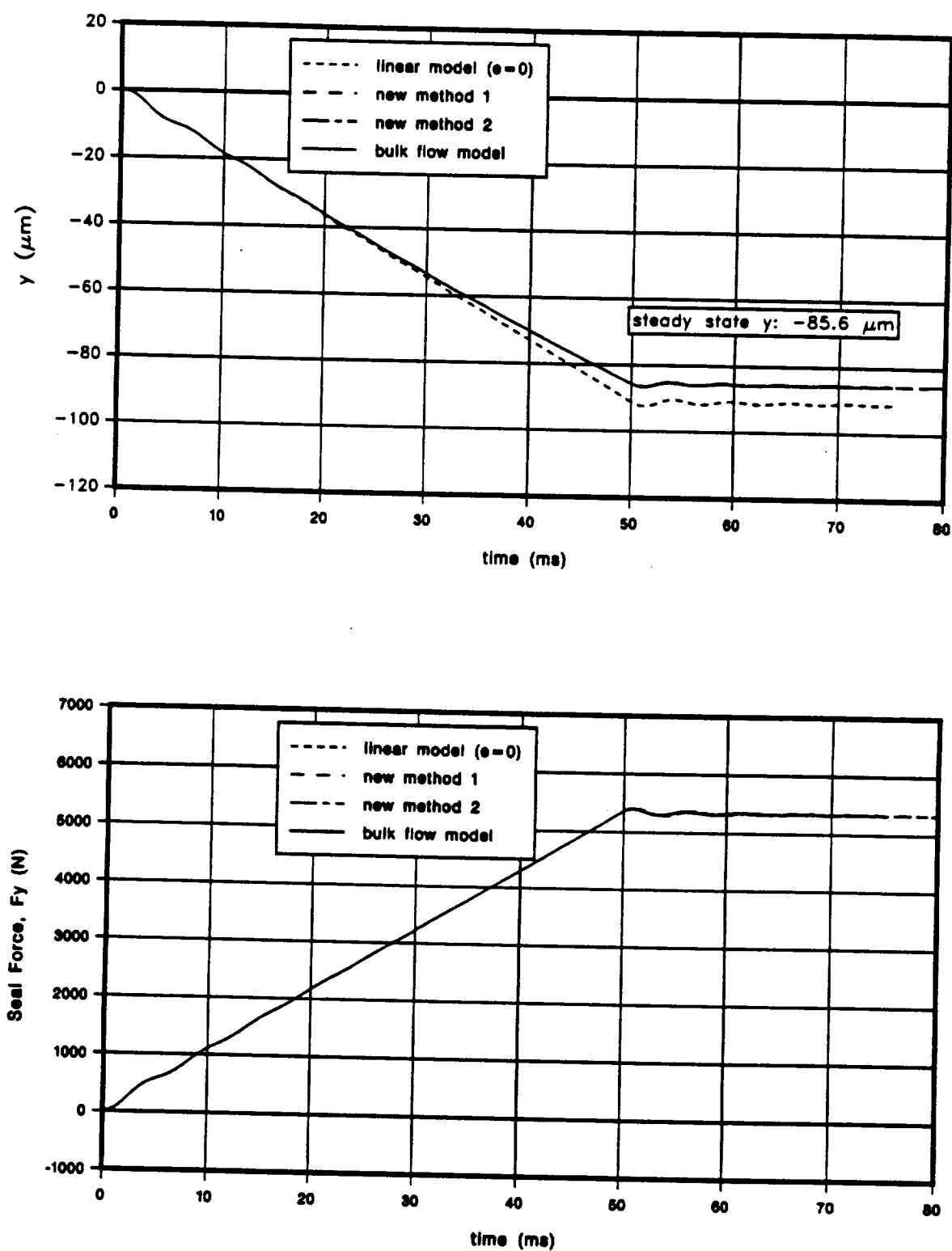


Figure 10.2 Gradually Applied Load, 5340 N (1200 lb), Disp. (y), Seal Force (F_y)

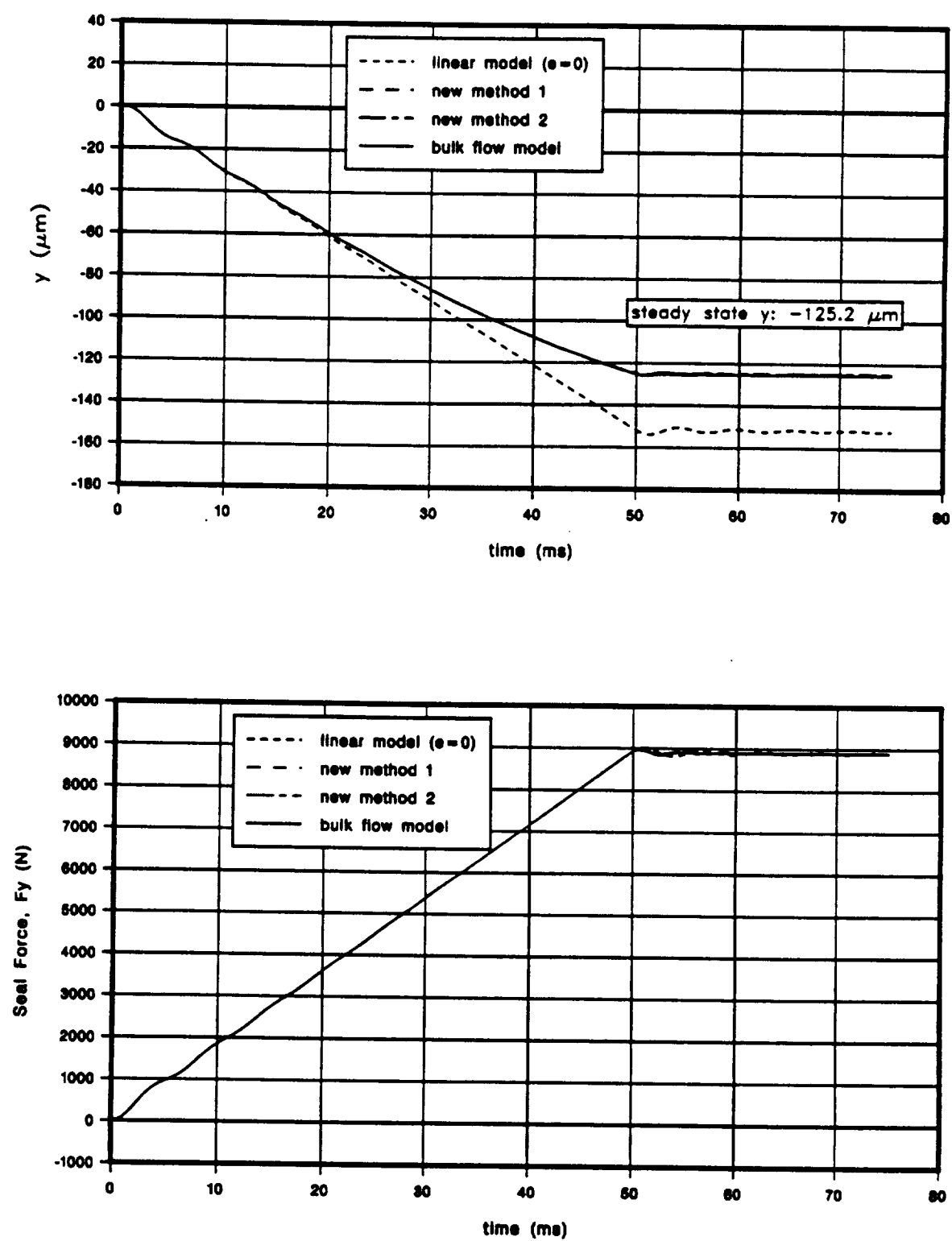


Figure 10.3 Gradually Applied Load, 8900 N (2000 lb), Disp. (y), Seal Force (F_y)

state values exactly, thus verifying the transient analysis solution procedure. The steady state values used for comparison are obtained independently using a separate solution process.

2. Linear model ($\epsilon = 0$) yields good results for small displacements. At higher eccentricities (beyond 0.3–0.4 eccentricity ratio) there is a marked difference between this model and the actual model (Figure 10.3). This example illustrates the need for a better model than linear model ($\epsilon = 0$) for motion with large eccentricities.
3. The results of new method-1 and new method-2 exactly match with those of the bulk flow model.
4. On a more important note, unrelated to the transient analysis, these results validate the solution procedure of the dynamic analysis developed in earlier chapters, zeroth order as well as first order solutions. The results of this transient analysis establishes the equivalence between the bulk flow model based motion and the corresponding motion described by the linear model of Eq.7.1 based on dynamic coefficients extracted from the first order solution. Generally, it is taken for granted that these two solution match for small motion. These results demonstrate, for the first time for seals, this equivalence. This exercise also may be used as a check case for the first order solution to verify that the dynamic coefficients extracted from the first order solution are indeed the correct coefficients. In other words, this study may be used as a check case for for the solution procedure, zeroth and first order solutions.

10.1.1 Steady State Seal Forces vs. Spring Forces

In a seal analysis, steady state seal forces are computed as function of eccentricity by integrating the zeroth order pressure distribution along the length of the seal. The two components of the seal force are used to estimate the load bearing capacity of the seal. In the context of the new methods 1 and 2, these forces may be thought of as forces due to spring stiffnesses as damping and inertia forces are non-existent when the rotor is in a steady state operating position. The component forces f_{kxx} , f_{kxy} , f_{kyx} and f_{kyy} in the new method-1 and new method-2 represent the forces due to direct and cross coupled stiffnesses.

Seal forces F_x and F_y shown in Figure 10.4 Seal forces F_{seal-x} and F_{seal-y} shown in Figure 8.9 are computed using the seal code as a function of eccentricity along the X axis. If the new analysis developed is accurate, these forces should be the same as the spring forces given below.

Seal forces F_x and F_y shown in Figure 10.4 are computed using the seal code *TAMUSEAL-III* as a function of eccentricity along the X axis. If the new analysis developed is accurate, these forces should be the same as the spring forces given below.

$$F_{seal-x} = f_{kxx} + f_{kxy} \quad (10.2)$$

$$F_{seal-y} = f_{kyx} + f_{kyy} \quad (10.3)$$

The plot in Figure 10.4 shows the steady state forces computed using both these approaches. The results match exactly further validating the two new methods.

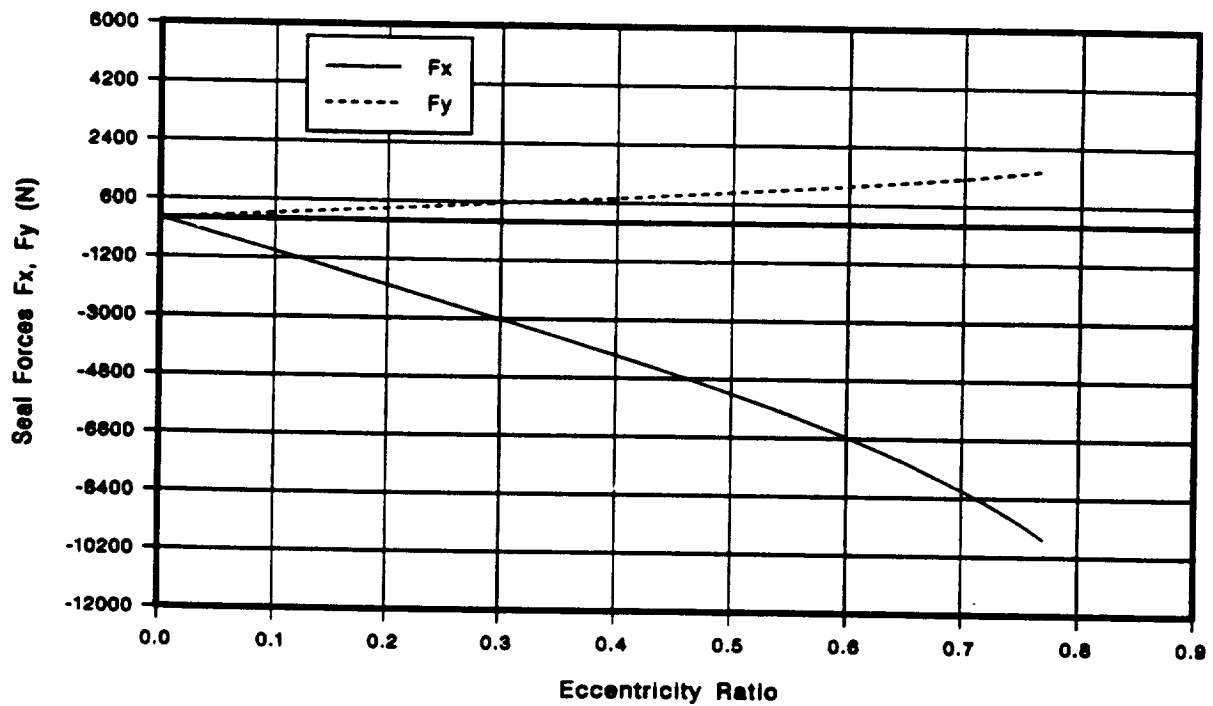


Figure 10.4 Steady State Seal Forces for Seal Unit 3-02, from Seal Code

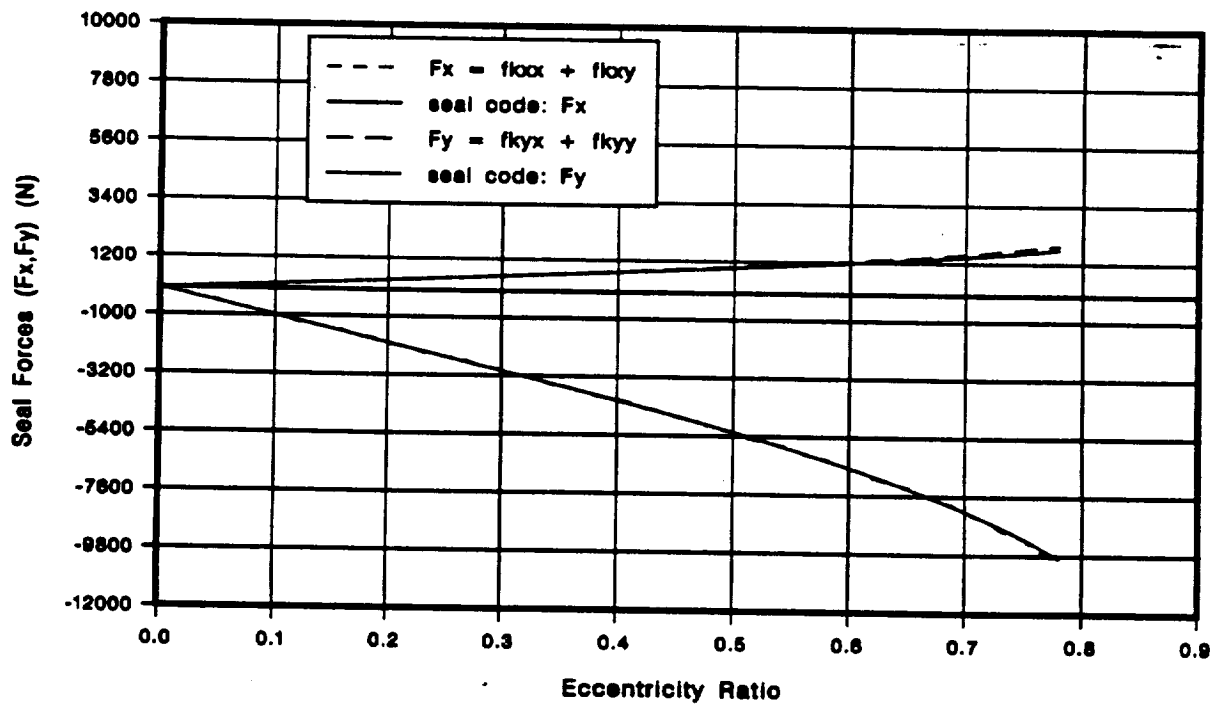


Figure 10.5 Steady State Seal Forces vs. Spring Forces, New Methods-1,2

10.2 Harmonic Loads (Sinusoidal Function)

In this test case, a series of loads at a frequency of 100Hz are applied to the rotor. This type of forcing function is typical of the loading on the rotor due to an unbalance. The external forcing function used for this test case is given below.

$$\begin{aligned} F_y(t) &= F_s \sin(2\pi ft) \\ F_x(t) &= 0 \end{aligned} \quad (10.4)$$

where F_s is the amplitude and f is the circular frequency in Hz.

The loads used are 1780N (400lb) and 5340N (1200lb) at a frequency of 100 Hz. The plots shown in Figures 10.6–10.9 refer to this case. There is excellent agreement between the bulk flow model and the all the three approximate models for 1780N (400lb) and 3560N (800lb) cases. For the 5340N (1200lb) case shown in Figure 10.8, the linear model ($\epsilon = 0$) starts to deviate from the actual model. However, the new methods gives exact results.

An important conclusion that can be drawn from this case is that the the linear model ($\epsilon = 0$) is accurate even for relatively large displacements provided the rotor vibrates about the same static operating point and the set of dynamic coefficients used correspond to that operating point. This is interesting since the basic assumption of the linear model ($\epsilon = 0$) is that it is valid only for a small motion about the operating point.

For the next case shown in Figure 10.9, the oscillating rotor is forced to move to an eccentric position by the application of the following forcing function.

$$\begin{aligned} F_y(t) &= (20t) F_c + F_s \sin(2\pi ft) \quad 0 < t \leq 0.05s \\ &= F_c + F_s \sin(2\pi ft) \quad t > 0.05s \end{aligned}$$

$$F_x(t) = 0 \quad (10.5)$$

where F_c is a constant load.

This example (Figure 10.9) clearly shows the effect of the movement of the rotor operating position away from the centered position as predicted by the bulk flow model vis-a-vis the same motion predicted by linear model ($\epsilon = 0$). There is an appreciable difference between these two models. The two new methods give almost exact results.

The following conclusions may be drawn based on these test cases.

1. The example case in Figure 10.8 refers to the large eccentric motion type-1 mentioned in Chapter VII. The case in Figure 10.9 refers to large eccentric motion type-2.
2. An annular seal operates almost like a linear element for steady state motion about a given static point.
3. The linear model ($\epsilon = 0$) gives good results even for relatively large rotor displacements ($\epsilon > 0.4$). For example, if the rotor is whirling about a static operating point, this model yields acceptable results even for large displacements if the set of dynamic coefficients corresponding to this operating point are used.
4. However, the above statement is not true in the case of the transient motion shown in shown in Figure 10.9 where there is actual movement of the center of rotor to an eccentric position.
5. The two new methods agree exactly with the actual model both for steady state as well as transient operation.

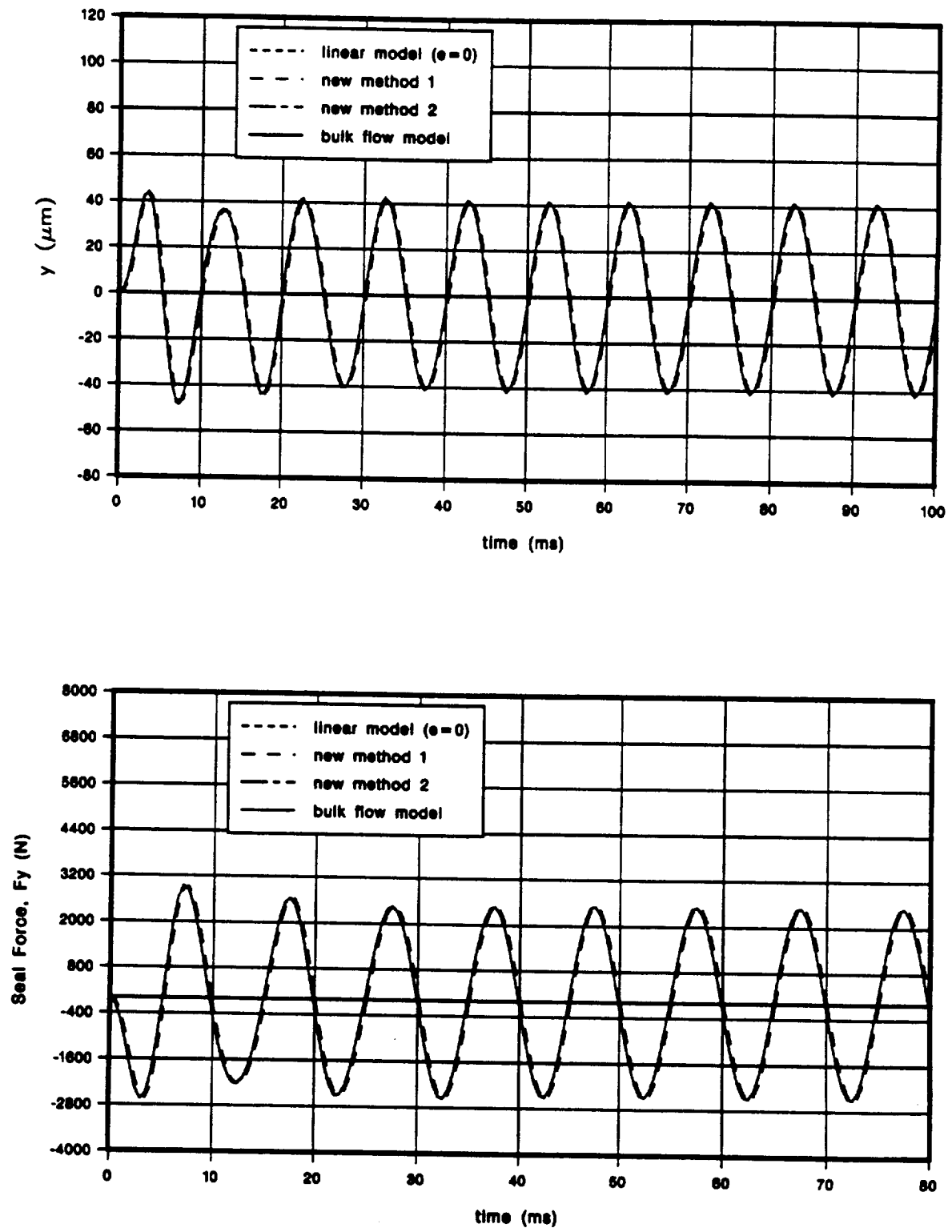


Figure 10.6 Harmonic Load, 1780N (400lb) at 100Hz, Disp. (y), Seal Force (F_y)

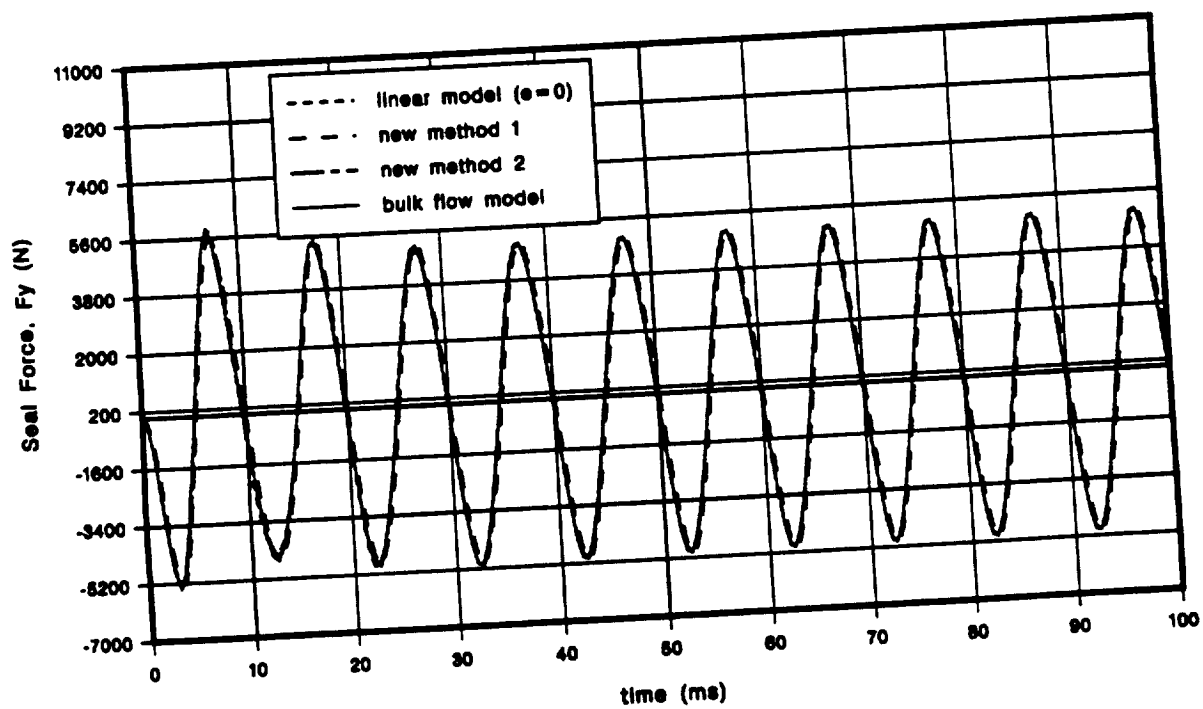
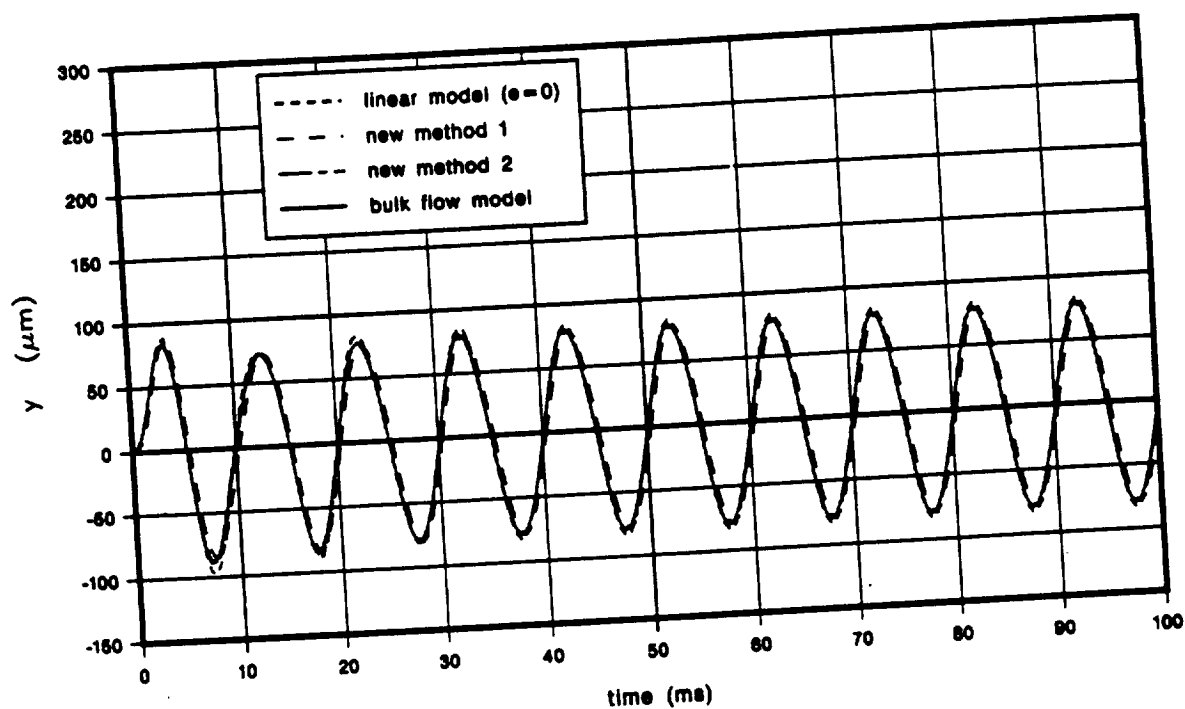


Figure 10.7 Harmonic Load, 3560N (800lb) at 100Hz, Disp. (y), seal Force (F_y)

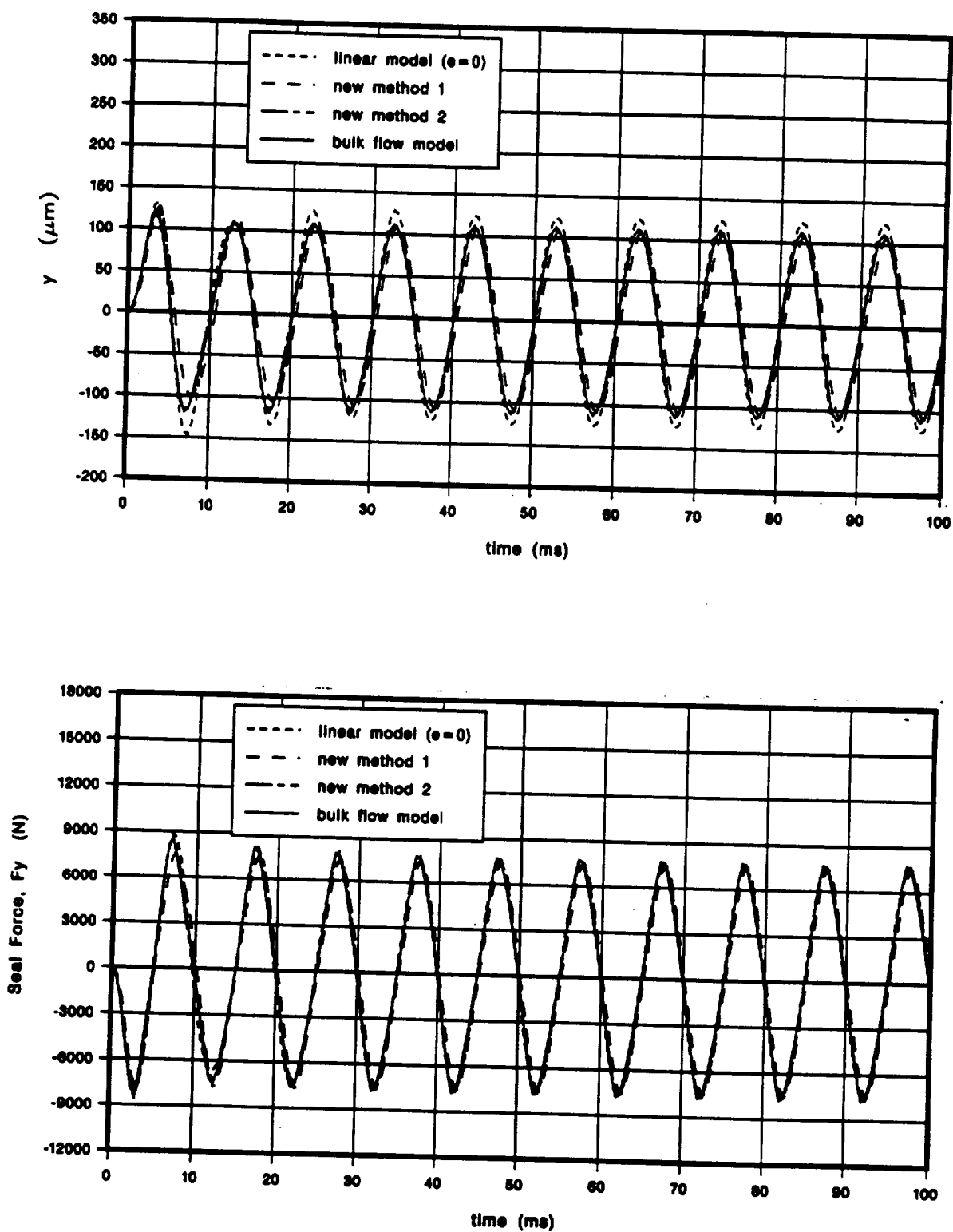


Figure 10.8 Harmonic Load, 5340N (1200lb) at 100Hz, Disp. (y), seal Force (F_y)

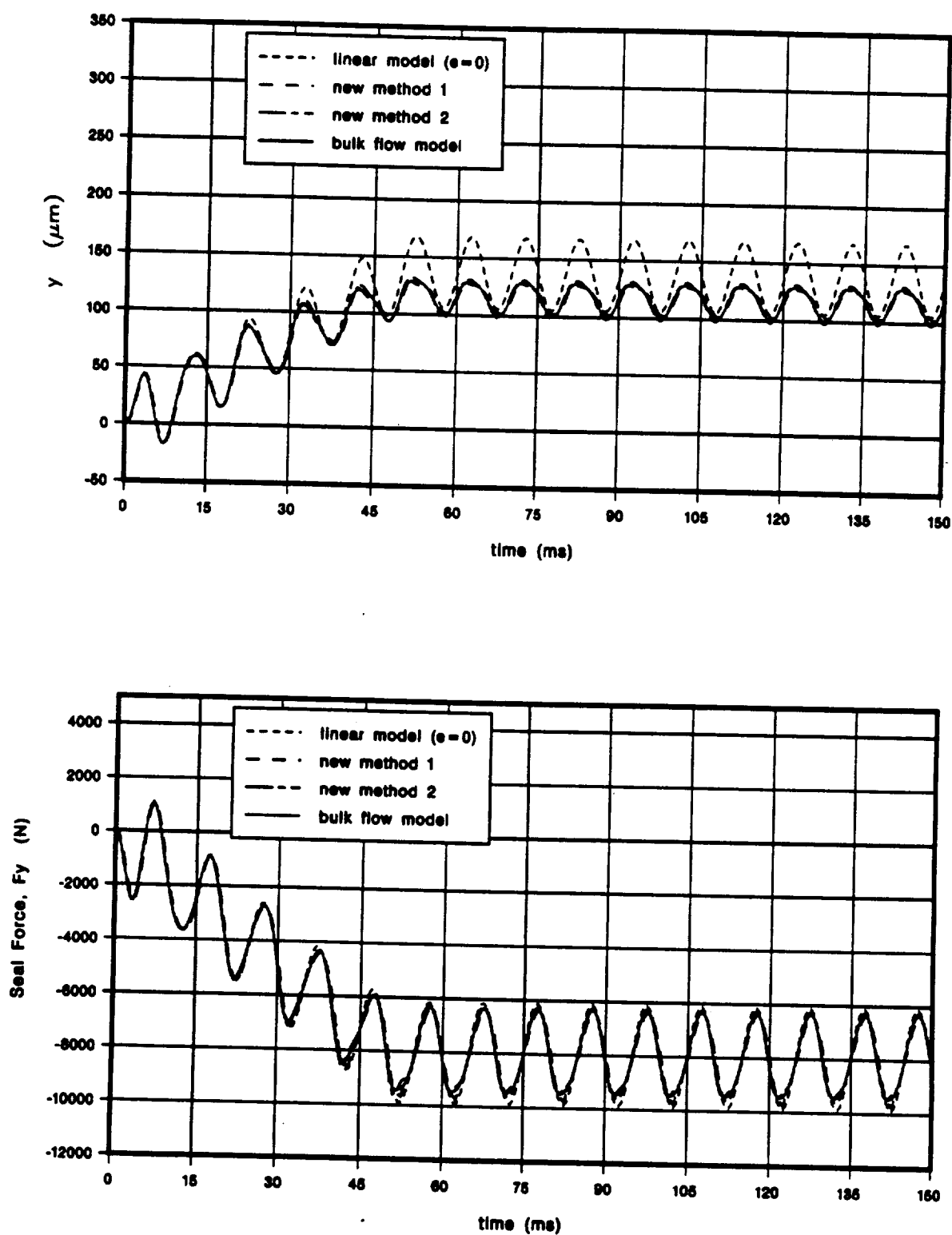


Figure 10.9 Harmonic Load (eccentric), 1340N (300lb), 100Hz, Disp. (y), Force (F_y)

10.3 High Frequency Loads (Sinusoidal Function)

The rotor of the SSME turbopump runs at about 25000 rpm, i.e., about 417 Hz. Any unbalance forces in the rotor system will vary as a function of this frequency. To study the effect of such unbalance forces at very high frequencies, different harmonic loads at 500 Hz and 1000Hz are applied to the rotor and the transient motion is observed. The loads applied are 2225N (500lb) and 15570N (3500lb) at 500Hz, 17800N (4000lb) and 3560N (8000lb) at 1000Hz.

The forcing function is similar to the previous case.

$$\begin{aligned} F_y(t) &= F_s \sin(2\pi ft) \\ F_x(t) &= 0 \end{aligned} \quad (10.6)$$

The results are shown in Figures 10.10–10.12 for the 500Hz case and in Figures 10.13–10.14 for 1000Hz case. Again, as in the case of harmonic loads at 100 Hz, there is good correspondence between the bulk flow model and the other three methods at both 500 Hz and 1000 Hz cases. Also, these results confirm that the two new methods work at any frequency.

To look at the motion away from the centered position, the rotor is forced to an eccentric position and the results in Figure 10.12 once again clearly show the difference the linear model ($\epsilon = 0$) and the actual model. Also, the results of new method-1 and new method-2 exactly match those of the actual model.

The external forcing function for this case is given below.

$$\begin{aligned} F_y(t) &= (20t) F_c + F_s \sin(2\pi ft) \quad (0 < t \leq 0.05s) \\ &= F_c + F_s \sin(2\pi ft) \quad (t > 0.05s) \\ F_x(t) &= 0 \end{aligned} \quad (10.7)$$

10.3.1 Fluid Inertia Forces at High Frequencies

The plots shown in Figures 10.10–10.14 may be studied to observe the effect of fluid inertia forces at very high frequencies. The results of the three approximate methods based on linear model compare very well with the bulk flow model results. These results show that the effects of fluid inertia effects at very high frequencies do not show any significant difference from the bulk flow model.

10.4 Suddenly Applied Loads (Step Function)

In this type of loading, the load is applied suddenly similar to a step function. The resulting motion after the transient state settles to the gradually applied load case discussed earlier. The loads applied are 1780N (400lb), 3560N (800lb) and 5340N (1200lb). This motion is almost similar to an impulse or shock load as the rise time t_r is much smaller than the time period T_n of the system. This is a good test case for the two new methods because of the rapidly varying motion. The results for this case are shown in Figures (10.15–10.17).

The linear model ($\epsilon = 0$) for 5340N (1200lb) case in Fig. 10.17 shows that the motion not only has a different overshoot but is also quite a bit out of phase and it settles to the wrong steady state value. The new method-2 has some overshoot, but maintains the phase and settles to the expected steady state value.

The forcing function for this case is,

$$\begin{aligned}
 F_y(t) &= 0 \quad (t = 0) \\
 &= -F_c \quad (t > 0) \\
 F_x(t) &= 0
 \end{aligned} \tag{10.8}$$

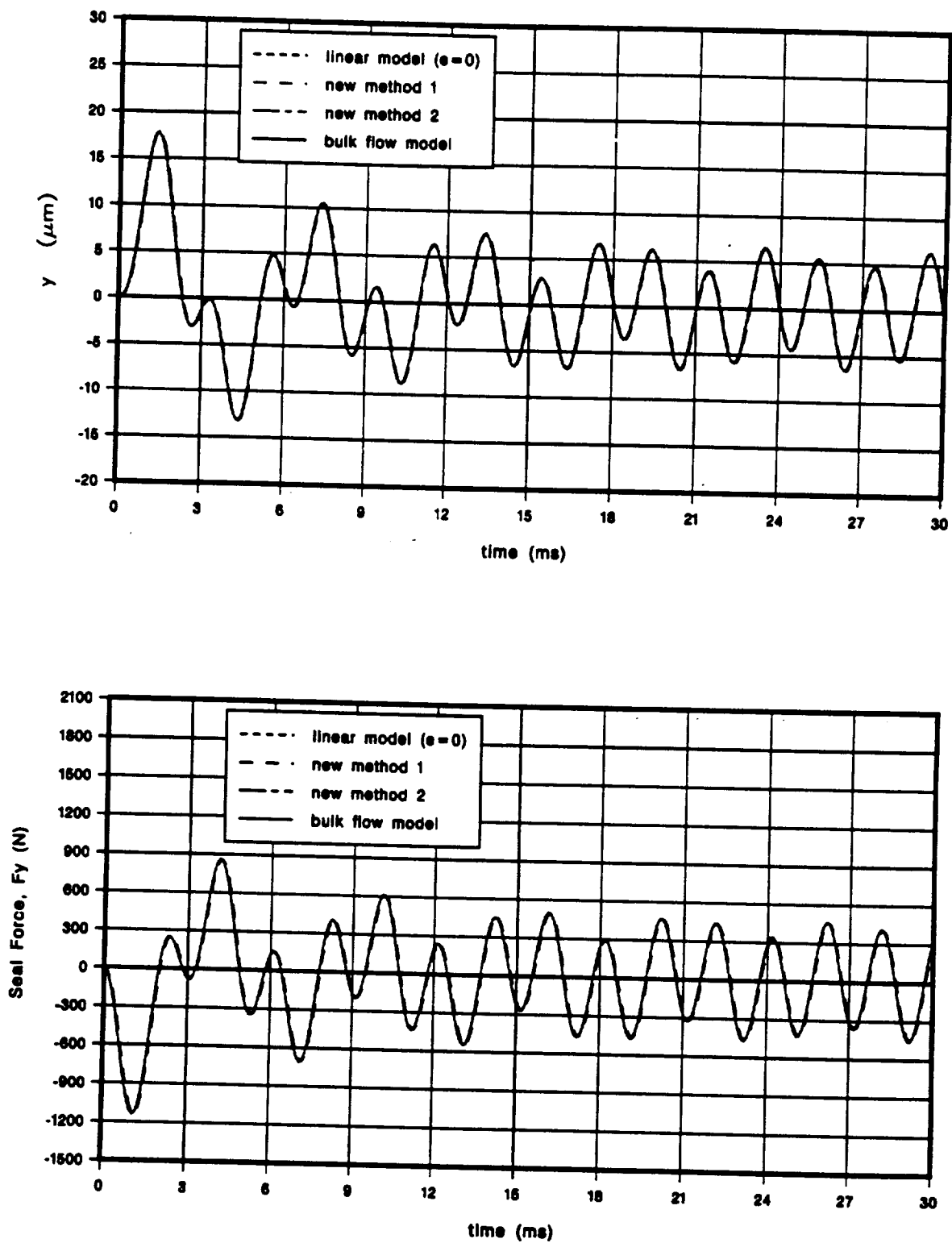


Figure 10.10 High Frequency Load, 2225N (500lb) at 500Hz, Disp. (y), Seal Force (F_y)

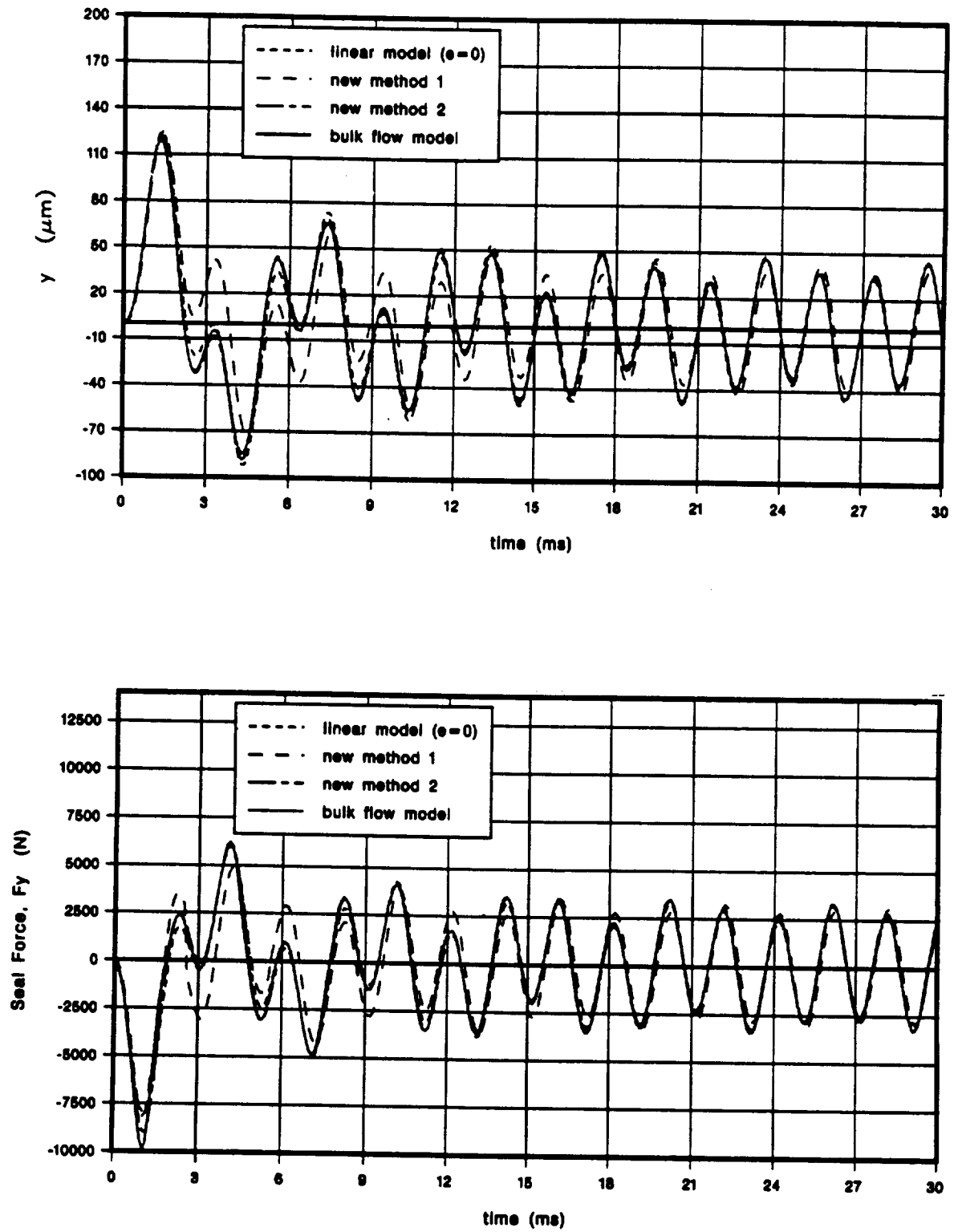


Figure 10.11 High Frequency Load, 15570N (3500lb) at 500Hz, Disp. (y), Force (F_y)

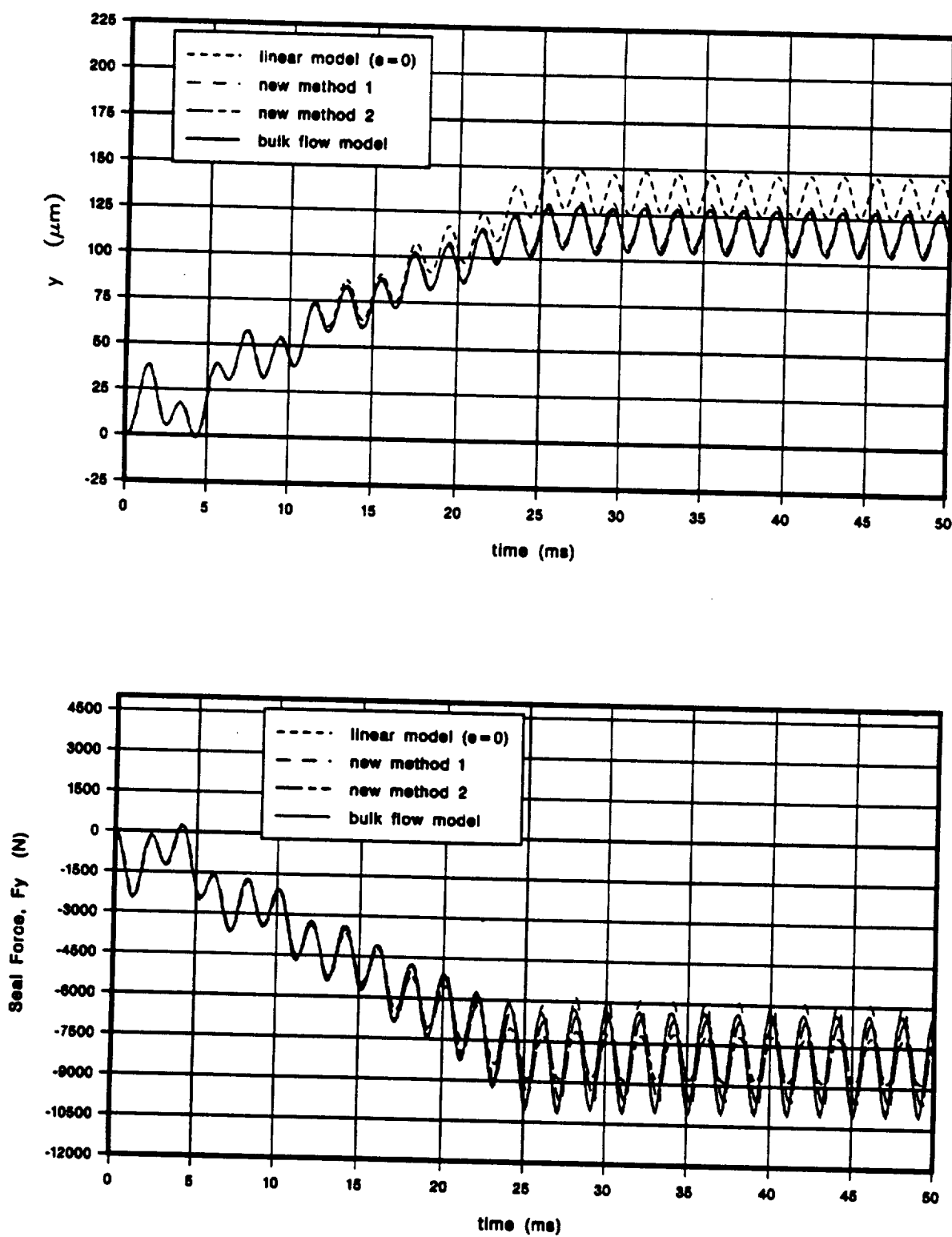


Figure 10.12 High Frequency Load (eccentric), 4450N at 500Hz, Disp. (y), Force (F_y)

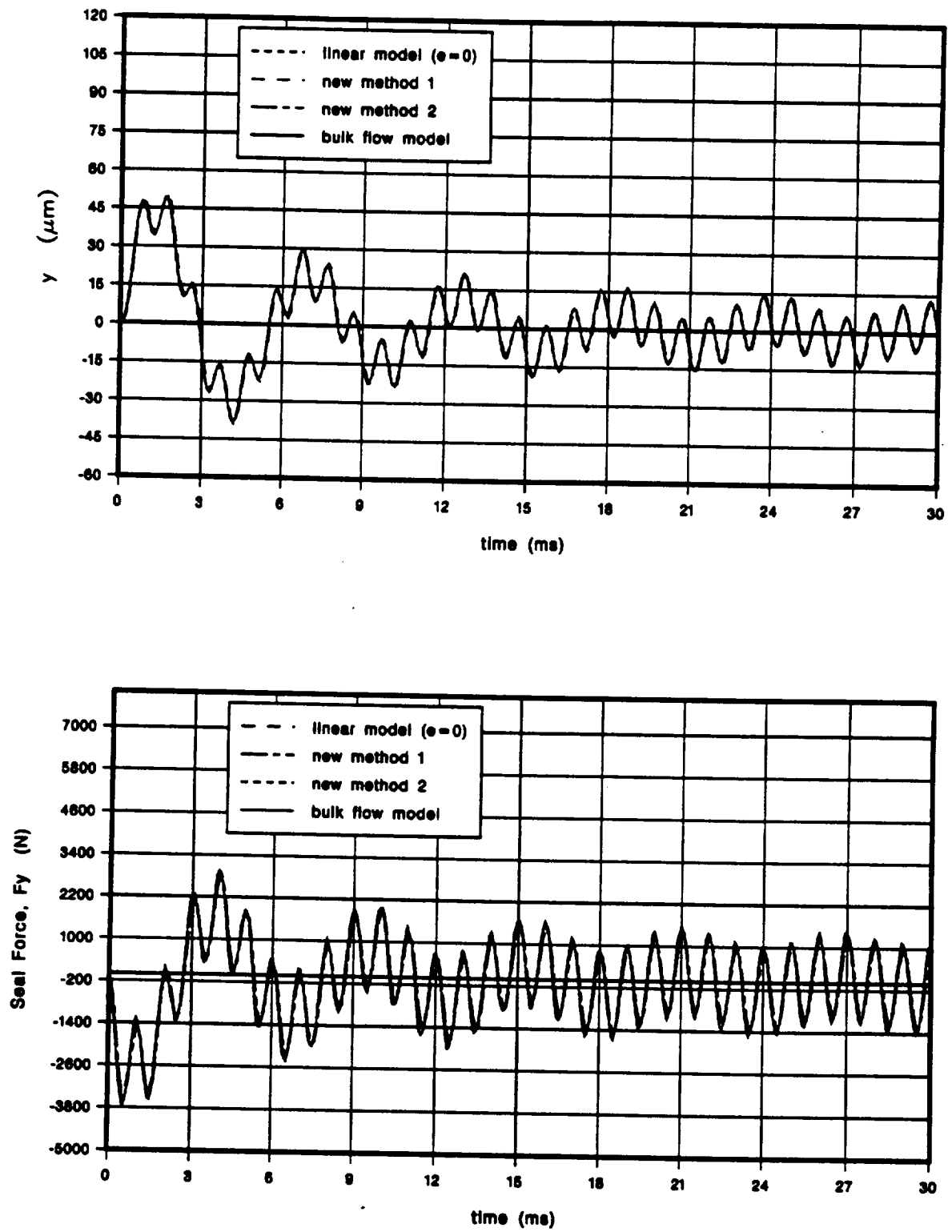


Figure 10.13 High Frequency Load, 17800N (4000lb) at 1000Hz Disp. (y), Force (F_y)

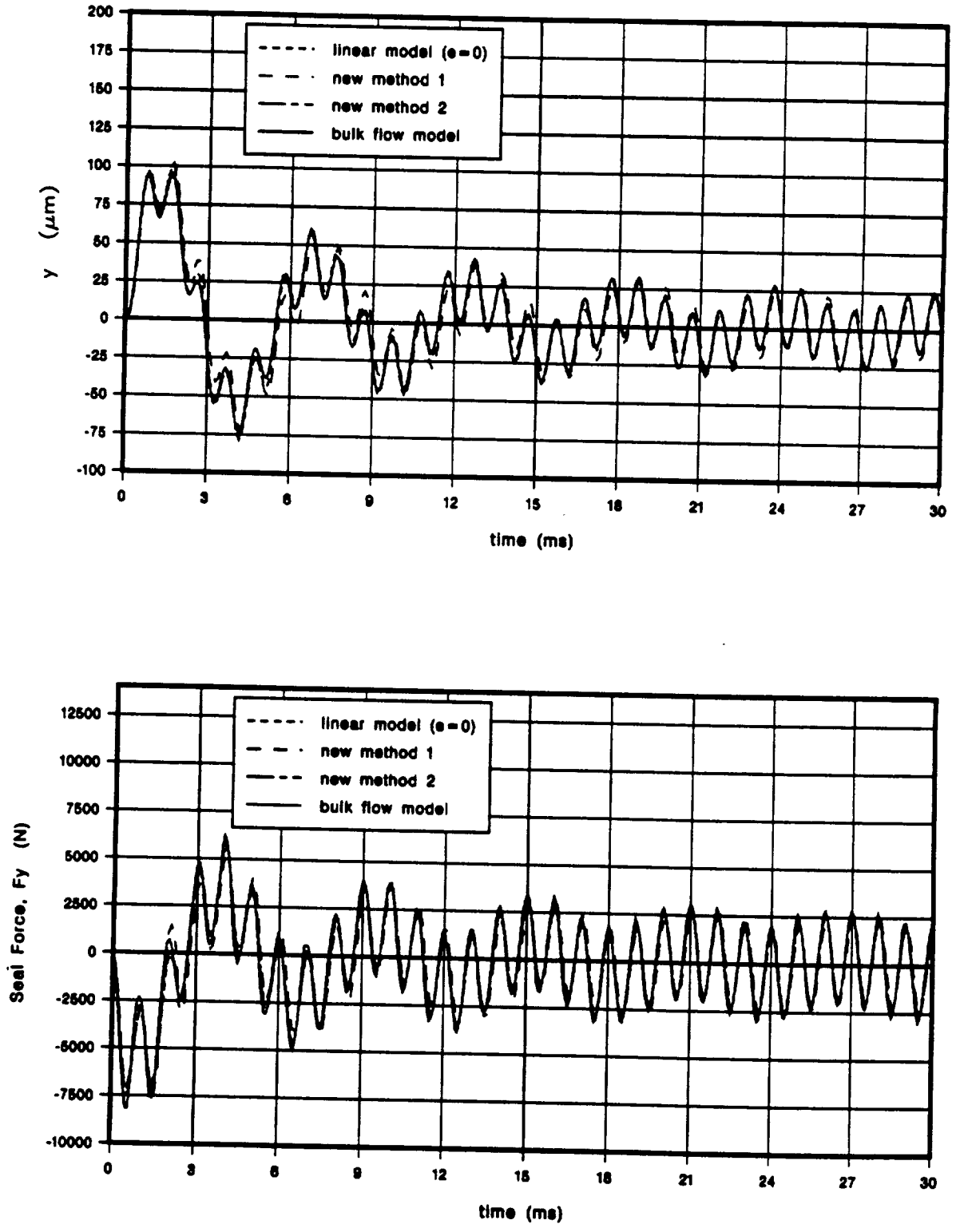


Figure 10.14 High Frequency Load, 35600N (8000lb) at 1000Hz, Disp. (y), Force (Fy)

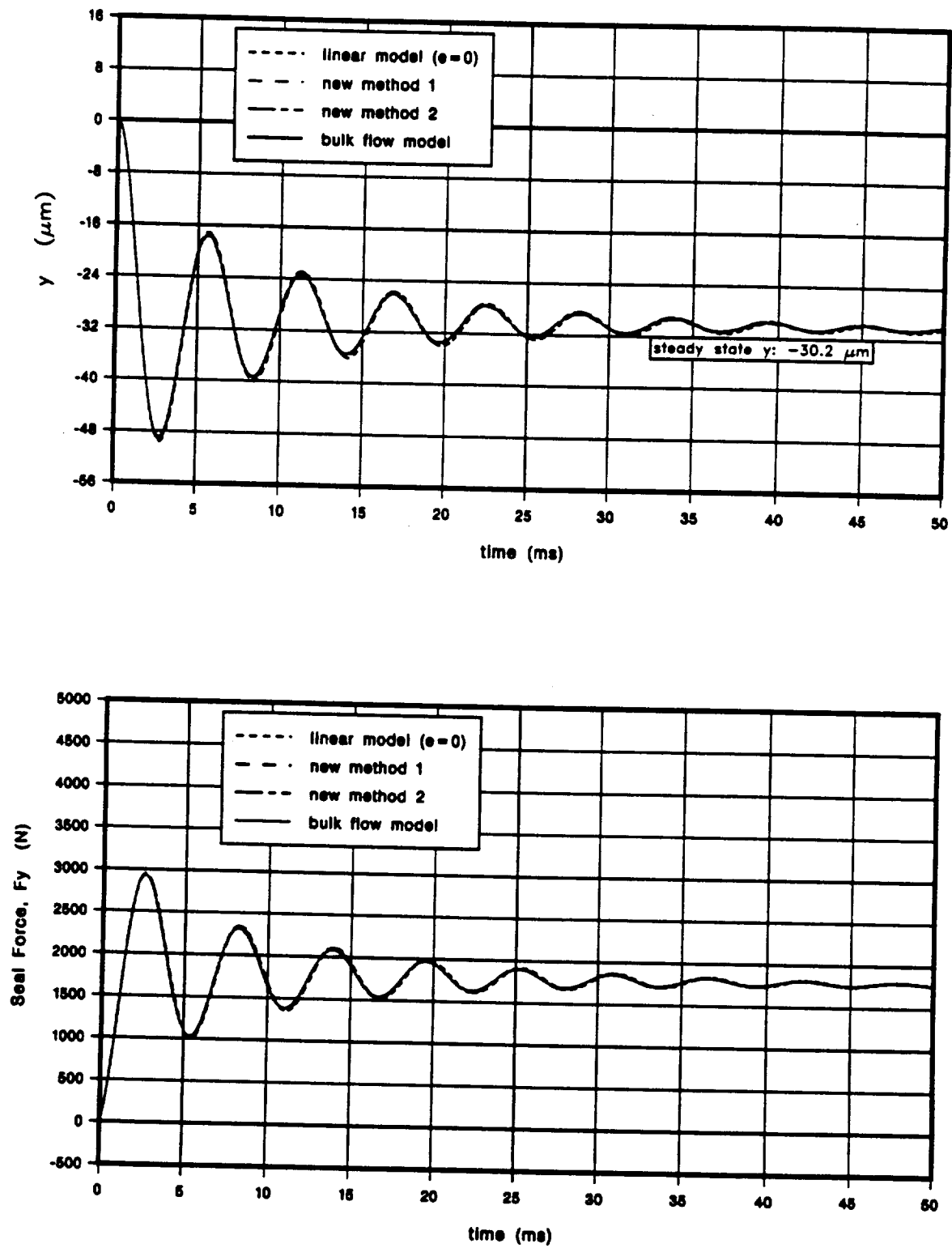


Figure 10.15 Suddenly Applied Load, 1780N (400lb), Disp. (y), seal Force (F_y)

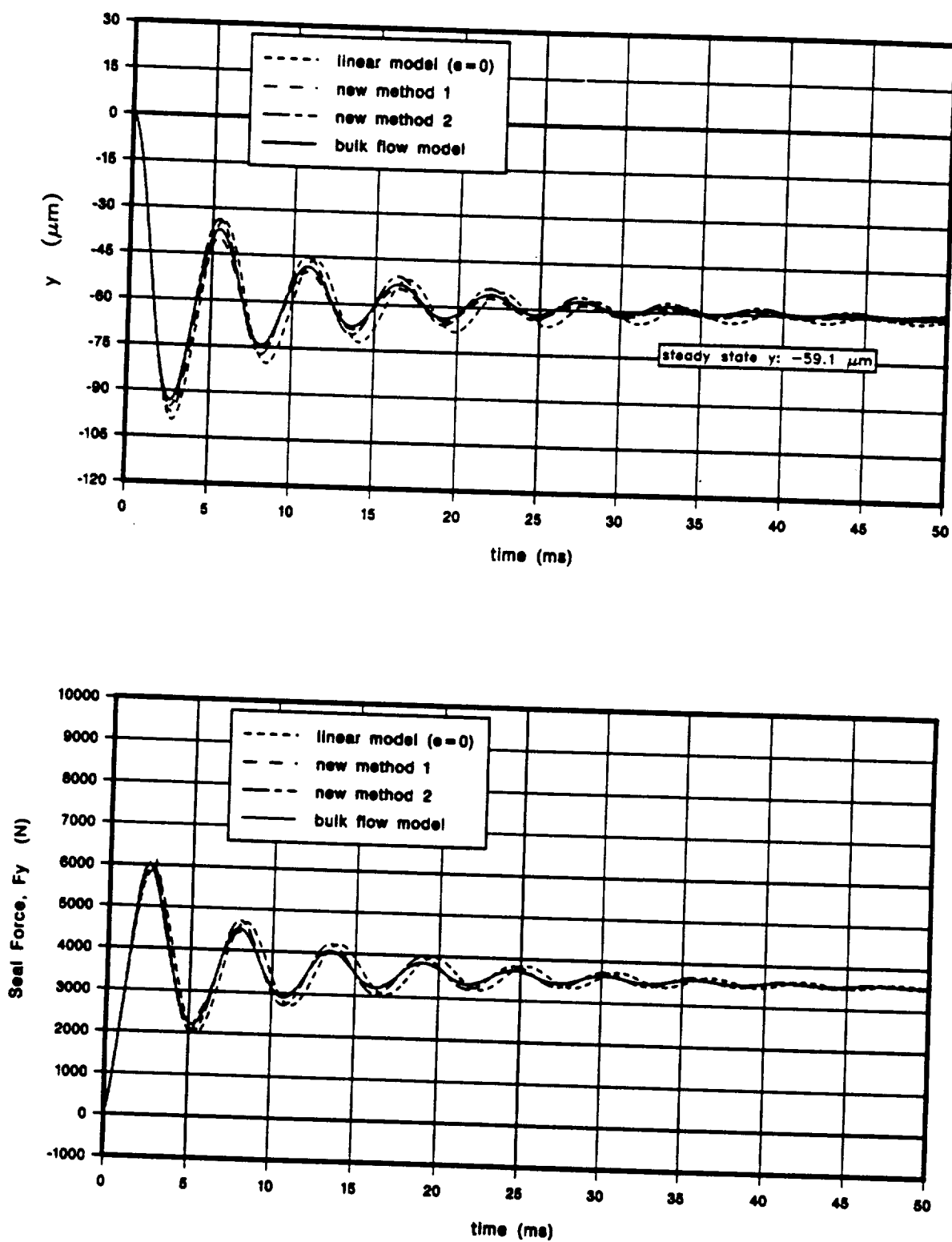


Figure 10.16 Suddenly Applied Load, 3560N (800lb), Disp. (y), Seal Force (F_y)

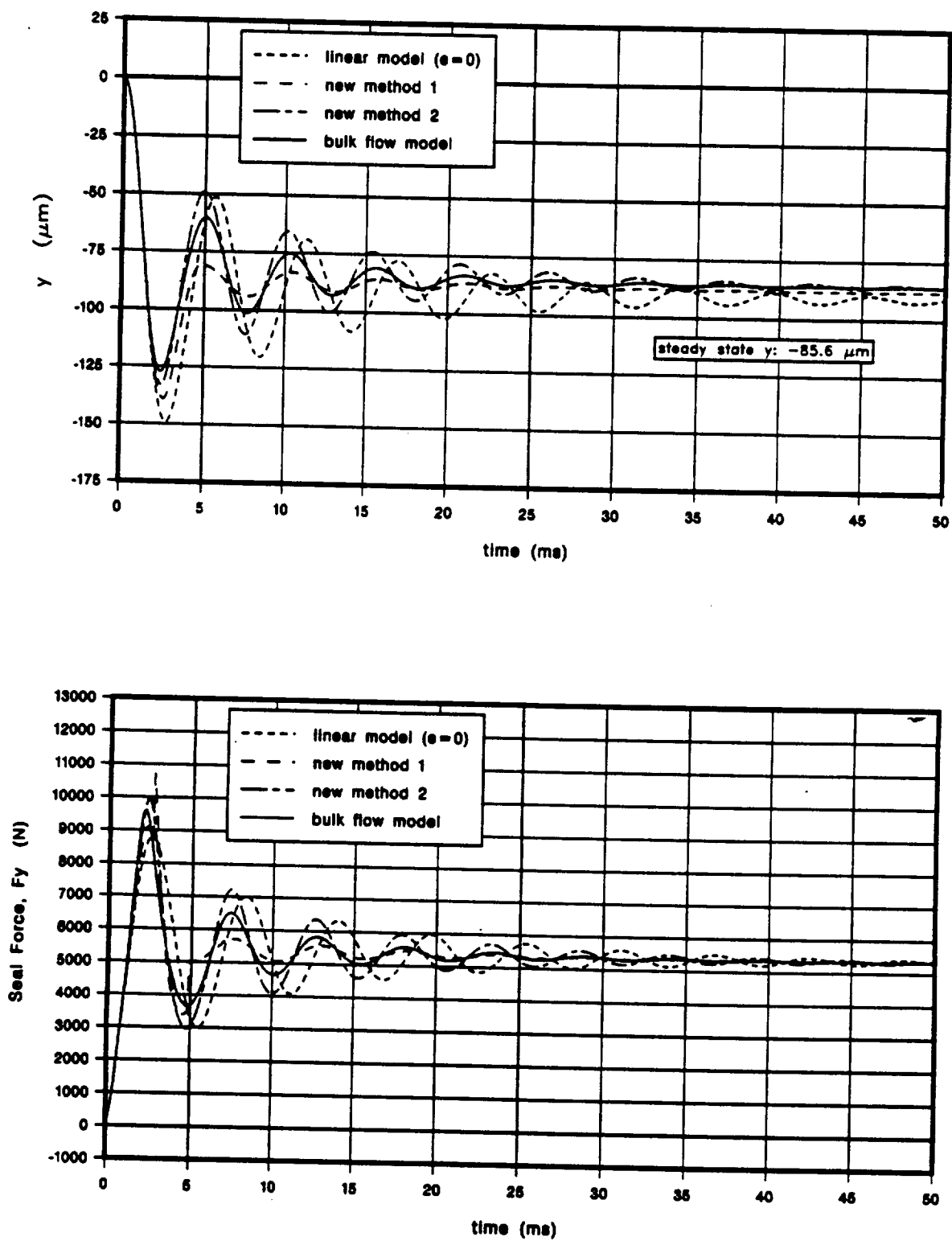


Figure 10.17 Suddenly Applied Load, 5340N (1200lb), Disp. (y), Seal Force (F_y)

10.5 Impulse Loads (Impulse Function)

This form of excitation occurs over a very short period of time. Let t_d be the time of force duration and t_n the time period of the system. If $t_d \ll t_n$ then the applied force is classified as an impulse or shock load. Impulse is a force applied over a short period of time and is defined as,

$$I = \int_0^{t_d} f(t) dt \quad (10.9)$$

where $f(t)$ is the forcing function and I is the impulse. The units of impulse are N-s or N-ms. As long as $t_d \ll t_n$, the form of $f(t)$ is not important.

The effect of an impulse on a mass-spring system is to give the mass an initial velocity given by,

$$\dot{x}(0) = \frac{I}{m} \quad (10.10)$$

and an initial displacement of zero.

$$x(0) = 0 \quad (10.11)$$

where m is mass of the system.

In this example case, impulse loads of 2225N-ms (500lb-ms), 4450N-ms (1000lb-ms) and (1800lb-ms) are applied at time $t = 0.025s$ and the motion studied. An impulse of 2250N-ms (500 lb-ms) refers to an impulse function of a load of 2225N(500lb) acting over a period of 1 ms. Of all the types of loading considered so far, this type of load results in maximum overshoot and generally a very rapid varying motion. The results for this case are shown in Figures. 10.18–10.21.

For motion at an eccentricity, the following forcing function is used. with $F_c =$

1500lb and $I = 500\text{lb-ms}$.

$$\begin{aligned}
 F_y(t) &= (40t)F_c \quad (0 < t \leq 0.025s) \\
 &= F_c + I\delta(t - 0.50) \quad (t > 0.025s) \\
 F_x(t) &= 0
 \end{aligned} \tag{10.12}$$

It is interesting to note that the transient motion predicted by linear model ($\epsilon = 0$) in Figure 10.21 is almost 180° out of phase with the actual motion.

10.6 Combination Loads

For the final simulation exercise, all the different loads considered in the previous simulations are applied simultaneously. The forcing function for this case is given below.

$$\begin{aligned}
 F_y(t) &= (40t)F_c + F_s \sin(2\pi ft) \quad (0 < t < 0.025s) \\
 &= F_c + F_s \sin(2\pi ft) + I\delta(t - 0.03) + I\delta(t - 0.038) \quad (0.025 < t < 0.05s) \\
 F_x(t) &= 0
 \end{aligned} \tag{10.13}$$

where

$$F_c = 1300 \text{ lb}$$

$$F_s = 1000 \text{ lb}$$

$$f = 500 \text{ Hz}$$

$$I = 500 \text{ lb-ms}$$

and the impulse is applied at $t = 0.03s$ and $0.038s$.

The results for this case are shown in Figure 10.22.

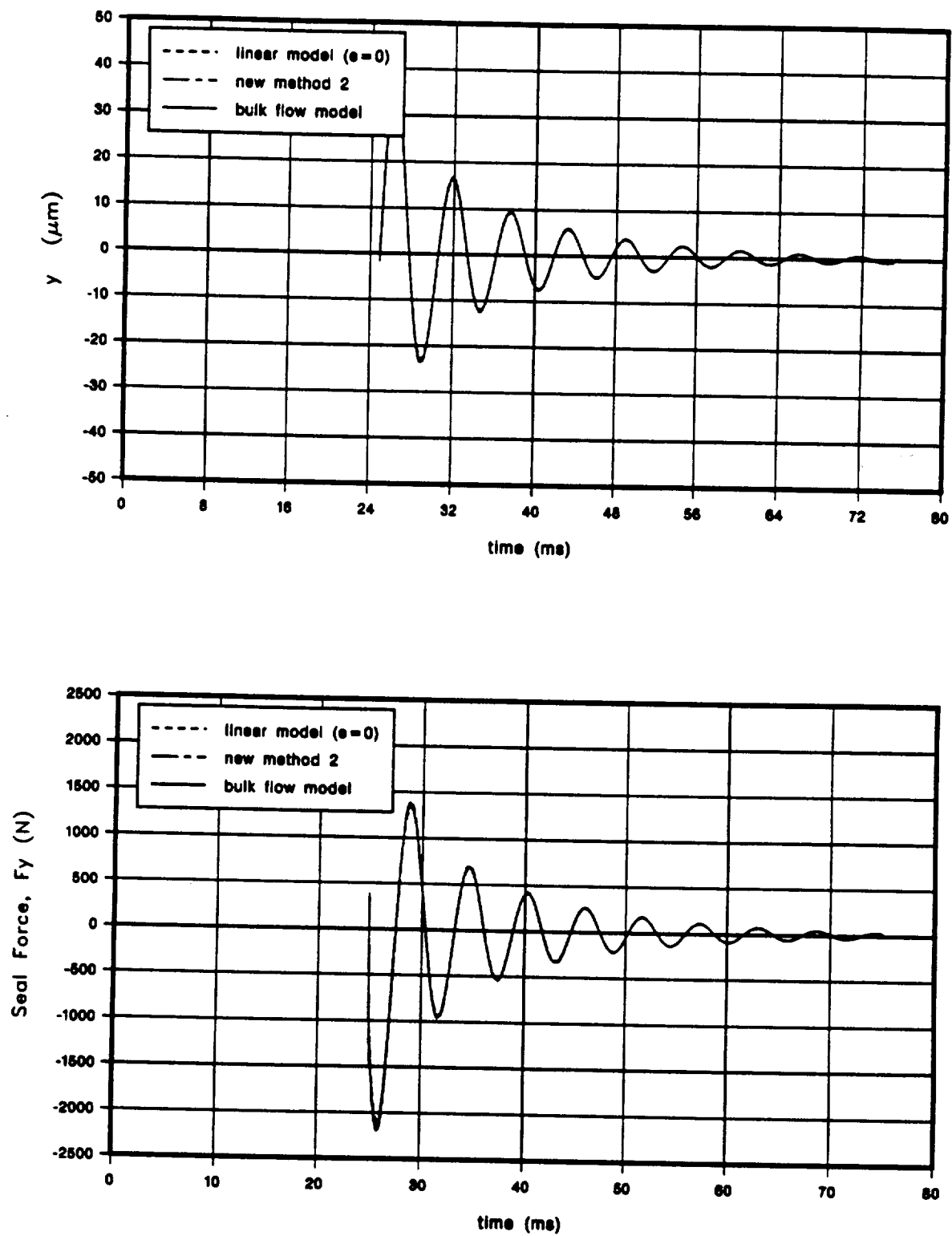


Figure 10.18 Impulse Load, 2225N-ms (500lb-ms), Disp. (y), Seal Force (F_y)

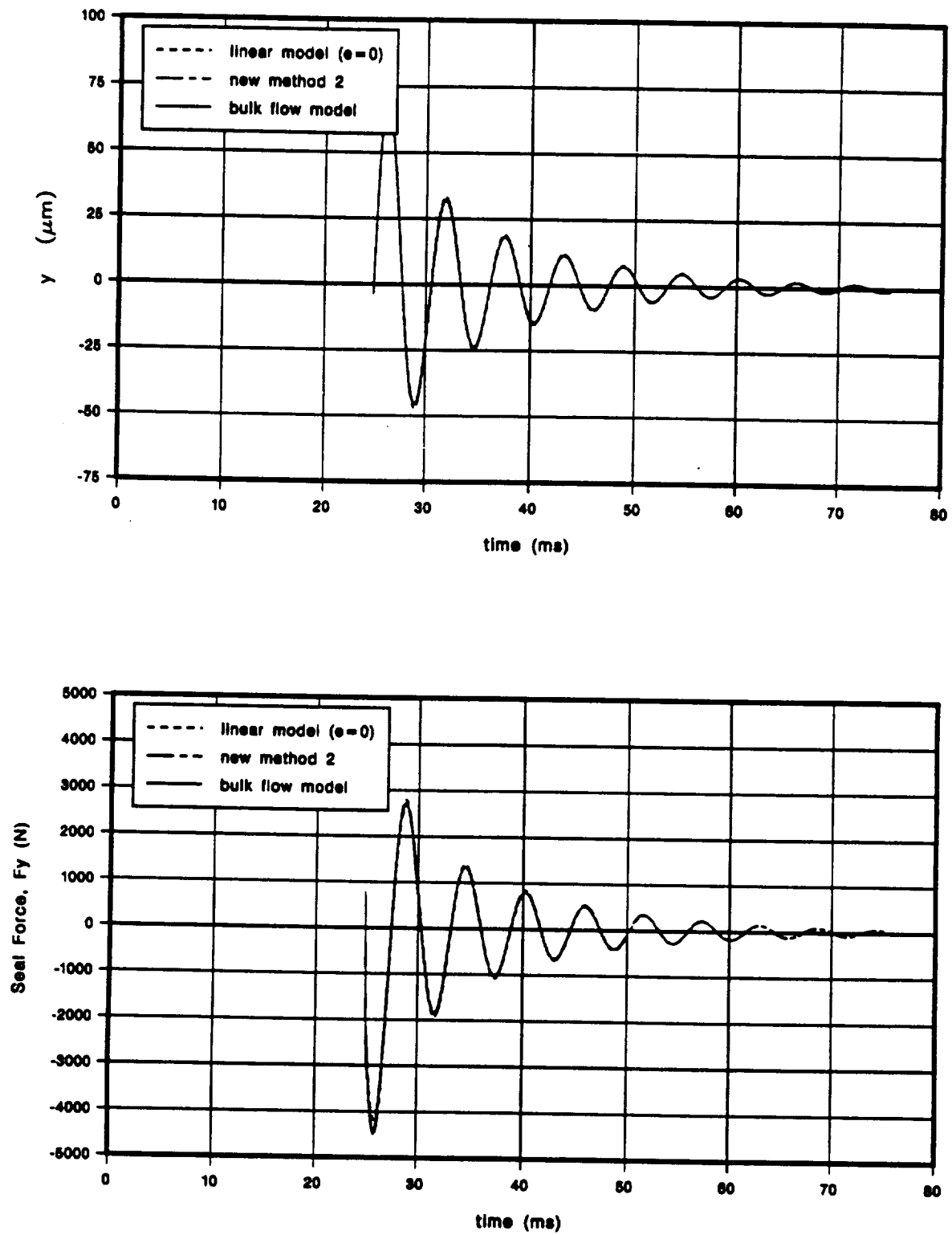


Figure 10.19 Impulse Load, 4450N-ms (1000lb-ms), Disp. (y), Seal Force (F_y)

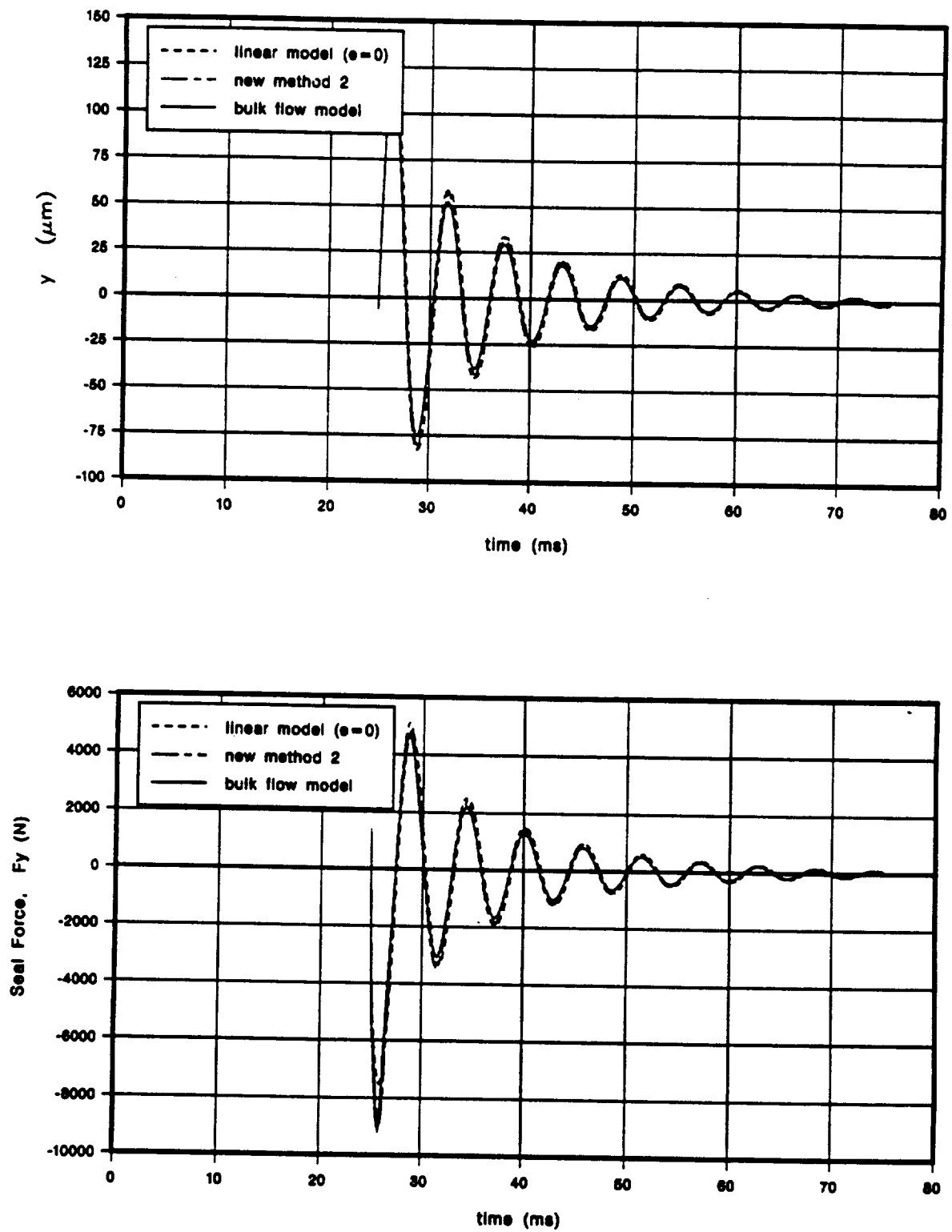


Figure 10.20 Impulse Load, 8000N-ms (1800lb-ms), Disp. (y), Seal Force (F_y)

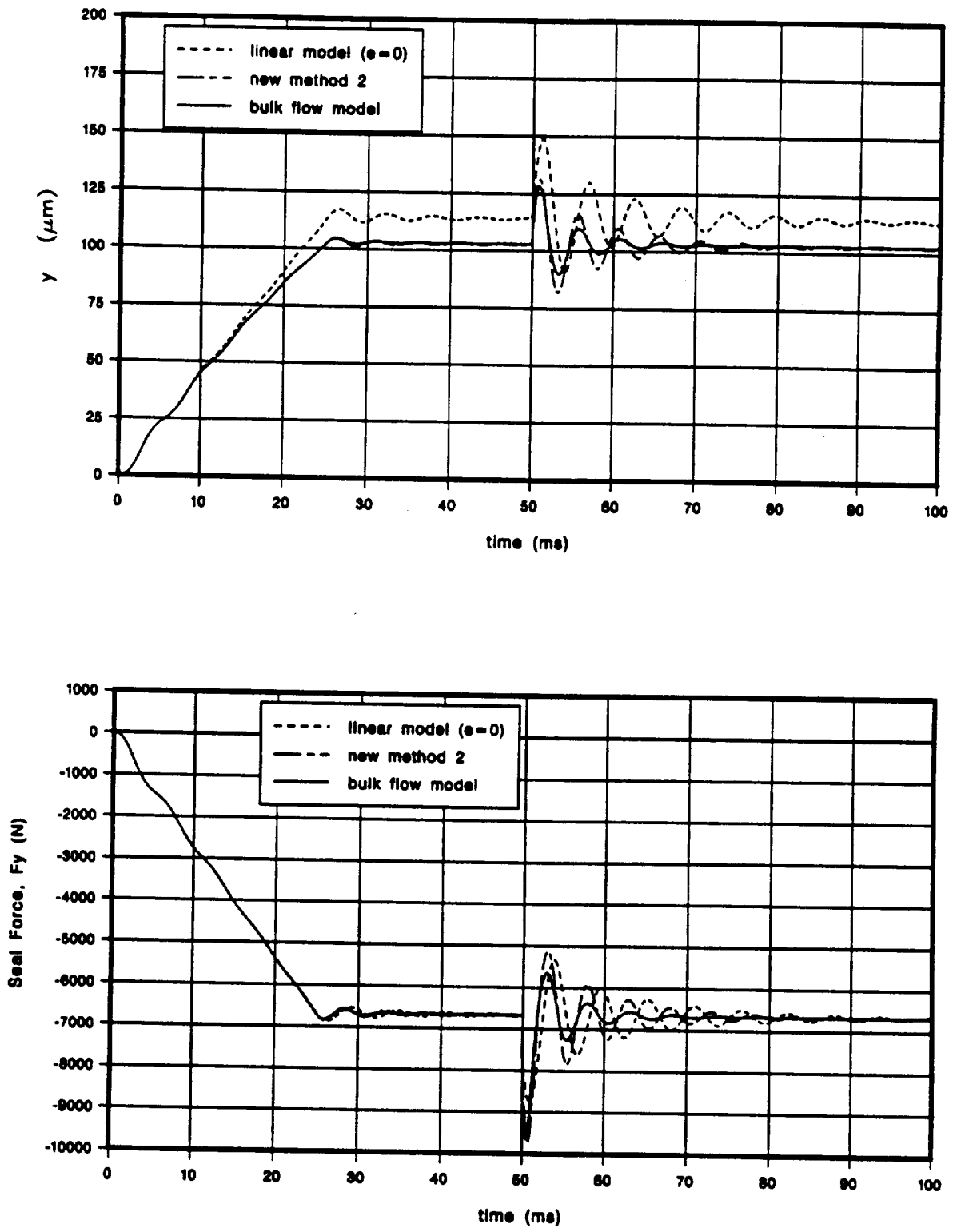


Figure 10.21 Impulse Load (eccentric), 2225N-ms (500lb-ms), Disp. (y), Force (F_y)

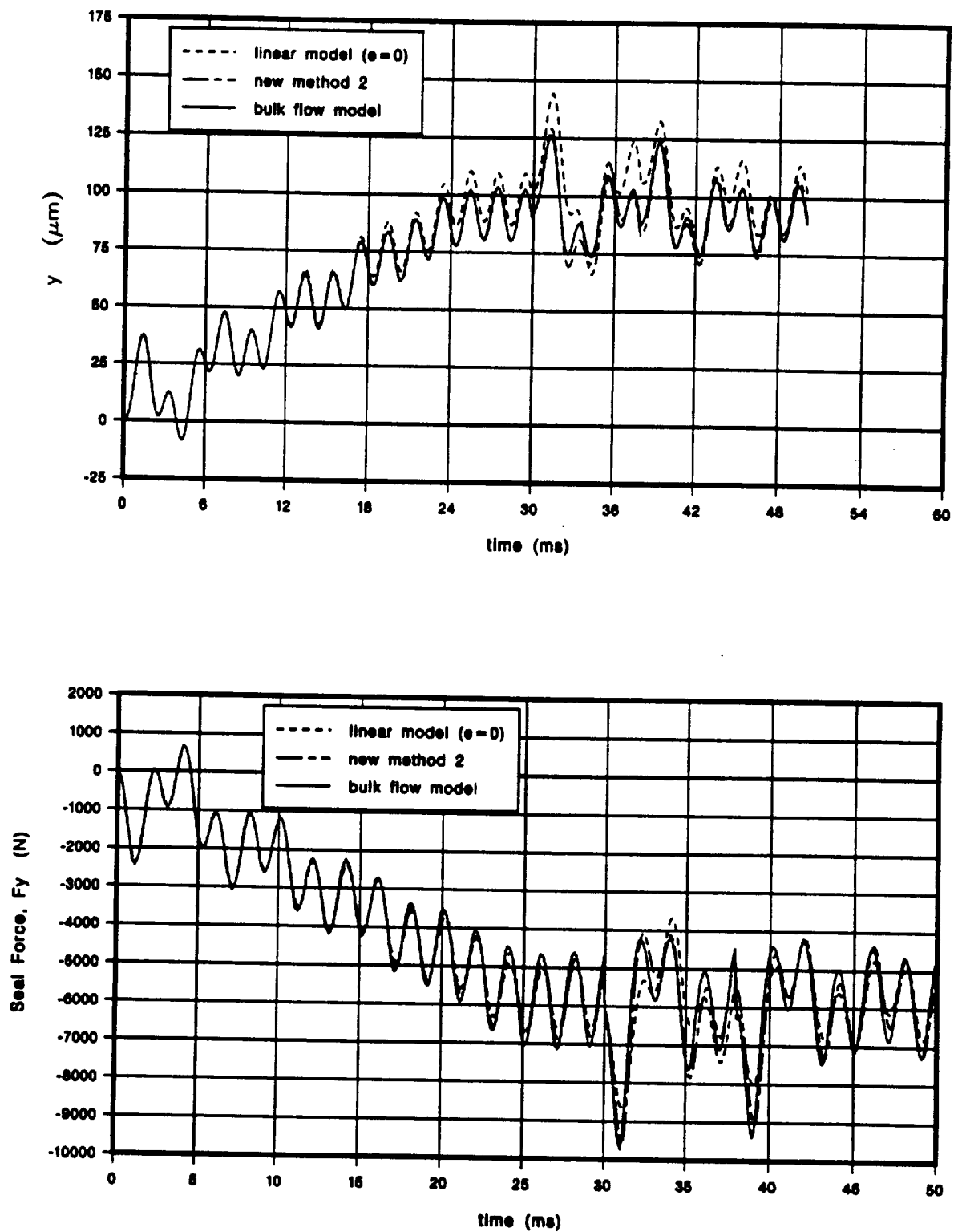


Figure 10.22 Combination Loads, Disp. (y), Seal Force (F_y)

10.7 Comparison between Bulk Flow Model and Linear Model ($\epsilon = 0$)

In Chapter VII, *large eccentric motion* of the rotor has been classified into the following two types.

1. Motion with a large amplitude about a static operating point, such as oscillation about the centered position.
2. A similar motion, but with center of the rotor moving in an arbitrary fashion away from the center of the seal.

The results from this study confirm the following general observations for *large eccentric motion*.

1. Linear model ($\epsilon = 0$) gives good results as long the the rotor vibrates about a static operating point, in this case the centered position, and the set of dynamic coefficients used in the model correspond to this point. For this type of motion, this model is accurate even for relatively large displacements ($\epsilon > 0.4$) and the seal behaves like a linear element.
2. As this operating point moves away from the centered position, the results start deviating from the actual model and these deviations get bigger as the eccentricity increases, i.e. for $\epsilon > 0.4$.

10.8 Comparison between Bulk Flow Model and New Method

The new method-1 and new method-2 give almost similar results for motion with *smoothly* varying displacement, velocity and acceleration profiles. For this type of motion the summation technique of new method-1 works well. However, for motion with rapidly varying displacement and velocity profiles with abrupt changes in function values (sharp peaks and valleys) the summation or integration process encounters

problems in some cases. An example of this case is given in Figure 10.23. In this simulation, an impulse of 1800lb-ms is applied to the rotor and due to the sudden change in velocity and acceleration i.e., discontinuities in the motion, the results are not accurate. Also, for new method-1 the time step Δt is critical for accurate evaluation of the integrals in Eqs. (8.47–8.58) using summation method. The effect of time step on the accuracy of this method is shown in Figure 10.24. The first case with a fine time step gives exact results. The second case with a coarse time step results in an erroneous simulation.

However, new method-2 is impervious to such problems as integration is carried out only with respect to displacement and total fluid force is computed at each time step.

The following observations may be made about these two approaches.

1. The results show virtually no difference between new method-1 and new method-2, indicating that past motion has practically no effect on the current state of motion for the bulk flow model used.
2. These two methods vastly simplify the computational procedure compared to the bulk flow model

10.9 Conclusions

This work examines the differences between the linear model ($\epsilon = 0$) and the actual bulk flow model for large eccentric motion of the rotor. This study confirms considerable deviations between the two models as the rotor is moved to a large eccentric position away from the center of the seal.

An innovative method to model the seal forces more accurately than the current model is developed and tested extensively for various types of transient motion.

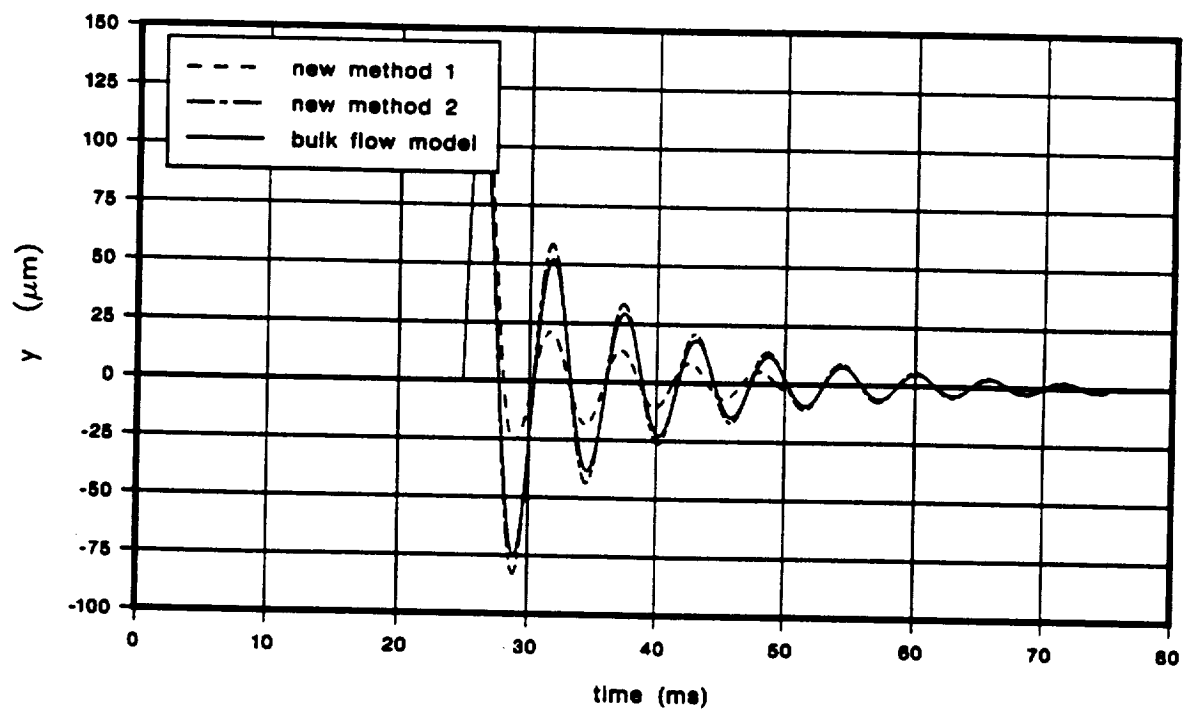


Figure 10.23 Limitations of Method-I: Discontinuities in Integrals

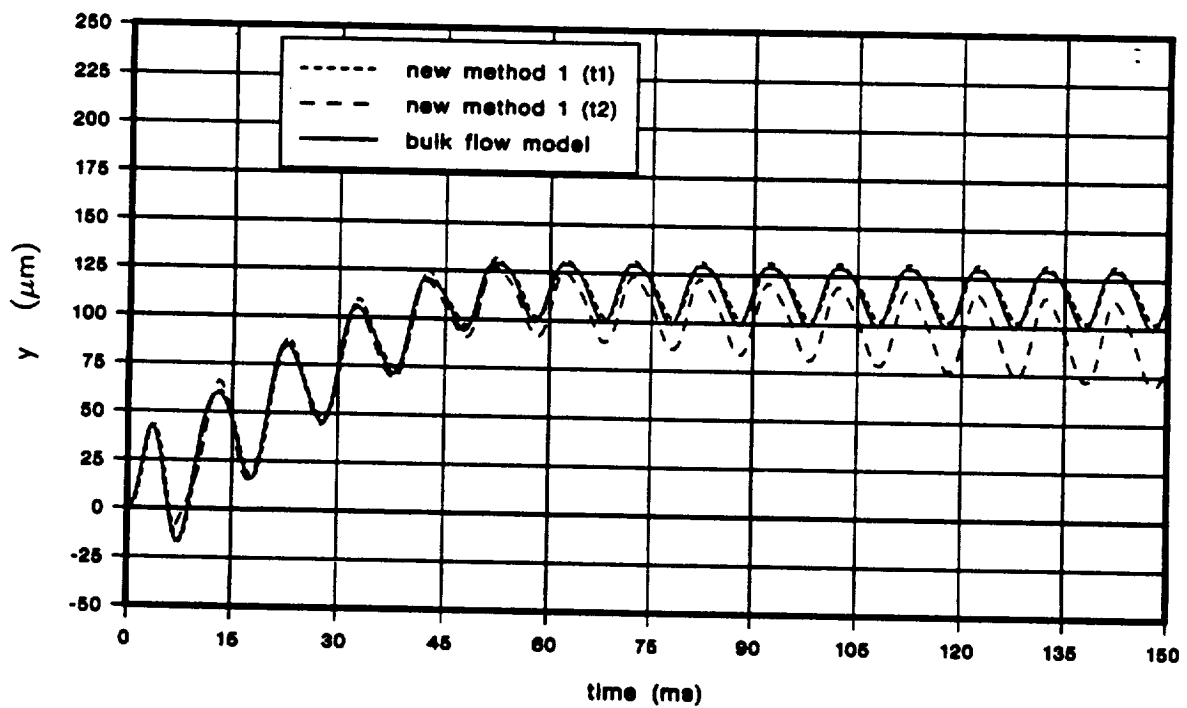


Figure 10.24 Limitations of Method-I: Dependence on Δt

The following tasks are accomplished in this study.

1. Developed transient analysis capability using the original bulk flow governing equations.
2. Established the validity of the transient analysis procedure by comparing the transient analysis results with the steady state results values obtained from *TAMUSEAL-III*.
3. Established equivalence between linearized coefficients based transient motion and the same motion as predicted by the original governing equations.
4. The linear model ($\epsilon = 0$) gives good results as long as the rotor vibrates about the centered position or a fixed static operating point (with corresponding set of dynamic coefficients). This model is valid even for relatively large displacements about this point. For this type of motion, the seal almost acts like a *linear* element.
5. However, if the rotor operating position moves away from the centered position such as in a transient motion, the results show appreciable differences between the linear model currently in use and the actual bulk flow model for eccentricity ratios above 0.4, the point at which the linear model ($\epsilon = 0$) starts deviating from the actual model, and there exists a need for a more accurate model in this region.
6. Developed a new method and tested it for various types of transient motion. This method is valid for any type of motion including motion at large eccentricities.

7. For the bulk flow model , fluid inertia forces are not significant even at very high frequencies.

CHAPTER XI

SEAL CODES

To implement the analysis developed in earlier chapters, a series of codes were written as a part of this research. All the following codes are currently being used at NASA Marshall Space Flight Center as primary tools of seal analysis and design of the interstage seals of SSME-ATD-HPOTP. Brief details of these various codes are given below.

11.1 Tamuseal-I

- Concentric seal analysis.
- Original Nelson and Nguyen model.
- Straight, tapered and axially varying profiles.
- Moody's and Hirs' friction models.
- Constant properties.
- Very good agreement with check cases.
- Runs on UNIX based workstation, VAX.

11.2 Tamuseal-II

- Eccentric seal analysis
- Constant properties.
- Improved dynamic analysis.

- Moody's and Hirs' friction model.
- Arbitrary profile, axial and circumferential.
- Distorted seal profile analysis.
- External load and eccentricity based analysis.
- Efficient and better mathematical algorithms.
- Good agreement with check cases.
- Runs on UNIX based workstation, VAX, and CRAY.

11.3 Tamuseal-III

- Eccentric seal analysis.
- Constant properties.
- Variable properties from NIST12 (LOX and LH2)
- Improved dynamic analysis.
- Moody's and Hirs' friction model.
- Arbitrary profile, axial and circumferential.
- Distorted profile analysis.
- External load and eccentricity based analysis.
- Efficient mathematical algorithms.
- Good agreement with check cases.
- Runs on UNIX based workstation, VAX, and CRAY.

11.4 Tamuseal-IV

- Eccentric seal analysis.
- Constant properties.
- Variable properties.
- Thermal Effects with variable fluid properties.
- Improved dynamic analysis.
- Moody's and Hirs' friction model.
- Arbitrary profile, axial and circumferential.
- Distorted profile analysis.
- External load and eccentricity based analysis.
- Efficient and better mathematical algorithms.
- Very good agreement with check cases.
- Runs on UNIX based workstation, VAX, and CRAY.

11.5 Transeal

This is the code developed for the study of transient analysis with an annular seal. It has the ability to do the following simulations. Given time dependent displacement, velocity and acceleration of the center of the rotor, the code computes the transient seal forces as a function of time using one of the following four models.

- Original bulk flow governing equations.

- Linear seal model ($\epsilon = 0$) with dynamic coefficients computed at zero eccentricity.
- Using New Method-I.
- Using New Method-II.

CHAPTER XII

CONCLUSIONS

In this work, a new dynamic analysis for liquid annular seals with arbitrary profile is developed based on a method originally proposed by Nelson and Nguyen. The following modifications are made to improve the original method.

1. Improved zeroth order solution based on cubic splines versus FFT method of Nelson and Nguyen. The improved method shows better convergence at higher eccentricities and yields solution for cases where the original method had failed.
2. A more exact first order solution based on continuous interpolation of first order variables. A new set of equations are derived for dynamic analysis.

The analysis developed is extended for cryogenic seals for the following models.

1. Constant fluid properties.
2. Variable fluid properties.
3. Thermal effects (energy equation) with variable fluid properties (concentric case).

A unified solution procedure that is valid for both Moody's friction model and Hirs' friction model is developed. Dynamic coefficients based on external load specification are introduced for seals for the first time. The analysis can be used to model seals which support a pre-load.

Arbitrary profile seals are discussed with reference to an elliptical seal. Unique differences that exist between regular straight or tapered circular cross-section seals and arbitrary profile seals with a circumferentially varying clearance are analyzed.

A study on the effect of orientation of minimum film thickness system on computed dynamic coefficients is conducted. A general distorted interstage seal of SSME-ATD-HPOTP is analyzed as an arbitrary profile seal and the results are compared to an average clearances profile seal.

The predictions of current analysis are compared with a number of experimental and theoretical cases from seal literature. Based on the comparative studies the following conclusions are drawn.

1. Good comparison with original Nelson and Nguyen method (1988a,1988b). Better results for cases where the original method had failed.
2. Good comparison with Childs' (1985) Hir's and Moody's friction model based analyses.
3. Good comparison with Scharrer and Nelson (1990), except for a discrepancy noted in their results.
4. The deviation between current analysis (variable properties) and San Andres' analysis increase with eccentricity. These differences vary from case to case.
5. The difference between current analysis (thermal effects with variable properties) and San Andres agree well for the concentric case, except for cross coupled stiffness.

The work on transient analysis with an annular seal examined the differences between linearized coefficients based motion and the actual motion based on bulk flow governing equations. This study confirms considerable deviations between the two models as the rotor is forced to an eccentric position of $\epsilon > 0.4$.

Based on this study an equivalence is established between linearized coefficients based motion and the same motion based on bulk flow governing equations for small

motion. This study may be used to compare the accuracy of solution (dynamic coefficients) of a particular dynamic analysis.

An innovative method to model non-linearities in seal forces is developed. This method models seal forces more accurately than the model based on a single set of dynamic coefficients. This method is tested extensively for various types of transient motion.

The following conclusions are drawn from this study.

1. Linear model ($\epsilon = 0$) gives good results as long as the rotor vibrates about the centered position or a fixed static operating point (with corresponding set of dynamic coefficients). This model is valid even for relatively large displacements about this point. For this type of motion, the seal almost acts like a *linear* element.
2. However, if the rotor operating position moves away from the centered position such as in a transient motion, the results show appreciable differences between the above linear model and the actual bulk flow model, for eccentricity ratios above 0.4. This is roughly the cutoff point where the linear model starts deviating from the bulk flow model. and there exists a need for a more accurate model in this region.

12.1 Future Work

One of the areas of improvement for the bulk flow model is the treatment of entrance and exit loss coefficients. Typically, in a seal analysis these coefficients are treated as constants. It is an accepted fact that these loss coefficients vary with the inlet and exit geometries and Reynolds number. A more realistic model for this loss coefficient would be a varying coefficient around the inlet and exit circumferences.

The other area of improvement for high pressure seals is the inclusion of elastic deformation of the seal housing. Some preliminary studies (Iwatsubo, 1987) have already been done in this area. Future work should combine all these various analyses into a combined thermoelastic-hydrodynamic (TEHD) analysis.

REFERENCES

- Allaire, P.E., Gunter, E.J., Lee, C.P., and Barrett, L.E., 1978, "The Dynamic Analysis of the Space Shuttle Main Engine-High Pressure Fuel Turbopump Interstage Annular Seals," University of Virginia, Charlottesville, VA, Report No. UVA/528140/ME76/103.
- Black, H.F., 1969, "Effects of Hydraulic Forces in Annular Pressure Seals on the Vibrations of Centrifugal Pump Rotors," *Journal of Mechanical Engineering Science*, Vol. II, pp. 206-213.
- Black, H.F., and Jenssen, D.N., 1970, "Dynamic Hybrid Bearing Characteristics of Annular-Controlled Leakage Seals," *Institute of Mechanical Engineers*, Vol. 184, pp. 92-100.
- Childs, D.W., 1983a, "Dynamic Analysis of Turbulent Annular Seals Based on Hirs Lubrication Equations," *ASME Journal of Lubrication Technology*, Vol. 105, pp. 429-436.
- Childs, D.W., 1983b, "Finite-Length Solutions for Rotordynamic Coefficients of Turbulent Annular Seals," *ASME Journal of Lubrication Technology*, Vol. 105, pp. 437-444.
- Childs, D.W., 1984, "Finite-Length Solutions for the Rotordynamic Coefficients of Constant Clearance and Convergent-Tapered Annular Seals," Third International Conference on Vibrations and Rotating Machinery, Sep. 1-12, University of York, York, England, pp. 120-126.
- Childs, D.W., and Kim, C.H., 1985, "Analysis and Testing for Rotordynamic Coefficients of Turbulent Annular Seals with Different Directionally Homogeneous

- Surface Roughness Treatment for Rotor and Stator Elements," *ASME Journal of Tribology*, Vol. 107, pp. 296-306.
- Childs, D.W., 1987, "Fluid-Structure Interaction Forces at Pump Impeller Shroud Surfaces for Rotordynamic Calculations," *Rotating Machinery Dynamics*, ASME, Vol 2, pp. 581-504.
- Falco, M., Mimmi, G., Pizzigoni, B., Marengo, G., and Negri, G., 1984, "Plain Seal Dynamic Behaviour - Experimental and Analytical Results," Third International Conference on Vibrations in Rotating Machinery, Sep. 11-13, University of York, York, pp. 151-158.
- Falco, M., Mimmi, G., and Marengo, G., 1986, "Effects of Seals on Rotor Dynamics," Proceedings of the International Conference on Rotordynamics, Sep. 1-4, Tokyo, Japan, pp 102-106.
- Hirs, G.G., 1973, "A Bulk-Flow Theory for Turbulence in Lubricating Films," *ASME Journal of Lubrication Technology*, Vol. 105, pp. 137-146.
- Iwatsubo, T., Yang, B.S., 1987, "The Effects of Elastic Deformation on Seal Dynamics," The 1987 ASME Design Technology Conferences - 11th Biennial Conference on Mechanical Vibration and Noise, Sep. 27-30, Boston, MA, pp. 435-440.
- Kanki, H., and Kawakami, T., 1984, "Experimental Study on the Dynamic Characteristics of Pump Annular Seals," Third International Conference on Vibrations in Rotating Machinery, University of York, England, pp. 159-166.
- Launder, B.E., and M. Leschziner, 1978, "Flow in Finite Width Thrust Bearings Including Inertial Effects, I-Laminar Flow, II-Turbulent Flow," *ASME Journal*

of Lubrication Technology, Vol. 100, pp.330-345.

Lindsey, W.T., 1993, "Experimental Versus Theoretical Comparison of the Effects of Taper and Static Eccentricity on the Rotordynamic Coefficients of Short, Smooth, High-Speed, Liquid Annular Seals", Master's Thesis, Texas A&M University, College Station, Texas.

McCarty, R.D., NBS Standard Reference Database 12, 1986, "Thermophysical Properties of Fluids, MIPROPS-86," Thermophysics Division, Center for Chemical Engineering, National Bureau of Standards, Boulder, Colorado.

Nelson, C.C., 1984, "Analysis for Leakage and Rotordynamic Coefficients of Surface Roughened Tapered Annular Gas Seals," *ASME Journal of Engineering for Power*, Vol. 106, No. 4, pp. 927-934.

Nelson, C.C., Nguyen, D.T., 1987, "Comparison of Hirs' Equation with Moody's Equation for Determining Rotordynamic Coefficients of Annular Pressure Seals," *ASME Journal of Tribology*, Vol. 109, pp. 144-148.

Nelson, C., Nguyen, D.T., 1988a, "Analysis of Eccentric Annular Seals: Part I - A New Solution Using Fast Fourier Transforms for Determining Hydrodynamic Force," *ASME Journal of Tribology*, Vol 110, pp. 335-360.

Nelson, C., and Nguyen, D.T., 1988b, "Analysis of Eccentric Annular Seals: Part II - Effects of Eccentricity on Rotordynamic Coefficients," *ASME Journal of Tribology*, Vol. 110, pp. 361-366.

Nguyen, D.T., 1988, "Analysis of Eccentric Annular Pressure Seals: A New Solution Procedure for Determining Reactive Force and Rotordynamic Coefficients", Ph.D. Dissertation, Texas A&M University, College Station, TX.

Patankar, S.V., "Numerical Heat Transfer and Fluid Flow," Hemisphere Publishing Corporation, New York, McGraw-Hill.

San Andres, L., 1991, "Analysis of Variable Properties Turbulent Annular Seals", *ASME Journal of Tribology*, Vol. 113, pp. 694-702.

San Andres, L., Yang, Z., Childs, D.W., 1992, "Thermal Effects in Cryogenic Liquid Annular Seals - Part II: Numerical Solution and Results," ASME/STLE Tribology Conference, San Diego, CA. Oct. 18-21. 1992.

Scharrer, J.K., and D.J. Nunez, 1989, "The SSME HPFTP Wavy Interstage Seal: I - Seal Analysis," Proceedings of the 1989 ASME Vibrations Conference, Machinery Dynamics - Applications and Vibration Control Problems, DE-Vol. 18-2.

Scharrer, J.K. and Nelson, C.C., 1990, "Rotordynamic Coefficients for Partially Tapered Annular Seals: Part I - Incompressible Flow", *ASME Journal of Tribology*, Vol. 112, pp. 404-411.

Simon, J., and Frene J., 1989, "Static and Dynamic Characteristics of Turbulent Annular Eccentric Seals: Effect of Convergent-Tapered Geometry and Variable Fluid Properties," *ASME Journal Of Tribology*, Vol. 111, pp. 378-385.

Simon, J., and Frene J., 1992, "Analysis of Incompressible Flow in Annular Pressure Seals", *ASME Journal of Tribology*, Vol 114, pp. 431-438.

von Pragenau, G.L., "Damping Seals for Turbomachinery," NASA Technical Paper 1987, March 1982.

Yang, Z., San Andres, L., Childs, D.W., 1992, "Thermal Effects in Cryogenic Liquid Annular Seals - Part I: Theory and Approximate Solution", ASME/STLE

Tribology Conference, San Diego, CA, Oct. 18-21.

APPENDIX A

CONSTANT PROPERTIES MODEL

Zeroth Order (Steady State) Equations:

$$\begin{bmatrix} \rho_0 h_0 & 0 & 0 \\ 0 & \rho_0 h_0 u_0 & 0 \\ \rho_0 h_0 u_0 & 0 & h_0 \end{bmatrix} \begin{Bmatrix} \frac{\partial u_0}{\partial z} \\ \frac{\partial v_0}{\partial z} \\ \frac{\partial p_0}{\partial z} \end{Bmatrix} = \begin{bmatrix} F_u \\ F_v \\ F_p \end{bmatrix} \quad (\text{A.1})$$

where

$$F_u = -\rho_0 u_0 \frac{\partial h_0}{\partial z} - \frac{\rho_0 v_0}{R} \frac{\partial h_0}{\partial \beta} - \frac{\rho_0 h_0}{R} \frac{\partial v_0}{\partial \beta} \quad (\text{A.2})$$

$$F_v = -\frac{\rho_0 h_0 v_0}{R} \frac{\partial v_0}{\partial \beta} - \frac{h_0}{R} \frac{\partial p_0}{\partial \beta} - \rho_0 \left\{ f_{r0} \frac{u_0}{2} \sqrt{u_0^2 + (v_0 - w)^2} + f_{s0} \frac{v_0}{2} \sqrt{u_0^2 + v_0^2} \right\} \quad (\text{A.3})$$

$$F_p = -\frac{\rho_0 h_0 v_0}{R} \frac{\partial v_0}{\partial \beta} - \rho_0 \left\{ f_{r0} \frac{(v_0 - w)}{2} \sqrt{u_0^2 + (v_0 - w)^2} + f_{s0} \frac{v_0}{2} \sqrt{u_0^2 + v_0^2} \right\} \quad (\text{A.4})$$

First Order (Perturbed) Equations: Continuity:

$$h_0 \frac{\partial u_0}{\partial z} + \frac{h_0}{R} \frac{\partial v_0}{\partial \beta} + \frac{\partial h_0}{\partial z} u_1 + \frac{1}{R} \frac{\partial h_0}{\partial \beta} v_1 = -\frac{\partial h_0}{\partial t} - u_0 \frac{\partial h_0}{\partial z} - \frac{v_0}{R} \frac{\partial h_0}{\partial \beta} - \left(\frac{\partial u}{\partial z} + \frac{1}{R} \frac{\partial v}{\partial \beta} \right) h_1 \quad (\text{A.5})$$

Axial Momentum:

$$h_0 u_0 \frac{\partial u_0}{\partial z} + \frac{h_0}{\rho_0} \frac{\partial p_0}{\partial z} + \frac{h_0 v_0}{R} \frac{\partial u_0}{\partial \beta} + h_0 \frac{\partial u_0}{\partial t} + A_u u_1 + A_v v_1 = A_h h_1 \quad (\text{A.6})$$

Circumferential Momentum:

$$h_0 u_0 \frac{\partial v_0}{\partial z} + \frac{h_0 v_0}{R} \frac{\partial v_0}{\partial \beta} + \frac{h_0}{\rho_0 R} \frac{\partial p_0}{\partial \beta} + h_0 \frac{\partial v_0}{\partial t} + B_u u_1 + B_v v_1 = B_h h_1 \quad (\text{A.7})$$

The coefficient expressions A_u, A_v etc., in the above first order equations are defined below.

$$A_u = h_0 \frac{\partial u_0}{\partial z} + u_0^2 \left(\frac{\bar{F}_{so}}{U_{so}} + \frac{\bar{F}_{ro}}{U_{ro}} \right) + (F_{so}U_{so} + F_{ro}U_{ro}) \quad (\text{A.8})$$

$$A_v = \frac{h_0}{R} \frac{\partial u_0}{\partial \beta} + u_0 \left\{ v_0 \frac{\bar{F}_{so}}{U_{so}} + (v_0 - w) \frac{\bar{F}_{ro}}{U_{ro}} \right\} \quad (\text{A.9})$$

$$A_h = -\frac{1}{\rho_0} \frac{\partial p_0}{\partial z} - u_0 \frac{\partial u_0}{\partial z} - \frac{v_0}{R} \frac{\partial v_0}{\partial \beta} + \frac{u_0}{h_0} (H_{so}U_{so} + H_{ro}U_{ro}) \quad (\text{A.10})$$

$$B_u = h_0 \frac{\partial v_0}{\partial z} + u_0 \left\{ v_0 \frac{\bar{F}_{so}}{U_{so}} + (v_0 - w) \frac{\bar{F}_{ro}}{U_{ro}} \right\} \quad (\text{A.11})$$

$$B_v = \frac{h_0}{R} \frac{\partial v_0}{\partial \beta} + v_0^2 \frac{\bar{F}_{so}}{U_{so}} + (v_0 - w)^2 \frac{\bar{F}_{ro}}{U_{ro}} + F_{so}U_{so} + F_{ro}U_{ro} \quad (\text{A.12})$$

$$B_h = -\frac{1}{R\rho_0} \frac{\partial p_0}{\partial \beta} - u_0 \frac{\partial v_0}{\partial z} - \frac{v_0}{R} \frac{\partial v_0}{\partial \beta} + \frac{1}{h_0} \{ v_0 H_{so}U_{so} + (v_0 - w) H_{ro}U_{ro} \} \quad (\text{A.13})$$

$$(\text{A.14})$$

with further definitions for Moody's and Hirs' friction factors and their dependent terms, $f_{so}, f_{ro}, F_{so}, F_{ro}$ etc., given in Appendix D.

The first-order governing equations are expressed in terms of the $a_i(z, \beta)$ and $b_i(z, \beta)$ functions as;

$$\begin{aligned} \frac{h_0}{\rho} \frac{\partial a_1}{\partial z} + (A_u - u_0 \frac{\partial h}{\partial z}) a_3 + h_0 \omega a_4 (A_v - \frac{u_0}{R} \frac{\partial h}{\partial \beta}) a_5 &= -\frac{h_0 v_0}{R} \frac{\partial a_3}{\partial \beta} + \frac{h_0 u_0}{R} \frac{\partial a_5}{\partial \beta} \\ &- c_* [(A_h + u_0 (\frac{\partial u}{\partial z} + \frac{1}{R} \frac{\partial v}{\partial \beta})) \cos \beta - \frac{u_0 v_0}{R} \sin \beta] \end{aligned} \quad (\text{A.15})$$

$$\begin{aligned} \frac{h_0}{\rho} \frac{\partial a_2}{\partial z} - h_0 \omega a_3 + (A_u - u_0 \frac{\partial h}{\partial z}) a_4 + (A_v - \frac{u_0}{R} \frac{\partial h}{\partial \beta}) a_5 &= c_* \omega u_0 \cos \beta - \frac{h_0 v_0}{R} \frac{\partial a_4}{\partial \beta} \\ &+ \frac{h_0 u_0}{R} \frac{\partial a_6}{\partial \beta} \end{aligned} \quad (\text{A.16})$$

$$h_0 \frac{\partial a_3}{\partial z} + \frac{\partial h}{\partial z} a_3 + \frac{1}{R} \frac{\partial h}{\partial \beta} a_5 = c_* [(\frac{\partial u}{\partial z} + \frac{1}{R} \frac{\partial v}{\partial \beta}) \cos \beta - \frac{v_0}{R} \sin \beta] - \frac{h_0}{R} \frac{\partial a_5}{\partial \beta} \quad (\text{A.17})$$

$$h_0 \frac{\partial a_4}{\partial z} + \frac{\partial h}{\partial z} a_4 + \frac{1}{R} \frac{\partial h}{\partial \beta} a_6 = -c_* \omega \cos \beta - \frac{h_0}{R} \frac{\partial a_6}{\partial \beta} \quad (\text{A.18})$$

$$h_0 u_0 \frac{\partial a_5}{\partial z} + B_u a_3 + B_v a_5 + h_0 \omega a_6 = -c_* B_h \cos \beta - \frac{h_0}{R \rho} \frac{\partial a_1}{\partial \beta} - \frac{h_0 v_0}{R} \frac{\partial a_5}{\partial \beta} \quad (\text{A.19})$$

$$h_0 u_0 \frac{\partial a_6}{\partial z} + B_u a_4 - h_0 \omega a_5 + B_v a_6 = -\frac{h_0}{R \rho} \frac{\partial a_2}{\partial \beta} - \frac{h_0 v_0}{R} \frac{\partial a_6}{\partial \beta} \quad (\text{A.20})$$

$$\begin{aligned} \frac{h_0}{\rho} \frac{\partial b_1}{\partial z} + (A_u - u_0 \frac{\partial h}{\partial z}) b_3 + h_0 \omega b_4 + (A_v - \frac{u_0}{R} \frac{\partial h}{\partial \beta}) b_5 &= -c_* \omega u_0 \sin \beta - \frac{h_0 v_0}{R} \frac{\partial b_3}{\partial \beta} \\ &+ \frac{h_0 u_0}{R} \frac{\partial b_5}{\partial \beta} \end{aligned} \quad (\text{A.21})$$

$$\begin{aligned} \frac{h_0}{\rho} \frac{\partial b_2}{\partial z} - h_0 \omega b_3 + (A_u - u_0 \frac{\partial h}{\partial z}) b_4 + (A_v - \frac{u_0}{R} \frac{\partial h}{\partial \beta}) b_6 &= \\ -c_* [(A_h + u_0 (\frac{\partial u}{\partial z} + \frac{1}{R} \frac{\partial v}{\partial \beta})) \sin \beta + \frac{u_0 v_0}{R} \cos \beta] - \frac{h_0 v_0}{R} \frac{\partial b_4}{\partial \beta} + \frac{h_0 u_0}{R} \frac{\partial b_6}{\partial \beta} \end{aligned} \quad (\text{A.22})$$

$$h_0 \frac{\partial b_3}{\partial z} + \frac{\partial h}{\partial z} b_3 + \frac{1}{R} \frac{\partial h}{\partial \beta} b_5 = c_* \omega \sin \beta - \frac{h_0}{R} \frac{\partial b_5}{\partial \beta} \quad (\text{A.23})$$

$$h_0 \frac{\partial b_4}{\partial z} + \frac{\partial h}{\partial z} b_4 + \frac{1}{R} \frac{\partial h}{\partial \beta} b_6 = c_* [\frac{v_0}{R} \cos \beta + (\frac{\partial u}{\partial z} + \frac{1}{R} \frac{\partial v}{\partial \beta}) \sin \beta] - \frac{h_0}{R} \frac{\partial b_6}{\partial \beta} \quad (\text{A.24})$$

$$h_0 u_0 \frac{\partial b_5}{\partial z} + B_u b_3 + B_v b_5 + h_0 \omega b_6 = -\frac{h_0}{R \rho} \frac{\partial b_1}{\partial \beta} - \frac{h_0 v_0}{R} \frac{\partial b_5}{\partial \beta} \quad (\text{A.25})$$

$$h_0 u_0 \frac{\partial b_6}{\partial z} + B_u b_4 - h_0 \omega b_5 + B_v b_6 = -c_* B_h \sin \beta - \frac{h_0}{R \rho} \frac{\partial b_2}{\partial \beta} - \frac{h_0 v_0}{R} \frac{\partial b_6}{\partial \beta} \quad (\text{A.26})$$

APPENDIX B

VARIABLE PROPERTIES MODEL

Zeroth Order (Steady State) Equations:

$$\begin{bmatrix} \rho_0 h_0 & 0 & h_0 u_0 \frac{\partial \rho_0}{\partial p_0} \\ 0 & \rho_0 h_0 u_0 & 0 \\ \rho_0 h_0 u_0 & 0 & h_0 \end{bmatrix} \begin{Bmatrix} \frac{\partial u_0}{\partial z} \\ \frac{\partial v_0}{\partial z} \\ \frac{\partial p_0}{\partial z} \end{Bmatrix} = \begin{bmatrix} F_u \\ F_v \\ F_p \end{bmatrix} \quad (\text{B.1})$$

where

$$F_u = -\rho_0 u_0 \frac{\partial h_0}{\partial z} - \frac{\rho_0 v_0}{R} \frac{\partial h_0}{\partial \beta} - \frac{\rho_0 h_0}{R} \frac{\partial v_0}{\partial \beta} - \frac{h_0 v_0}{R} \frac{\partial \rho_0}{\partial p_0} \frac{\partial p_0}{\partial \beta} \quad (\text{B.2})$$

$$F_v = -\frac{\rho_0 h_0 v_0}{R} \frac{\partial v_0}{\partial \beta} - \frac{h_0}{R} \frac{\partial p_0}{\partial \beta} - \rho_0 \left\{ f_{r0} \frac{u_0}{2} \sqrt{u_0^2 + (v_0 - w)^2} + f_{s0} \frac{v_0}{2} \sqrt{u_0^2 + v_0^2} \right\} \quad (\text{B.3})$$

$$F_p = -\frac{\rho_0 h_0 v_0}{R} \frac{\partial v_0}{\partial \beta} - \rho_0 \left\{ f_{r0} \frac{(v_0 - w)}{2} \sqrt{u_0^2 + (v_0 - w)^2} + f_{s0} \frac{v_0}{2} \sqrt{u_0^2 + v_0^2} \right\} \quad (\text{B.4})$$

First Order (Perturbed) Equations: Continuity:

$$\begin{aligned} & \frac{\rho_0 v_0}{R} \frac{\partial h_1}{\partial \beta} + \frac{\rho_0 h_0}{R} \frac{\partial v_1}{\partial \beta} + \frac{v_0 h_0}{R} \frac{\partial p_1}{\partial \beta} + \rho_0 h_0 \frac{\partial u_1}{\partial z} + u_0 h_0 \frac{\partial p_1}{\partial z} + h_0 A_{p1} \frac{\partial p_1}{\partial t} \\ & + A_u u_1 + A_v v_1 + A_p p_1 = -\rho_0 u_0 \frac{\partial h_1}{\partial z} - \rho_0 \frac{\partial h_1}{\partial t} - A_h h_1 \end{aligned} \quad (\text{B.5})$$

Axial Momentum:

$$\begin{aligned} & \frac{h_0 v_0}{R} \frac{\partial u_1}{\partial \beta} + h_0 u_0 \frac{\partial u_1}{\partial z} + \frac{h_0}{\rho_0} \frac{\partial p_1}{\partial z} + h_0 \frac{\partial u_1}{\partial t} + B_u u_1 + B_v v_1 + B_p p_1 \\ & = B_h h_1 \end{aligned} \quad (\text{B.6})$$

Circumferential Momentum:

$$\begin{aligned} \frac{h_0 v_0}{R} \frac{\partial v_1}{\partial \beta} + \frac{h_0}{\rho_0 R} \frac{\partial p_1}{\partial \beta} + h_0 u_0 \frac{\partial v_1}{\partial z} + h_0 \frac{\partial v_1}{\partial t} + C_u u_1 + C_v v_1 + C_p p_1 \\ = C_h h_1 \end{aligned} \quad (\text{B.7})$$

The coefficient expressions A_u, A_v etc., in the above first order equations are defined below.

$$A_u = \rho_0 \frac{\partial h_0}{\partial z} + h_0 \frac{\partial \rho_0}{\partial z} \quad (\text{B.8})$$

$$A_v = \frac{\rho_0}{R} \frac{\partial h_0}{\partial \beta} + \frac{h_0}{R} \frac{\partial \rho_0}{\partial \beta} \quad (\text{B.9})$$

$$A_p = \frac{v_0}{R} \frac{\partial h_0}{\partial \beta} + \frac{h_0}{R} \frac{\partial v_0}{\partial \beta} + u_0 \frac{\partial h_0}{\partial z} + h_0 \frac{\partial u_0}{\partial z} \quad (\text{B.10})$$

$$A_{\rho 1} = \frac{\partial \rho_0}{\partial p_0} \quad (\text{B.11})$$

$$A_p = A_{\rho 1} A_{\rho 1} \quad (\text{B.12})$$

$$A_h = \frac{\rho_0}{R} \frac{\partial v_0}{\partial \beta} + \frac{v_0}{R} \frac{\partial \rho_0}{\partial \beta} + \rho_0 \frac{\partial u_0}{\partial z} + u_0 \frac{\partial \rho_0}{\partial z} \quad (\text{B.13})$$

$$A_{\rho 1} = \frac{\partial \rho_0}{\partial p_0} \quad (\text{B.14})$$

$$A_{\mu 1} = \frac{\partial \mu_0}{\partial p_0} \quad (\text{B.15})$$

$$B_u = h_0 \frac{\partial u_0}{\partial z} + u_0^2 \left(\frac{\bar{F}_{r0}}{U_{r0}} + \frac{\bar{F}_{s0}}{U_{s0}} \right) + F_{r0} U_{r0} + F_{s0} U_{s0} \quad (\text{B.16})$$

$$B_v = \frac{h_0}{R} \frac{\partial u_0}{\partial \beta} + u_0 \left\{ v_0 \frac{\bar{F}_{s0}}{U_{s0}} + (v_0 - w) \frac{\bar{F}_{r0}}{U_{r0}} \right\} \quad (\text{B.17})$$

$$B_p = -\frac{h_0}{\rho_0^2} - \frac{u_0}{\rho_0} \{ G_{s0} U_{s0} + G_{r0} U_{r0} \} \quad (\text{B.18})$$

$$B_h = -\frac{1}{\rho_0} \frac{\partial p_0}{\partial z} - u_0 \frac{\partial u_0}{\partial z} - \frac{v_0}{R} \frac{\partial u_0}{\partial \beta} + \frac{u_0}{h_0} (H_{s0} U_{s0} + H_{r0} U_{r0}) \quad (\text{B.19})$$

$$B_{\mu} = \frac{u_0}{\mu_0} (G_{s0} U_{s0} + G_{r0} U_{r0}) \quad (\text{B.20})$$

$$B_p = B_{\rho} A_{\rho 1} + B_{\mu} A_{\mu 1} \quad (\text{B.21})$$

$$C_u = h_0 \frac{\partial v_0}{\partial z} + u_0 \left\{ v_0 \frac{\bar{F}_{so}}{U_{so}} + (v_0 - w) \frac{\bar{F}_{ro}}{U_{ro}} \right\} \quad (\text{B.22})$$

$$C_v = \frac{h_0}{R} \frac{\partial v_0}{\partial \beta} + v_0^2 \frac{\bar{F}_{so}}{U_{so}} + (v_0 - w)^2 \frac{\bar{F}_{ro}}{U_{ro}} + F_{so} U_{so} + F_{ro} U_{ro} \quad (\text{B.23})$$

$$C_p = -\frac{1}{\rho_0} \left[\frac{h_0}{R \rho_0} \frac{\partial p_0}{\partial \beta} + \{v_0 G_{so} U_{so} + (v_0 - w) G_{ro} U_{ro}\} \right] \quad (\text{B.24})$$

$$C_\mu = \frac{1}{\mu_0} \{v_0 G_{so} U_{so} + (v_0 - w) G_{ro} U_{ro}\} \quad (\text{B.25})$$

$$C_h = -\frac{1}{R \rho_0} \frac{\partial p_0}{\partial \beta} - u_0 \frac{\partial v_0}{\partial z} - \frac{v_0}{R} \frac{\partial v_0}{\partial \beta} + \frac{1}{h_0} \{v_0 H_{so} U_{so} + (v_0 - w) H_{ro} U_{ro}\} \quad (\text{B.26})$$

$$C_p = C_p A_{p1} + C_\mu A_{\mu 1} \quad (\text{B.27})$$

with further definitions for Moody's and Hirs' friction factors and their dependent terms, $f_{so}, f_{ro}, F_{so}, F_{ro}$ etc., given in Appendix D.

The first-order governing equations are expressed in terms of the $a_i(z, \beta)$ and $b_i(z, \beta)$ functions as;

$$\begin{aligned} h_0 u_0 (A_{p1} - \frac{1}{u_0^2}) \frac{\partial a_1}{\partial z} + (A_p - \frac{\rho_0}{u_0} B_p) a_1 + h_0 \omega A_{p1} a_2 + (A_u - \frac{\rho_0}{u_0} B_u) a_3 \\ - \frac{h_0 \omega \rho_0}{u_0} a_4 + (A_v - \frac{\rho_0}{u_0} B_v) a_5 = - \frac{c_s \rho_0 v_0}{R} \sin \beta + c_s A_h \cos \beta \\ - \frac{h_0 \rho_0}{R} \frac{\partial a_5}{\partial \beta} - \frac{h_0 v_0 A_{p1}}{R} \frac{\partial a_1}{\partial \beta} + \frac{c_s \rho_0 B_h}{u_0} + \frac{h_0 \rho_0 v_0}{R u_0} \frac{\partial a_3}{\partial \beta} \end{aligned} \quad (\text{B.28})$$

$$\begin{aligned} h_0 u_0 (A_{p1} - \frac{1}{u_0^2}) \frac{\partial a_2}{\partial z} - h_0 \omega A_{p1} a_1 + (A_p - \frac{\rho_0}{u_0} B_p) a_2 + \frac{h_0 \omega \rho_0}{u_0} a_3 \\ + (A_u - \frac{\rho_0}{u_0} B_u) a_4 + (A_v - \frac{\rho_0}{u_0} B_v) a_5 = - c_s \rho_0 \omega \cos \beta - \frac{h_0 \rho_0}{R} \frac{\partial a_6}{\partial \beta} \\ - \frac{h_0 v_0}{R} \frac{\partial a_2}{\partial \beta} + \frac{h_0 \rho_0 v_0}{R u_0} \frac{\partial a_4}{\partial \beta} \end{aligned} \quad (\text{B.29})$$

$$\begin{aligned} h_0 \rho_0 (1 - A_{p1} u_0^2) \frac{\partial a_3}{\partial z} + (A_p - \rho_0 u_0 A_{p1} B_p) a_1 + h_0 \omega A_{p1} a_2 \\ + (A_u - \rho_0 u_0 A_{p1} B_u) a_3 - h_0 \omega \rho_0 A_{p1} a_4 + (A_v - \rho_0 u_0 A_{p1} B_v) = - \frac{c_s \rho_0 v_0}{R} \sin \beta \end{aligned}$$

$$\begin{aligned}
& + c_* A_h \cos \beta - \frac{h_0 \rho_0}{R} \frac{\partial a_5}{\partial \beta} - \frac{h_0 v_0}{R} A_{\rho 1} \frac{\partial a_1}{\partial \beta} + c_* B_h \rho_0 u_0 A_{\rho 1} \cos \beta \\
& + \frac{h a \rho_0 u_0 v_0}{R} A_{\rho 1} \frac{\partial a_3}{\partial \beta}
\end{aligned} \tag{B.30}$$

$$\begin{aligned}
& h_0 \rho_0 (1 - u_0^2 A_{\rho 1}) \frac{\partial a_4}{\partial z} - h_0 \omega A_{\rho 1} a_1 + (A_p - \rho_0 u_0 A_{\rho 1} B_p) a_2 + h_0 \omega \rho_0 u_0 A_{\rho 1} a_3 \\
& + (A_u - \rho_0 u_0 A_{\rho 1} B_u) a_4 + (A_v - \rho_0 u_0 A_{\rho 1} B_v) a_6 = -c_* \rho_0 \omega \cos \beta - \frac{h_0 \rho_0}{R} \frac{\partial a_6}{\partial \beta} \\
& - \frac{h_0 v_0}{R} A_{\rho 1} \frac{\partial a_2}{\partial \beta} + \frac{h_0 \rho_0 u_0 v_0}{R} A_{\rho 1} \frac{\partial a_4}{\partial \beta}
\end{aligned} \tag{B.31}$$

$$\begin{aligned}
& h_0 u_0 \frac{\partial a_5}{\partial z} + C_p a_1 + C_u a_3 + C_v a_5 + h_0 \omega a_6 = -c_* C_h \cos \beta \\
& - \frac{h_0 v_0}{R} \frac{\partial a_5}{\partial \beta} - \frac{h_0}{R \rho_0} \frac{\partial a_1}{\partial \beta}
\end{aligned} \tag{B.32}$$

$$\begin{aligned}
& h_0 u_0 \frac{\partial a_6}{\partial z} + C_p a_2 + C_u a_4 - h_0 \omega a_5 + C_v a_6 = -\frac{h_0 v_0}{R} \frac{\partial a_6}{\partial \beta} \\
& - \frac{h_0}{R \rho_0} \frac{\partial a_2}{\partial \beta}
\end{aligned} \tag{B.33}$$

$$\begin{aligned}
& h_0 u_0 (A_{\rho 1} - \frac{1}{u_0^2}) \frac{\partial b_1}{\partial z} + (A_p - \frac{\rho_0}{u_0} B_p) b_1 + (A_u - \frac{\rho_0}{u_0} B_u) a_3 - \frac{h_0 \omega A_{\rho 1}}{u_0} b_4 \\
& + (A_v - \frac{\rho_0}{u_0} B_v) b_5 = -c_* \rho_0 \omega \sin \beta - \frac{h_0 \rho_0}{R} \frac{\partial b_6}{\partial \beta} - \frac{h_0 v_0}{R} A_{\rho 1} \frac{\partial b_1}{\partial \beta} \\
& + \frac{h_0 \rho_0 v_0}{R u_0} \frac{\partial b_3}{\partial \beta}
\end{aligned} \tag{B.34}$$

$$\begin{aligned}
& h_0 u_0 (A_{\rho 1} - \frac{1}{u_0^2}) \frac{\partial b_2}{\partial z} - h_0 \omega A_{\rho 1} b_1 + (A_p - \frac{\rho_0}{u_0} B_p) b_2 + \frac{h_0 \omega \rho_0}{u_0} b_3 \\
& + (A_u - \frac{\rho_0}{u_0} B_u) b_4 + (A_v - \frac{\rho_0}{u_0} B_v) b_6 = \frac{c_* \rho_0 v_0}{R} \cos \beta + c_* A_h \sin \beta \\
& - \frac{h_0 \rho_0}{R} \frac{\partial b_5}{\partial \beta} - \frac{h_0 v_0 A_{\rho 1}}{R} \frac{\partial b_2}{\partial \beta} + \frac{c_* \rho_0 B_h}{u_0} \sin \beta + \frac{h_0 \rho_0 v_0}{R u_0} \frac{\partial b_4}{\partial \beta}
\end{aligned} \tag{B.35}$$

$$h_0 \rho_0 (1 - A_{\rho 1} u_0^2) \frac{\partial b_3}{\partial z} + (A_p - \rho_0 u_0 A_{\rho 1} B_p) b_1 + h_0 \omega A_{\rho 1} b_2$$

$$\begin{aligned}
& + (A_u - \rho_0 u_0 A_{\rho 1} B_u) b_3 - h_0 \omega \rho_0 A_{\rho 1} b_4 + (A_v - \rho_0 u_0 A_{\rho 1} B_v) b_5 = c_* \rho_0 \omega \sin \beta \\
& - \frac{h_0 \rho_0}{R} \frac{\partial b_6}{\partial \beta} - \frac{h_0 v_0}{R} A_{\rho 1} \frac{\partial b_1}{\partial \beta} + \frac{h_0 \rho_0 u_0 v_0}{R} A_{\rho 1} \frac{\partial b_4}{\partial \beta} \quad (B.36)
\end{aligned}$$

$$\begin{aligned}
& h_0 \rho_0 (1 - u_0^2 A_{\rho 1}) \frac{\partial b_4}{\partial z} - h_0 \omega A_{\rho 1} a_1 + (A_p - \rho_0 u_0 A_{\rho 1} B_p) b_2 + h_0 \omega \rho_0 u_0 A_{\rho 1} b_3 \\
& + (A_u - \rho_0 u_0 A_{\rho 1} B_u) b_4 + (A_v - \rho_0 u_0 A_{\rho 1} B_v) b_5 = \frac{c_* \rho_0 v_0}{R} \cos \beta + c_* A_h \sin \beta \\
& - \frac{h_0 \rho_0}{R} \frac{\partial b_5}{\partial \beta} - \frac{h_0 v_0}{R} A_{\rho 1} \frac{\partial b_2}{\partial \beta} + c_* B_h \rho_0 u_0 A_{\rho 1} \sin \beta + \frac{h_0 \rho_0 u_0 v_0}{R} A_{\rho 1} \frac{\partial b_4}{\partial \beta} \quad (B.37)
\end{aligned}$$

$$\begin{aligned}
h_0 u_0 \frac{\partial b_5}{\partial z} + C_p b_1 + C_u b_3 + C_v b_5 + h_0 \omega b_6 & = - \frac{h_0 v_0}{R} \frac{\partial b_6}{\partial \beta} \\
& - \frac{h_0}{R \rho_0} \frac{\partial b_1}{\partial \beta} \quad (B.38)
\end{aligned}$$

$$\begin{aligned}
h_0 u_0 \frac{\partial b_6}{\partial z} + C_p b_2 + C_u b_4 - h_0 \omega b_5 + C_v b_6 & = -c_* C_h \sin \beta \\
& - \frac{h_0 v_0}{R} \frac{\partial b_5}{\partial \beta} \frac{h_0}{R \rho_0} \frac{\partial b_2}{\partial \beta} \quad (B.39)
\end{aligned}$$

APPENDIX C

THERMAL EFFECTS WITH VARIABLE PROPERTIES MODEL

Zeroth Order (Steady State) Equations:

$$\begin{bmatrix} \rho_0 h_0 & 0 & h_0 u_0 \frac{\partial \rho_0}{\partial p_0} & h_0 u_0 \frac{\partial \rho_0}{\partial T_0} \\ 0 & \rho_0 h_0 u_0 & 0 & 0 \\ \rho_0 h_0 u_0 & 0 & h_0 & 0 \\ 0 & 0 & T \beta_v h_0 u_0 & -\rho_0 C_p h_0 u_0 \end{bmatrix} \begin{bmatrix} \frac{\partial u_0}{\partial z} \\ \frac{\partial v_0}{\partial z} \\ \frac{\partial \rho_0}{\partial z} \\ \frac{\partial T_0}{\partial z} \end{bmatrix} = \begin{bmatrix} F_u \\ F_v \\ F_p \\ F_T \end{bmatrix} \quad (C.1)$$

where

$$F_u = -\rho_0 u_0 \frac{\partial h_0}{\partial z} - \frac{\rho_0 v_0}{R} \frac{\partial h_0}{\partial \beta} - \frac{\rho_0 h_0}{R} \frac{\partial v_0}{\partial \beta} - \frac{h_0 v_0}{R} \frac{\partial \rho_0}{\partial p_0} \frac{\partial p_0}{\partial \beta} - \frac{h_0 v_0}{R} \frac{\partial \rho_0}{\partial T_0} \frac{\partial T_0}{\partial \beta} \quad (C.2)$$

$$F_v = -\frac{\rho_0 h_0 v_0}{R} \frac{\partial v_0}{\partial \beta} - \frac{h_0}{R} \frac{\partial p_0}{\partial \beta} - \rho_0 \left\{ f_{s0} \frac{v_0}{2} \sqrt{u_0^2 + v_0^2} + f_{r0} \frac{u_0}{2} \sqrt{u_0^2 + (v_0 - w)^2} \right\} \quad (C.3)$$

$$F_p = -\frac{\rho_0 h_0 v_0}{R} \frac{\partial v_0}{\partial \beta} - \rho_0 \left\{ f_{s0} \frac{v_0}{2} \sqrt{u_0^2 + v_0^2} + f_{r0} \frac{(v_0 - w)}{2} \sqrt{u_0^2 + (v_0 - w)^2} \right\} \quad (C.4)$$

$$F_T = \rho_0 C_p \frac{h_0 v_0}{R} \frac{\partial T_0}{\partial \beta} - T_0 \beta_v \frac{h_0 v_0}{R} \frac{\partial p_0}{\partial \beta} + Q_s - \omega R \left[\frac{h_0}{2R} \frac{\partial p_0}{\partial \beta} + \frac{\mu_0}{4h_0} \left\{ \frac{v_0}{2} f_{s0} R_{s0} - \frac{(v_0 - w)}{2} f_{r0} R_{r0} \right\} \right] - u_0 \rho_0 \left\{ f_{s0} \frac{v_0}{2} \sqrt{u_0^2 + v_0^2} + f_{r0} \frac{u_0}{2} \sqrt{u_0^2 + (v_0 - w)^2} \right\} - v_0 \rho_0 \left\{ f_{s0} \frac{v_0}{2} \sqrt{u_0^2 + v_0^2} + f_{r0} \frac{(v_0 - w)}{2} \sqrt{u_0^2 + (v_0 - w)^2} \right\} \quad (C.5)$$

The first order equations are given in Appendix B.

APPENDIX D

FRICTION FACTORS

term	Moody's Model	Hirs' Model
f_{so}	$f_{soM} = \frac{0.0055}{4} [1 + (10^4 \frac{e_s}{h_0} + 10^6 \frac{1}{R_{so}})^{1/3}]$	$f_{soH} = n_s R_{so}^{m_s}$
f_{ro}	$f_{roM} = \frac{0.0055}{4} [1 + (10^4 \frac{e_r}{h_0} + 10^6 \frac{1}{R_{ro}})^{1/3}]$	$f_{roH} = n_r R_{ro}^{m_r}$
g_{so}	$g_{soM} = \frac{0.0055 \times 10^4}{12 R_{so}} (10^4 \frac{e_s}{h_0} + 10^6 \frac{1}{R_{so}})^{-2/3}$	$g_{soH} = -m_s n_s [R_{so}]^{m_s}$
g_{ro}	$g_{roM} = \frac{0.0055 \times 10^4}{12 R_{ro}} (10^4 \frac{e_r}{h_0} + 10^6 \frac{1}{R_{ro}})^{-2/3}$	$g_{roH} = -m_r n_r [R_{ro}]^{m_r}$
h_{so}	$h_{soM} = \frac{0.0055}{12} (10^4 \frac{e_s}{h_0} + 10^6 \frac{1}{R_{so}})^{1/3}$	$h_{soH} = -m_s n_s [R_{so}]^{m_s}$
h_{ro}	$h_{roM} = \frac{0.0055}{12} (10^4 \frac{e_r}{h_0} + 10^6 \frac{1}{R_{ro}})^{1/3}$	$h_{roH} = -m_r n_r [R_{ro}]^{m_r}$
F_{so}	$f_{soM}/2$	$f_{soH}/2$
F_{ro}	$f_{roM}/2$	$f_{roH}/2$
G_{so}	$g_{soM}/2$	$g_{soH}/2$
G_{ro}	$g_{roM}/2$	$g_{roH}/2$
H_{so}	$h_{soM}/2$	$h_{soH}/2$
H_{ro}	$h_{roM}/2$	$h_{roH}/2$
\bar{F}_{so}	$(f_{soM} - g_{soM})/2$	$(f_{soH} - g_{soH})/2$
\bar{F}_{ro}	$(f_{roM} - g_{roM})/2$	$(f_{roH} - g_{roH})/2$
U_{so}	$\sqrt{u_0^2 + v_0^2}$	$\sqrt{u_0^2 + v_0^2}$
U_{ro}	$\sqrt{u_0^2 + (v_0 - w)^2}$	$\sqrt{u_0^2 + (v_0 - w)^2}$
R_{so}	$\frac{2\rho_0 h_0}{\mu_0} \sqrt{u_0^2 + v_0^2}$	$\frac{2\rho_0 h_0}{\mu_0} \sqrt{u_0^2 + v_0^2}$
R_{ro}	$\frac{2\rho_0 h_0}{\mu_0} \sqrt{u_0^2 + (v_0 - w)^2}$	$\frac{2\rho_0 h_0}{\mu_0} \sqrt{u_0^2 + (v_0 - w)^2}$

APPENDIX E

CLEARANCE FUNCTIONS FOR ELLIPTICAL SEAL

The clearance functions for the elliptical seal are given in the next table as;

<i>straight profile</i>	<i>linear profile</i>	<i>quadratic profile</i>
$f_1(z) = a_1$	$f_1(z) = a_1 + a_2 z$	$f_1(z) = a_1 + a_2 z + a_3 z^2$
$f_2(z) = b_1$	$f_2(z) = b_1 + b_2 z$	$f_2(z) = b_1 + b_2 z + b_3 z^2$
$\frac{\partial f_1}{\partial z} = 0$	$\frac{\partial f_1}{\partial z} = a_2$	$\frac{\partial f_1}{\partial z} = a_2 + 2a_3 z$
$\frac{\partial f_2}{\partial z} = 0$	$\frac{\partial f_2}{\partial z} = b_2$	$\frac{\partial f_2}{\partial z} = b_2 + 2b_3 z$
$a_1 = R + c_i$	$a_1 = R + c_i$	$a_1 = R + c_i$
	$a_2 = \frac{1}{L}(c_e - c_i)$	$a_2 = \frac{-1}{L}(c_e - 4c_m + 3c_i)$
		$a_3 = \frac{2}{L^2}(c_e - 2c_m + c_i)$
$b_1 = R + (1 - \delta)c_i$	$b_1 = R + (1 - \delta)c_i$	$b_1 = R + (1 - \delta)c_i$
	$b_2 = \frac{1}{L}(1 - \delta)(c_e - c_i)$	$b_2 = \frac{-1}{L}(1 - \delta)(c_e - 4c_m + 3c_i)$
		$b_3 = \frac{2}{L^2}(1 - \delta)(c_e - 2c_m + c_i)$

Gradients of the clearance function for elliptical seal are given by;

$$c(z, \beta) = \sqrt{(f_1(z)\cos\beta)^2 + (f_2(z)\sin\beta)^2} - R \quad (\text{E.1})$$

$$\frac{\partial c}{\partial z} = \frac{f_1 f_1' \cos^2 \beta + f_2 f_2' \sin^2 \beta}{\sqrt{(f_1 \cos \beta)^2 + (f_2 \sin \beta)^2}} \quad (\text{E.2})$$

$$\frac{\partial c}{\partial \beta} = \frac{(f_2^2 - f_1^2) \cos \beta \sin \beta}{\sqrt{(f_1 \cos \beta)^2 + (f_2 \sin \beta)^2}} \quad (\text{E.3})$$

APPENDIX F

EQUATION OF STATE

The modified Benedict-Webb-Rubens Equation of state is given below.

$$\begin{aligned}
 p = & \rho RT + \\
 & \rho^2(G(1)T + G(2)T^{1/2} + G(3) + G(4)/T + G(5)/T^2) + \\
 & \rho^3(G(6)T + G(7) + G(8)/T + G(9)/T^2) + \\
 & \rho^4(G(10)T + G(11) + G(12)/T) + \rho^5(G(13)) + \\
 & \rho^6(G(14)/T + G(15)/T^2) + \rho^7(G(16)/T) + \\
 & \rho^8(G(17)/T + G(18)T^2) + \rho^9(G(19)/T^2) + \\
 & \rho^3(G(20)/T^2 + G(21)/T^3) e^{\gamma\rho^2} + \\
 & \rho^5(G(22)/T^2 + G(23)/T^4) e^{\gamma\rho^2} + \\
 & \rho^7(G(24)/T^2 + G(25)/T^3) e^{\gamma\rho^2} + \\
 & \rho^9(G(26)/T^2 + G(27)/T^4) e^{\gamma\rho^2} + \\
 & \rho^{11}(G(28)/T^2 + G(29)/T^3) e^{\gamma\rho^2} + \\
 & \rho^{13}(G(30)/T^2 + G(31)/T^3 + G(32)/T^4) e^{\gamma\rho^2}
 \end{aligned} \tag{F.1}$$

The expression for viscosity is given by,

$$\mu = \mu_0(T) + \mu_1(T)\rho + \mu_2(\rho, T) \tag{F.2}$$

$$\mu_0 = \sum_{i=1}^9 G_{\nu}(i)T^{(4-i)/3} \tag{F.3}$$

$$\mu_1(T) = F_{\nu}(1) + F_{\nu}(2) \{F_{\nu}(3) - \ln(T/F_{\nu}(4))\}^2 \tag{F.4}$$

$$\mu_2(\rho, T) = e^{F(\rho, T)} - e^{G(T)} \tag{F.5}$$

$$F(\rho, T) = E_{\nu}(1) + E_{\nu}(2)H(\rho) + E_{\nu}(3)\rho^{0.1} +$$

$$E_{\nu}(4)H(\rho)/T^2 + E_{\nu}(5)\rho^{0.1}/T^{1.5} + \\ E_{\nu}(6)/T + E_{\nu}(7)H(\rho)/T \quad (\text{F.6})$$

$$G(T) = E_{\nu}(1) + E_{\nu}(2)/T \quad (\text{F.7})$$

$$H(\rho) = \rho^{0.5}(\rho - E_{\nu}(8))/E_{\nu}(8) \quad (\text{F.8})$$

The variation of density with respect to pressure (isothermal case), $\frac{\partial \rho}{\partial p}$ ($1/\frac{\partial p}{\partial \rho}$) is given as,

$$\frac{\partial p}{\partial \rho} = RT + \\ 2\rho(G(1)T + G(2)T^{1/2} + G(3) + G(4)/T + G(5)/T^2) + \\ 3\rho^2(G(6)T + G(7) + G(8)/T + G(9)/T^2) + \\ 4\rho^3(G(10)T + G(11) + G(12)/T) + 5\rho^4(G(13)) + \\ 6\rho^5(G(14)/T + G(15)/T^2) + 7\rho^6(G(16)/T) + \\ 8\rho^7(G(17)/T + G(18)T^2) + 9\rho^8(G(19)/T^2) + \\ \{3\rho^2 + 2\gamma\rho^4\}(G(20)/T^2 + G(21)/T^3) e^{\gamma\rho^2} + \\ \{5\rho^4 + 2\gamma\rho^6\}(G(22)/T^2 + G(23)/T^4) e^{\gamma\rho^2} + \\ \{7\rho^6 + 2\gamma\rho^8\}(G(24)/T^2 + G(25)/T^3) e^{\gamma\rho^2} + \\ \{9\rho^8 + 2\gamma\rho^{10}\}(G(26)/T^2 + G(27)/T^4) e^{\gamma\rho^2} + \\ \{11\rho^{10} + 2\gamma\rho^{12}\}(G(28)/T^2 + G(29)/T^3) e^{\gamma\rho^2} + \\ \{13\rho^{12} + 2\gamma\rho^{14}\}(G(30)/T^2 + G(31)/T^3 + G(32)/T^4) e^{\gamma\rho^2} \quad (\text{F.9})$$

The variation of viscosity with respect to pressure (isothermal case), $\frac{\partial \mu}{\partial p}$ ($\frac{\partial \mu}{\partial \rho} \times \frac{\partial \rho}{\partial p}$) is given below.

$$\frac{\partial \mu}{\partial \rho} = \mu_1(T) + e^{F(\rho, T)} \left[\frac{\partial H}{\partial \rho} \left\{ E_{\nu}(2) + E_{\nu}(4) \frac{1}{T^2} + E_{\nu}(7) \frac{1}{T} \right. \right.$$

$$+ \frac{0.1}{\rho^{0.9}} \{E_\nu(3) + E_\nu(5) \frac{1}{T^{1.5}}\}] \quad (\text{F.10})$$

$$\frac{\partial H}{\partial \rho} = \frac{1}{E_\nu(8)} \left[\frac{0.5}{\rho^{0.5}} \{\rho - E_\nu(8)\} + \rho^{0.5} \right] \quad (\text{F.11})$$

$$B_{\mu 1} = \frac{\partial \mu}{\partial \rho} \quad (\text{F.12})$$

$$A_{\rho 1} = \frac{\partial \rho}{\partial p} \quad (\text{F.13})$$

$$A_{\mu 1} = \frac{\partial \mu}{\partial p} \quad (\text{F.14})$$

$$A_{\mu 1} = A_{\rho 1} \times B_{\mu 1} \quad (\text{F.15})$$

APPENDIX G

LIQUID SEAL DATA

The following data is for Childs and Lindsey (1993)

<i>Seal Data for Childs/Lindsey (1993) Case</i>	
seal length, L	13.13 mm
rotor radius, R	76.20 mm
c_i	nominal values are given in Chapter VI
c_e	for measured values see Lindsey (1993)
fluid	water at 54.5°C
density, ρ	985.25 kg/m ³
viscosity μ	0.5268×10^{-3} Pa-s
pressure drop, Δp	1.38 Mpa, 2.41 Mpa, 3.45 Mpa
rotor speed, N	10200 rpm, 17400 rpm, 24600 rpm
friction factor	Moody Model
relative roughness $e_r/2c_r$	0.001 (rotor)
relative roughness $e_s/2c_s$	0.001 (stator)
pre-swirl ratio	see table in Lindsey (1993)
inlet loss, ξ_i	0.1
exit pressure recovery, ξ_e	1.0

The following data is for Childs and Kim (1985) case.

<i>Seal Data for Childs & Kim (1985) Case</i>	
seal length, L	16.66 mm (0.656 in)
rotor radius, R	48.39 mm (1.905 in)
c_i	0.224 mm (0.0088 in)
c_e	0.158 mm (0.0062 in)
c_s	0.191 mm (0.0075 in)
fluid	liquid oxygen
density, ρ	1121.26 kg/m ³ (70.0 lbm/ft ³)
viscosity μ	1.292×10^{-4} Pa-s (2.70×10^{-6} lb-s/ft ²)
pressure drop, Δp	32.26 MPa (4700 psi)
rotor speed, N	23700 rpm
friction factor	Hirs Model
roughness m_r, n_r	-0.0980, 0.01091 (rotor)
roughness m_s, n_s	-0.0433, 0.03120 (stator)
pre-swirl ratio	0.3
inlet loss, ξ_i	0.1
exit pressure recovery, ξ_e	1.0

The following data is for Sharrer and Nelson (1990) case.

<i>Seal Data for Sharrer & Nelson (1990) Case</i>	
seal length, L	22.20 mm (0.874 in)
rotor radius, R	42.50 mm (1.673 in)
c_i	0.381 mm (0.015 in)
c_e	0.127 mm (0.005 in)
c_s	0.127 mm (0.005 in)
fluid	liquid oxygen
density, ρ	1124 kg/m ³ (70.0 lbm/ft ³)
viscosity μ	1.34×10^{-4} Pa-s (2.70×10^{-6} lb-s/ft ²)
pressure drop, Δp	44.82 MPa (6500 psi)
rotor speed, N	30000 rpm
friction factor	Hirs Model
roughness m_r, n_r	-0.2500, 0.0790 (rotor)
roughness m_s, n_s	-0.1360, 0.0697 (stator)
pre-swirl ratio	0.8
inlet loss, ξ_i	0.25
exit pressure recovery, ξ_e	1.0

The following data is for Scharrer and Nunez (1989) case.

<i>Seal Data for Sharrer & Nunez (1989) Case</i>	
seal length, L	45.70 mm (1.8 in)
rotor radius, R	45.50 mm (1.79 in)
nominal c_i	0.107 mm (0.0042 in)
nominal c_e	0.089 mm (0.0035 in)
c_s	0.089 mm (0.0035 in)
fluid	liquid oxygen
density, ρ	1124 kg/m ³ (70.0 lbm/ft ³)
viscosity μ	1.34×10^{-4} Pa-s (2.70×10^{-6} lb-s/ft ²)
pressure drop, Δp	14.93 MPa (2165 psi)
rotor speed, N	37360 rpm
friction factor	Hirs Model
relative roughness m_r, n_r	-0.25, 0.079 (rotor)
relative roughness m_s, n_s	-0.136, 0.0697 (stator)
pre-swirl ratio	0.6
inlet loss, ξ_i	0.25
exit pressure recovery, ξ_e	1.0

The following data is for Jenssen (1970) case.

<i>Seal Data for Jenssen (1970) Case</i>	
seal length, L	50.80 mm (2.0 in)
rotor radius, R	24.76 mm (0.975 in)
c_i	0.272 mm (0.0107 in)
c_e	0.272 mm (0.0107 in)
c_s	0.272 mm (0.0107 in)
fluid	water
density, ρ	1000 kg/m ³ (62.43 lbm/ft ³)
viscosity μ	1.30×10^{-3} Pa-s (2.72×10^{-5} lb-s/ft ²)
pressure drop, Δp	0.344, 1.034, 1.724 MPa (50,150,250 psi)
rotor speed, N	3000, 5000, 7000 rpm
friction factor	Moody Model
relative roughness $e_r/2c_s$	0.0 (rotor)
relative roughness $e_s/2c_s$	0.0000748 (stator)
pre-swirl ratio	0.3
inlet loss, ξ_i	0.4
exit pressure recovery, ξ_e	1.0

The following data is for Falco *et al.* (1986) case.

<i>Seal Data for Falco et al. (1986) Case</i>	
seal length, L	40 mm (1.57 in)
rotor radius, R	80 mm (3.15 in)
c_i	0.36 mm (0.0142 in)
c_e	0.36 mm (0.0142 in)
c_s	0.36 mm (0.0142 in)
fluid	water
density, ρ	1000 kg/m ³ (62.43 lbm/ft ³)
viscosity μ	1.0×10 ⁻³ Pa-s (2.10×10 ⁻⁵ lb-s/ft ²)
pressure drop, Δp	1.0 MPa (145 psi)
rotor speed, N	4000 rpm
friction factor	Moody Model
relative roughness $e_r/2c_s$	0.0044 (rotor)
relative roughness $e_s/2c_s$	0.0083 (stator)
pre-swirl ratio	0.3
inlet loss, ξ_i	0.3
exit pressure recovery, ξ_e	1.0

The following data is for Kanki and Kawakami (1984) case.

<i>Seal Data for Kanki & Kawakami (1984) Case</i>	
seal length, L	200 mm (7.87 in)
rotor radius, R	100 mm (3.94 in)
c_i	0.50 mm (0.0197 in)
c_e	0.50 mm (0.0197 in)
c_s	0.50 mm (0.0197 in)
fluid	water
density, ρ	1000 kg/m ³ (62.43 lbm/ft ³)
viscosity μ	1.0×10^{-3} Pa-s (2.10×10^{-5} lb-s/ft ²)
pressure drop, Δp	0.98 MPa (142 psi)
rotor speed, N	2000 rpm
friction factor	Moody Model
relative roughness $e_r/2c_s$	0.0033 (rotor)
relative roughness $e_s/2c_s$	0.0033 (stator)
pre-swirl ratio	0.0
inlet loss, ξ_i	0.1
exit pressure recovery, ξ_e	1.0

The following data is for Allaire *et al.* (1976) case.

<i>Seal Data for Allaire et al. (1976) Case</i>	
seal length, L	40.6 mm (1.60 in)
rotor radius, R	39.9 mm (1.57 in)
c_i	0.14 mm (0.0055 in)
c_e	0.14 mm (0.0055 in)
c_s	0.14 mm (0.0055 in)
fluid	liquid hydrogen
density, ρ	57.657 kg/m ³ (3.6 lbm/ft ³)
viscosity μ	7.4396 $\times 10^{-6}$ Pa-s (1.5538 $\times 10^{-7}$ lb-s/ft ²)
pressure drop, Δp	7.26 MPa (1050 psi)
rotor speed, N	23700 rpm
friction factor	Moody Model
relative roughness $e_r/2c_r$	0.00 (rotor)
relative roughness $e_s/2c_s$	0.000001 (stator)
pre-swirl ratio	0.5
inlet loss, ξ_i	0.1
exit pressure recovery, ξ_e	1.0

The following data is for San Andres *et al.* (1992)

<i>Seal Parameters for San Andres et al. (1992)</i>	
seal length, L	45.70 mm (0.656 in)
rotor radius, R	45.50 mm (1.905 in)
c_i	0.127 mm (0.00587 in)
c_e	0.127 mm (0.00581 in)
c_s	0.127 mm (0.00587 in)
fluid	liquid oxygen
density, ρ	variable prop. from NIST12 (MIPROPS)
viscosity μ	variable prop. from NIST12 (MIPROPS)
inlet pressure, π	18.31 MPa (2621 psi)
exit pressure, p_e	3.378 Mpa (483 psi)
rotor speed, N	37360 rpm
friction factor	Moody Model
relative roughness, $e_r/2c_s$	0.0 (rotor)
relative roughness, $e_s/2c_s$	0.044 (stator)
pre-swirl ratio	0.6
inlet loss, ξ_i	0.25
exit pressure recovery, ξ_e	1.0

The following data is for elliptical seal case.

<i>Seal Parameters for Elliptical Seal</i>	
seal length, L	16.66 mm (0.656 in)
rotor radius, R	48.39 mm (1.905 in)
c_i	0.069 mm (0.00273 in)
c_e	0.099 mm (0.00390 in)
c_s	0.069 mm (0.00273 in)
fluid	liquid oxygen
density, ρ	1041.7 kg/m ³ (65.03 lbm/ft ³)
viscosity μ	1.296×10^{-4} Pa-s (0.188×10^{-6} lb-s/ft ²)
pressure drop, Δp	25.39 MPa (3681 psi)
rotor speed, N	22700 rpm
friction factor	Moody Model
relative roughness, $c_r/2c_s$	0.0 (rotor)
relative roughness, $c_s/2c_s$	0.03 (stator)
pre-swirl ratio	0.2
inlet loss, ξ_i	0.33
exit pressure recovery, ξ_e	1.0

The following data is for the distorted seal case.

<i>Seal Parameters for Distorted Seal Unit 9-01</i>	
seal length, L	16.66 mm (0.656 in)
rotor radius, R	48.39 mm (1.905 in)
average c_i	0.149 mm (0.00587 in)
average c_e	0.148 mm (0.00581 in)
nominal clearance c_n	0.149 mm (0.00587 in)
fluid	liquid oxygen
density, ρ	1041.7 kg/m ³ (65.03 lbm/ft ³)
viscosity μ	1.296×10^{-4} Pa-s (0.188×10^{-8} lb-s/ft ²)
pressure drop Δp	35.25 MPa (5112 psi)
rotor speed, N	25000 rpm
friction factor	Moody Model
relative roughness, $e_r/2c_n$	0.0 (rotor)
relative roughness, $e_s/2c_n$	0.8518 (stator)
pre-swirl ratio	0.2
inlet loss, ξ_i	0.3
exit pressure recovery, ξ_e	1.0

The following data is for seal unit 3-02 used in transient simulations.

<i>Seal Parameters for Seal Unit 3-02</i>	
seal length, L	16.6 mm (0.656 in)
rotor radius, R	45.7 mm (1.80 in)
c_i	0.174 mm (0.00687 in)
c_e	0.148 mm (0.00581 in)
nominal clearance c_s	0.149 mm (0.00581 in)
fluid	liquid oxygen
density, ρ	1041.7 kg/m ³ (65.03 lbm/ft ³)
viscosity μ	1.296×10^{-4} Pa-s (0.188×10^{-8} lb-s/ft ²)
pressure drop Δp	35.25 MPa (5112 psi)
rotor speed, N	25000 rpm
friction factor	Moody Model
relative roughness, $e_r/2c_s$	0.0 (rotor)
relative roughness, $e_s/2c_s$	0.8518 (stator)
pre-swirl ratio	0.2
inlet loss, ξ_i	0.3
exit pressure recovery, ξ_e	1.0

C-4